"Photo-responsive Microgels"

Von der Fakultät für Mathematik, Informatik und Naturwissenschaften der RWTH Aachen University zur Erlangung des akademischen Grades eines Doktors der Naturwissenschaften

genehmigte Dissertation

vorgelegt von

Dazril Izrar Phua, M.Sc.

aus Singapur

Berichter: Universitätsprofessor Prof. Dr. Andrij Pich

Universitätsprofessor Prof. Dr. Alexander Böker

Tag der mündlichen Prüfung: 14.10.2016

For my parents and Shahreena

"Knock, And He'll open the door
Vanish, And He'll make you shine like the sun
Fall, And He'll raise you to the heavens
Become nothing, And He'll turn you into everything."

Rumi

Acknowledgement

الحَمْدُ لله I got through this PhD journey relatively intact. For this I would like to express my gratitude and give thanks where its due, to those who have made it a positive sum of experiences.

First and foremost, to the key people who have been directly involved and pivotal in the successful completion of my work. To my supervisor Prof Andrij Pich, thank you for welcoming me into your research group and the guidance provided. Prof Dan Demco, thank you for the time and effort with the NMR measurements and little talks, even when you did not have to. Dr Rostislav Vinokur, thank you for sharing your expertise on LEDs and making them work on the ALV and skilfully crafting the LEDs that were so very crucial to my work, even assembling a second set when the first vanished. Thank you to Dr Juri Zakrevski for the discussions on and analyses of UV/vis spectroscopic measurements.

Thank you to the colleagues (many amongst whom I would consider as friends) at the DWI who have kindly assisted me with measurements and provided their insights:

- Yaodong and Hang for their introductions to and help with the Nanoscope AFM
- Dr. Khosrow Rahimi and Christian Bergs for their patience and expertise with cryo-TEM
- Peng Huan, Sabrina Mallmann and Steve Rütten for their expertise with cryo-FESEM
- Andreea Balaceanu and Krisztian Herman for putting my data through the Flory-Rehner treatment
- Michael Kather for entertaining my questions, requests and providing useful tips
- Thomas Tigges for assistance with confocal microscopy

There have been some good memories with colleagues of the Pich group that I will remember for a long time, especially that very cool and smart trickery (Zosel!) to get me to attend the enjoyable bachelors' day out, shortly before my big day. Shahreena and I also appreciate it that some of you made it down to Singapore.

To Amelina AYTF and Elfeiz, thank you for being generous with the access to the journals.

Badminton was great exercise and a welcome diversion - Greatly improved my skills thanks to Veit, Debra, Thomas, Stefan and Sebastian. Thanks to Patrick for putting me through my paces as well with squash.

I'm grateful for friends who have provided much needed distractions from afar via regular Whatsapp & FB correspondences and/or by way of travel companionship: Raf, Faye, JS, Weebs, Amy, Hieu, Ahmad, Khairul, Lester, Azman and Henrik & family.

This has also been a journey of personal growth and I am thankful to have met good people with the biggest hearts along the way to see me through it: Marscie and family, Helmiah and family, Monsieur Flo Damas (who is actually Singaporean at heart), Jah and Ludwig, and Linda. I enjoy your company and it was always nice and truly a blessing having somewhere to go to which felt like home.

I had the good fortune to meet my beautiful significant other, my cheerleader; your support, presence, patience and love warm my heart and make me feel so very grateful.

To family at home, especially my parents: you have given so much and continue to. It's good to be back <3

I did not make this journey alone, and that is well worth remembering. There are many more friends that I will stop short of mentioning by name, but whose company I will miss and hope to keep in touch with.

A final thanks to Dominik & Debra for kindly agreeing to submit this dissertation on my behalf.

Abstract

In the field of smart materials, employing light as a stimulus is advantageous. Light can be manipulated with high degrees of spatial and temporal control, and applied remotely, without direct contact to the system under study. It is therefore non-invasive, does not contaminate the system or produce unwanted side reactions. The extent or rate of photo-reaction from light stimulation can additionally be tuned by varying the intensity, wavelength, and direction of polarization of the light.

Microgels as a class of smart material, endowed with a photo-responsive property is the focus of this work. Novel microgel systems were synthesized via precipitation polymerization to include photo-sensitive moieties. The changes in the particle size due to light and/or temperature stimuli were detected via dynamic light scattering (DLS). Light stimulus in the form of UV irradiation or visible light was applied *in situ* during DLS measurements by means of optical fiber-coupled LEDs.

In Chapter 2, dual thermo- and photo-responsive microgels are described. *N*-Vinylcaprolactam (VCL) was used as the functional monomer to impart the thermo-sensitive property to the microgels. 4-[(4-Methacryloyloxy)phenylazo] benzenesulfonic acid (ABSA) was used as a water-soluble, photo-switchable co-monomer. *N,N'*-Methylenebisacrylamide (BIS) cross-linked the polymeric chains to produce the microgel particles. In a low regime of ABSA incorporation (< 10 wt. %) as pendant groups, the P(VCL-BIS-ABSA) microgels displayed volume phase transition temperatures that were shifted to lower temperatures relative to P(VCL-BIS) microgels. Under UV irradiation (λ = 365 nm), the P(VCL-BIS-ABSA) microgels deswelled by up to 28% of their sizes in the native, dark-adapted state. The photo-response was more pronounced in the microgel with higher ABSA content. The UV-induced deswelling is found to be reversible, through irradiation with visible light (λ = 450 nm). A mechanism for volume collapse caused by UV stimulus in these microgels is proposed and deduced to be analogous to that caused solely by a temperature stimulus.

Microgels similar to those in Chapter 2 but with higher ABSA incorporation (20-30 wt. %) are described in Chapter 3. These microgels, in their native state, were detected by DLS, cryo-TEM and AFM to exist as pairs of particles in dimeric assemblies. These assemblies could not be disrupted by temperature and/or photo stimuli. However, they were separated by the addition of a small volume of dilute KCl solution as a chaotropic agent followed by a short period of mechanical agitation by ultra-sonication. The abundance of ABSA pendant groups bearing sulfonic acid terminal ends is believed to lead to extensive complexation of the sulfonic acid

groups of ABSA to the C=O groups of the VCL units (strong charged-assisted hydrogen bonding) and to the formation of H-aggregates (π-π stacking interactions) of the azobenzene moieties. This resulted in the formation of inter- and intra-particle cross-links, which act in concert to suppress the thermo- and photo-responses of the particles.

Azobenzene-based cross-linkers and VCL were used to produce dual thermo- and photo-responsive microgels in Chapter 4. Low feed amounts of azo cross-linkers were used for polymerization ($\leq$ 1.0 mol %). The UV-induced deswelling of these microgels was found to be less significant that in the microgels described in Chapter 2.

Non-temperature responsive microgels in Chapter 5 were synthesized with 2-acetoacetoxyethyl methacrylate (AAEM) as the main monomer. AAEM contains the *β*-dicarbonyl moiety which exhibits both enol and diketo structures that should interconvert through a tautomeric equilibrium. In their native states, the P(AAEM) chains in the microgels exist predominantly in the enol form and is tautomerized to the diketo form with UV (λ = 254 nm) irradiation. The diketo tautomer preferentially forms hydrogen bonds with water molecules, thereby causing an increased swelling and larger hydrodynamic radii of the particles that were detected by DLS. The addition of hydrophilic reagents during polymerization alters the topology and consequently the hydrophilicity of the internal micro-environment and porosity of the microgel network. By introducing greater hydrophilicity in the network, we obtained particles with less restricted topology that swelled more rapidly and isotropically. Increased hydrophilicity of the network, however, mitigates the extent of photo-induced swelling and increases the possibility of aggregation. We did not achieve the back-isomerization of the diketo form to the enol form, and hence, the increased swelling was irreversible.

List of Abbreviations and Symbols

Chemicals

AAEM	2-Acetoacetoxyethyl methacrylate
ACMA	2,2'-azobis(*N*-(2-carboxyethyl)-2-methyl-propionamidine)
AMPA	2,2'-azobis(2-methylpropionamidine) dihydrochloride
BIS	*N,N'*-Methylenebisacrylamide
CTAB	Cetyltrimethylammonium bromide
NIPAM	*N*-Isopropylacrylamide
SDS	Sodium dodecyl sulfate
VCL	*N*-Vinylcaprolactam

Instruments and Methods

AFM	Atomic Force Microscopy
DLS	Dynamic Light Scattering
Cryo-FESEM	Cryogenic Field Emission Scanning Electron Microscopy
Cryo-TEM	Cryogenic Transmission Electron Microscopy
NMR	Nuclear Magnetic Resonance
SANS	Small-Angle Neutron Scattering
UV	Ultraviolet

General Abbreviations and Symbols

LCST	Lower Critical Solution Temperature
MW	Molecular Weight
MWCO	Molecular Weight Cut-off
R_h	Hydrodynamic Radius
VPTT	Volume Phase Transition Temperature

Content

Chapter 1. Introduction

1.1. Synthesis of microgels …………………………………………………………………10

1.2. Thermo-responsive microgels …………………………………………………………..11

1.3. Photo-responsive polymer systems ……………………………………………………12

1.4. Photo-responsive microgels ……………………………………………………………...17

1.5. Purpose of study

1.5.1. Motivation ……………………………………………………………………………………20

1.5.2. Aim ……………………………………………………………………………………………...21

1.5.3. Outline of dissertation ………………………………………………………………….....21

1.6. References ………………………………………………………………………………….....25

Chapter 2. The Reversible Thermo- and Photo-Responsive Behavior of Copolymer Microgels of *N*-Vinylcaprolactam and 4-[(4-Methacryloyloxy)phenylazo] benzenesulfonic acid

2.1. Introduction ………………………………………………………………………………36

2.2. Experimental section

2.2.1. Materials ……………………………………………………………………………………37

2.2.2. Microgel synthesis …………………………………………………………………………38

2.2.3. Characterization ……………………………………………………………………………38

2.3. Theory

2.3.1. Flory-Rehner theory for homopolymeric microgel with homogeneous cross-linking density ……………………………………………………………………………………...40

2.4. Results and discussion

2.4.1. Determination of the amount of ABSA comonomer incorporated into Microgels ……………..43

2.4.2. Photo-isomerization behavior of free ABSA comonomer and of ABSA incorporated into microgel ……………………………………………………………………………….....43

2.4.3. Investigation of the thermo- and photo-responsive properties of microgels via DLS measurements ……………………………………………………………………………….45

2.4.4. Raman and ATR spectroscopic investigation of microgel photo-response ……….51

2.4.5. Probing of VCL microgel internal morphology by high-resolution ^{1}H MAS transverse relaxation (T_2) NMR measurements …………………………………………………..53

2.4.6. Description of microgel photo-response based on Flory-Rehner model …………..55

2.4.7. Morphology and topography of P(VCL-BIS$_{1.5}$-ABSA$_{4.5}$) microgel before and after UV irradiation ……………………………………………………………………………………...59

2.5. Conclusion ……………………………………………………………………………………...61

2.6. Outlook …………………………………………………………………………………….....62

2.7. References ………………………………………………………………………………….....63

Appendix 2 ……………………………………………………………………………………...69

Chapter 3. The Effect of the High Loading of 4-[(4-Methacryloyloxy) phenylazo] benzenesulfonic acid (ABSA) on the Thermo- and Photo-Responsive Properties of P(VCL-bis-ABSA) Microgels and on the Self-Assembly of the Linear P(VCL-ABSA) Copolymer

3.1. Introduction …………………………………………………………………………................75
3.2. Experimental section
3.2.1. Materials …………………………………………………………………………….........77
3.2.2. Microgel and linear polymer syntheses …………………………………………….........77
3.2.3. Characterization ……………………………………………………………………........78
3.3. Results and discussion
3.3.1. Morphology and topography of P(VCL-bis$_{1.5}$-ABSA$_{6.0}$) and P(VCL-bis$_{1.5}$-ABSA$_{10}$) Microgels ……………………………………………………………………………….........80
3.3.2. The origin of clustering ……………………………………………………………........82
3.3.3. Investigation of the thermo- and photo-responsive properties of dimeric assemblies of P(VCL-bis$_{1.5}$-ABSA$_x$) microgels via DLS measurements ……………………………......84
3.3.4. Investigation of the thermo- and photo-responsive properties of single particles of P(VCL-bis$_{1.5}$-ABSA$_x$) microgels via DLS measurements …………………………….......87
3.3.5. Self-assembly of P(VCL-ABSA$_{10}$) chains in THF/water mixture ………………........91
3.3.6. Investigation of the thermo- and photo-responsive properties of nanospheres assembled from linear P(VCL-ABSA$_{10}$) chains ………………………………….............95
3.3.7. Investigation of the fluorescence behavior of P(VCL-bis$_{1.5}$-ABSA$_x$) microgels and nanospheres assembled from linear P(VCL-ABSA$_{10}$) chains …………………………......96
3.3.8. Possibility for higher order aggregation of microgel particles ……………….............97
3.4. Conclusion ……………………………………………………………………………..........97
3.5. Outlook ………………………………………………………………………....................99
3.6. References ……………………………………………………………………………..........99
Appendix 3 ………………………………………………………………………………........106

Chapter 4. Thermo- and Photo-Responsive Properties of *N*-Vinylcaprolactam Microgels containing Azobenzene-based Cross-linkers

4.1. Introduction …………………………………………………………………………...110
4.2. Experimental section
4.2.1. Materials ……………………………………………………………………………...113
4.2.2. Cross-linker syntheses ……………………………………………………………........113
4.2.3. Microgel synthesis …………………………………………………………………......118
4.2.4. Microgel characterization …………………………………………………………........119
4.3. Results and discussion
4.3.1. Morphology of microgel on Si substrate ………………………………………….......120
4.3.2. Thermo-responsive behavior of microgels ………………………………….............121
4.3.3. Photo-responsive behavior of microgels ………………………………….............123

4.4. Conclusion ……………………………………………………………………………….........127
4.5. References …………………………………………………………………………..........128
Appendix 4 ……………………………………………………………………………….............130

Chapter 5. UV-induced Swelling of Microgel Particles containing *β*-Dicarbonyl Groups
5.1. Introduction ……………………………………………………..............................135
5.2. Experimental section
5.2.1. Materials ……………………………………………………………........................136
5.2.2. Polymerization ……………………………………………………………...................137
5.2.3. Characterization ………………………………………………………………..............138
5.3. Results and discussion
5.3.1. Synthesis and particulate nature of non-chemically cross-linked microgels ………………………………………………………………………………........140
5.3.2. Tautomeric nature of AAEM monomer and AAEM unit within microgel Particle ………………………………………………………………………………….........142
5.3.3. Detection of photo-ketonization …………………………………………….............144
5.3.4. Photo-ketonization-induced swelling of microgel ……………………….............146
5.4. Conclusion …………………………………………………………………….............153
5.5. Outlook ………………………………………………...153
5.6. References ……………………………………………………………………..............154
Appendix 5 ………………………………………………………………………..................159

Chapter 6. Summary ……………………………………………………………………..............162

CHAPTER 1. Introduction

Microgel research has gained steady invigoration in recent decades,[1(1)] after a period of lull since the term was first mentioned by Baker *et al.* in 1949.[1(2)] Saunders *et al.* assert that colloidal particles with properties that are characteristic of microgels were prepared as early as 1935 by Staundinger and Husemann.[1(3),1(4)] Microgels are cross-linked polymeric networks that exist as soft spherical particles in the colloidal size regime. They range in size from 10 nm to the lower micrometer range.[1(1)] They can be chemically or physically cross-linked and remain stable and swollen in the solvent they are dispersed in, usually water, due to the thermodynamic compatibility of the polymer chains with the solvent molecules. Their degree of swelling is therefore governed by the polymer-polymer, polymer-solvent and solvent-solvent interactions, which in turn depend on their ionic/nonionic or hydrophilic/ hydrophobic natures, degree of cross-linking, and external conditions.[1(1)]

In solution, the microgel particles usually remain spherical. They also tend to have fuzzy morphologies with dangling polymer chains protruding from their surfaces.[1(5)] This is an indication of their inherent softness resulting in interfacial properties that can be very different from those of classical rigid latex particles. The average cross-linking density of the networks can be varied to influence the softness of the particles, which has implications for the use of such particles at surfaces and interfaces. For instance, they can be deformed and even flattened at the oil/water interface.[1(6)]

Microgel particles have porous internal structures with high surface area to volume ratio. Consequently, they possess the ability to react quickly to changes in their external environment. This dynamic response of microgels to changes in their environment places them in the category of smart materials. Environmental stimuli such as temperature,[1(1a)] pH,[1(7)] ionic strength,[1(8)] solvent composition,[1(9)] and light[1(10)] lead to a drastic change in degree of swelling and correlated properties such as volume and density. Because of their attractive properties, microgels have found applications in bio-sensing, separation techniques, catalysis, and drug delivery, amongst others.[1(1),1(11),1(12)]

1.1. Synthesis of microgels

The most common synthetic route is the polymerization of the monomers and cross-linkers in a dilute homogeneous mixture with a suitable solvent, or in emulsions where the reactive components are suspended in micro-droplets. Microgels can also be formed from the physical self-assembly of polymer chains or from the post-polymerization cross-linking of polymer chains in homogeneous phase or within micro-droplets. The third approach involves the mechanical disruption of macrogels into microgels by grinding or photolithographic techniques.[1(1b-c),1(3),1(11)]

1.2. Thermo-responsive microgels

The bulk of the reported microgels have been based on hydrophilic and thermo-responsive *N*-substituted poly(acrylamides) and poly(methacrylamides).[1(13)] Most commonly reported are microgels of poly(*N*-isopropylacrylamide) or P(NIPAM) for short.[1(14)] Such microgels undergo rapid volume change over a narrow temperature range, at the volume phase transition temperature (VPTT). The VPTTs of the microgels usually coincide with the lower critical solution temperature (LCST) of the corresponding linear polymer chains. In the case of P(NIPAM), the VPTT stands at around 32ºC. Microgels based on homopolymers or copolymers of the other *N*-substituted poly(acrylamides) and poly(methacrylamides) such as poly(*N*-ethyl-*N*-methylacrylamide),[1(15)] poly(*N*-cyclopropylacrylamide)[1(16)] and poly(*N,N'*-diethylacrylamide)[1(17)] have been reported to display VPTTs in the range between 30-56°C.

The amide functionalities in these microgels act as both H-bond donors and acceptors. The alkyl groups on the other hand cause hydrophobic structuring of water, which results in entropically controlled polymer-polymer interactions. Heating above their VPTTs leads to the disruption of hydrogen bonds with water molecules, the expulsion of structured water and the increased dominance of hydrophobic polymer-polymer interactions. These series of events eventually lead to the collapse in volume of the particles.[1(18)]

Another important class of thermo-responsive microgels are those based on cyclic vinylamides. Amongst them, poly(*N*-Vinylcaprolactam) P(VCL) is most relevant, namely for biotechnological applications since it exhibits a VPTT of ~ 32ºC, which is close to physiological conditions. The thermo-sensitive property of P(VCL) was first observed in 1957[1(19)] by Shostakovski *et al.* but it would take several decades before the first hydrogel based on P(VCL) was reported in 1996 by Makhaeva *et al*.[1(20)] Soon after, Gao *et al.* synthesized the first P(VCL)-based microgels in 1999.[1(21)] They reported that the P(VCL)-based microgels display similar swelling/deswelling behavior as P(NIPAM) microgels, with the difference that VCL forms hydrogen bonding interactions with water molecules through a H-bond acceptor in the form of its polar C=O moiety and has no H-bond donor groups. Throughout the last decade, research into P(VCL)-based microgels have grown and continues to do so.[1(22)]

Microgels based on P(VCL) are superior to the ones based on P(NIPAM) mainly because they less cytotoxic.[1(23)] Hence, P(VCL) microgels have gained increased attention since they are more biocompatible for therapeutic purposes, and show better stability against hydrolysis under physiological conditions. Additionally, the VPTT of P(VCL) decreases with increasing polymer chain length and concentration, leading to microgel systems with simpler control over the coil-to-globule transition *via* modification of molecular weight. Furthermore, it is known for its high complexing ability and good film-forming properties, which are advantageous for many applications.[1(23)]

1.3. Photo-responsive polymer systems

Light as a stimulus has several advantages. It can be applied with high degrees of spatial and temporal control. Since the application of light is usually remotely done without direct contact, it is non-invasive and does not contaminate the system or lead to unwanted side reactions. The extent or rate of photo-reaction from light stimulation can additionally be tuned by varying the intensity, wavelength, and polarization direction of the light.[1(24)] As a result, the response of the system can be kinetically controlled or made to occur in stepwise fashion.

Irie and co-workers pioneered research into photo-responsive polymer systems since the late 1970s.[1(25)] The prevailing strategy for producing photo-responsive or photo-triggerable polymeric systems involve dispersing photo-sensitive molecules within polymers either via chemical linkage or physical interactions.[1(24)] The inclusion of the photo-sensitive group as a monomeric unit or included in a post-polymerization step are commonly employed strategies. An important factor to consider for effective photo-transformation of polymeric systems with molecularly embedded photo-sensitive groups is the number or concentration and nature of the groups.[1(26)] Furthermore, the photo-sensitive group should have a high molar extinction coefficient to be able to absorb light effectively and undergo photochemical reactions with high efficiency so that the irradiance of light necessary to trigger the reaction is at a reasonable level. When a biotechnological application is the goal, the photo-sensitive group employed should ideally absorb at a wavelength that is compatible with the physiological system. Sterenborg *et al*. recommends a wavelength no shorter than ~340 nm and ideally, much longer, into the near infrared region.[1(27)]

The commonly employed photo-sensitive compounds can be broadly divided into two categories; those that are photo-switchable and others that are photo-labile. Photo-switchable groups are those that exhibit photochromism. A chemical species exhibit photochromism when it can undergo a reversible transformation between two states, induced in one or both directions by electromagnetic radiation of different wavelengths.[1(28)] Common photochromic groups are azobenzene, spiropyran, diarylethene, fulgide, salicylideneaniline, and coumarin.[1(29)] Less commonly employed are malachite green leuconitriles and β-diketone derivatives.[1(30)] Their structures are shown in Scheme 1(1). Photo-labile groups differ from photo-switchable ones in one main criterion, the reversibility between states. Photo-labile groups cannot return to their original states due to photo-induced cleavage of bond(s) that occur upon activation. Pyrenylalkyl and *o*-nitrobenzyl esters are some of the common functional groups that belong to this category and they are depicted in Scheme 1(2).[1(24a),1(31)] Photo-switching from one form to the other, and the photo-cleavage of photo-labile groups result in modifications of the geometry and/or structure of the systems and their electron distributions. These are often accompanied by spectral changes in absorption and/or emission, which can be manifested as a color change or changes in physical or chemical properties. Examples of such properties are conductivity, refractive index, dipole moment, dielectric constant, chelate formation, ion dissociation, phase transitions, solubility, and viscosity.[1(29a)] The changes in these properties have been exploited to exert control over assembly properties of amphiphilic block copolymers and hybrid particles, for instance.[1(31),1(32)] A third class of photo-responsive compounds is one that relies on the photo-thermal effect of metal nanoparticles such as gold. These nanoparticles often absorb light in the near infrared region causing their electrons to be excited by the surface plasmon resonance phenomenon. The excited electrons lose energy quickly and the energy loss upon relaxation is released as a phonon that heats up the external environment of the nanoparticles.[1(33)]

When a photo-responsive group is incorporated into a hydrophilic polymer network, dual thermo- and photo-responsive polymers can be produced. The group of Irie *et al*. adopted this strategy in creating the first dual thermo- and photo-responsive hydrophilic copolymer in 1988.[1(29b)] They produced P(NIPAM) copolymers that contained azobenzene moieties as side chain groups. They reported the increase in the LCST of the P(NIPAM-Azo) copolymer upon switching of the azo groups from the less polar *trans* form to the more polar *cis* form.[1(29b)] Since then, other examples of thermo- and photo-responsive polymers and block copolymers based on have been published.[1(34)] A dual thermo- and photo- responsive copolymer can additionally be made pH-responsive when one of the co-monomers possesses an acidic functionality.[1(35)]

More recently, Jochum *et al*. worked intensively on producing thermo- and photo-responsive copolymers.[1(36)] They synthesized polyacrylamides containing different amounts of azobenzene moieties via a polymer analogous reaction between the reactive precursor polymer poly(pentafluorophenylacrylate) with *N*-(2- aminoethyl)-4-(2-phenyldiazenyl)benzamide and either isopropylamine, cyclopropylamine, diethylamine or ethylmethylamine.[1(37)] In another study, they reported telechelic thermo- and photo-responsive polymers based on poly(oligo(ethylene glycol) methyl ether methacrylate) P(OEGMA) that were functionalized with azobenzene end groups. They achieved this through a series of reactions involving a reversible addition fragmentation chain transfer (RAFT) polymerization using a functionalized chain transfer agent (CTA), and the post-modification of the telechelic reactive end groups through a polymer analogous reaction with amino-functionalized azobenzene.[1(38)] In both these instances, the polymers displayed reversible light- and temperature-controlled phase transitions in water. Higher values for the lower critical solution temperature (LCST) were also recorded after UV irradiation of the aqueous polymer solutions as a result of the increased polarity of *cis*-azobenzene. The reported LCST increases depended upon the ratio of azobenzene units and reached up to 7°C. In a third system containing azobenzene photochromes, Jochum *et al*. produced block copolymers of ethyleneoxide and NIPAM that were functionalized with azobenzene pendant groups. They could control the reversible formation of micellar structures from these block copolymers as well as cause light-induced disruption and re-formation of the micelles in water.[1(39)] Jochum and co-workers also synthesized other thermo- and photo-responsive polymers containing salicylideneaniline and fulgimide moieties.[1(40)]

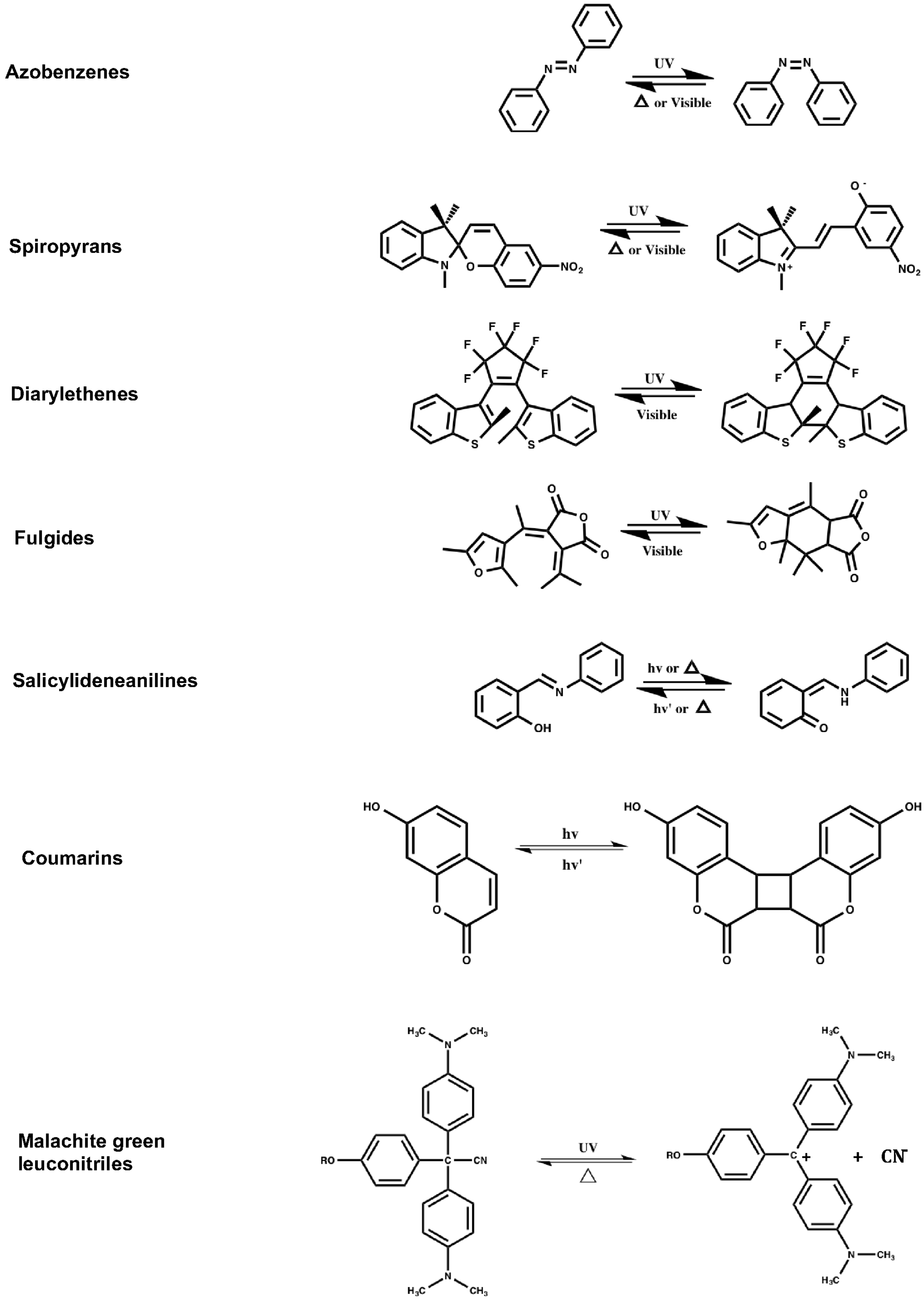

Scheme 1(1). Photo-reactions of common photochromic compounds. Adapted from Ercole *et al*. and Trenor *et al*.[1(29a,d)]

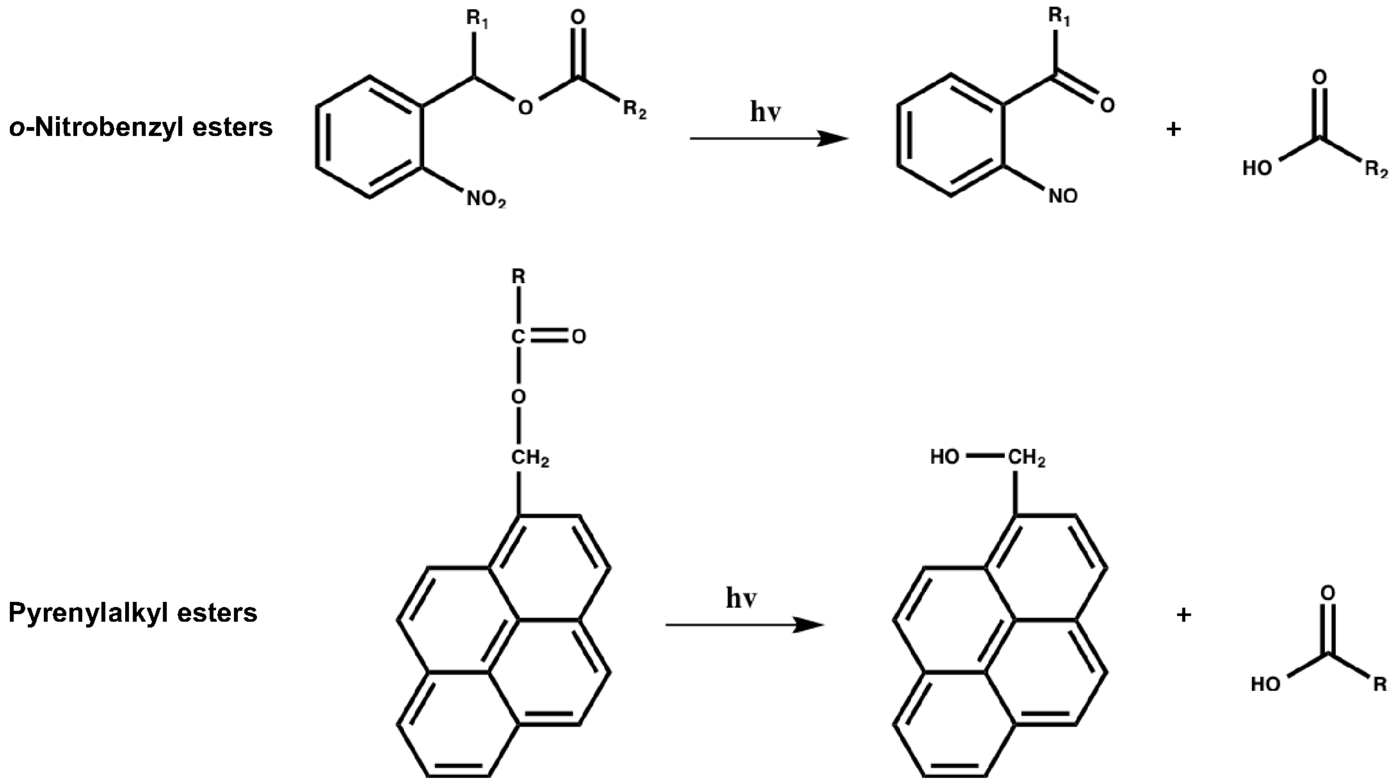

Scheme 1(2). Photo-reactions of common photo-activated molecules. Adapted from Klinger and Zhao.[1(24a),1(31)]

Interests in using photo-switchable and photo-labile systems to modify biopolymers to produce smart biomaterials and surfaces for biotechnological applications have also grown.[1(29a)] In the field of biotechnology, biomolecules such as enzymes and channel proteins have been conjugated most commonly to photo-labile groups to introduce photo-triggers for their biological activity. A suitable functional group in a key location of the biomolecule should be conjugated to a photo-labile protecting group. This approach is known as *caging*. This renders the biomolecule inactive until the caging group is cleaved by light.[1(41)] Conjugation to a photo-switch, on the other hand, enables a reversible photochemistry, thereby enabling many cycles of alternate production of active/inactive states.[1(34e),1(42)]

1.4. Photo-responsive microgels

On the back of photo-responsive polymers, various groups have gone down to the nanoscale to introduce the photo-responsive property into colloidal particles. This has been a topic of perennial interest in recent years since nanoparticles are attractive vehicles or carriers for cargo and can unload them upon rapid response to environmental stimuli.[1(43)] Moreover, nanoparticles can be (self) assembled into higher order architectures, increasing their application potential.[1(44)]

While photo-responsive micelles and polymersomes assembled from amphiphilic (block) copolymers are fairly common,[1(45)] work into the design and synthesis of photo-responsive microgels in aqueous systems is still a relatively nascent field. Several reports of photo-responsive microgels have been based on the use of photochromic azobenzenes, spiropyrans, and coumarins. Microgels with photo-labile *o*-nitrobenzyl derivatives have also been reported, as well as microgels containing gold nanoparticles that exhibit photo-thermal effects.

One of the earliest reported photo-responsive microgels was prepared by Hirakura *et al.* in 2004.[1(46)] The microgels were prepared via the intermolecular self-assembly of the polysaccharide pullulan chains that bear spiropyran groups. The association of spiropyran groups acts as cross-linking points between chains. The microgels swell or deswell according to the proportion of merocyanine (Mer) to spiropyran (Sp) form, with the higher content of the ionic ring-opened merocyanine form causing increased swelling. These physically cross-linked microgels do not disassemble probably because at the photostationary state, both the Mer and Sp forms coexist and can complex with each other.

Garcia *et al.* also developed microgels bearing spiropyran groups. They synthesized P(NIPAM-*co*-allylamine) microgels coupled to a spiropyran via an amide bond. They report the photo-, thermal- and pH-responsive properties of the aqueous microgel dispersion. Hence the swelling behavior of the microgel can be modulated using these three orthogonal types of external stimuli.[1(47)]

Coumarin functional groups have in general been introduced as hydrophobic pendant groups in amphiphilic polymer chains which then assemble into photo-responsive polymer micelles.[1(48)] Adjacent coumarin groups undergo quick and reversible photo-dimerizations via alternate irradiations with UV lights of different wavelengths, resulting in reversible changes in the morphology of the micelles. He *et al.* reported the formation of nanogels from the photo-dimerization reaction of coumarin side groups in a block copolymer that was first assembled into micelles.[1(49)] The photo-crosslinking was partially reversible resulting in swelling of nanogel particles with a volume increase of about 90%. Huang *et al.* employed cross-linkers based on 7-amino coumarin moieties to investigate the influence of the cross-linker's structure on the photo-degradation and photo-swelling behavior of the constructed polystyrene microgels.[1(50)] Upon irradiation, the dimerized coumarin moieties in the cross-linkers were cleaved, leading to the photo-degradation of the cross-linking points and the subsequent change in cross-linking density of the network, which then allowed the photo-regulated swelling of the microgels. In this case, the photo-cleavage of the coumarin dimers were not reported to be reversible. In the third reported case of microgels containing coumarin moieties, Wang *et al*. synthesized amphiphilic copolymers bearing coumarin-based co-monomers.[1(51)] The polymers were found to assemble into microgels due to inter-/intra-molecular hydrophobic interactions, especially of the hydrophobic coumarin units. The coumarin units could be dimerized and de-dimerized via cyclic irradiation with UV lights of wavelengths 365 nm and 254 nm respectively and they were able to show the photo-triggered release of the hydrophobic dye Nile Red upon de-dimerization of the coumarin units.

Microgels functionalized with photo-labile *o*-nitrobenzyl derivatives have been reported.[1(52)] For instance, Klinger *et al.* used divinyl functionalized cross-linkers based on *o*-nitrobenzyl derivatives to produce poly(methyl methacrylate) (PMMA) microgels.[1(52d)] They were able to induce the swelling and/or degradation of the microgel by tuning the wavelength, and doses and intensities of the UV source.

Microgel systems, which are photo-responsive based on a photo-thermal mechanism have also gained substantial attention. Such systems are often hybrid systems based on the inclusion of metal nanoparticles, especially that of gold. The photo-thermal effect produced by gold nanoparticles upon absorption of infrared light has been exploited to induce the phase transition in hybrid, thermo-responsive P(NIPAM)- or PEG-based microgels.[1(53)]

The most widely used photochrome, azobenzenes, have also been investigated as the photo-responsive moiety in microgels. Via the *trans-cis* isomerization of the azobenzene, the swelling degrees of the microgels can be reversibly modulated. For instance, Zhang *et al.* synthesized separate linear chains bearing azobenzene and *β*-cyclodextrin (*β*-CD) groups respectively. Via the supramolecular interaction of azobenzene with *β*-CD, the chains assembled into physically cross-linked networks, which were then subsequently cross-linked covalently via other functional groups to form microgel networks. They report the reversible dissociation and association of the β-CD/azobenzene by alternate UV and visible light irradiations, resulting in the reversible size control of the microgel particles.[1(54)] More recently, Zhu and co-workers synthesized poly(*N*-isopropylacrylamide-*co*-acrylic acid) microgels and subsequently grafted on azobenzene moieties as pendant groups via a condensation reaction.[1(55)] They reported the slight increase in VPTT of the microgel when the *trans* azobenzene moieties were converted to the *cis* form. When an α-cyclodextrin (α–CD) solution was added to a solution of the microgel, host–guest interactions between *trans*-azobenzene pendant groups and α–CD formed. The resultant supramolecular microgel complex exhibited a higher VPTT than the uncomplexed microgel. The microgel complex was shown to display a photo-controllable shift in its VPTT with trans/cis isomerization of the azobenzene moieties which caused the disruption or re-formation of the host-guest interactions.

The groups of Vincent and Santer separately designed microgel particles, whose sizes could be manipulated, not by the incorporation of a photo-sensitive group within the polymer network, but as a result of the physical interactions between the microgels and photo-responsive molecules added into the colloidal dispersion. Vincent and co-workers relied on the use of hydrophobically-modified and positively-charged azobenzene-based organic salts that could be absorbed by P(NIPAM-co-acrylic acid) particles. UV-induced transformation of the salt to more polar *cis* form reduced the hydrophobic attraction between the salt and the microgel particles, leading to some desorption of the salt from the microgel. The reversible absorption and desorption of the positively-charged salts affect the net charge on the negatively charged microgels and as a result, the diameter of the particles varied accordingly.[1(56)]

Santer and co-workers, on the other hand, utilized an azobenzene-containing surfactant to achieve reversible photo-control of the swelling behavior of P(NIPAM-*co*-allyl acetic acid) microgel particles via the binding/unbinding of the surfactant. They report the collapse of the microgel upon addition of the surfactant above a critical concentration. UV-induced transformation to the *cis* form of the surfactant cause its unbinding from the hydrophobic microgel and in turn led to its swelling. The re-binding of the surfactant proceeds via blue light irradiation, which re-isomerizes the surfactant to its more hydrophobic *trans* conformation, thereby increasing its affinity to bind to the microgel.[1(57)]

The group of Serpe used an azobenzene crosslinker, 4,4′-di(acrylamido)-azobenzene to synthesize P(NIPAM) microgels. With these microgels, they have a system where they could control particle volume via temperature or light. The particles shrink reversible with temperature while they swell reversibly with alternate application of UV and visible lights.[1(58)] Richtering and co-workers focused on the physical chemistry of azobenzene isomerization within polymeric colloidal particles.

They characterized the isomerization dynamics of azobenzenes functionalized as side chains and as cross-linkers in colloids with a poly(butyl methacrylate) (PBMA) backbone via femtosecond fluorescence up-conversion spectroscopy. They compared these isomerization data with those of the free azobenzene comonomer and cross-linker in solution. Their investigations revealed significantly longer excited-state lifetimes of the cis form in the polymer, which led them to deduce that the lifetimes could be controlled by varying the tightness of the surrounding matrix.[1(59)]

1.5 Purpose of study

1.5.1. Motivation

Microgels have been extensively investigated and are especially suited for quick, multi-responses to external stimuli. Light as a stimulus is of growing interest since it can be easily controlled, accurately focused on specific areas for the required time, and switched to the required wavelengths and intensities. Additionally it is a generally non-invasive and non-contaminating stimulus for biological systems, and should lead to rapid response in microgels.

While research into photo-responsive polymeric systems has been ongoing since the pioneering work of Irie *et al.*,[1(1)] the work into synthesis and characterization of similarly photo-responsive colloids such as microgels and especially of intelligent functional materials therefrom is relatively scant and still in its nascent stages. When endowed together with responsiveness to other triggers such as temperature, colloidal particles that are versatile and multi-responsive can be obtained. The possibility for targeted tuning of the properties of materials is appealing from the point of view of creating new multi-responsive, intelligent materials. Such a research trajectory should be undertaken with a view toward expanding the classes of functional microgels and developing a greater scope for their applications in actuators, membrane technology, micro-optomechanical systems, microfluidic systems, microsensor arrays, biomedical devices and photo-pharmacology.[1(2)]

The exact effect of incorporation of photo-sensitive units in microgels on their phase transition behavior has not been completely unraveled, which may be different from that in macroscopic polymeric systems. This ties in with addressing some of the ongoing themes and challenges associated with research into microgels including the precise elucidation of the internal particle structure for the better understanding of its correlation with the particle properties. The control of particle size, size distribution, and homogeneity of cross-linking density remain critical considerations, especially when working with novel combinations of monomers. The selective incorporation of functional groups and the controlled distribution of these groups in the microgel matrix, while achieving particles with good colloidal stability, are additional important considerations. Strategies and protocols for the assembly of mono-dispersed microgel particles into higher order architectures should also be further explored. The fabrication of novel microgel particles or even microgel hybrids with anisotropic shapes and morphology could prove challenging but could also offer enhanced surface properties and great engineering potential in advanced supracolloidal material design.[1(3)]

1.5.2. Aim

The aim of this work is the synthesis of photo-responsive microgels with controlled chemical structures and characterization of their responses to different stimuli like light and temperature in aqueous solutions. The incorporation of an azobenzene comonomer or an azobenzene cross-linker into poly(*N*-vinylcaprolactam) (PVCL) networks yields systems sensitive to both temperature and light. Meanwhile, microgels of poly(acetoacetoxyethyl methacrylate) (PAAEM) are responsive to UV irradiation and the influence of different hydrophilic co-monomers on the extent of UV-induced swelling is investigated.

One of the main challenges in this endeavor is in the synthesis of microgels where we can achieve control over the amount of photo-sensitive groups incorporated and their distribution within the microgel matrix. The other significant challenge is the characterization of the microgel behavior in aqueous solution.

We therefore sought to produce relatively small, monodispersed microgels with diameters lower than 500 nm that possess good colloidal stability, and to understand the mechanism of the photo-triggered swelling-deswelling by probing the internal structure and discerning the interactions between photo-responsive groups, polymer segments and water molecules. Furthermore, the surface topology of the microgels, their deformation into anisotropic structures as well as the potential for their self-assembly and aggregation are pertinent concerns.

Elucidation of the structure-property relationship would facilitate future work toward gaining more precise control over the swelling-deswelling behavior and properties and to develop targeted strategies for assembly and/or disassembly on desired surfaces and interfaces using external stimuli.

1.5.3. Outline of dissertation

The main characterization techniques employed in this dissertation are the established colloidal science techniques of dynamic light scattering (DLS), UV/vis spectroscopy, atomic force microscopy (AFM), cryogenic transmission electron microscopy (cryo-TEM), cryogenic field emission scanning electron microscopy (cryo-FESEM) and proton nuclear magnetic resonance spectroscopy (^{1}H NMR). The operating principles of these techniques will not be discussed in detail for the sake of brevity. Readers are advised to refer to comprehensive texts available elsewhere.

All measurements, results, their analyses and description as well as theoretical discussion that I use in this dissertation were done and written by me or by students under my supervision. I list an abstract of each chapter below that emphasizes the novelties in each study presented. Within the conclusion of each chapter, I summarize the main findings of the work, and offer suggestions and recommendations for possible future lines of study. Below is an outline of the studies presented in the subsequent chapters.

Chapter 2: *N*-Vinylcaprolactam (VCL) and 4-[(4-methacryloyloxy)phenylazo] benzenesulfonic acid (ABSA) were copolymerized and chemically cross-linked with *N,N'*-methylenebisacrylamide (bis) to prepare reversible thermo- and photo-responsive P(VCL-bis-ABSA) microgels via surfactant-free precipitation polymerization in water. ABSA is incorporated as pendant groups in amounts of less than 10 wt.% relative to the VCL co-monomer.

In situ irradiation within the dynamic light scattering (DLS) instrument was used to investigate the volume phase transition information of the microgels under both orthogonal and combined application of temperature and light stimuli. This was then modeled by the Flory-Rehner theory and is shown to describe and aid the preliminary understanding of the main features in the volume phase transition of these photo-responsive microgels. Interestingly, the microgels rapidly deswell upon UV irradiation when the thermodynamically stable *trans*-ABSA pendant groups are converted to the more polar *cis* form at temperatures below their VPTT. This UV-induced deswelling phenomenon is believed to originate primarily from the disruption of hydrogen bonding interaction between water molecules and the carbonyl group of VCL caused by the approach of the sulfonic acid groups of *cis*-ABSA toward the polymer chain backbone. This approach of the polar *cis*-ABSA also facilitates increased hydrophobic interactions in the network. The mechanism of volume collapse caused by UV stimulus in these microgels is therefore analogous to that caused by a temperature stimulus.

N.B. A large part of this chapter has been accepted as a paper in *Langmuir*: Phua, D. I.; Herman, K.; Balaceanu, A.; Zakrevski, J.; Pich, A. Reversible Size Modulation of Aqueous Microgels via Orthogonal or Combined Application of Thermo- and Photo-Triggers. *Langmuir* Just Accepted Manuscript **2016**, **DOI**: 10.1021/acs.langmuir.6b00241

Chapter 3: P(VCL-bis-ABSA) microgels were synthesized via the same procedure as that employed in Chapter 2. In this chapter, a high amount of ABSA was incorporated (between 22 wt% and 28 wt. %). In this high regime of ABSA incorporation, we find that supramolecular forces between ABSA and VCL units and between ABSA units themselves become significant. The abundance of ABSA pendant groups bearing sulfonic acid terminal ends leads to extensive complexation of the sulfonic acid groups of ABSA to the C=O groups of the VCL units (strong charged-assisted hydrogen bonding) and to the formation of H-aggregates (π-π stacking interactions) of the azobenzene moieties. The presence of these non-covalent interactions affects the particle architecture and morphology in solution. Observations of the microgels under cryo-TEM and AFM indicate that the microgels in their native solutions exist as pairs of particles in dimeric assemblies with dangling chains on their peripheries. The supramolecular interactions exist both as intra- and inter-particle forces, forming both intra- and inter-particle physical cross-links. As a result, the phase transition behavior of the microgels is affected in a non-monotonous manner, depending on the amount of incorporated ABSA pendant groups. The dimeric assemblies could not be disrupted by temperature or light stimuli but was disrupted by the addition of a small volume of dilute KCl solution as a chaotropic agent followed by a short period of mechanical agitation by ultra-sonication.

Linear P(VCL-ABSA) chains were synthesized using the same microgel polymerization procedure without the addition of BIS cross-linker in order to exploit the supramolecular forces to explore the possibility for self-assembly. The linear polymer chains were found to self-assemble into a mixture of dense nanospheres and vesicle-like nanospheres in 75% w/w solution of water in THF as detected by DLS and cryo-TEM. Disruption of these nanospheres by UV irradiation and their subsequent re-assembly by re-stirring in the dark were also detected by DLS. Finally, confocal microscopic investigation revealed the fluorescent nature of both the microgel particles and the self-assembled nanospheres and this can be attributed to the confinement of a large amount of ABSA pendant groups, resulting in a suppression of the *trans*-*cis* isomerization.

Chapter 4: This chapter looks into the incorporation of azobenzene cross-linkers into P(VCL) microgel networks and investigates the coupling of the change in the end-to-end distance upon *trans*-to-*cis* isomerization of the cross-linker on the deswelling of the microgel network. No additional chemical cross-linker, such as *N*,*N*'-methylenebisacrylamide (BIS) was used to obtain stable microgel particles. By incorporating azobenzene cross-linkers into P(VCL) microgel, the effect of cooperative and simultaneous contraction of the *trans*-azobenzene to *cis*-

azobenzene cross-linkers could lead to a significant deswelling of the microgel matrix. The use of different azobenzene cross-linkers that differed in the length of alkyl spacers on the *para* carbon atoms was also investigated. The length of spacer could possibly influence the size of microgels and interactions of azobenzenes with each other and with the VCL units. Lengthening of the spacers should enhance the flexibility of the resultant microgel matrix, thereby facilitating and increasing the rate of the *trans*-*cis* isomerization. Furthermore, the flexibility of the spacers should also tend to increase the cross-linker's mobility even under ambient conditions, which should facilitate the propensity for *cis* azobenzene moieties to associate with each other. All things considered, by increasing the spacer lengths, the *cis* moieties could possibly approach each other in space within the microgel matrix to result in increased hydrophobic interactions. Increased hydrophobic interaction should then enhance the deswelling of the microgels upon UV-induced *trans*-to-*cis* isomerization of the cross-linkers.

Chapter 5: 2-Acetoacetoxyethyl methacrylate (AAEM) is a monomeric *β*-dicarbonyl compound (*β*-DCC) which exhibits both enol and diketo structures that interconvert through a tautomeric equilibrium. The enol form can be converted to the diketo form with UV irradiation of 254 nm. We investigated the photo-responsive behavior of P(AAEM) microgels in this chapter.

A series of monodispersed, spherical P(AAEM) microgels were synthesized via surfactant-free precipitation polymerization in water. UV/vis spectroscopy and attenuated total reflectance studies reveal that on a molecular level, all of the P(AAEM) microgels undergo a rapid photo-ketonization process upon UV irradiation (λ = 254 nm). In this photo-ketonization process, the chelated enol tautomer in P(AAEM) is converted to the diketo form which preferentially forms hydrogen bonding interactions with water molecules, thereby leading to the increase in hydrodynamic radii of the particles. The swelling was detected by DLS. The addition of hydrophilic co-monomers during polymerization alters the topology and consequently the hydrophilicity of the internal microenvironment and porosity of the microgel network. This affects the speed and degree of swelling of the microgels upon UV irradiation because the tautomeric equilibrium is influenced by the hydrophilicity of the network. By introducing greater hydrophilicity in the network, we obtain particles with less restricted topology and achieve faster and more homogeneous swelling. Increased hydrophilicity of the network, however, mitigates the extent of photo-induced swelling and increases the possibility of aggregation.

Chapter 6 provides a summary of the overall work.

1.6. REFERENCES

1(1) (a) Pelton, R. Temperature-Sensitive Aqueous Microgels. *Adv. Colloid Interf. Sci.* **2000,** *85*, 1-33, (b) Pich, A.; Richtering, W. Eds., *Chemical Design of Responsive Microgels*; Springer: Berlin, 2010. (c) Fernandez-Nieves, A.; Wyss, H.; Mattsson, J.; Weitz, D. A., *Microgel Suspensions: Fundamentals and Applications*; Wiley: Weinheim, 2011. (d) Pelton, R.; Hoare, T., Microgels and Their Synthesis: An Introduction. In *Microgel Suspensions*; Wiley-VCH Verlag GmbH & Co. KGaA: Weinheim, 2011; pp 1-32

1(2) Baker, W. O. Microgel, A New Macromolecule. *Ind. Engin. Chem.* **1949,** *41*, 511-520.

1(3) (a) Saunders, B. R.; Vincent, B. Microgel particles as Model Colloids: Theory, Properties and Applications. *Adv. Colloid Interf. Sci.* **1999,** *80*, 1-25, (b) Saunders, B. R.; Laajam, N.; Daly, E.; Teow, S.; Hu, X.; Stepto, R. Microgels: From Responsive Polymer Colloids to Biomaterials. *Adv. Colloid Interf. Sci.* **2009,** *147–148*, 251-262.

1(4) Staudinger, H.; Husemann, E., Über hochpolymere Verbindungen, 116. Mitteil.: Über das begrenzt quellbare Polystyrol. *Berichte der deutschen chemischen Gesellschaft (A and B Series)* **1935,** *68*, 1618-1634.

1(5) Berndt, I.; Pedersen, J. S.; Lindner, P.; Richtering, W. Structure of Doubly Temperature Sensitive Core-Shell Microgels Based on Poly-*N*-Isopropylacrylamide and Poly-*N*-Isopropylmethacrylamide. *Progr. Colloid Polym. Sci.* **2006**, *133*, 35-40.

1(6) (a) Schmidt, S.; Liu, T.; Rütten, S.; Phan, K. H.; Möller, M.; Richtering, W. Influence of Microgel Architecture and Oil Polarity on Stabilization of Emulsions by Stimuli-Sensitive Core-Shell Poly(*N*-isopropylacrylamide-*co*-methacrylic acid) Microgels: Mickering versus Pickering Behavior? *Langmuir* **2011**, *27*, 9801-9806. (b) Wu, Y.; Wiese, S.; Balaceanu, A.; Richtering, W.; Pich, A. Behavior of Temperature-Responsive Copolymer Microgels at the Oil/Water Interface. *Langmuir* **2014**, *30*, 7660-7669. (c) Schneider, F.; Balaceanu, A.; Feoktystov, A.; Pipich,V.; Wu, Y.; Allgaier, J.; Pyckhout-Hintzen, W.; Pich, A.; Schneider, G. J. Monitoring the Internal Structure of Poly(*N*-vinylcaprolactam) Microgels with Variable Cross-Link Concentration. *Langmuir* **2014**, *30*, 15317−15326.

1(7) (a) Tan, B. H.; Tam, K. C., Review on the Dynamics and Micro-Structure of pH-Responsive Nano-Colloidal Systems. *Adv. Colloid Interf. Sci.* **2008,** *136*, 25-44. (b) Schroeder, R.; Rudov, A. A.; Lyon, L. A.; Richtering, W.; Pich, A.; Potemkin, I. I. Electrostatic Interactions and Osmotic Pressure of Counterions Control the pH-

Dependent Swelling and Collapse of Polyampholyte Microgels with Random Distribution of Ionizable Groups. *Macromolecules* **2015**, *48*, 5914-5927.

1(8) Shibayama, M.; Ikkai, F.; Inamoto, S.; Nomura, S.; Han, C. C. pH and Salt Concentration Dependence of the Microstructure of Poly(*N*-isopropylacrylamide-*co*-acrylic acid) Gels. *J. Chem. Phys.* **1996,** *105*, 4358-4366.

1(9) Hofmann, C. H.; Plamper, F. A.; Scherzinger, C.; Hietala, S.; Richtering, W. Cononsolvency Revisited: Solvent Entrapment by *N*-Isopropylacrylamide and *N*,*N*-Diethylacrylamide Microgels in Different Water/Methanol Mixtures. *Macromolecules* **2012,** *46*, 523-532.

1(10) Nayak, S.; Lyon, L. A. Photoinduced Phase Transitions in Poly(*N*-isopropylacrylamide) Microgels. *Chem. Mater.* **2004,** *16*, 2623-2627.

1(11) (a) Loxley, A.; Vincent, B. Equilibrium and Kinetic Aspects of the pH-Dependent Swelling of Poly(2-vinylpyridine-*co*-styrene) Microgels. *Colloid Polym. Sci.***1997**, *275*, 1108. (b) Baran, T.; Arica, M. Y.; Denizli, A.; Hasirci, V. Comparison of ß-galactosidase Immobilization by Entrapment In and Adsorption on Poly(2-hydroxyethylmethacrylate) Membranes. *Polym. Int.***1997**, *44*, 530-536. (c) Robinson, D. N.; Peppas, N. A. Preparation and Characterization of pH-Responsive Poly(methacrylic acid-g-ethylene glycol) Nanospheres. *Macromolecules* **2002**, *35*, 3668-3674. (d) Alarcon, C. D. H.; Pennadam, S.; Alexander, C. Stimuli Responsive Polymers for Biomedical Applications. *Chem. Soc. Rev.* **2005**, *34*, 276-285. (e) Freitag, R.; Panayitou, M.; Pohner, C.; Vandevyver, C.; Wandrey, C.; Hilbrig, F. Synthesis and Characterization of Thermo-Responsive Poly(*N*,*N*'-Ethylacrylamide) Microgels. *React. Funct. Polym.* **2007**, *67*, 807. (f) Saunders, B. R.; Laajam, N.; Daly, E.; Teow, S.; Hu, X. H.; Stepto, R. Microgels: From Responsive Polymer Colloids to Biomaterials. *Adv. Colloid Interf. Sci.* **2009**, *147-148*, 251-262. (g) Klinger, D.; Landfester, K. Stimuli-Responsive Microgels for the Loading and Release of Functional Compounds: Fundamental Concepts and Applications. *Polymer* **2012**, *53*, 5209-5231.

1(12) (a) Froimowicz, P.; Klinger, D.; Landfester, K. Photoreactive Nanoparticles as Nanometric Building Blocks for the Generation of Self-Healing Hydrogel Thin Films. *Chem. Eur. J.* **2011**, *17*, 12465. (b) Tsai, H.-Y.; Vats, K.; Yates, M. Z.; Benoit, D. S. W. Two-Dimensional Patterns of Poly(*N*-Isopropylacrylamide) Microgels to Spatially Control Fibroblast Adhesion and Temperature-Responsive Detachment. *Langmuir* **2013**, *29*, 12183–12193.

1(13) Dimitrov, I.; Trzebicka B.; Müller, A. H. E.; Dworak, A.; Tsvetanov, C. B. Thermosensitive Water-Soluble Copolymers with Doubly Responsive Reversibly

Interacting Entities. *Prog. Polym. Sci.* **2007**, *32*, 1275-1343 and references therein.

1(14) Pelton, R. H.; Chibante, P. Preparation of Aqueous Latices with *N*-Isopropylacrylamide. *Colloids and Surfaces* **1986,** *20*, 247-256.

1(15) Plate, N. A.; Lebedeva, T. L.; Valuev, L. I. Lower Critical Solution Temperature in Aqueous Solutions of *N*-Alkyl-Substituted Polyacrylamides. *Polym. J.* **1999**, *31*, 21-27.

1(16) Maeda, Y.; Nakamura, T.; Ikeda, I. Changes in the Hydration States of Poly(*N*-alkylacrylamide)s during Their Phase Transitions in Water Observed by FTIR Spectroscopy. *Macromolecules* **2001**, *34*, 1391-1399.

1(17) Idziak, I.; Avoce, D.; Lessard, D.; Gravel, D.; Zhu, X. X. Thermosensitivity of Aqueous Solutions of Poly(*N*,*N*-diethylacrylamide). *Macromolecules* **1999**, *32*, 1260-1263.

1(18) Keerl, M.; Smirnovas, V.; Winter, R.; Richtering, W. Copolymer Microgels from Mono- and Disubstituted Acrylamides: Phase Behavior and Hydrogen Bonds. *Macromolecules* **2008**, *41*, 6830-6836.

1(19) Shostakovski, M. F.; Sydelkovskaya, F. P. *Vesnik Akad. Nauk SSSR* **1957**, *7*, 127.

1(20) Makhaeva, E. E.; Thang, L. T. M.; Starodubzev, S. G.; Khohlov, A. R. Thermoshrinking Behavior of Poly(Vinylcaprolactam) Gels in Aqueous Solution. *Macromol. Chem. Phys.* **1996**, *197*, 1973.

1(21) Gao, Y.; Au-Yeng, S. C. F.; Wu, C. Interaction between Surfactant and Poly(*N*-Vinylcaprolactam) Microgels. *Macromolecules* **1999**, *32*, 3674–3677.

1(22) (a) Boyko, V.; Pich, A.; Lu, Y.; Richter, S.; Arndt, K.-F.; Adler, H.-J. P. Thermo-Sensitive Poly(*N*-vinylcaprolactam-*co*-acetoacetoxyethyl methacrylate) Microgels: 1-Synthesis and Characterization. *Polymer* **2003**, *44*, 7821-7827. (b) Boyko, V. *N*-Vinylcaprolactam based Bulk and Microgels: Synthesis, Structural Formation and Characterization by Dynamic Light Scattering. Ph.D. Dissertation, University of Technology, Dresden, Germany, 2004 and references therein. (c) Balaceanu, A.; Demco, D. E.; Möller, M.; Pich, A. Microgel Heterogeneous Morphology Reflected in Temperature-Induced Volume Transition and 1H High-Resolution Transverse Relaxation NMR. The Case of Poly(*N*-vinylcaprolactam) Microgel. *Macromolecules* **2011**, *44*, 2161–2169. (d) Wang, Y.; Nie, J.; Chang, B.; Sun, Y.; Yang, W. Poly(vinylcaprolactam)-Based Biodegradable Multiresponsive Microgels for Drug Delivery. *Biomacromolecules* **2013,** *14*, 3034-3046.

1(23) Ramos, J.; Imaz, A.; Forcada, J. Temperature-sensitive Nanogels: Poly(*N*-Vinylcaprolactam) versus Poly(*N*-Isopropylacrylamide). *Polym. Chem.* **2012**, *3*, 852-856 and references therein.

1(24) (a) Klinger, D. Light-Sensitive Polymeric Nanoparticles based on Photo-cleavable Chromophores. Ph.D Dissertation, Johannes Gutenberg-Universität, Mainz, Germany, 2011, and references therein. (b) Irie, M. Diarylethenes for Memories and Switches. *Chem. Rev.* **2000**, *100*, 1685-1716. (c) Yokoyama, Y. Fulgides for Memories and Switches. *Chem. Rev.* **2000**, *100*, 1717-1740. (d) Berkovic, G.; Krongauz, V.; Weiss, V. Spiropyrans and Spirooxazines for Memories and Switches. *Chem. Rev.* **2000**, *100*, 1741-1754.

1(25) (a) Smets, G.; Breaken, J.; Irie, M. Photomechanical Effects in Photochromic Systems. *Pure Appl. Chem.* **1978**, *50*, 845-856. (b) Irie, M.; Menju, A.; Hayashi, K. Photoresponsive Polymers. Reversible Solution Viscosity Change of Poly(methylmethacrylate) Having Spirobenzopyran Side Groups. *Macromolecules* **1979**, *12*, 1176-1180. (c) Irie, M.; Schnabel, W. Photoresponsive Polymers. Dynamics of Conformational Changes of Polyamides with Backbone Azobenzene Groups. *Macromolecules* **1981**, *14*, 1246 – 1249. (d) Irie, M.; Hirano, Y.; Hashimoto, S.; Hayashi, K. Photoresponsive Polymers. 2. Reversible Solution Viscosity Change of Polyamides having Azobenzene Residues in the Main Chain. *Macromolecules* **1981**, *14*, 262 – 267. (e) Menju, A.; Hayashi, K.; Irie, M. Photoresponsive Polymers. 3. Reversible Solution Viscosity Change of Poly(methacrylic acid) having spirobenzopyran Pendant Groups in Methanol. *Macromolecules* **1981**, *14*, 755 – 758. (f) Irie, M.; Hayashi, K.; Menju, A. Photoresponsive Polymers IV. Photocontrol of Viscosity and pH-Value in Aqueous Systems using Poly(Methacrylic acid) having Spirobenzipyran Side Groups. *Polym. Photochem.* **1981**, *1*, 233 – 242. (g) Irie, M.; Tanaka, H. Photoresponsive Polymers. 5. Reversible Solubility Change of Polystyrene having Azobenzene Pendant Groups. *Macromolecules* **1983**, *16*, 210 – 214. (h) Irie, M. Light-Induced Reversible pH Change. *J. Am. Chem. Soc.* **1983**, *105*, 2078 – 2079.

1(26) Masuda, S.; Sertova, N.; Petkov, I. Photochemical Behavior of Poly(Ethylacryloylacetate) and Poly(Acryloylacetone) films. *J. Polym. Sci. Part A: Polym. Chem.* **1997**, *35*, 3683–3688.

1(27) (a) Sterenborg, H. J. C. M., Van Gemert, M. J. C., Kamphorst, W., Wolbers, J. G., and Hogervorst, W. The Spectral Dependence of the Optical Properties of Human Brain. *Lasers in Medical Science* **1989**, *4*, 221-227. (b) Smith, A. M.; Mancini, M. C.; Nie, S. Bioimaging: Second Window for *in vivo* Imaging. *Nat. Nanotechnol.* **2009**, *4*, 710 – 711.

1(28) Crano, J. C.; Guglielmetti, R. J. Eds., *Organic Photochromic and Thermochromic Compounds*; Kluwer Academic Publishers: New York, 2002.

1(29) (a) Ercole, F.; Davis, T. P.; Evans, R. A. Photo-Responsive Systems and Biomaterials: Photochromic Polymers, Light-Triggered Self-Assembly, Surface Modification, Fluorescence Modulation and Beyond. *Polym. Chem.* **2010**, *1*, 37-54 and references therein. (b) Kungwatchakun,D.; Irie, M. Photoresponsive Polymers. Photocontrol of the Phase Separation Temperature of Aqueous Solutions of Poly-[*N*-isopropylacrylamide-*co*-*N*-(4-phenylazophenyl)acrylamide]. *Makromol. Chem. Rapid Commun.* **1988**, *9*, 243-246. (c) Chujo, Y.; Sada, K.; Saegusa, T. Polyoxazoline having a coumarin moiety as a pendant group. Synthesis and Photogelation. *Macromolecules* **1990**, *23*, 2693-2697. (d) Trenor, S. R., Shultz, A. R., Love, B. J. & Long, T. E. Coumarins in Polymers: from Light Harvesting to Photo-Cross-Linkable Tissue Scaffolds. *Chem. Rev.* **2004**, *104*, 3059–3077. (e) Sumaru, K.; Ohi, K.; Takagi, T.; Kanamori, T.; Shinbo, T. Photoresponsive Properties of Poly(*N*-Isopropylacrylamide) Hydrogel Partly Modified with Spirobenzopyran. *Langmuir* **2006**, *22*, 4353-4356. (f) Jochum, F. D.; Theato, P. Temperature- and Light-Responsive Polyacrylamides Prepared by a Double Polymer Analogous Reaction of Activated Ester Polymers. *Macromolecules* **2009**, *42*, 5941-5945. (g) Zhao, Y.; Bertrand, J.; Tong, X.; Zhao, Y. Photo-Cross-Linkable Polymer Micelles in Hydrogen-Bonding-Built-Layer-by-Layer Films. *Langmuir* **2009**, *25*, 13151-13157. (h) Jochum, F. D.; Forst, F. R.; Theato, P. PNIPAM Copolymers Containing Light-Responsive Chromophores: A Method Toward Molecular Logic Gates. *Macromol. Rapid Commun.* **2010**, *31*, 1456-1461. (i) Satoh, T.; Sumaru, K.; Takagi, T.; Kanamori, T. Fast-Reversible Light-Driven Hydrogels Consisting of Spirobenzopyran-functionalized Poly(*N*-Isopropylacrylamide) *Soft Matter* **2011**, *7*, 8030-8034.

1(30) (a) Irie, M.; Kungwatchakun, D. Photoresponsive polymers. Mechanochemistry of Polyacrylamide Gels having Triphenylmethane Leuco Derivatives. *Makromol. Chem. Rapid Commun*. **1984**, *5*, 829-832. (b) Irie, M.; Kungwatchakun, D. Photoresponsive Polymers. 8. Reversible Photostimulated Dilation of Polyacrylamide Gels having Triphenylmethane Leuco Derivatives. *Macromolecules* **1986**, *19*, 2476-2480. (c) Mamada, A.; Tanaka, T.; Kungwatchakun, D.; Irie, M. Photoinduced Phase Transition of Gels. *Macromolecules* **1990**, *23*, 1517-1519. (d) Jiang, Y.; Wan, P.; Xu, H.; Wang, Z.; Zhang, X. Facile Reversible UV-Controlled and Fast Transition from Emulsion to Gel by Using a Photoresponsive Polymer with a Malachite Green Group. *Langmuir* **2009**, *25*, 10134-10138. (e) Ishikawa, M.; Kitamuru, N.; Masuhara, H.;

Irie, M. Size Effect on Photoinduced Volume Change of Polyacrylamide Microgels containing Triphenylmethane Leuco Cyanide. *Makromol. Chem. Rapid Commun.* **1991**, *12*, 687-690. (f) Watanabe, T.; Akiyama, M.; Totani, K.; Kuebler, S. M.; Stellacci, F.; Wenseleers, W.; Braun, K.; Marder, S. R.; Perry, J. W. Photoresponsive Hydrogel Microstructure Fabricated by Two-Photon Initiated Polymerization. *Adv. Funct. Mater.* **2002**, *12*, 611-614.

1(31) Zhao, Y. Photocontrollable block copolymer micelles: what can we control? *J. Mater. Chem.* **2009**, *19*, 4887-4895 and references therein.

1(32) (a) Han, M.; Hara, M. Intense Fluorescence from Light-Driven Self-Assembled Aggregates of Nonionic Azobenzene Derivative. *J. Am. Chem. Soc.* **2005**, *127*, 10951-10955. (b) Han, M. R.; Hara, M. Chain Length-Dependent Photoinduced Formation of Azobenzene Aggregates. *New J. Chem.* **2006**, *30*, 223-227. (c) Han, M. R.; Hirayama, Y.; Hara, M. Fluorescence Enhancement from Self-Assembled Aggregates: Substituent Effects on Self-Assembly of Azobenzenes. *Chem. Mater.* **2006**, *18*, 2784-2786. (d) Han, M. R.; Hashizume, D.; Hara, M. Self-Assembly of Long-Lived *cis*-Azobenzenes into Crystalline Nanoparticles. *New J. Chem.* **2007**, *31*, 1746-1750.

1(33) Gong, H.; Yang, Y.; Chen, X.; Zhao, D.; Chen, X.; Chen, Y.; Yan, M.; Li, Q.; Qiu, M. Gold Nanoparticle Transfer through Photothermal Effects in a Metamaterial Absorber by Nanosecond Laser. *Scientific Reports* **2014**, *4*, 6080.

1(34) (a) Kroeger, R.; Menzel, H.; Hallensleben, M. L. Light Controlled Solubility Change of Polymers: Copolymers of *N,N*-dimethylacrylamide and 4-phenylazophenyl acrylate. *Macromol. Chem. Phys.* **1994**, *195*, 2291- 2298. (b) Akiyama, H.; Tamaoki, N. Polymers derived from *N*-Isopropylacrylamide and Azobenzene-Containing Acrylamides: Photoresponsive Affinity to Water. *J. Polym. Sci. A. Polym. Chem.* **2004**, *42*, 5200-5214. (c) Akiyama, H.; Tamaoki, N. Synthesis and Photoinduced Phase Transitions of Poly(*N*-isopropylacrylamide) Derivative Functionalized with Terminal Azobenene Units. *Macromolecules* **2007**, *40*, 5129-5132. (d) Luo, C.; Zuo, F.; Ding, X.; Zheng, Z.; Cheng, X.; Peng, Y. Light-triggered Reversible Solubility of α-Cyclodextrin and Azobenzene Moiety Complexes in PDMAA-*co*-PAPA via Molecular Recognition. *J. Appl. Polym. Sci.* **2007**, *107*, 2118- 2125. (e) Shimoboji, T.; Larenas, E.; Fowler, T.; Kulkarni, S.; Hoffman, A. S.; Stayton, P. S. Photoresponsive Polymer-Enzyme Switches. *Proc. Natl. Acad. Sci. U. S. A.* **2002**, *99*, 16592-16596. (f) Ravi, P.; Sin, S. L.; Gan, L. H.; Gan, Y. Y.; Tam, K. C.; Xia, X. L.; Hu, X. New Water Soluble Azobenzene-Containing Diblock Copolymers: Synthesis and Aggregation Behavior. *Polymer* **2005**, *46*, 137-146. (g) Zhao, Y.; Tremblay, L.; Zhao, Y. Doubly Photoresponsive and Water-Soluble Block Copolymers: Synthesis and Thermosensitivity. *J. Polym. Sci. Part A Polym. Chem.* **2010**, *48*, 4055-4066. (h) Desponds, A.; Freitag, R. Synthesis and Characterization of Photoresponsive *N*-Isopropylacrylamide Cotelomers. *Langmuir* **2003**, *19*, 6261–6270. (i) Boissiere, O.; Han, D.; Tremblay, L.; Zhao, Y. Flower micelles of poly(*N*-isopropylacrylamide) with Azobenzene Moieties Regularly Inserted into the Main Chain. *Soft Matter* **2011**, *7*, 9410–9415.

1(35) Li, L.; Xing, X.; Liu, Z. Triply-Responsive (Thermo/Light/pH) Copolymeric Hydrogel of *N*-Isopropylacrylamide with an Azobenzene-Containing Monomer. *J. Appl. Polym. Sci.* **2012**, *124*, 1128–1136.

1(36) Jochum, F. D.; Theato, P. Temperature- and Light-Responsive Smart Polymer Materials. *Chem. Soc. Rev.* **2013**, *42*, 7468-7483.

1(37) Jochum, F. D.; Theato, P. Temperature and Light Sensitive Copolymers Containing Azobenzene Moieties Prepared via a Polymer Analogous Reaction. *Polymer* **2009**, *50*, 3079- 3085.

1(38) Jochum, F. D.; zur Borg, L.; Roth, P. J.; Theato, P. Thermo- and Light-Responsive Polymers Containing Photoswitchable Azobenzene End Groups. *Macromolecules* **2009**, *42*, 7854-7862.

1(39) Jochum, F. D.; Theato, P. Thermo- and Light responsive Micellation of Azobenzene Containing Block Copolymers. *Chem. Commun.* **2010**, *46*, 6717-6719.

1(40) (a) Jochum, F. D.; Theato, P. Temperature- and Light-Responsive Polyacrylamides Prepared by a Double Polymer Analogous Reaction of Activated Ester Polymers. *Macromolecules* **2009**, *42*, 5941-5945. (b) Jochum, F. D.; Forst, F. R.; Theato, P. PNIPAM Copolymers Containing Light-Responsive Chromophores: A Method Toward Molecular Logic Gates. *Macromol. Rapid Commun.* **2010**, *31*, 1456-1461.

1(41) Goeldner, M.; Givens, R., Eds. *Dynamic Studies in Biology: Phototriggers, Photoswitches and Caged Biomolecules*; Wiley-VCH Verlag GmbH & Co; Weinheim, 2005.

1(42) (a) Stankovic, C. J.; Heinemann, S. H.; Schreiber, S. L. Photo-Modulated Ion Channels based on Covalently Linked Gramicidins. *Biochem. Biophys. Acta.* **1991**, *1061*, 163-170. (b) Wooley, G. A.: Jaikaran, A. S. I.; Zhang, Z.; Peng, S. Design of Regulated Ion Channels Using Measurements of Cis-Trans Isomerization in Single Molecules. *J. Am. Chem. Soc*. **1995**, *117*, 4448- 4454. (c) Borisenko, V.; Burns, D. C.; Zhang, Z.; Woolley, G. A. Optical Switching of Ion-Dipole Interactions in a Gramicidin Channel Analogue. *J. Am. Chem. Soc.* **2000**, *122*, 6364-6370. (d) Feringa, B. L.; Browne, W. R. Eds. *Molecular Switches*;

Wiley-VCH: Weinheim, 2011. (e) Durr, H.; Bouas-Laurent, H., Eds. *Photochromism: Molecules and Systems, Revised Ed*.; Elsevier: Amsterdam, 2003. (f) Banghart, M.; Borges, K.; Isacoff, E.; Trauner, D.; Kramer, R. H. Light-Activated Ion Channels for Remote Control of Neuronal Firing. *Nat. Neurosci.* **2004**, *7*, 1381-1386.

1(43) (a) Wang, Z.; Wang, P.; Tang, X. J. Synthesis of Light-Induced Expandable Photoresponsive Polymeric Nanoparticles for Triggered Release. *ChemPlusChem* **2013**, *78*, 1273-1281 and references therein. (b) Rwei, A. Y.; Wang, W.; Kohane, D. S. Photoresponsive Nanoparticles for Drug Delivery. *Nano Today* **2015**, *10*, 451-467 and references therein.

1(44) (a) Whitesides, G. M.; Grzybowski, B. Self-Assembly at All Scales. *Science* **2002**, *295*, 2418-2421. (b) Klajn, R.; Bishop, K. J. M.; Grzybowski, B. A. Light-Controlled Self-Assembly of Reversible and Irreversible Nanoparticle Suprastructures. *PNAS* **2007**, *104*, 10305–10309. (c) Das, S.; Ranjan, P.; Maiti, P. S.; Singh, G.; Leitus, G.; Klajn, R. Dual-Responsive Nanoparticles and their Self-Assembly. *Adv. Mater.* **2013**, *25*, 422–426.

1(45) (a) Kita-Tokarczyk, K.; Grumelard, J.; Haefele, T.; Meier, W. Block Copolymer Vesicles – using Concepts from Polymer Chemistry to Mimic Biomembranes. *Polymer* **2005**, *46*, 3540-3563. (b) Lin, L.; Feng, Z.; Yu, Q.; Yan, Z.; Yen, C.-C.; Yu, Y. Self-Assembly and Photoresponsive Behavior of Amphiphilic Diblock Copolymers Containing Azobenzene Moieties. *Mol. Cryst. Liq. Cryst.* **2009**, *508*, 214-225. (c) Wang, C.; Chen, Q.; Xu, H.; Wang, Z.; Zhang, X. Photoresponsive Supramolecular Amphiphiles for Controlled Self-Assembly of Nanofibers and Vesicles. *Adv. Mater.* **2010**, *22*, 2553-2555. (d) Cabane, E.; Malinova, V.; Menon, S.; Palivan, C. G.; Meier, W. Photoresponsive polymersomes as smart, triggerable nanocarriers. *Soft Matter* **2011**, *7*, 9167-9176. (e) Boissiere, O.; Han, D.; Tremblay, L.; Zhao, Y. Flower Micelles of Poly(*N*-Isopropylacrylamide) with Azobenzene Moieties Regularly Inserted into the Main Chain. *Soft Matter* **2011**, *7*, 9410–9415. (f) Lee, J. S.; Feijen, J. Polymersomes for Drug Delivery: Design, Formation and Characterization. *J. Control. Release* **2012**, *161*, 473-483. (g) Han, M.; Okui, Y.; Hirade, T. Light-Responsive Microstructures capable of Pyrene Monomer Fluorescence Switching. *J. Mater. Chem. C* **2013**, *1*, 3448-3453.

1(46) Hirakura, T.; Nomura, Y.; Aoyama, Y.; Akiyoshi, K. Photoresponsive Nanogels Formed by the Self-Assembly of Spiropyrane-Bearing Pullulan That Act as Artificial Molecular Chaperones. *Biomacromolecules* **2004**, *5*, 1804-1809 and references therein.

1(47) Garcia, A.; Marquez, M.; Cai, T.; Rosario, R.; Hu, Z.; Gust, D.; Hayes, M.; Vail, S. A.; Park, C.-D. Photo-, Thermally, and pH-Responsive Microgels. *Langmuir* **2007**, *23*, 224-229.

1(48) (a) Tian, Y.; Akiyama, E.; Nagase, Y.; Kanazawa, A.; Tsutsumib, O.; Ikeda, T. Synthesis and Investigation of Photophysical and Photochemical Properties of New Side-Group Liquid Crystalline Polymers containing Coumarin Moieties. *J. Mater. Chem.* **2004**, *14*, 3524-3531. (b) Barberis, V. P.; Mikroyannidis, J. A.; Cimrov_a, V. J. Coumarin-containing Poly(fluorenediylvinylene)s: Synthesis, Photophysics, and Electroluminescence. *Polym. Sci., Part. A: Polym. Chem*. **2006**, *44*, 5750-5762. (c) Jiang, J. Q.; Qi, B.; Lepage, M.; Zhao, Y. Polymer Micelles Stabilization on Demand through Reversible Photo-Cross-Linking. *Macromolecules* **2007**, *40*, 790-792. (d) Fu, Q.; Cheng, L. L.; Zhang, Y.; Shi, W. F. Preparation and Reversible Photo-Crosslinking/ Photo-Cleavage Behavior of 4-Methylcoumarin Functionalized Hyperbranched Polyester. *Polymer* **2008**, *49*, 4981-4988. (e) He, J.; Tong, X.; Tremblay, L.; Zhao, Y. Corona-Cross-Linked Polymer Vesicles Displaying a Large and Reversible Temperature-Responsive Volume Transition. *Macromolecules* **2009**, *42*, 7267-7270. (f) Jiang, J. Q.; Feng, Y.; Wang, H. M.; Liu, X. Y.; Zhang, S. W.; Chen, M. Q. Synthesis and Micellization of Photosensitive Amphiphilic Comblike SMA Polymer. *Acta Phys. Chim. Sin.* **2008**, *24*, 2089-2095. (g) He, J.; Zhao, Y.; Zhao, Y. Photoinduced Bending of a Coumarin-Containing Supramolecular Polymer. *Soft Matter* **2009**, *5*, 308-310. (21) Zhao, Y. Rational Design of Light-Controllable Polymer Micelles. *Chem. Rec*. **2007**, *7*, 286-294. (h) Dahmane, S.; Lasia, A.; Zhao, Y. Electrochemically Active Block Copolymer Micelles Containing Coumarin Moieties. *Macromol. Chem. Phys*. **2008**, *209*, 1065-1072. (i) Zhao, Y. Photocontrollable Block Copolymer Micelles: What Can We Control? *J. Mater. Chem.* **2009**, *19*, 4887-4895. (j) Zhao, Y.; Bertrand, J.; Tong, X.; Zhao, Y. Photo-Cross-Linkable Polymer Micelles in Hydrogen-Bonding-Built-Layer-by-Layer Films. *Langmuir* **2009**, *25*, 13151-13157. (k) Jiang, J.; Shu, Q.; Chen, X.; Yang, Y.; Yi, C.; Song, X.; Liu, X.; Chen, M. Photoinduced Morphology Switching of Polymer Nanoaggregates in Aqueous Solution. *Langmuir* **2010**, *26*, 14247–14254.

1(49) He, J.; Tong, X.; Zhao, Y. Photoresponsive Nanogels Based on Photocontrollable Cross-Links. *Macromolecules* **2009**, *42*, 4845-4852.

1(50) Huang, Q.; Bao, C.; Ji, W.; Wang, Q.; Zhu, L. Photocleavable Coumarin Crosslinkers based Polystyrene Microgels: Phototriggered Swelling and Release. *J. Mater. Chem***. 2012**, *22*, 18275-18282.

1(51) Wang, M. H.; Kim, J.-C. Microgels of Poly(hydroxyethyl acrylate-*co*-coumaryl acrylate-*co*-octadecyl acrylate): Photo-Responsive Release. *Colloid Polym. Sci.* **2013,** *291*, 2319-2327.

1(52) (a) Yin, J.; Hu, H.; Wu, Y.; Liu, S. Thermo- and light-regulated fluorescence resonance energy transfer processes within dually responsive microgels. *Polym. Chem.* **2011**, *2*, 363-371. (b) Klinger, D.; Landfester, K. Dual Stimuli-Responsive Poly(2-hydroxyethyl methacrylate-*co*-methacrylic acid) Microgels Based on Photo-Cleavable Cross-Linkers: pH-Dependent Swelling and Light-Induced Degradation. *Macromolecules* **2011**, *44*, 9758-9772. (c) Klinger, D.; Landfester, K. Polymeric Photoresist Nanoparticles: Light-Induced Degradation of Hydrophobic Polymers in Aqueous Dispersion. *Macromol. Rapid Commun.* **2011**, *32*, 1979-1985. (d) Klinger, D.; Landfester, K. Photo-Sensitive PMMA Microgels: Light-Triggered Swelling and Degradation. *Soft Matter* **2011**, *7*, 1426-1440.

1(53) (a) Gorelikov, I.; Field, L. M.; Kumacheva, E. Hybrid Microgels Photoresponsive in the Near-Infrared Spectral Range. *J. Am. Chem. Soc*. **2004**, *126*, 15938-15939. (b) Das, M.; Sanson, N.; Fava, D.; Kumacheva, E. Microgels Loaded with Gold Nanorods: Photothermally Triggered Volume Transitions under Physiological Conditions. *Langmuir* **2007**, *23*, 196-201. (c) Kawano, T.; Niidome, Y.; Mori, T.; Katayama, Y.; Niidome, T. PNIPAM Gel-Coated Gold Nanorods for Targeted Delivery Responding to a Near-Infrared Laser. *Bioconjugate Chem*. **2009**, *20*, 209-212. (d) Wu, W.; Sheh, J.; Banerjee, P.; Zhou, S. Water-Dispersible Multifunctional Hybrid Nanogels for Combined Curcumin and Photothermal Therapy. *Biomaterials* **2011**, *32*, 598-609.

1(54) Zhang, H.-J.; Xin, Y.; Yan, Q.; Zhou, L.-L.; Peng, L.; Yuan, J.-Y. Facile and Efficient Fabrication of Photoresponsive Microgels via Thiol-Michael Addition. *Macromol Rapid Commun*. **2012,** *33*, 1952-1957.

1(55) Zhu, L.; Zhao, C.; Zhang, J.; Gong, D. Photocontrollable Volume Phase Transition of an Azobenzene Functionalized Microgel and its Supramolecular Complex. *RSC Adv.* **2015**, *5*, 84263-84268.

1(56) Fan, K.; Bradley, M.; Vincent, B. Photo-Responsive Properties of Poly(NIPAM-co-AAc) Microgel Particles with Absorbed, Hydrophobically Modified Organic Salts. *J. Colloid Interf. Sci.* **2012**, *368*, 287–291.

1(57) Zakrevskyy, Y.; Richter, M.; Zakrevska, S.; Lomadze, N.; von Klitzing, R.; Santer, S. Light-Controlled Reversible Manipulation of Microgel Particle Size Using Azobenzene-Containing Surfactant. *Adv. Funct. Mater.* **2012**, *22*, 5000-5009.

1(58) Zhang, Q. M.; Li, X.; Islam, M. R.; Wie, M.; Serpe, M. J. Light Switchable Optical Materials from Azobenzene Crosslinked Poly(*N*-Isopropylacrylamide)-based Microgels. *J. Mater. Chem. C* **2014**, *2*, 6961-6965.

1(59) Bahrenburg, J.; Renth, F.; Temps, F.; Plamper, F.; Richtering, W. Femtosecond Spectroscopy Reveals Huge differences in the Photoisomerisation Dynamics between Azobenzenes Linked to Polymers and Azobenzenes in Solution. *Phys. Chem. Chem. Phys.* **2014**, *16*, 11549-11554.

CHAPTER 2. The Reversible Thermo- and Photo-Responsive Behavior of Copolymer Microgels of *N*-Vinylcaprolactam and 4-[(4-Methacryloyloxy)phenylazo] benzenesulfonic acid

2.1. Introduction

Light is a resource that is available in abundance and can be easily harnessed and exploited. It functions as an important stimulus in nature where organisms detect and respond to light in various ways, for instance, in photosynthesis, for their vision and in the maintenance of circadian rhythms. Its application within the clinical or research environment can be further expanded in the development of intelligent stimuli-responsive materials. Its use as a stimulus is attractive because it is an orthogonal, exogenous, non-chemical trigger that can be controlled with high temporal and spatial resolution. Advances in the exploitation of light as a stimulus are spread across a wide spectrum. This includes the development of artificial light-harvesting antennae for practical applications such as in sustainable energy production,[2(1)] photo-switchable proteins that report on tumor cells,[2(2)] polymer systems that possess photo-responsive functionality for control over molecular motion,[2(3)] controlled drug delivery vehicles,[2(4)] sensors,[2(5)] and polymer-enzyme switches.[2(6)]
Attention has also been focused on incorporating a photo-responsive property into soft materials such as gels to control their physicochemical properties. Especially attractive are photo-switchable systems. To this end, photochromic groups such as fulgimides,[2(7)] coumarins,[2(8)] and spiropyrans[2(9)] have been employed. Azobenzene has been the most commonly used of all since its synthesis is relatively convenient, and it exhibits good and fast reversibility between the *trans* and *cis* states by alternate irradiation using two distinct wavelengths.[2(10)] The UV-triggered variation in the polarity of azobenzene between the less polar *trans* to the more polar *cis* forms has often been used to increase the hydrophilicity of azobenzene-containing polymeric gel systems.[2(1)] For instance, Zhang *et al.* developed photo-switchable optical materials from azobenzene cross-linked poly(*N*-isopropylacrylamide)-based microgels that exhibited increased swelling upon isomerization of the azo moiety from *trans* to *cis*.[2(12)] Furthermore, Zakrevskyy *et al.* demonstrated the reversible swelling and deswelling of poly(*N*-isopropylacrylamide)-based microgels via UV and visible light isomerization respectively, of a photosensitive azobenzene-containing surfactant interacting with the microgel particles.[2(13)] Less frequently observed, on the other hand, is the deswelling phenomenon of the polymeric network when the azobenzene moiety is switched from the less polar *trans* state to the more polar *cis*

state.[2(14)] Moreover, in all these reports, azobenzene-containing compounds have either been incorporated into *N*-isopropylacrylamide (NIPAM) or *N,N*-dimethylacrylamide (DMA) to yield thermo- and photo-responsive copolymers.

In this chapter, we focus on poly(*N*-vinylcaprolactam) (PVCL) microgels, which combine unique properties like biocompatibility, temperature-responsiveness and adaptability to different solvents.[2(15)] Our approach involves synthesizing thermo- and photo-responsive copolymeric microgels via surfactant-free precipitation polymerization of *N*-vinylcaprolactam (VCL) as the thermo-responsive unit with a water-soluble azobenzene comonomer 4-[(4-methacryloyloxy)phenylazo] benzenesulfonic acid (ABSA) as the photo-responsive pendant group. To the best of our knowledge, we report the first instance of rapid and significant deswelling of P(VCL)-based microgels upon UV-induced *trans*-to-*cis* isomerization of small amounts (≤ 10 wt. %) of incorporated azobenzene pendant groups within the microgel matrix. The variation in the content of the pendant groups allows modulation of the photo-triggered volume change. The deswelling can be reversed thermally or by irradiation with visible light. Based on the characterization of the internal microgel structure we propose a mechanism for the photo-induced swelling-deswelling of the microgels.

2.2. Experimental Section

2.2.1. Materials

N-Vinylcaprolactam (VCL) (Sigma-Aldrich, of 98% purity) was purified by a high-vacuum distillation at 80°C. The azobenzene comonomer 4-[(4-methacryloyloxy)phenylazo] benzenesulfonic acid (ABSA) was synthesized according to a previously reported procedure[2(16)] and its ^{1}H NMR spectrum can be found in Fig. A2(6) of Appendix 2. *N,N'*-Methylenebis(acrylamide) (BIS) cross-linker was obtained from Sigma-Aldrich and used as received. The initiator, 2,2'-azobis[*N*-(2-carboxyethyl)-2 methylpropionamidine]hydrate (ACMA), was purchased from (Wako Pure Chemical Industries, Ltd., Specialty Chemicals) and used as received. Deuterium oxide (D_2O, 99.9%) was obtained from Deutero GmbH and used as received.

UV and visible light light-emitting diodes (LEDs). The following LEDs were purchased and then handcrafted and fashioned in-house for use with the dynamic light scattering instrument. Gen 2 Emitter LZ1-00UV00 (365 nm, LED Engin, Inc.) was coupled to an optical fiber from (CeramOptec) to produce an irradiance of 100 mW cm^{-2}. RLT365-10E UV LED 5 mm (365 nm, 1.0 mW cm^{-2}, Roithner LaserTechnik

GmbH), and LED450 (InGaN, 450 nm, 1.0 mW cm^{-2}, Roithner LaserTechnik GmbH) were also employed.

2.2.2. Microgel synthesis

Microgels were synthesized in deionized water via surfactant-free precipitation polymerization, according to a procedure modified from that reported by Boyko *et al*.[2(17)] In a typical procedure, the polymerization is carried out in a double-wall glass reactor equipped with a stirrer. Half the amount of VCL and half the BIS cross-linker amount were dissolved in 80 ml deionized water and added into the reactor and stirred for 30 min at 70 °C under continuous purging with nitrogen. Subsequently, 5 mL aqueous solution of ACMA initiator was added under continuous stirring into the reactor. The reaction mixture turned turbid 30 s after initiation. At the 30 s mark after the appearance of turbidity, a 15 ml solution containing the remaining VCL monomer, BIS cross-linker and all of the ABSA comonomer was added with a syringe over a period of 1 min under positive flow of nitrogen. The reaction stirred for 6 h at 70°C. The respective amounts of VCL, ABSA, BIS and ACMA are listed in Table 2(1) and the steps in the microgel synthesis are represented in Scheme 2(1).

Table 2(1). Amount of monomers used in the synthesis of microgels.

Microgel	VCL [mmol]	$ABSA_{feed}$ [mmol]	$ABSA_{feed}$ wt. %	$ABSA_{incorp.}$ wt. %
P(VCL-$bis_{1.5}$)	10	-	-	-
P(VCL-$bis_{1.5}$-$ABSA_{1.5}$)	9.85	0.15	3.7	6.1
P(VCL-$bis_{1.5}$-$ABSA_{4.5}$)	9.55	0.45	10.5	10.1

*The nomenclature used in this chapter for the microgels are based on the feed amounts of BIS and ABSA (indicated in subscripts in mol%).

2.2.3. Characterization

UV/vis-spectroscopy. Spectra were measured from 800-200 nm with a scan rate of 600 nm/min on a Cary 100Bio UV-Visible Spectrophotometer from Varian. A quartz cuvette was used for the measurement and a quartz cuvette filled with deionized water was used as a reference.

Dynamic light scattering (DLS). The size of the microgel particles was measured with an ALV/LSE-5004 Dynamic Light Scattering (DLS) goniometer with a Multiple Tau Digital Correlator and Electronics. The instrument is equipped with a laser light wavelength of 633 nm and the scattered light was detected at a scattering angle set to 90°. The samples were measured at 20 °C and the temperature fluctuations were below 0.1 °C. Microgel samples were highly diluted (*c* < 0.01 wt %) with water for chromatography from Merck Millipore and subsequently filtered through a 1.2 μm filter before measurements were performed to eliminate dust, aggregation and impurities. The hydrodynamic radius R_h was calculated from second order cumulant fits via the Stokes-Einstein equation. For temperature-dependent measurements, samples were measured between 10 and 60°C, in steps of 3°C and the temperature fluctuations were kept below 0.1°C. Three runs of 120 s each were performed at each temperature in order to calculate the standard deviation. The volume phase transition temperature (VPTT) of each microgel was determined as the inflection point of the temperature-dependent light scattering curve.

***In situ* irradiation within the DLS instrument.** The photo-induced size changes of the microgels at different temperatures were measured within the DLS instrument. Samples were allowed to equilibrate thermally at the respective temperatures for 10 minutes. The LED (λ = 365 nm or 450 nm) was placed 0.5 cm above the meniscus of the microgel solution in the DLS cuvette (Fig. A2(1) of Appendix 2 shows the *in situ* irradiation set-up for investigation of photo-responsive behaviour via DLS). At each temperature, six runs of 10 s each were performed and repeated for over fifteen minutes to monitor the photo-responsive effect over time.

Atomic force microscopy (AFM). AFM images were recorded using a tapping mode on a Veeco Nanoscope Atomic Force Microscope. Cantilevers (NanoWorld, Neuchâtel, Switzerland) with resonance frequency of 250 – 300 kHz and spring constant of 42 N m^{-1} were used. The deposition of microgels on a silicon wafer was carried out on a spin-coater (Convac 1001S, Germany) at a speed of 3000 rpm for 30 s. The silicon wafer used for deposition was previously cleaned by sonication in isopropanol for 10 minutes, dried with an air stream, and treated with UV/O_2 for 15 minutes. The concentration of microgel solution used for spin coating was 1.0 mg/mL. At this microgel concentration, sufficient amount of particles could be adsorbed and be evenly distributed on the silicon wafer without clustering. For the measurement of UV-irradiated sample of P(VCL-$BIS_{1.5}$-$ABSA_{4.5}$), the native 1.0 mg/ml microgel aqueous solution was first irradiated by placing the UV LED (365 nm, 100 mW cm^{-2}) at a height of 0.5 cm above the meniscus of the solution. This irradiated solution was subsequently spin-coated according to the same procedure as above.

Fourier transform Raman spectroscopy. P(VCL-$BIS_{1.5}$) microgel was analyzed with a FT-Raman Bruker Optics Spectrometer, model RFS 100/S, equipped with a

Nd:YAG 1064 nm laser, operating at a power of 200mV. 1000 scans were performed to obtain the spectrum with a spectral resolution of 4 cm^{-1}.

Attenuated total reflectance (ATR). Microscopic attenuated total reflectance Fourier transform infrared (ATR FT-IR) spectra were collected on a Thermo Nicolet Nexus 470 FT-IR spectrometer supplemented with a Ge crystal (2 mm, 45° face angle) overhead ATR cell from Specac. An amount of 1 µL of microgel dispersion was placed directly on the Ge crystal and each spectrum was collected on the liquid-substrate interface.

Proton nuclear magnetic resonance spectroscopy (^{1}H NMR). The ^{1}H NMR spectra of the microgels under magic-angle sample spinning (MAS) conditions were measured on a wide-bore AV700 Bruker NMR spectrometer operating at 700 MHz with a cross-polarization magic-angle sample spinning (MAS) probe head. The rotor frequency and the sample temperature were v_R = 7 kHz and 24 ± 0.5 °C, respectively. For all measurements, the recycle delay was 5 s, the radiofrequency pulse length was 1.9 µs, and the dwell time was 10 µs. For all measurements, 5 wt.% microgel in D_2O was used and the spectra were calibrated relative to the water peak.

The high-resolution MAS transverse magnetic relaxation (T_2) NMR measurements were performed at 700.2378 MHz proton frequency on the Bruker AV700 NMR spectrometer. Solution of of P(VCL-$BIS_{1.5}$-$ABSA_{4.5}$) microgel in D_2O was used for the measurements. The same rotor frequency, recycle delay, dwell time, and temperature as for ^{1}H spectra were employed. The decay of transverse magnetization relaxation was measured using spin-echo pulse sequence: $90°_x$ – t – $180°_x$ – t – spin echo – (acquisition), where t is the echo time.[2(18)] Half of the spin echo decay was detected and Fourier transformed. The normalized integral intensity of various resonances was fitted by two-exponential decay functions using Origin® 8.6 software. The errors of the fits were found to be smaller than 10%.

2.3. Theory

2.3.1. Flory-Rehner theory for homopolymeric microgel with homogeneous cross-linking density

In the Flory-Rehner polymer gel swelling theory, an assumption is made that the free energy change on swelling has two separable and additive contributions, one from the free energy of mixing and the other, the free energy of elastic deformation.[2(19)] In the case of a neutral microgel system, the two contributions are the mixing of the polymer and the solvent, and the network elasticity as a result of cross-linking the polymer chains.[2(20)] Considering these terms for a microgel system at equilibrium, an explicit equation of state that relates the temperature and the hydrodynamic radius of homopolymeric and homogeneously cross-linked microgels can be derived as shown in equation (1). A detailed derivation of equation (1) and comprehensive theoretical descriptions of microgel swelling theories can be found elsewhere.[2(20-23)]

$$T_{\Pi=0} = \varphi_0^2 A\Theta \left(\frac{R_{H0}}{R_H}\right)^6 / \left\{ \frac{N\nu_s}{N_A V_0}\left[\frac{1}{2}\left(\frac{R_{H0}}{R_H}\right)^3 - \left(\frac{R_{H0}}{R_H}\right)\right] - \varphi_0\left(\frac{R_{H0}}{R_H}\right)^3 - ln\left[1-\varphi_0\left(\frac{R_{H0}}{R_H}\right)^3\right] + \varphi_0^2\left(A-\frac{1}{2}\right)\left(\frac{R_{H0}}{R_H}\right)^6 - \varphi_0^3\chi_1\left(\frac{R_{H0}}{R_H}\right)^9 \right\} \qquad (1)$$

where,

N: number of subchains is defined as the polymer chain between two subsequent cross-link points

φ: polymer volume fraction in the particle

χ_1: Flory parameter that accounts for the polymer-polymer and polymer-solvent interactions, and for the quality of the solvent

A = $(2\Delta S + k_B)/2k_B$ is the second virial coefficient

Θ = $2\Delta H/(2\Delta S + k_B)$ is the ***Θ*** temperature of the polymer-solvent system

ΔS and ***ΔH*** are the corresponding entropic and enthalpic changes and k_B is the Boltzmann constant.

Equation (1) makes the approximation that accounts for the concentration dependence of the Flory interaction parameter, χ, through the following relationship with the polymer volume fraction ϕ:

$\chi = \chi_0 + \phi\chi_1$

where χ_0 is given by the expression

$\chi_0 = ½ - A(1 - \theta/T)$

It is known that the typical synthesis procedure of microgels via precipitation polymerization with BIS as cross-linker leads to a radial distribution of cross-linking density, i.e. a more cross-linked core and a looser corona.[2(20),2(21),2(24)] Similarly, we expect our microgels to exhibit such structural inhomogeneities. However, we believe that since we employed a two-step synthesis procedure where the BIS cross-linker is added in equal amounts in succession, the distribution of cross-linking density is expected to be more homogeneous. In order to investigate the morphology of our microgels, we have opted to apply the equation of state for a homopolymeric microgel with a homogeneous distribution of cross-links. A homopolymeric model is a good approximation of our system because of the much higher proportion of VCL monomers (>89 wt.%) in our microgels[2(25)] and for the reason stated above, that the cross-linking density in our microgels should be rather homogeneous. Simplifying the analysis and reducing the time required for data acquisition were also important considerations.

The experimental data of the native microgels were fitted into equation (1) and their parameters N, Θ, A, and χ_1 were obtained. Since there must be no change in the number of subchains after irradiating the microgels, the size-temperature data of the irradiated microgels were fitted with the same equation of state, but this time with the N values fixed and equal to those of their respective native counterparts. The parameters obtained from the fits are listed in Table 2(3).

2.4. Results and discussion

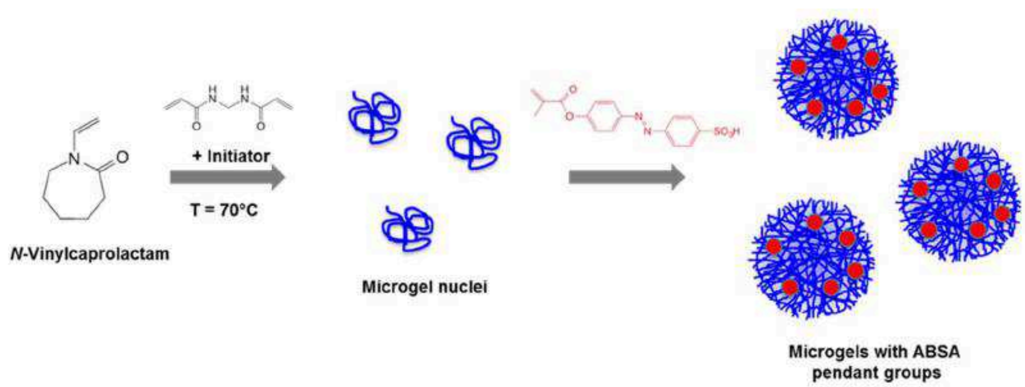

Scheme 2(1). Schematic representation of the microgel synthesis via surfactant-free precipitation polymerization.

2.4.1. Determination of the amount of ABSA comonomer incorporated into microgels

The actual amount of ABSA incorporated into each microgel was determined via UV/vis spectroscopy. A calibration curve (Fig. A2(2), Appendix 2) of the absorbance of ABSA was first recorded. The absorbance due to P(VCL-$BIS_{1.5}$) was subtracted from the absorbance of the P(VCL-BIS-ABSA) microgels. The absorbance maxima due to the π - π* transition of the *trans* isomer in the respective P(VCL-BIS-ABSA) microgels were then compared with the absorbance in the calibration curve and the estimated amount of ABSA incorporated was determined and shown in Table 2(1).

2.4.2. Photo-isomerization behavior of free ABSA comonomer and of ABSA incorporated into microgel

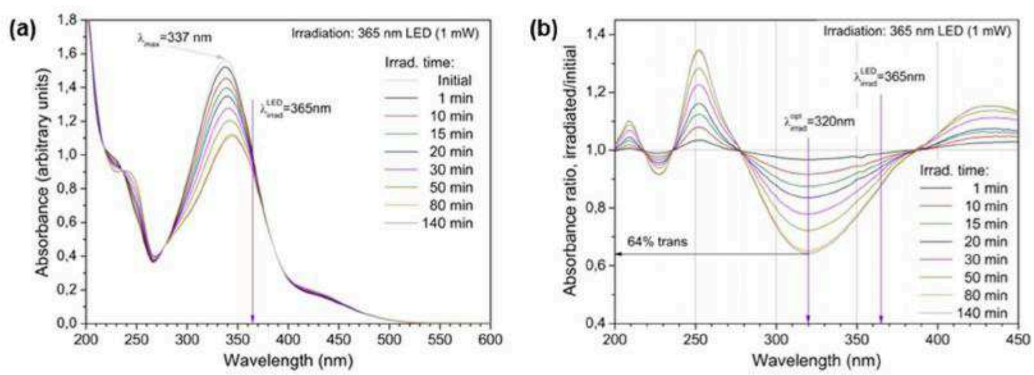

Figure 2(1). Change in the absorbance of (a) ABSA with UV irradiation over time, and (b) Ratio of extinction coefficient spectra after irradiation divided by the initial (dark) spectrum. The *trans*-isomer composition at the photo-stationary state after 140 min of UV irradiation is indicated in Fig. 1b as 64%.

The photo-isomerization behavior of the ABSA in water as free comonomer and as a pendant group incorporated into P(VCL-$BIS_{1.5}$-$ABSA_{1.5}$) and P(VCL-$BIS_{1.5}$-$ABSA_{4.5}$) microgels was investigated using UV/vis spectroscopy. The solutions were irradiated with 365 nm LED (1.0 mW cm^{-2}). Changes in the UV/vis spectra of the free comonomer after different exposure times are shown in Fig. 2(1a). As can be seen, the saturation of the *trans-cis* isomerization process was reached after about one hour of irradiation. This is the so-called steady state where further irradiation does not result in spectral changes. It should be noted, that very similar isomerization behavior with the same saturation exposure period was also measured for ABSA incorporated into the microgels. This is an indication that the isomerization process is not hindered by spatially-confined environments of the microgel matrix. The reversible *cis*-*trans* relaxation in the dark was also investigated spectroscopically by allowing the ABSA monomer solution to relax thermally in the dark for up to 22 hours. The relaxation spectra, as depicted in Fig. A2(3) of Appendix 2, indicate that the spectral changes associated with thermal relaxation are small and the lifetime of the *cis* isomer can be deduced to be very long, in the order of days.

The initial spectrum in Fig. 2(1a) corresponds to the dark state, in which azobenzene units stay predominantly in the *trans* conformation. The absorption band with maximum at 337 nm corresponds to *π*-*π** transition of the *trans* isomer and the band with maximum at about 240 nm corresponds to the absorption of the *π*-conjugated benzene rings.[2(26)] Exposure to UV light of λ = 365 nm leads to *trans*-*cis* isomerization of ABSA. The absorption spectrum of the *cis* isomer is characterized by two maxima: (i) blue-shifted maxima associated with the *π*-*π** transition below 300 nm and (ii) *n*-*π** transition with maximum at about 430 nm. As there is only partial conversion to the *cis* state, the exact position of these transitions cannot be determined.

The isomeric composition of the irradiated ABSA in its free monomeric state in water as well as and in P(VCL-$BIS_{1.5}$-$ABSA_{4.5}$) microgel solution after irradiation were assessed in a similar fashion as reported by Zakrevskyy *et al*.[2(27)] The spectra after irradiation were divided by the initial (dark) spectrum and the obtained absorption ratios are shown in Fig. 2(1b). In the spectral range near 320 nm, a minimum is observed, whose position is mostly independent of the exposure dose. As the absorption of the *cis* isomer in this range is minimal and the *trans* isomer absorption is much higher, the ratio corresponds to the approximate concentration of the *trans* conformation of ABSA. Thus, in the steady state only 36% of ABSA is converted to the *cis* form. Very similar conversion ratios were obtained for ABSA, which is incorporated into microgel. This is a further indication that the isomerization properties of the ABSA unit are not influenced by the microgel matrix.

Low conversion to the *cis* state can be explained by the irradiation wavelength of the LED used. As can be seen from Fig. 2(1b), exposure to 365 nm does not exactly match the minimum of the *cis* isomer. As a result, both the *trans*-to-*cis* isomerization and the reverse *cis*-to-*trans* isomerization are induced at this irradiation wavelength. This leads then to the steady state where an equilibrium conversion is attained. Much higher *cis* concentrations should be obtained by using monochromatic irradiation at wavelengths close to 320 nm. Nonetheless, even with the partial isomerization yield, we were able to detect significant volume changes in the irradiated microgels.

2.4.3. Investigation of the thermo- and photo-responsive properties of microgels via DLS measurements

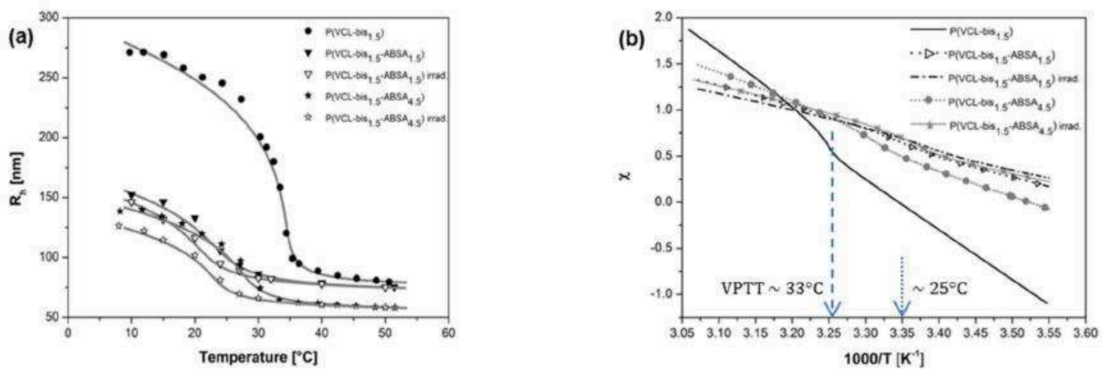

Figure 2(2). (a) Size-temperature data of the microgels obtained from DLS and fitted with equation of state (1) in the homogeneous morphology approximation (solid line), (b) Plot of Flory interaction parameter, χ, as a function of temperature. VPTT of P(VCL-BIS$_{1.5}$) is indicated with an arrow at around 33°C.

The size-temperature data obtained from dynamic light scattering (DLS) measurements is shown in Fig. 2(2a). The size-temperature data were further analyzed using a theoretical model of Flory and Rehner, modified for the case of a homopolymeric, homogeneous microgel system.[2(20)] The fitting with equation (1) is shown as the solid lines in Fig. 2(2a). The data reveal the attainment of particles with narrow particle size distributions and show that the P(VCL-BIS-ABSA) microgels possess a thermo-responsive property. However, there is a decrease in the swelling capacity of the ABSA-containing microgels relative to the P(VCL-BIS$_{1.5}$) microgel. This is especially apparent in the R_h of P(VCL-BIS$_{1.5}$) microgel at 20°C, which is almost double that of the ABSA-containing microgels. This is further supported by the data in Fig. 2(2b), which shows that the Flory interaction parameter, χ, of P(VCL-BIS$_{1.5}$) is lower than that of ABSA-containing microgels at temperatures below its VPTT. This indicates that P(VCL-BIS$_{1.5}$) has a higher affinity for water than the ABSA-containing microgels. A possible explanation is that relatively large parts of the carbonyl groups of the VCL units in P(VCL-BIS$_{1.5}$-ABSA$_{1.5}$) and P(VCL-BIS$_{1.5}$-ABSA$_{4.5}$) are not extensively hydrogen-bonded to water molecules, even below the VPTT probably because they are in crowded positions near the backbone,[2(28)] due to the presence of bulky and hydrophobic benzene rings of ABSA. The introduction of the relatively rigid and bulky ABSA units, interspersed between the VCL units, decreases the rotational freedom of the monomer units along the main chain. This leads ultimately to a decrease in chain flexibility which is associated with less effective solvation of the polymer chains in the microgel network. The hydrophobicity of the double benzene rings of azobenzene also plays a part in diminishing the hydrogen-bonded water network around the C=O groups of the VCL monomer units. In P(VCL), on the other hand, the hydrogen bonding of water molecules to the C=O groups of VCL along the main chain is expected to be relatively unrestricted since a syndiotactic arrangement of the VCL units along the main chain is the preferred conformation.[2(29)] In such a conformation, good solvation of the polymer chains occurs. VPTT is known to depend on the balance between the hydrophilicity/hydrophobicity of the comonomers and the resultant balance of the polar and unpolar regions in the network.[2(30)] Hence, the ABSA-containing microgels exhibit a lower VPTT than the P(VCL-$BIS_{1.5}$) microgel and show a broad transition centered around 24°C as seen in Fig. 2(2a).

It could be argued that the hydrophilic sulfonic acid groups of ABSA can be additionally hydrated because of the presence of three hydrogen bonding sites. This would favor the increased swelling of the microgel. However this does not seem to be the case in our system. It could be possible that the hydroxyl group of the sulfonic moieties preferentially interact with carbonyl groups of VCL units on adjacent subchains within the confined space of the three-dimensional microgel matrix, thereby reducing hydration of the polymer. The sulfonic acid moiety could also be forming hydrogen bonding interactions with the water molecules already hydrogen bonded to the carbonyl groups of the VCL main chain.[2(31)] This results in a cooperative network of hydrogen bonds involving polarized molecules of water forming complete bridges between SO_3H and C=O groups. This could be energetically favorable due to minimization of steric hindrance.[2(32)] This would then mean that the sulfonic acid groups, on their own, do not draw in additional water molecules for hydration and at the same time minimize the size of the hydration shell around the VCL main chain.

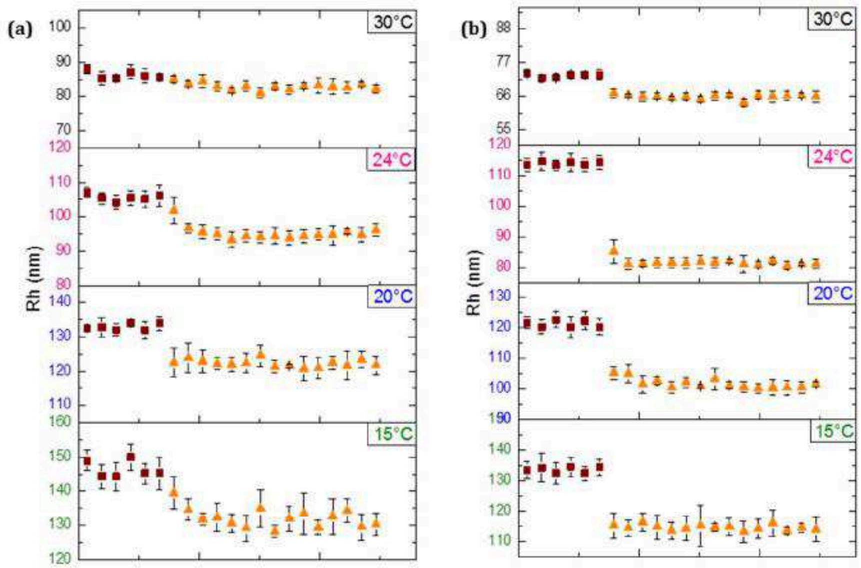

(c)

Temperature [°C]	% decrease in R_h
15	9.7
20	8.0
24	9.8
30	3.7

(d)

Temperature [°C]	% decrease in R_h
15	14.3
20	15.7
24	28.6
30	9.4

Figure 2(3). Investigation of the photo-responsive behavior of (a) P(VCL-$BIS_{1.5}$-$ABSA_{1.5}$), and (b) P(VCL-$BIS_{1.5}$-$ABSA_{4.5}$) microgels irradiated (λ = 365 nm, 100 mW cm^{-2}) at different temperatures. ■ points represent the R_h of the microgels in their native states while ▲ points represent the R_h reached with UV irradiation. Each measurement point represents the mean of 6 x 10 seconds acquisitions in the DLS instrument. Percentage deswelling* of (c) P(VCL-$BIS_{1.5}$-$ABSA_{1.5}$), and (d) P(VCL-$BIS_{1.5}$-$ABSA_{4.5}$) at the different temperatures. *Values were calculated based on the mean R_h values before and after irradiation.

A substantial body of literature concerning polymeric systems bearing azobenzene units also describes the improved hydrophilicity with the increase in polarity on switching to the *cis* form.[2(11)] However, as seen in Fig. 2(3), UV irradiation triggered rapid deswelling of the P(VCL-$BIS_{1.5}$-$ABSA_{1.5}$) and P(VCL-$BIS_{1.5}$-$ABSA_{4.5}$) microgels at temperatures below their VPTT. This seemingly counterintuitive phenomenon is actually not without precedence. Liu *et al.* studied the lower critical solution temperature (LCST) properties of poly(*N*-isopropylacrylamide) chains containing both hydrophilic oligo(ethylene oxide) and azobenzene [12-aminoundecylamido-4-phenylazobenzene (i.e. azobenzene dye with a dodecyl spacer)] introduced at varying integration levels. They found that beyond 11 mol% of azobenzene incorporation, the photo-conversion of azobenzene from the *trans* apolar isomer to the *cis* polar form led to the decrease in the LCST of the polymer by up to 5°C. They attributed this behavior to the formation of hydrophobic associates between *cis* azobenzene groups.[2(33)]

We do not however believe that the formation of hydrophobic associates between *cis*-ABSA pendant groups is the primary cause of the UV-induced dehydration in our microgels since the amount of incorporated ABSA is lower than was reported by Liu and co-workers and ABSA is attached to the polymer backbone via a shorter spacer and contains a relatively large sulfonic acid terminal group. We propose a mechanism for the UV-induced deswelling that is illustrated in Scheme 2(2). The *trans*-to-*cis* isomerization of the ABSA pendant group is not expected to be energetically expensive to the microgel system since it is provided from an external source. The *cis* form has a higher free-volume requirement than the *trans* form[2(34)] and within the confined environment of a subchain, the *cis* form is expected to bend toward the main chain. The network then seeks both entropic and enthalpic compensation to accommodate the *cis*-ABSA. Via ATR measurements, the disruption of hydrogen bonding of water molecules to the carbonyl of VCL is evident (see discussion in the next section). The rapid exclusion of water upon UV irradiation (see Fig. 2(3)) suggests that the hydrophobic state is energetically favorable. There is an entropic gain from the loss of water molecules from the network but also an increase in enthalpy from the breaking of the hydrogen bonding of water molecules to the carbonyl group of VCL. The increase in attractive hydrophobic interactions between the *cis*-ABSA and the VCL main chain most probably offsets this enthalpic increase. Furthermore, the sulfonic acid end group could contribute to the rapid disruption of hydrogen bonding interactions of water molecules to the carbonyl group of VCL upon isomerization of ABSA from the *trans* to *cis* state. The positive component of the amide of PVCL is known for its strong complexing ability to organic anions, leading to the formation of a charge-assisted hydrogen bonding interaction between the sulfonic acid group and C=O of VCL.[2(35)]

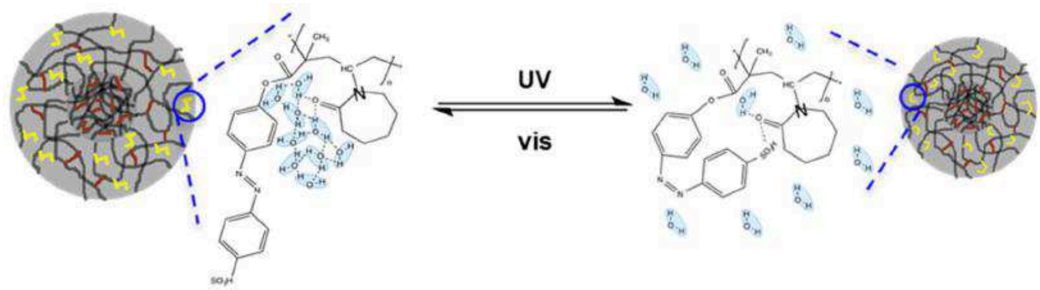

Scheme 2(2). Proposed mechanism of the photo-induced swelling-deswelling phenomenon of P(VCL-BIS-ABSA) microgels.

The percentage deswelling is higher for P(VCL-$BIS_{1.5}$-$ABSA_{4.5}$) and this is indicative of the cooperative effect of having a higher concentration of azobenzene groups.[2(36)] Fig. 2(3) shows that the photo-induced deswelling is most significant close to the VPTT of the microgels and starts to diminish above this temperature. Close to its VPTT, the hydrophobic interactions associated with chain collapse become stronger. Above their respective VPTTs, the photo-responsive effect is abated since water molecules are already removed from the network due to the heat-induced disruption of hydrogen bonding. Moreover, the UV-induced shrinking of the microgel is superceded by the temperature-induced hydrophobic-driven chain collapse. P(VCL-$BIS_{1.5}$) microgel was also investigated with UV irradiation within the DLS instrument. As seen in Fig. A2(4b) of Appendix 2, the variations in size of the P(VCL-$BIS_{1.5}$) microgel were marginal and could be attributed to minor temperature fluctuations. Fig. 2(2a) shows that the irradiated samples have their VPTT lowered by a further ~2°C compared to their native microgels. The irradiated microgel networks contain more unpolar regions than their native counterparts because of the increase in hydrophobic interactions between the polar *cis*-ABSA and the VCL main chain. The effect of employing UV LED (λ = 365 nm) of different irradiances on the UV-induced deswelling behavior of P(VCL-$BIS_{1.5}$-$ABSA_{4.5}$) was investigated via DLS and shown in Fig. A2(4a) of Appendix 2. 365 nm LED (100 mW cm^{-2}) caused a rapid deswelling, and a constant R_h value was reached after about 3 minutes of irradiation time. With LED of λ = 365 nm (1.0 mW cm^{-2}), having 100x lower irradiance, the deswelling process occurred gradually and the R_h appears to reach a constant value, that is on average, marginally higher than those attained using λ = 365 nm (100 mW cm^{-2}). This data suggest that with UV of lower irradiance but of the same wavelength, the eventual deswollen R_h value that would be attained would be similar to that achieved using UV of higher irradiance. It should, however, require a longer irradiation time to reach.[2(37)] Fig. 2(4) demonstrates the reversibility of the UV-induced deswelling. Immediately upon removal of the UV irradiation, the microgel particles of P(VCL-BIS$_{1.5}$-ABSA) appear to exhibit a slight thermal relaxation. The length of time required for thermal relaxation of the UV-irradiated microgel back to its original size in the native state is most probably correlated to the lifetime of the *cis* isomer of ABSA. The use of blue light (λ = 450 nm, 1.0 mW cm^{-2}) accelerated the re-swelling of the microgel particles but they do not regain their original size. This could be attributed to the fact that the *trans* isomer also absorbs at this wavelength. A limiting factor could also be the irradiance value of the blue light used which is 1.0 mW cm^{-2} compared to the 100 mW cm^{-2} of the 365 nm LED.

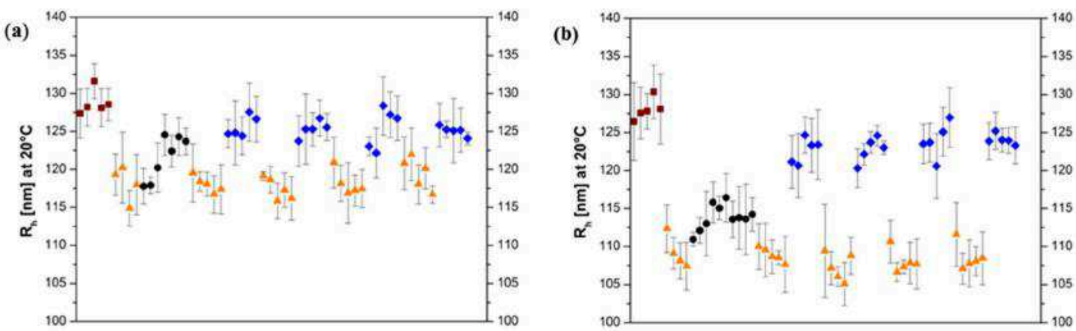

Figure 2(4). Investigation of the photo-switchability in size of (a) P(VCL-BIS$_{1.5}$-ABSA$_{1.5}$), and (b) P(VCL-BIS$_{1.5}$-ABSA$_{4.5}$) at 20°C, over several cycles, via DLS measurements. ■ points represent the R_h of the microgels in their native states, points represent the R_h reached with UV irradiation (λ = 365 nm, 100 mW cm^{-2}), ● points represent the R_h of the particles upon removal of UV and left to relax in the dark, and ◆ points represent the R_h attained with blue light irradiation (λ = 450 nm, 1.0 mW cm^{-2}). Each measurement point represents the mean of 6 x 10 seconds acquisitions in the DLS instrument.

2.4.4. Raman and ATR spectroscopic investigation of microgel photo-response

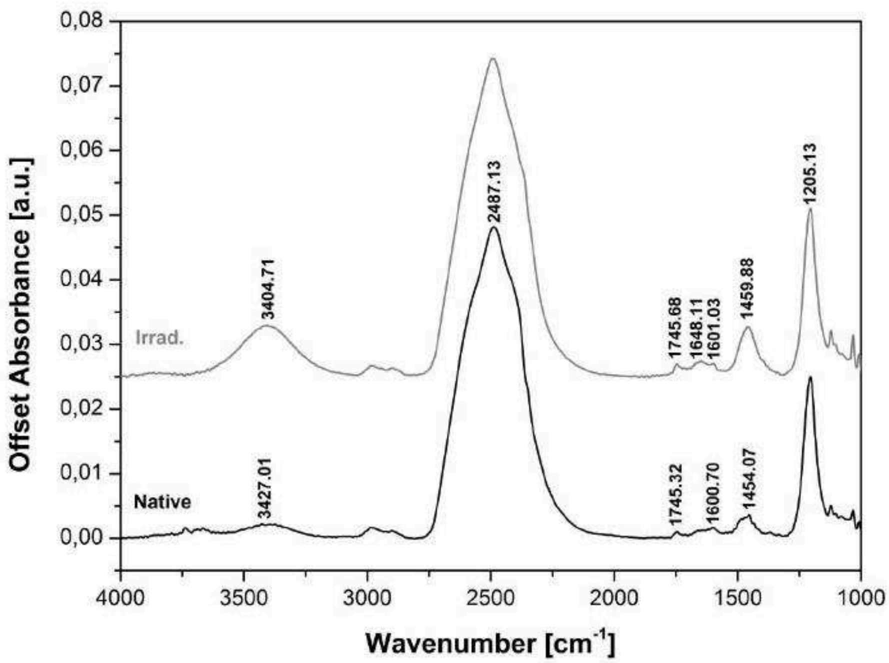

Figure 2(5). ATR spectra of (a) Native P(VCL-$BIS_{1.5}$-$ABSA_{4.5}$) in D_2O, and (b) P(VCL-$BIS_{1.5}$-$ABSA_{4.5}$) in D_2O irradiated with UV (λ = 356 nm, 100 mW cm^{-2}) for 15 minutes.

Swelling of P(VCL) microgels is due to hydrogen bonding of its highly polar C=O moieties to water molecules and conversely the deswelling can be attributed to the disruption of H-bonding between the C=O moieties and water molecules followed by the hydrophobic dehydration of C-H groups.[2(38)] The probing of changes in the absorption frequencies of the C=O moieties via IR spectroscopic techniques is therefore helpful in elucidating the mechanism of water loss from the microgel upon irradiation. Furthermore, the C=O side groups of P(VCL) is particularly sensitive because of their larger degree of freedom in relation to the backbone. They therefore display a faster response than the backbone during both hydration and dehydration of the network.[2(38a)]

We performed Raman spectroscopic measurement of neat P(VCL-$BIS_{1.5}$), as shown in Fig. A2(5) of Appendix 2, and ATR measurements of P(VCL-$BIS_{1.5}$-$ABSA_{4.5}$) microgel sample shown in Fig. 2(5). We were interested in determining how the C=O absorption band(s) of VCL in a P(VCL-BIS-ABSA) microgel change after UV irradiation and in doing so attempt to understand the mechanism of UV-induced deswelling phenomenon. P(VCL-$BIS_{1.5}$-$ABSA_{4.5}$) was redispersed in D_2O at a 10 wt% concentration, under ambient conditions. The microgel in D_2O can be assumed to be in their native swollen state. D_2O was selected as a solvent instead of H_2O in order to avoid the overlap of the bending mode of water (1500-1700 cm^{-1}) with the important absorption bands needed for analysis, namely the C=O related stretching vibrations (1645-1570 cm^{-1}) of P(VCL). It is nonetheless unavoidable that D_2O does contain trace amounts of HDO and H_2O molecules and that the bending modes of HOD and HOH do contribute minimally to the absorption band in the spectral region 1500-1700 cm^{-1}. The maximum absorbance for water stretching vibrations in single bounce mode ATR is typically low at 0.15.[2(39)] Nonetheless, ATR as a technique remains particularly useful in distinguishing between waters of hydration from bulk water of aqueous suspensions.

According to Liu *et al*., the C=O stretching vibrations of P(VCL) occur in the region between 1550-1700 cm^{-1}.[2(38b)] Via a curve fitting procedure, they attributed the band at 1640 cm^{-1} to anhydrous C=O stretching, 1610 cm^{-1} to C=O with a single H-bonding interaction with H_2O molecule and 1590 cm^{-1} to C=O with two H-bonding interactions to H_2O molecules. Shifts in these bands to lower wavenumbers are indicative of further hydration of primary H-bonded structures.[2(38b)] We observe the anhydrous C=O stretching vibration *v*(free C=O) at ~1632 cm^{-1} in the Raman spectrum (Fig. A2(5) of Appendix 2) of lyophilized P(VCL-$BIS_{1.5}$) microgel. This band is weak in the spectrum of 10 wt% P(VCL-$BIS_{1.5}$-$ABSA_{4.5}$) in D_2O (see Fig. 2(5)), and appears at ~1650cm^{-1}. Instead, a more prominent absorption band appears at ~1600 cm^{-1}. This band could be ascribed to C=O groups that are doubly H-bonded to water molecules, *v*(doubly H-bonded C=O). All the absorption bands, meaningful to our discussion and their corresponding assignments, are presented in Table A2(1) of Appendix 2. A comparison of the spectra of native P(VCL-$BIS_{1.5}$-$ABSA_{4.5}$) and UV-irradiated P(VCL-$BIS_{1.5}$- $ABSA_{4.5}$) is shown in Fig. 2(5). Of particular interest are the bands at ~1600 cm^{-1} *v*(doubly H-bonded C=O) and ~1648 cm^{-1} *v*(free C=O). The intensity of the band at 1648 cm^{-1} appears to increase relative to that of the band at 1599 cm^{-1} upon UV irradiation. This is indicative of the increase in anhydrous C=O groups upon UV irradiation. Concomitantly, there appears to be an increase in absorption intensity of the broad band associated with the stretching band of bulk water *v*(H_2O) + *v*(HOD). In the spectrum of native P(VCL-$BIS_{1.5}$-$ABSA_{4.5}$), this band appears to have a peak centered at ~3427 cm^{-1} while this peak is shifted to lower frequency (~3405 cm^{-1}) in the spectrum of irradiated P(VCL-$BIS_{1.5}$-$ABSA_{4.5}$). This indicates that upon UV irradiation, the water molecules H-bonded to C=O groups are transformed to free molecules in bulk water. The shift to lower frequency can be explained by the formation of water clusters in the bulk water. The Raman and ATR data therefore provide a qualitative confirmation to our hypothesis that the isomerization of ABSA side groups from the *trans* to *cis* isomer occurs such that the ABSA pendant group bends toward the P(VCL) backbone thereby causing the dehydration of the VCL units.

2.4.5. Probing of VCL microgel internal morphology by high-resolution ^{1}H MAS transverse relaxation (T_2) NMR measurements

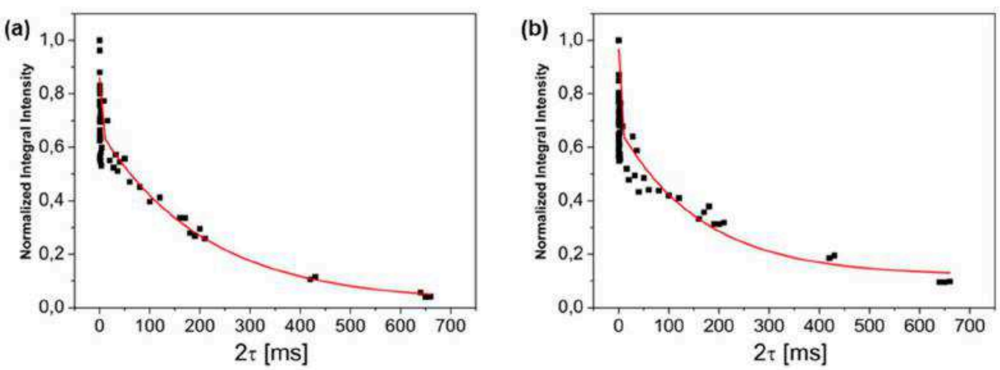

Figure 2(6). ^{1}H NMR transverse relaxation decay by spin echo fitted with biexponential decay function (solid line) of P(VCL-BIS$_{1.5}$-ABSA$_{4.5}$) with concentration of 5 wt.% in D_2O in its (a) native, and (b) irradiated (365 nm, 100 mW cm^{-2}, 15 min) states at 24°C.

We measured the T_2 decay values of P(VCL-BIS$_{1.5}$-ABSA$_{4.5}$) by the spin echo method (Table 2(2)) and also compared the aggregate integral intensities of all the VCL proton signals ($\boldsymbol{I}_{VCL}$) of the native sample of P(VCL-BIS$_{1.5}$-ABSA$_{4.5}$) with those of the irradiated sample (see Fig. 2(6)). From the T_2 values, we recognize heterogeneity in the internal morphology of the microgel. This is inevitable when the BIS cross-linker is more reactive than VCL and leads to what is usually described as a core-shell structure where a more highly cross-linked core is separated from a less densely cross-linked corona by diffuse boundaries.[2(40)]

Table 2(2). Transverse relaxation times (T_2) of protons in the aliphatic region (0-2 ppm) of P(VCL-BIS$_{1.5}$-ABSA$_{4.5}$), under native and UV-irradiated conditions. The fits of the T_2 decays by spin echo were performed using a biexponential function.

	$T_{2,short}$* [ms]	$T_{2,long}$* [ms]
Native	0.23	209.9
UV-irradiated	0.04	0.166

*Errors are of the order of 10%.

The core has a shorter T_2 value ($T_{2,short}$) than the corona ($T_{2,long}$) and their respective values in the native and irradiated microgels are presented in Table 2(2). UV-induced decrease in T_2 is much more significant in the less densely cross-linked corona, indicating that a less cross-linked network is more sensitive to UV irradiation and that the UV-induced shrinking in P(VCL-BIS$_{1.5}$-ABSA$_{4.5}$) particles occurs primarily in the corona.

The $\boldsymbol{I}_{VCL}$ show a clear decrease upon irradiation. This indicates a more restricted motion of the VCL chain after UV irradiation which is similar to the increasingly restricted motions of the chains in the gel network as the temperature increases.[2(41)] In its native state, the microgel particle is more swollen compared to the irradiated particle. The spaces between the polymer chains are larger and the correlation time (the time between rotations) is smaller. The transverse relaxation time is therefore longer and the resonance lines in the NMR spectrum of the native microgel appear narrower and better resolved. With UV irradiation, the microgel particles deswell, the motions of the protons become hindered due to the diminished space between polymer chains, the correlation time becomes larger, the transverse relaxation time decreases, and the resonance lines broaden or shrink, leading to a decrease in integral intensity. In keeping with our proposed mechanism (Scheme 2(2)), the approach of the *cis*-ABSA pendant group toward the P(VCL) backbone favors the increase in hydrophobic interactions between the polar *cis* ABSA and the VCL units. These interactions arise from a dipole/induced dipole interaction of the aromatic benzene rings with the aliphatic ring of VCL and via the interaction of the sulfonic acid end group with the amide group of the caprolactam ring which is probably a combination of both hydrogen bonding and electrostatic interactions.[2(29),2(32),2(35),2(42)]

2.4.6. Description of microgel photo-response based on Flory-Rehner model

Equation (1) was used to model the size-temperature data of the native microgels and their irradiated counterparts. The fitting parameters obtained are listed in Table 2(3). We analyzed how these parameters change with the amount as well as with the isomeric nature of the ABSA side group. Table 2(3) shows that the polymer volume fraction, ϕ_0, of all three microgels are very similar and this is unsurprising since the cross-linker to total monomer ratio as well as the concentration of monomer in water in the feed solution were kept constant. The Flory interaction parameter χ is a crucial parameter obtained from the fit and accounts for the polymer-polymer and polymer-solvent interactions and is responsible for the collapse of the microgel particle.[2(43)] The changes and differences in χ elucidates the change in the quality of the solvent for the polymer gel.[2(25)] In a good solvent where the polymer-solvent interaction is more favorable than the polymer-polymer interaction, χ assumes a lower value. In systems possessing a lower critical VPTT, χ increases with temperature since solvent quality becomes increasingly poorer. Our microgels exhibit this same tendency as shown in Fig. 2(2b). Below the VPTT, the Flory interaction parameter scales linearly with 1/T, but not above this temperature.

Table 2(3). Fit parameters obtained from the homogeneous homopolymeric Flory-Rehner model.

	P(VCL-bis$_{1.5}$)	P(VCL-bis$_{1.5}$-ABSA$_{1.5}$)	P(VCL-bis$_{1.5}$-ABSA$_{1.5}$) irrad.	P(VCL-bis$_{1.5}$-ABSA$_{4.5}$)	P(VCL-bis$_{1.5}$-ABSA$_{4.5}$) irrad.
N	179823	377121	377121	136021	136021
Θ	307.78	297.6	296.11	301.15	298.25
A	-17.47	-6.37	-5.24	-8.63	-5.35
χ_1	0.38	0.33	0.42	0.31	0.45
Φ_0	0.9	0.87	0.8	0.9	0.8

Fig. 2(2b) also shows how the χ value varies as a function of ABSA comonomer content and as a function of UV irradiation, over the investigated temperature range. At temperatures below 25°C, seen on the right side of Fig. 2(2b), the P(VCL-BIS$_{1.5}$) microgel displays a much lower χ than the other two microgels. This indicates a higher affinity for water than the ABSA-containing microgels. This has been attributed in the earlier section to the relatively unrestricted hydrogen bonding of water molecules to the C=O groups of VCL arranged syndiotactically along the main chain, thus promoting good solvation of the polymer chains. P(VCL-$BIS_{1.5}$-$ABSA_{4.5}$) appears to have a slightly higher affinity for water than P(VCL-$BIS_{1.5}$-$ABSA_{1.5}$) at temperatures below 25°C. Its higher ABSA content favors more extensive polymer-water interactions most probably due to the presence of hydrophilic methacrylic ester unit and a sulfonic acid end group.[2(44)] Irradiated P(VCL-BIS-ABSA) microgels show lower affinity for water than their native counterparts, especially at temperatures below 20°C. Irradiated microgels contain a higher proportion of *cis* azobenzene which as discussed earlier promotes disruption of hydrogen bonding interactions with water molecules and increased hydrophobic interactions with the polymer backbone. Additionally, there could be a small contribution to the increased polymer-polymer interactions from the attractive dipole-dipole interaction between adjacent *cis* azobenzene moieties within the network. Both these interactions are expected to increase with the total dipole concentration.[2(36),2(45)] A combination of these forces promotes stronger polymer-polymer interactions relative to polymer-water interactions, resulting in higher χ values for the irradiated microgels.

The left side of Fig. 2(2b) shows the relationship between χ and 1000/T above the VPTT of the microgels. We observe that above its VPTT, P(VCL-$BIS_{1.5}$) has a lower affinity for water than the P(VCL-$BIS_{1.5}$-ABSA) microgels. The absence of ABSA side groups allows closer approach of the polymer chains due to smaller excluded volume effect within the chain segments and therefore stronger hydrophobic interactions between the chains. P(VCL-$BIS_{1.5}$-ABSA) microgels in their native states have lower affinities for water than their irradiated counterparts. Presumably this could be attributed to the *trans* azobenzene side groups in the native gels allowing closer ordering and greater attractive interactions of the chains in their collapsed states. In the collapsed state, the cooperative effect of more extensive *trans* azobenzene - *trans* azobenzene interactions could also account for the lower affinity for water of P(VCL-$BIS_{1.5}$-$ABSA_{4.5}$) compared to P(VCL-$BIS_{1.5}$-$ABSA_{1.5}$).

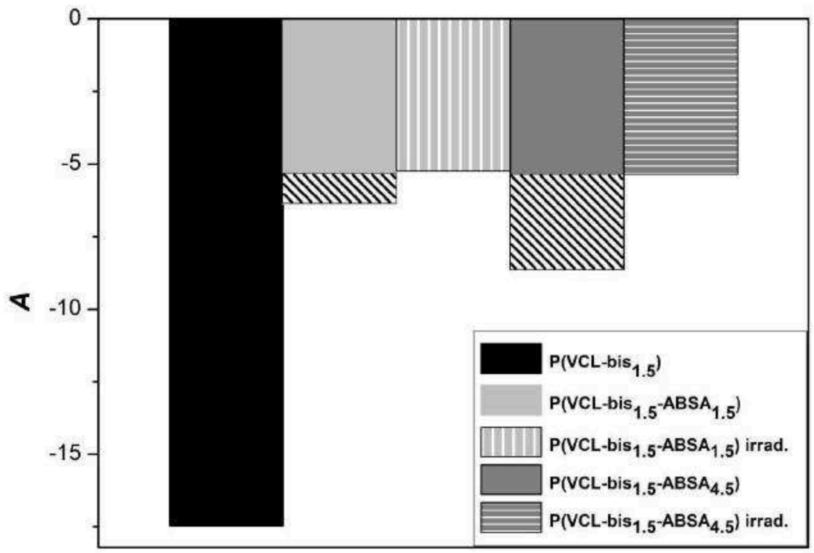

Figure 2(7). Graph of the values of the second virial coefficients, *A*, of the microgels, as obtained from the fit with equation of state (1). The shaded regions (oblique lines) show the difference in *A* quantity between UV-irradiated and native microgels and is proportional to the Δ*S* associated with the volume changes due solely to UV stimulus.

Table 2(3) shows that the θ values of P(VCL-BIS-ABSA) microgels are lower than that of P(VCL-BIS) microgel. The values decrease further in the irradiated microgels. These results agree with the decrease in VPTT observed in the DLS size-temperature data (Fig. 2(2a)). θ represents the spinodal temperature of the microgel particles at which the collapse is complete and usually has a higher value compared to the measured VPTT, which is often, and also in our case defined as the inflexion point of the swelling curve where the second derivative is zero.[2(25)] From the second virial coefficients, *A*, presented in Fig. 2(7), a measure of the average entropic change associated with deswelling caused solely by light stimulus can be estimated. The magnitude of the second virial coefficient, *A*, is proportional to the change in entropy during transition from the swollen to deswollen state. P(VCL-BIS$_{1.5}$) shows the greatest *ΔS* because of the largest volume of water excluded during deswelling. The values of *A* in Fig. 2(7) of the irradiated microgels samples (-5.2) were computed from the fit of the size-temperature data of the respective microgel solutions subjected to both UV and temperature stimuli. Below the VPTT, we can assume that the volume decrease can be attributed solely to the UV stimulus. Above the VPTT, the UV stimulus does not trigger any additional macroscopic volume decrease in the collapsed microgels, as shown by our dynamic light scattering measurements in Fig. 2(3). Since the irradiated microgels and their native counterparts have the same end collapsed hydrodynamic size, the difference in *A* values (regions shown in Fig. 2(7) that are shaded with oblique lines) between the irradiated and native microgels can be assumed to be proportional to the ΔS associated with the volume change due solely to UV stimulus. These values should be taken with some degrees of error and represent mean values, since the volume changes due to UV stimulus is not entirely uniform at the different temperatures below VPTT. The ΔS associated with the volume change due solely to the UV stimulus is greater in P(VCL-$BIS_{1.5}$-$ABSA_{4.5}$) than in P(VCL-$BIS_{1.5}$-$ABSA_{1.5}$), and can be understood from the higher hydrophobic interactions in the network with higher ABSA content. As a corollary, the magnitude of *A* computed for the irradiated microgels are proportional to the ΔS associated solely with the temperature-induced transition. With this in mind, the ΔS for P(VCL-$BIS_{1.5}$-$ABSA_{1.5}$) and P(VCL-$BIS_{1.5}$-$ABSA_{4.5}$) under temperature stimulus can be seen to be very similar. This can be attributed to the fact that these microgels contain similar amounts of VCL and BIS.

2.4.7. Morphology and topography of P(VCL-$BIS_{1.5}$-$ABSA_{4.5}$) microgel before and after UV irradiation

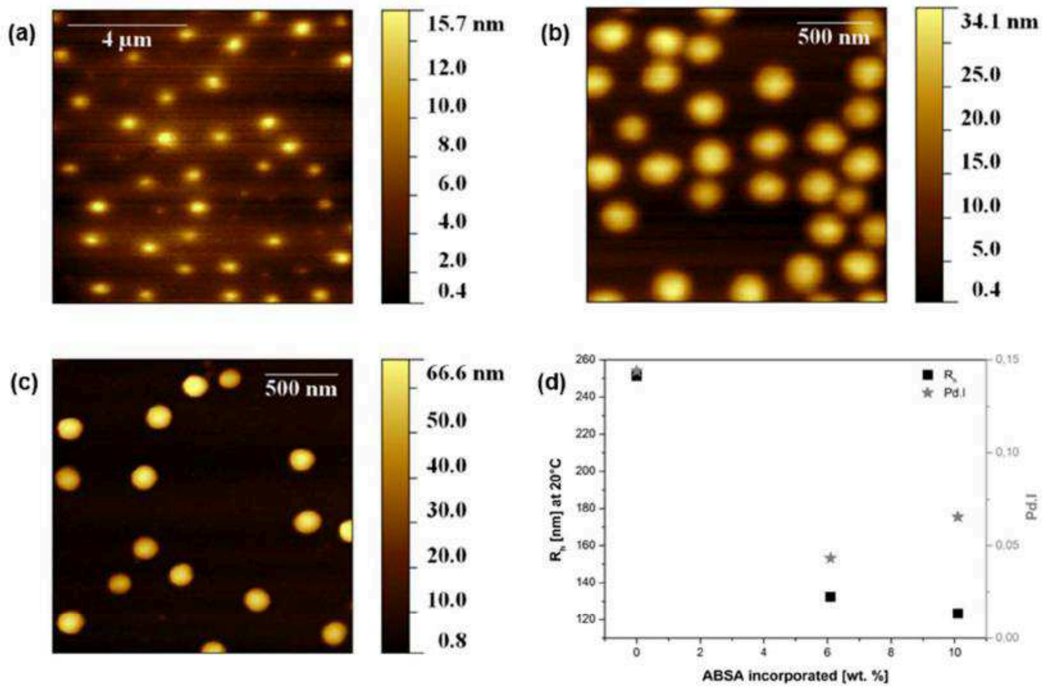

Figure 2(8). AFM topography images of (a) P(VCL-$BIS_{1.5}$), (b) P(VCL-$BIS_{1.5}$-$ABSA_{1.5}$), and (c) P(VCL-$BIS_{1.5}$-$ABSA_{4.5}$). (d) R_h of microgels, obtained via a cumulant fit and as measured in DLS at 20°C, as a function of incorporated ABSA amount.

AFM was employed to investigate the morphology and topography of the microgels on a hydrophilized Si substrate. Fig. 2(8a) shows that the P(VCL-$BIS_{1.5}$) particles are strongly deformed and flattened on the Si substrate in contrast to the P(VCL-$BIS_{1.5}$-ABSA) particles (seen in Fig. 2(8b) and 2(8c)) which appear harder. The size of the individual particles of P(VCL-$BIS_{1.5}$) in Fig. 2(8a) are around doubled that observed by DLS. Meanwhile, the sizes of P(VCL-$BIS_{1.5}$-$ABSA_{1.5}$) and P(VCL-$BIS_{1.5}$-$ABSA_{4.5}$) in Fig. 2(8b) and 2(8c) respectively correspond well with the sizes obtained in DLS. These observations correlate well with the evidence that P(VCL-$BIS_{1.5}$) is softer since it has a higher degree of swelling than the other microgels. Presumably the ABSA moieties incorporated within the P(VCL-$BIS_{1.5}$-ABSA) microgels provide stronger structural integrity to the particles since they are less deformed on the Si substrate. We also investigated the difference in the height profiles and morphologies of P(VCL-$BIS_{1.5}$-$ABSA_{4.5}$) microgel particles before and after 15 minutes of UV (λ = 365nm, 100 mW cm^{-2}) irradiation. UV irradiation was performed on the same P(VCL-$BIS_{1.5}$-

ABSA$_{4.5}$) microgel solution before it was spin-coated onto a silicon wafer. Fig. 2(9a) and 2(9b) show the 3D representations of the native and irradiated P(VCL-BIS$_{1.5}$-ABSA$_{4.5}$) particles respectively while Fig. 2(9c) shows the typical height cross-section profiles of the native and irradiated P(VCL-BIS$_{1.5}$-ABSA$_{4.5}$) microgel particles, taken not of the same particle. The UV-irradiated particles showed a discernible decrease in particle height and an increase in lateral diameter compared to the native microgel particles imaged prior to UV exposure.

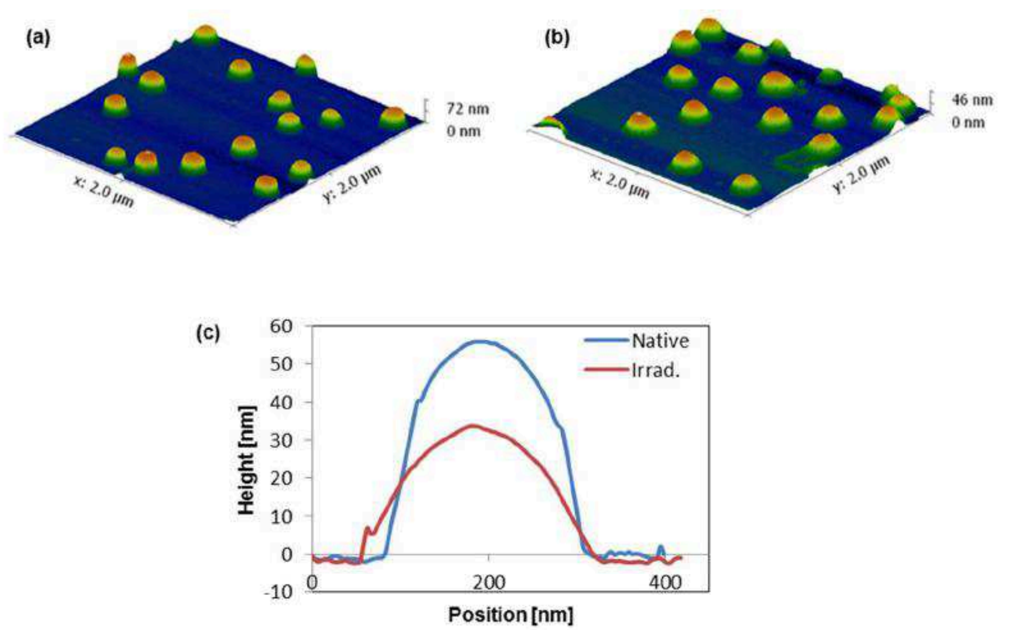

Figure 2(9). 3D representations of the AFM topography images of (a) Native P(VCL-BIS$_{1.5}$-ABSA$_{4.5}$), and (b) UV-irradiated P(VCL-BIS$_{1.5}$-ABSA$_{4.5}$). Typical height cross-section profiles of (c) P(VCL-BIS$_{1.5}$-ABSA$_{4.5}$) microgel particles before and after UV irradiation.

An evaluation was made on seven single particles each of native and irradiated P(VCL-BIS$_{1.5}$-ABSA$_{4.5}$) (Fig. 2(9a) and 2(9b), respectively). The average height and lateral diameter of the native and irradiated samples, respectively, were computed and compared (detailed information is found in Fig. A2(7) of Appendix 2). The average percentage decrease in height of the particles after UV irradiation was found to be ~38% while the average percentage increase in lateral diameter was close to 31%. This result provides evidence of more deformable particles after UV irradiation, analogous to the observations made of the height cross-section profiles of P(VCL-BIS) microgel particles with lower BIS cross-linking density.[2(40)] While they report that the increased deformation of their microgel particles arises from an increased softness of the particles as BIS cross-linking density decreases, the deformation in our irradiated microgel probably stems from a combination of deswelling and the formation of specific interactions with the Si substrate. This UV-induced deformation could have beneficial implications when using these microgels at interfaces, for instance in the formation of aqueous or non-aqueous simple and multiple emulsions to transport drug molecules. Microgels at the oil-water interface tend to adopt a flattened morphology and presumably, UV responsive P(VCL-bis-ABSA) particles could be further deformed at the interface under UV.[2(46)] This could significantly affect, for instance, how these microgels adsorb at interfaces and thereby influence the stability of emulsions formed by them.

2.5. Conclusion

N-Vinylcaprolactam was copolymerized in a two-step surfactant-free precipitation polymerization in water with 1.5 and 4.5 mol % feed amounts of a hydrophilic azobenzene comonomer, 4-[(4-Methacryloyloxy)phenylazo] benzenesulfonic acid, in order to prepare dual thermo- and photo-responsive microgels.

Size-temperature data obtained from dynamic light scattering measurements show that the azobenzene-containing microgels display volume phase transition temperatures that are shifted to lower temperatures relative to pure P(VCL-BIS) microgels. UV irradiation of λ = 365 nm induces the isomerization of *trans* ABSA side groups in P(VCL-BIS-ABSA) microgels, producing up to 36% *cis*-ABSA in the photo-stationary state. As a result of this *trans*-*cis* isomerization, the microgels deswell at temperatures below their VPTT by up to 28% of their sizes in the native state. This photo-response is especially pronounced for the microgel with 4.5 mol% feed amount of azobenzene comonomer and at a temperature of 24°C, which is in the vicinity of its VPTT. Above the VPTT of the microgels, no photo-response was detected by DLS. To our knowledge, this is the first reported instance of rapid and significant deswelling of P(VCL)-based microgels upon UV-induced *trans*-to-*cis* isomerization of small amounts (≤ 10 wt. %) of incorporated azobenzene pendant groups within the microgel matrix.

The mechanism for the UV-induced deswelling is analogous to that of a temperature induced deswelling of P(VCL-BIS) microgels. Within the microgels, the bent and bulky *cis*-ABSA side groups are most likely to be oriented toward the VCL units in the main chain. This results in increased hydrophobic interactions between the polar *cis* side groups with the main chain and causes a dehydrating effect on the VCL units as investigated via attenuated total reflection (ATR) and high-resolution

MAS transverse relaxation (T_2) NMR measurements. ATR investigation indicates the disruption of hydrogen bonding interaction of water molecules to the carbonyl groups while T_2 proton NMR relaxometry indicate the hydrophobic dehydration of the VCL units associated with the isothermal UV-induced deswelling of the P(VCL-BIS-ABSA) microgels. Additionally, the UV-induced deswelling was found to be reversible by application of blue light to trigger the back-isomerization of the azobenzene moieties from the *cis* to *trans* state.

An equation of state based on the Flory-Rehner theory that describes the swelling of homopolymeric microgels with homogeneous cross-link distribution was used to model the temperature- and photo-induced transitions of our microgels. This fitting and the Flory-Rehner parameters obtained from it provide a preliminary description of the microscopic mechanisms at play and the correlated changes in the morphology of the microgel network during temperature and photo-stimulations. It therefore aids in the initial understanding of the main features in the volume transition of these dual thermo- and photo-responsive microgels.

AFM investigations further reveal the mechanical robustness and responsive nature of the microgels. The organized motions occurring within the microgel network due to photo-stimulation resulted in nanoscale morphological and topographical changes when the irradiated microgels were adsorbed onto a hydrophilized Si substrate. The irradiated microgels were found to be more deformable than their native counterparts. This has important implications when considering the use of such microgels at interfaces or on membranes.

2.6. Outlook

The microgels synthesized here contain sulfonic acid moieties from the ABSA pendant groups. These negative charges can be used to bind cationic molecules including drugs, and metallic targets or aid in the formation of highly ordered nanostructures such as LbL assemblies. This would position the microgels as unique multi-responsive building blocks for the development of advanced smart functional materials, which are sensitive to non-invasive and easily controlled stimuli.

Azobenzenes bearing other functional groups could be considered. For instance, Han and co-workers reported that azobenzene derivatives containing a CN^- group are more polar in the thermodynamically stable *trans* form compared to the *cis* form.[2(45c)] It could be worthwhile to investigate the possibility of incorporating such an azobenzene moiety as a pendant group in P(VCL) microgels and determine if the deswelling extent could be larger than what we have reported here.

Red-shifting the photo-switching wavelength of the azobenzene moieties into the more physiologically benign region of the electromagnetic spectrum could extend the utility of such microgel particles for biomedical release applications, even within the intracellular environment.[2(47)] One strategy involves the 2,2'6,6'-*ortho*-tetramethoxy substitution of the phenyl rings which allow for the trans-to-cis and cis-to-trans photoisomerization to occur with green and blue light respectively.[2(48)] Another strategy is to exploit the two-photon absorption of the azobenzene moieties in photodynamic therapy, for instance.[2(49)]

2.7. REFERENCES

2(1) Croce, R.; van Amerongen, H. Natural Strategies for Photosynthetic Light Harvesting. *Nature Chem. Biol.* **2014**, *10*, 492–501.

2(2) Nedosekin, D. A.; Verkhusha, V. V.; Melerzanov, A. V.; Zharov, V. P.; Galanzha, E. I. *In Vivo* Photoswitchable Flow Cytometry for Direct Tracking of Single Circulating Tumor Cells. *Chem. Biol.* **2014**, *21*, 792-801.

2(3) Bellini, B.; Ackermann, J.; Klein, H.; Grave, C.; Dumas, P.; Safarov, V. Light-induced Molecular Motion of Azobenzene-containing Molecules: A Random-walk Model. *J. Phys.: Condens. Matter* **2006**, *18*, S1817-S1835.

2(4) (a) Lee, H.; Wu, W.; Oh, J. K.; Mueller, L.; Sherwood, G.; Peteanu, L.; Kowalewski, T.; Matyjaszewski, K. Light-induced Reversible Formation of Polymeric Micelles. *Angew. Chem. Int. Ed.* **2007**, *46*, 2453-2457.; (b) Tomatsu, I.; Peng, K.; Kros, A. Photoresponsive Hydrogels for Biomedical Applications. *Adv. Drug Deliv. Res.* **2011**, *63*, 1257-1266.; 2(c) Fomina, N.; Sankaranarayanan, J.; Almutairi, A. Photochemical Mechanisms of Light-triggered Release from Nanocarriers. *Adv. Drug Deliv. Rev.* **2012**, *64*, 1005-1020.; (d) Menon, J. U.; Jadeja, P.; Tambe, P.; Vu, K.; Yuan, B.; Nguyan, K. T. Nanomaterials for Photo-Based Diagnostic and Therapeutic Applications. *Theranostics* **2013**, *3*, 152-166.

2(5) Yu, G.; Cao, Y.; Wang, J.; McElvain, J.; Heeger, A. J. High Sensitivity Polymer Photosensors for Image Sensing Applications. *Synthetic Met.* **1999**, *102*, 904-907.

2(6) Shimoboji, T.; Larenas, E.; Fowler, T.; Kulkarni, S.; Hoffman, A.; Stayton, P. S. Photoresponsive Polymer–Enzyme Switches. *PNAS* **2002**, *99*, 16592-16596.

2(7) Jochum, F. D.; Forst, F. R.; Theato, P. PNIPAM Copolymers Containing Light-Responsive Chromophores: A Method Toward Molecular Logic Gates. *Macromol. Rapid Commun*. **2010**, *31*, 1456-1461.

2(8) (a) Chujo, Y.; Sada, K.; Saegusa, T. Polyoxazoline Having a Coumarin Moiety as a Pendant Group. Synthesis and Photogelation. *Macromolecules* **1990**, *23*, 2693-2697.; (b) Chen, Y.; Geh, J.-L. Copolymers Derived from 7-Acryloyloxy-4-methylcoumarin and Acrylates: 2. Reversible Photocrosslinking and Photocleavage. *Polymer* **1996**, *37*, 4481-4486.; (c) Yamamoto, H.; Kitsuki, T.; Nishida, A.; Asada, K.; Ohkawa, K. Photoresponsive Peptide and Polypeptide Systems. 13. Photoinduced Cross-Linked Gel and Biodegradation Properties of Copoly(l-lysine) Containing ε-7-Coumaryloxyacetyl-l-lysine Residues. *Macromolecules* **1999**, *32*, 1055-1061.; (d) He, J.; Tong, X.; Zhao, Y. Photoresponsive Nanogels Based on Photocontrollable Cross-Links. *Macromolecules* **2009**, *42*, 4845-4852.

2(9) (a) Hirakura, T.; Nomura, Y.; Aoyama, Y.; Akiyoshi, K. Photoresponsive Nanogels Formed by the Self-Assembly of Spiropyrane-Bearing Pullulan That Act as Artificial Molecular Chaperones. *Biomacromolecules* **2004**, *5*, 1804-1809.; (b) Sumaru, K.; Ohi, K.; Takagi, T.; Kanamori, T.; Shinbo, T. Photoresponsive Properties of Poly(*N*-isopropylacrylamide) Hydrogel Partly Modified with Spirobenzopyran. *Langmuir* **2006**, *22*, 4353–4356.; (c) Garcia, A.; Marquez, M.; Cai, T.; Rosario, R.; Hu, Z.; Gust, D.; Hayes, M.; Vail, S. A.; Park, C.-D. Photo-, Thermally, and pH-Responsive Microgels. *Langmuir* **2007**, *23*, 224-229.; (d) Satoh, T.; Sumaru, K.; Takagi, T.; Kanamori, T. Fast-reversible Light-driven Hydrogels Consisting of Spirobenzopyran-functionalized Poly(*N*-isopropylacrylamide). *Soft Matter* **2011**, *7*, 8030-8034.

2(10) Natansohn, A.; Rochon, P. Photoinduced Motions in Azo-Containing Polymers. *Chem. Rev.* **2002**, *102*, 4139-4176 and references therein.

2(11) (a) Kungwatchakun, D.; Irie, M. Photoresponsive polymers. Photocontrol of the Phase Separation Temperature of Aqueous Solutions of Poly-[*N*-isopropylacrylamide-co-*N*-(4-phenylazophenyl)acrylamide]. *Makromol. Chem. Rapid. Commun.* **1988**, *9*, 243-246.; (b) Kroeger, R.; Menzel, H.; Hallensleben, M. L. Light Controlled Solubility Change of Polymers: Copolymers of *N,N*-dimethylacrylamide and 4-phenylazophenyl acrylate. *Macromol. Chem. Phys.* **1994**, *195*, 2291-2298.; (c) Akiyama, H.; Tamaoki, N. Polymers Derived from *N*-isopropylacrylamide and Azobenzene-containing Acrylamides: Photoresponsive Affinity to Water. *J. Polym. Sci. A Polym. Chem.* **2004**, *42*, 5200-5214.; (d) Akiyama, H.; Tamaoki, N. Synthesis and Photoinduced Phase Transitions of Poly(*N*-isopropylacrylamide) Derivative Functionalized with Terminal Azobenzene Units. *Macromolecules* **2007**, *40*, 5129-5132.; (e) Jochum, F. D.; Theato, P. Temperature and Light Sensitive Copolymers Containing Azobenzene Moieties Prepared via a Polymer Analogous Reaction. *Polymer* **2009**, *50*, 3079–3085.; (f) Li, L.; Xing, X.; Liu, Z. Triply-responsive (Thermo/Light/pH) Copolymeric Hydrogel of *N*-Isopropylacrylamide with an Azobenzene-containing Monomer. *J. Appl. Polym. Sci.* **2012**, *124*, 1128-1136.; (g) Zhu, L.; Zhao, C.; Zhang, J.; Gong, D. Photocontrollable Volume Phase Transition of an Azobenzene Functionalized Microgel and its Supramolecular Complex. *RSC Adv.* **2015**, *5*, 84263-84268.

2(12) Zhang, Q. M.; Li, X.; Islam, M. R.; Wie, M.; Serpe, M. J. Light Switchable Optical Materials from Azobenzene Crosslinked Poly(*N*-isopropylacrylamide)-based Microgels. *J. Mater. Chem. C* **2014**, *2*, 6961-6965.

2(13) Zakrevskyy, Y.; Richter, M.; Zakrevska, S.; Lomadze, N.; von Klitzing, R.; Santer, S. Light-Controlled Reversible Manipulation of Microgel Particle Size Using Azobenzene-Containing Surfactant. *Adv. Funct. Mater.* **2012**, *22*, 5000-5009.

2(14) (a) Desponds, A.; Freitag, R. Synthesis and Characterization of Photoresponsive *N*-Isopropylacrylamide Cotelomers. *Langmuir* **2003**, *19*, 6261–6270.; (b) Boissiere, O.; Han, D.; Tremblay, L.; Zhao, Y. Flower Micelles of Poly(*N*-Isopropylacrylamide) with Azobenzene Moieties Regularly Inserted into the Main Chain. *Soft Matter* **2011**, *7*, 9410–9415.

2(15) (a) Ramos, J.; Imaz, A.; Forcada, J. Temperature-sensitive Nanogels: Poly(*N*-Vinylcaprolactam) versus Poly(*N*-Isopropylacrylamide). *Polym. Chem.* **2012**, *3*, 852-856.; (b) Wang, Y.; Nie, J.; Chang, B.; Sun, Y.; Yang, W. Poly(vinylcaprolactam)-Based Biodegradable Multiresponsive Microgels for Drug Delivery. *Biomacromolecules* **2013**, *14*, 3034-3046.; (c) Shen, L.; Pich, A.; Fava, D.; Wang, M.; Kumar, S.; Wu, C.; Scholes, G. D.; Winnik, M. A. Loading Quantum Dots into Thermo-responsive Microgels by Reversible Transfer from Organic Solvents to Water. *J. Mater. Chem.* **2008**, *18*, 763-770.; (d) Imaz, A.; Forcada, J. *N*-Vinylcaprolactam-based Microgels: Synthesis and Characterization. *J. Polym. Sci. Part A: Polym. Chem.* **2008**, *46*, 2510–2524.

2(16) Gong, C. B.; Wong, K. L.; Lam, M. H. W. Photoresponsive Molecularly Imprinted Hydrogels for the Photoregulated Release and Uptake of Pharmaceuticals in the Aqueous Media. *Chem. Mater.* **2008**, *20*, 1353-1358.

2(17) Boyko, V.; Pich, A.; Lu, Y.; Richter, S.; Arndt, K.-F.; Adler, H.-J. P. Thermo-sensitive Poly(*N*-Vinylcaprolactam-co-acetoacetoxyethyl methacrylate) Microgels: 1—Synthesis and Characterization. *Polymer* **2003**, *44*, 7821-7827.

2(18) Ernst, R. R.; Bodenhausen, G.; Wokaun, A. *Principles of Nuclear Magnetic Resonance in One and Two Dimensions*; Clarendon Press: Oxford, 1987.

2(19) Flory, P. J.; Rehner, J. Statistical Mechanics of Cross‐Linked Polymer Networks II. Swelling. *J. Chem. Phys.* **1943**, *11*, 521-526.

2(20) Balaceanu, A.; Demco, D. E.; Möller, M.; Pich, A. Microgel Heterogeneous Morphology Reflected in Temperature-Induced Volume Transition and ^{1}H High-Resolution Transverse Relaxation NMR. The Case of Poly(*N*-Vinylcaprolactam) Microgel. *Macromolecules* **2011**, *44*, 2161–2169.

2(21) Fernández-Barbero, A.; Fernández-Nieves, A.; Grillo, I.; López-Cabarcos, E. Structural Modifications in the Swelling of Inhomogeneous Microgels by Light and Neutron Scattering. *Phys. Rev. E* **2002**, *66*, 051803-051812.

2(22) Quesada-Perez, M.; Maroto-Centeno, J.A.; Forcadab, J.; Hidalgo-Alvarez, R. Gel Swelling Theories: The Classical Formalism and Recent Approaches. *Soft Matter* **2011**, *7*, 10536-10547.

2(23) Lietor-Santos, J. J.; Kim, C.; Lu, P. J.; Fernandez-Nieves, A.; Weitz, D. A. Gravitational Compression of Colloidal Gels. *Eur. Phys. J. E.* **2009**, *28*, 159-164.

2(24) Stieger, M.; Richtering, W.; Pedersen, J.S.; Linder, P. Small-angle Neutron Scattering Study of Structural Changes in Temperature Sensitive Microgel Colloids. *J. Chem. Phys.* **2004**, *120*, 6197-6206.

2(25) Hertle, Y.; Zeiser, M.; Hasenöhrl, C.; Busch, P.; Hellweg, T. Responsive P(NIPAM-co-NtBAM) Microgels: Flory–Rehner Description of the Swelling Behaviour. *Colloid Polym. Sci.* **2010**, *288*, 1047-1059.

2(26) Zhao, Y.; Ikeda, T. Eds. *Smart Light-Responsive Materials: Azobenzene-Containing Polymers and Liquid Crystals*; John Wiley & Sons: Hoboken, New Jersey, 2009.

2(27) Zakrevskyy, Y.; Roxlau, J.; Brezesinski, G.; Lomadze, N.; Santer, S. Photosensitive surfactants: Micellization and interaction with DNA *J. Chem. Phys*. **2014**, *140*, 044906-044908.

2(28) Maeda, Y.; Kubota, T.; Yamauchi, H. Hydration Changes of Poly(2-(2-methoxyethoxy)ethyl Methacrylate) during Thermosensitive Phase Separation in Water. *Langmuir* **2007**, *23*, 11259-11265.

2(29) Kirsh, E.Y. Water-soluble Poly(*N*-Vinylamides): Microstructure, Solvation, Conformational State and Complex Formation in Aqueous Solutions. *Prog. Polym. Sci.* **1993**, *18*, 519-542.

2(30) Keerl, M.; Smirnovas, V.; Winter, R.; Richtering, W. Copolymer Microgels from Mono- and Disubstituted Acrylamides: Phase Behavior and Hydrogen Bonds. *Macromolecules* **2008**, *41*, 6830-6836.

2(31) Boyko, V. *N*-Vinylcaprolactam based Bulk and Microgels: Synthesis, Structural Formation and Characterization by Dynamic Light Scattering. Ph.D. Dissertation, Dresden University of Technology, Dresden, Germany, 2004 and references therein.

2(32) Kirsh, E. Y. *Water Soluble Poly-N-Vinylamides: Synthesis and Physicochemical Properties*; John Wiley & Sons: Chichester, 1998.

2(33) Liu, Y.-J.; Pallier, A.; Sun, J.; Rudiuk, S.; Baigl, D.; Piel, M.; Marie, E.; Tribet, C. Non-monotonous Variation of the LCST of Light-responsive, Amphiphilic Poly(NIPAM) Derivatives. *Soft Matter* **2012**, *8*, 8446-8455.

2(34) El Halabieh, R. H.; Mermut, O.; Barrett, C. Using Light to Control Physical Properties of Polymers and Surfaces with Azobenzene Chromophores. *J. Pure Appl. Chem.* **2004**, *76*, 1445–1465.

2(35) (a) Qiu, Q.; Somasundaran, P.; Pethica, B. A. Hydrophobic Complexation of Poly(vinylcaprolactam) with Sodium Dodecyl Sulfate and Dodecyltrimethylammonium Bromide in Solution. *Langmuir* **2002**, *18*, 3482-3486 and references therein; (b) Son, S. U.; Reingold, J. A.; Carpenter, G. B.; Czech, P. T.; Sweigart, D. A. Charge-Assisted Hydrogen Bonding and Other Noncovalent Interactions in the Self-Assembly of the Organometallic Building Block $[(\eta^6\text{-hydroquinone})Rh(P(OPh)_3)_2]^+$ with a Range of Counteranions. *Organometallics* **2006**, *25*, 5276-5285 and references therein; (c) Fang, Y.; Nguyen, P.; Ivasenko, O.; Aviles, M. P.; Kebede, E.; Askari, M. A.; Ottenwaelder, X.; Ziener, U.; Sirid, O.; Cuccia, L. A. Charge-assisted Hydrogen Bond-directed Self-assembly of an Amphiphilic Zwitterionic Quinonemonoimine at the Liquid–solid Interface. *Chem. Commun.* **2011**, *47*, 11255–11257.

2(36) (a) Aalbers, A. B.; den Hartog, H. W. Gadolinium-doped SrF2: Dipole Strengths and Concentration Effects Influenced by Dipole-dipole Interactions. *Phys. Rev. B* **1979**, *19*, 2163.; (b) Cussó, F.; Aceituno, P.; Murrieta, H.; López, F. J. Dipole-dipole Interaction Effects on the Relative Stabilities of Dipoles in $NaCl:Mn^{2+}$. *Phys. Rev. B* **1985**, 3*1*, 8119-8123.

2(37) Toschchevikov, V.; Saphiannikova, M. Theory of Light-Induced Deformation of Azobenzene Elastomers: Effects of the Liquid-Crystalline Interactions and Biaxiality. *J. Phys. Chem. B* **2014**, *118*, 12297−12309.

2(38) (a) Sun, S.; Wu, P. Infrared Spectroscopic Insight into Hydration Behavior of Poly(*N*-vinylcaprolactam) in Water. *J. Phys. Chem. B* **2011**, *115*, 11609–11618.; (b) Liu, T.; Chen, J.; Sugihara, S.; Maeda, Y. Study on Hydration of Poly(*N*-Vinylcaprolactam) Microgels by Near-IR and Mid-IR Spectroscopy. *Colloid Polym. Sci.* **2012**, *290*, 763-767.

2(39) Lappi, S. E.; Smith, B.; Franzen, S. Infrared spectra of $H_2{}^{16}O$, $H_2{}^{18}O$ and D_2O in the Liquid Phase by Single-pass Attenuated Total Internal Reflection Spectroscopy. *Spectrochimica Acta Part A* **2004**, *60*, 2611-2619.

2(40) Schneider, F.; Balaceanu, A.; Feoktystov, A.; Pipich,V.; Wu, Y.; Allgaier, J.; Pyckhout-Hintzen, W.; Pich, A.; Schneider, G. J. Monitoring the Internal Structure of Poly(*N*-vinylcaprolactam) Microgels with Variable Cross-Link Concentration. *Langmuir* **2014**, *30*, 15317−15326.

2(41) (a) Bronstein, L. M.; Kostylev, M.; Tsvetkova, I.; Tomaszewski, J.; Stein, B.; Makhaeva, E. E.; Okhapkin, I.; Khokhlov, A. R. Core−Shell Nanostructures from Single Poly(*N*-Vinylcaprolactam) Macromolecules: Stabilization and Visualization. *Langmuir* **2005**, *21*, 2652-2655.; (b) Spěváček, J.; Hanyková, L.; Starovoytova. L. ^{1}H NMR Relaxation Study of Thermotropic Phase Transition in Poly(Vinyl methyl ether)/D_2O Solutions. *Macromolecules* **2004**, *37*, 7710–7718.; (c) Balaceanu, A.; Verkh, Y.; Demco, D. E.; Möller, M; Pich, A. Correlated Morphological Changes in the Volume Temperature Transition of Core–Shell Microgels. *Macromolecules* **2013**, *46*, 4882–4891.

2(42) Okhapkin, I. M.; Nasimova, I. R.; Makhaeva, E. E.; Khokhlov, A. R. Effect of Complexation of Monomer Units on pH- and Temperature-Sensitive Properties of Poly(*N*-vinylcaprolactam-co-methacrylic acid). *Macromolecules* **2003**, *36*, 8130-8138.

2(43) Erman, B.; Flory, P. J. Critical Phenomena and Transitions in Swollen Polymer Networks and in Linear Macromolecules. *Macromolecules* **1986**, 19, 2342–2353.

2(44) Atta, A. M. Swelling Behaviors of Polyelectrolyte Hydrogels Containing Sulfonate Groups. *Polym. Adv. Technol*. **2002**, *13*, 567-576.

2(45) (a) Han, M.; Hara, M. Intense Fluorescence from Light-Driven Self-Assembled Aggregates of Nonionic Azobenzene Derivative. *J. Am. Chem. Soc.* **2005**, *127*, 10951. (b) Han, M. R.; Hara, M. Chain Length-dependent Photoinduced Formation of Azobenzene Aggregates. *New J. Chem.* **2006**, *30*, 223-227. (c) Han, M. R.; Hirayama, Y.; Hara, M. Fluorescence Enhancement from Self-Assembled Aggregates: Substituent Effects on Self-Assembly of Azobenzenes. *Chem. Mater.* **2006**, *18*, 2784-2786.

2(46) (a) Destribats, M.; Lapeyre, V.; Wolfs, M.; Sellier, E.; Leal-Calderon, F.; Ravaine, V.; Schmitt, V. Soft microgels as Pickering Emulsion Stabilisers: Role of Particle Deformability. *Soft Matter*, **2011**, *7*, 7689-7698.; (b) Geisel, K.; Isa L.; Richtering, W. Unraveling the 3D Localization and Deformation of Responsive Microgels at Oil/Water Interfaces: A Step Forward in Understanding Soft Emulsion Stabilizers. *Langmuir*, **2012**, *28*, 15770-15776. (c) Pinaud, F.; Geisel, K.; Masse, P.; Catargi, B.; Isa, L.; Richtering, W.; Ravaine, V.; Schmitt, V. Adsorption of Microgels at an Oil–water Interface: Correlation Between Packing and 2D Elasticity. *Soft Matter* **2014**, *10*, 6963–6974.

2(47) (a) Sortino, S. Photoactivated Nanomaterials for Biomedical Release Applications. *J. Mater. Chem.* **2012**, *22*, 301-318 and references therein.; (b) Rwei, A. Y.; Wang, W.; Kohane, D. S. Photoresponsive Nanoparticles for Drug Delivery. *Nano Today* **2015**, *10*, 451-467.

2(48) Beharry, A. A. Characterization of Azobenzene-based Photo-switches and their Evaluation for *in vivo* Applications. Ph.D Dissertation, University of Toronto, Canada, 2012 and references therein.

2(49) (a) Croissant, J. *et al*. Two-Photon-Triggered Drug Delivery in Cancer Cells Using Nanoimpellers. *Angew. Chem. Int. Ed.* **2013**, *52*, 13813–13817.; (b) Moreno, J.; Gerecke, M.; Dobryakov, A. L.; Ioffe, I. N.; Granovsky, A. A.; Bleger, D.; Hecht, S.; Kovalenko, S. A. Two-Photon-Induced versus One-Photon-Induced Isomerization Dynamics of a Bistable Azobenzene Derivative in Solution. *J. Phys. Chem. B.* **2015**, *119*, 12281-12288.

APPENDIX 2

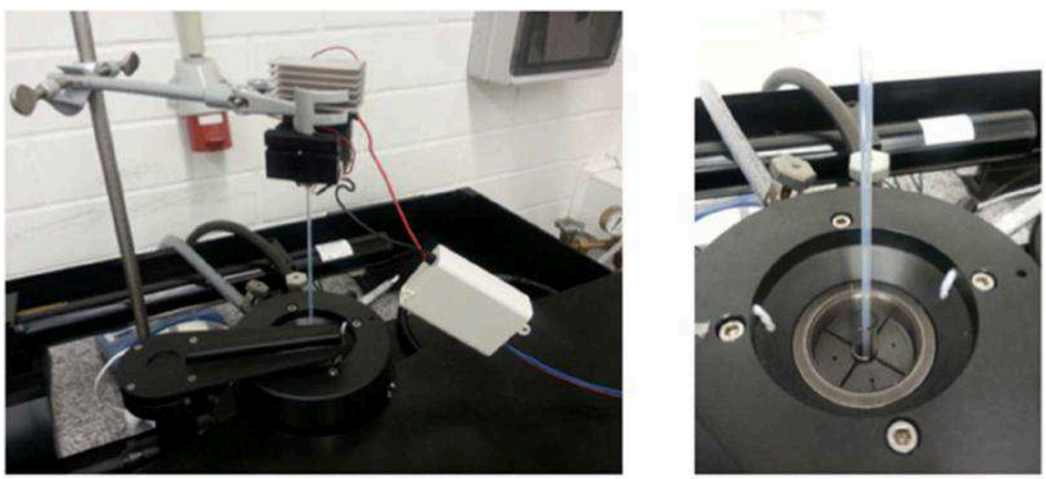

Figure A2(1). *in situ* irradiation set-up for investigation of photo-responsive behavior of microgels via DLS.

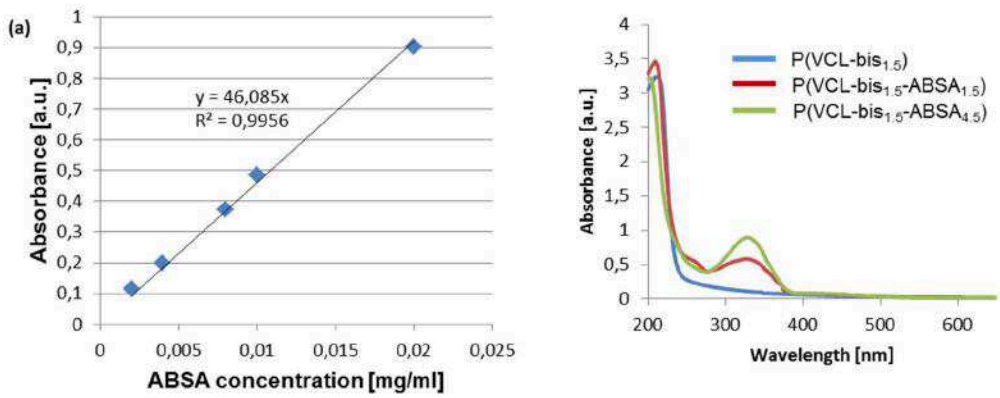

Figure A2(2). (a) Calibration curve of ABSA comonomer in distilled water, and (b) UV/vis spectra of the respective microgels at a concentration of 0.167 g/L in water.

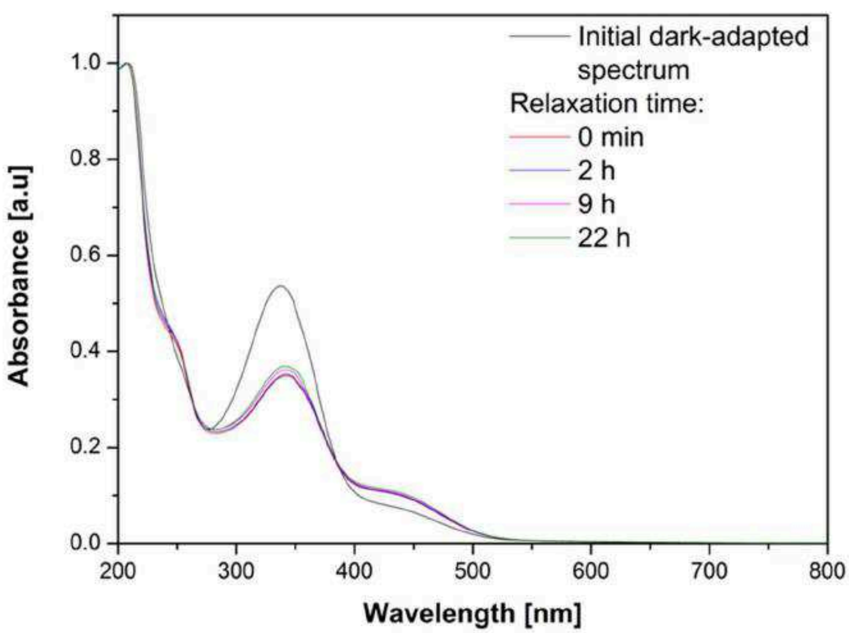

Figure A2(3). Relaxation in the dark of UV-irradiated ABSA.

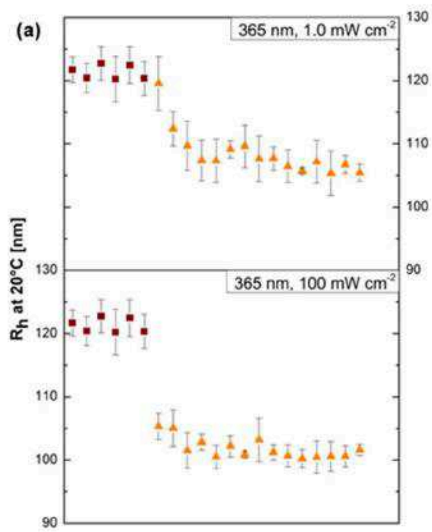

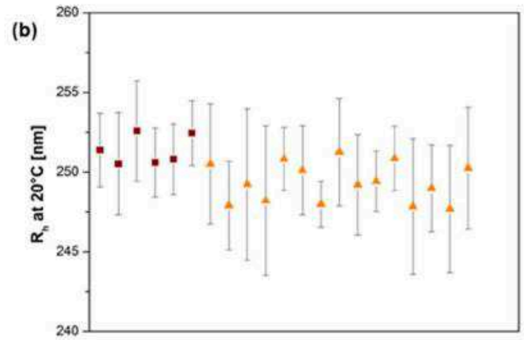

(c)

Microgel	$R_{h,24°C}$ in the native state [nm]	$R_{h,24°C}$ in the UV-irrad. state [nm]	% decrease in R_h upon UV irrad.
P(VCL-bis$_{1.5}$)	**132.9**	**129.4**	**1.5**
P(VCL-bis$_{1.5}$-ABSA$_{1.5}$)	**106.6**	**95.3**	**9.8**
P(VCL-bis$_{1.5}$-ABSA$_{4.5}$)	**113.9**	**81.3**	**28.6**

Figure A2(4). (a) The effect of employing different UV LEDs (λ = 365 nm, 1.0 mW cm^{-2} and 100 mW cm^{-2}) of different irradiances on the photo-responsive behavior of P(VCL-bis$_{1.5}$-ABSA$_{4.5}$) at 20°C, (b) Investigation of the photo-responsive behavior of P(VCL-bis$_{1.5}$) microgel irradiated (λ = 365 nm, 100 mW cm^{-2}) at 20°C, (c) Percentage decrease in R_h of microgels upon UV (365 nm, 100 mW) irradiation at 24°C. ■ points represent the R_h of the microgels in their native states while ▲ points represent the R_h reached with UV irradiation. Each point represents the mean of 6 x 10 seconds acquisitions in the DLS instrument.

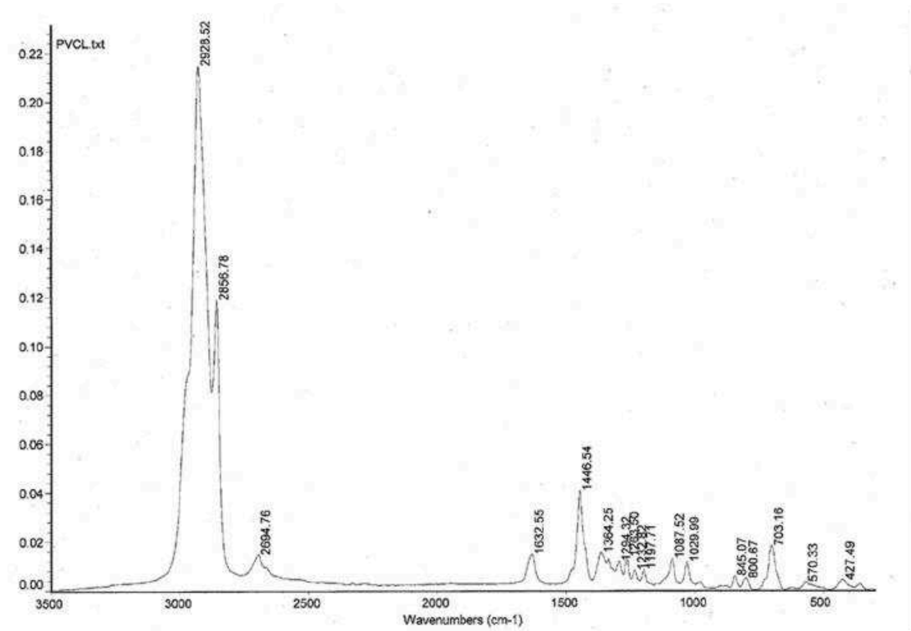

Figure A2(5). Raman spectrum of lyophilized P(VCL-bis$_{1.5}$).

Table A2(1). Assignment of IR absorption bands.

Assignment	Band (cm^{-1})
v(free C=O)	1650/1633
v(doubly H-bonded C=O)	1599
v(H_2O) + *v*(HOD)	3427

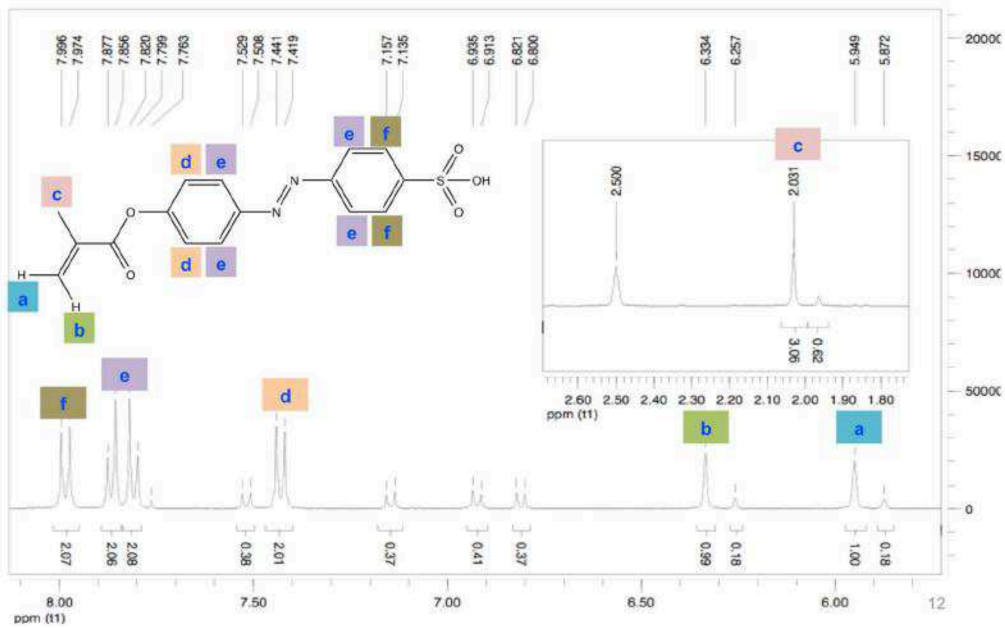

Figure A2(6). ^{1}H NMR of ABSA comonomer.

(a) Native P(VCL-$bis_{1.5}$-$ABSA_{4.5}$)

Particle	Diameter [nm] Horizontal	Diameter [nm] Vertical	Ave. Diameter [nm]	Height [nm] Horizontal	Baseline	Actual Height [nm] Horizontal	Height [nm] Vertical	Baseline	Actual Height [nm] Vertical	Ave. Height [nm]
1	211.3	215.3	213.3	51.0	-9.31	60.3	51.9	-9.41	60.6	60.4
2	215.3	199.3	207.3	57.0	-3.17	60.2	57.3	-2.71	60.0	60.1
3	215.3	199.3	207.3	51.8	-1.74	53.5	51.3	-1.35	52.7	53.1
4	211.3	195.3	203.3	49.9	-6.84	56.7	50.3	-7.18	57.5	57.1
5	211.3	207.3	209.3	50.2	-4.29	54.5	51.2	-3.90	55.1	54.8
6	227.2	207.3	217.3	50.2	-5.17	55.4	51.2	-6.21	57.4	56.4
7	215.3	187.4	201.3	52.5	-8.49	60.9	52.4	-6.96	59.4	60.2
8	219.3	191.4	205.3	66.8	2.71	64.1	66.7	3.25	63.4	63.7

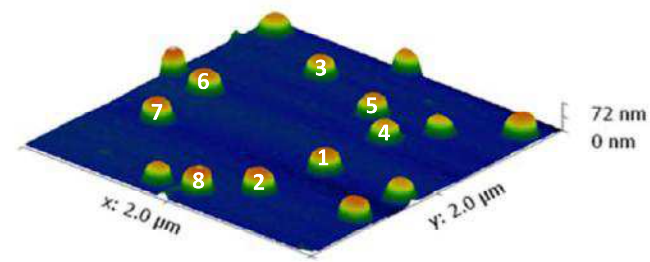

(b) UV-irradiated (365 nm, 100 mW cm^{-2}) P(VCL-$bis_{1.5}$-$ABSA_{4.5}$)

Particle	Diameter [nm] Horizontal	Diameter [nm] Vertical	Ave. Diameter [nm]	Height [nm] Horizontal	Baseline	Actual Height [nm] Horizontal	Height [nm] Vertical	Baseline	Actual Height [nm] Vertical	Ave. Height [nm]
1	273.4	261.7	267.6	34.9	-1.88	36.7	34.0	-1.84	35.8	36.3
2	285.2	261.7	273.4	34.9	-2.07	37.0	34.7	-3.94	38.7	37.8
3	281.3	277.3	279.3	33.7	-2.20	35.9	33.5	-3.26	36.7	36.3
4	296.9	281.3	289.1	36.6	-2.24	38.9	36.1	-2.22	38.3	38.6
5	257.8	250.0	253.9	32.1	-3.32	35.4	31.7	-3.20	34.8	35.1
6	269.5	265.6	267.6	34.7	-2.01	36.7	34.1	-0.74	34.9	35.8
7	269.5	269.5	269.5	31.4	-3.07	34.5	30.9	-1.72	32.6	33.5

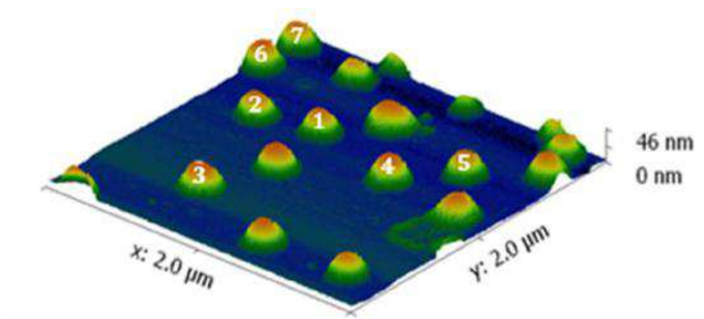

(c)

Difference in Ave. Diameter [nm]	63.4
% Increase in Diameter after irrad.	30.5
Difference in Ave. Height [nm]	22.0
% Decrease in height after irrad.	37.8

Figure A2(7). Analysis of the height profiles and lateral diameters of individual particles of (a) Native P(VCL-$bis_{1.5}$-$ABSA_{4.5}$), and (b) UV-irradiated P(VCL-$bis_{1.5}$-$ABSA_{4.5}$). *Horizontal* refers to the cross-section made across the particle along the *x*-axis while *vertical* refers to the cross-section made across the particle along the *y*-axis. (c) Summary of the average differences in height and diameter of the particles.

CHAPTER 3. The Effect of the High Loading of 4-[(4-Methacryloyloxy) phenylazo] benzenesulfonic acid (ABSA) on the Thermo- and Photo-Responsive Properties of P(VCL-bis-ABSA) Microgels and on the Self-Assembly of the Linear P(VCL-ABSA) Copolymer

3.1. Introduction

The design of smart systems and materials is inspired by nature's seemingly effortless and efficient ways in assembling functional systems for life's processes. By combining lessons from the mechanisms underlying natural systems and the knowledge in polymer and materials sciences, researchers have endeavored to produce functional materials, imbued with useful and interesting physicochemical properties that attempt to emulate the adaptive and intelligent behaviors in natural systems.

An area of particular interest in smart material research has been the field of responsive microgels. Here, the physico-chemical properties of the colloidal particles can be controlled by means of various external stimuli.[3(1)] Microgels represent an intermediate between linear polymers and macroscopic hydrogels, thereby combining advantages such as rapid phase transition, good structural integrity, and allowing for relative ease in tuning the polymer composition. They have found a wide range of uses and potential applications in surface science, sensors and biomaterials.[3(2)] Stimuli such as temperature and light are relatively non-invasive and can be remotely administered, especially to achieve control over the properties of the particles in a clean manner that would be compatible with biomedical applications.[3(3)] To this end, the thermo- and photo-responsive behavior of microgels composed of a thermo-responsive monomer *N*-vinylcaprolactam (VCL) and up to 10 wt. % of a photo-responsive comonomer 4-[(4-methacryloyloxy)phenylazo] benzenesulfonic acid (ABSA) were reported in Chapter 2. The microgel particles shrunk by up to 28 % upon UV irradiation (λ = 365 nm, 100 mW cm^{-2}). Furthermore, switchability between the deswollen and swollen states could be achieved by alternate application of UV and blue lights respectively, as described in Chapter 2.

In order to obtain greater functionality out of microgel particles, they should be organized into hierarchical structures such as films and colloidosomes.[3(5)] Self-assembly has been recognized as one of the few practical strategies for making ensembles of nanostructures.[3(5)] In practice, however, the bottom-up approach to create complex lattices and assemblies from microgel particles and from different colloidal particles in general, is not a trivial pursuit.[3(6)] The concept of supramolecular interactions is often employed in crystal engineering[3(7)] but can be adapted as a promising and targeted strategy to achieve controlled and stable bridging between microgel particles, en route to ordered, nanostructured materials for use in photonics, and sensing applications for instance.[3(6)] ABSA in itself can act as a supramolecular synthon since it bears basic structural motifs that can be formed and/or assembled by non-covalent, intermolecular interactions with neighboring, complementary motifs.[3(8)] The aromatic rings can be involved in π-π stacking interactions while the sulfonic acid end group is capable of specific and directional hydrogen bonding interactions. The primary supramolecular interaction in our VCL-ABSA system is expected to be the hydrogen bonding interactions between the sulfonic acid terminal groups of ABSA and the C=O groups of VCL. The formed hydrogen bond can be classified as a type of charge-assisted hydrogen bonding (CAHB). CAHB is a hydrogen bond that is accompanied by Coulombic interactions, leading to exceptionally strong electrostatic, yet flexible interactions between oppositely charged components.[3(9)] The binding energy of a CAHB is around 70 kJ mol^{-1}, which is up to four times that of a typical hydrogen bond.[3(9a,10)] As a comparison, the weakest covalent bond binding energy is close to 200 kJ mol^{-1}.[3(11)]

With this in mind, and seeking to develop a rational supramolecular strategy for inter-particle interactions, we employed the same polymerization procedure as before, to produce microgel particles with a higher loading of ABSA comonomer (20-30 wt. %). We find that with high ABSA loading, intra- and inter-particle, supramolecular interactions between comonomer units became extensive and dominant. As a result, the particles exhibit unique morphologies and differing responses to temperature and UV stimuli. We deduced from DLS and cryo-TEM measurements that the particles prefer to exist as stable dimeric assemblies in the native microgel dispersions. Single particles of the microgels possess dangling polymer chains on their peripheries, as revealed by cryo-TEM micrographs. The interlocking of the dangling chains through supramolecular forces is the expected origin for the formation of dimeric assemblies. The thermo- and photo-responsive behavior of the dimeric assemblies and single particles are discussed in terms of the strength of the intra-particle supramolecular forces. Additionally, via the same polymerization procedure and with the same feed ratio of VCL and ABSA, we synthesized linear chains of P(VCL-ABSA) by eliminating the addition of BIS cross-linker. These linear chains were found to self-assemble upon stirring in a 75 wt. % water/THF mixture into compact nanospheres and vesicle-like nanospheres via similar supramolecular forces. As detected via dynamic light scattering measurements, these nanospheres were found to be disrupted under UV irradiation and then re-formed when re-stirred for over a day in the dark. The P(VCL-bis$_{1.5}$-ABSA$_{10}$) microgel and the self-assembled nanospheres of P(VCL-ABSA$_{10}$) were also found to fluoresce with UV irradiation.

3.2. Experimental section

3.2.1. Materials

N-Vinylcaprolactam (VCL) (Sigma-Aldrich, 98% purity) was purified by a high-vacuum distillation at 80°C. The azobenzene comonomer 4-[(4-methacryloyloxy)phenylazo] benzenesulfonic acid (ABSA) was synthesized according to the procedure reported in Gong *et al*.[3(12)] *N,N'*-methylenebis(acrylamide) (BIS) cross-linker was obtained from Sigma-Aldrich and used as received. The initiator, 2,2'-azobis[*N*-(2-carboxyethyl)-2-methylpropionamidine]hydrate (ACMA), was purchased from (Wako Pure Chemical Industries, Ltd., Specialty Chemicals) and used as received. Tetrahydrofuran (THF) (LiChrosolv®, Merck Millipore) was used as received.

UV and visible light light-emitting diodes. The following LEDs were purchased and then handcrafted and fashioned in-house for use with the ALV instrument. Gen 2 Emitter LZ1-00UV00 (365 nm, LED Engin, Inc.) coupled to an optical fiber from (CeramOptec) to produce an irradiance of 100 mW cm^{-2}.

3.2.2. Microgel and linear polymer syntheses

P(VCL-bis$_{1.5}$-ABSA$_x$) microgels were synthesized via a two-step surfactant-free precipitation polymerization according to the same procedure reported in Chapter 2 and represented in Scheme 2(1). In a typical procedure, the polymerization is carried out in a double-wall glass reactor equipped with stirrer. Half the amount of VCL and half the cross-linker amount were dissolved in 80 ml deionized water and added into the reactor and stirred for 30 min at 70 °C under continuous purging with nitrogen. Subsequently, 5 mL aqueous solution of ACMA initiator was added under continuous stirring into the reactor. The reaction mixture turned turbid 30 s after initiation. At the 30 s mark after the appearance of turbidity, a 15 ml solution containing the remaining VCL monomer, BIS cross-linker and all of the ABSA comonomer were added with a syringe over a period of 1 min under positive flow of nitrogen. The reaction was left to stir for 6 h at 70°C. The reagents and their respective amounts used are listed in Table 3(1).

Table 3(1). Amount of Monomers Used and Incorporated during the Synthesis of Microgels.

Microgel	VCL [mmol]	$ABSA_{feed}$ [mmol]	$ABSA_{feed}$ [wt. %]	$ABSA_{incorp.}$ [wt. %]
P(VCL-$bis_{1.5}$-$ABSA_{6.0}$)	9.4	0.6	13.7	21.7
P(VCL-$bis_{1.5}$-$ABSA_{10}$)	9.0	1.0	21.7	28.1

*The nomenclature used in this paper for the microgels are based on the feed amounts of BIS and ABSA (indicated in subscripts in mol %).

The linear polymer P(VCL-Azo_{10}) was synthesized in deionized water following the same synthesis procedure as above, but without the addition of BIS cross-linker. Self-assembly of the linear chains into nanostructures was carried out by adding 0.3 ml polymer solution (having a concentration of 2 mg/ml) dropwise over 5 minutes into a continuously-stirred (400 rpm) solution of 0.6 ml THF and 0.1 ml 5% HCl solution. The mixture was left to stir for 24 h at 400 rpm. The self-assembled structures were subsequently fixed by heating the solution at 35°C for 10 minutes.

3.2.3. Characterization

UV/vis-spectroscopy. The spectra were measured from 800-200 nm with a scan rate of 600 nm/min on a Cary 100Bio UV-Visible Spectrophotometer from Varian. A quartz cuvette was used for the measurement and a quartz cuvette filled with deionized water was used as a reference.

UV/vis spectroscopic investigation of ABSA incorporated. The amount of ABSA incorporated into each microgel was determined via UV/vis spectroscopy via the same method described in Chapter 2. The approximate amounts of ABSA incorporated were determined and shown in Table 3(1). The absorption spectra of the microgels are shown in Fig. A3(1) of Appendix 3.

Dynamic light scattering (DLS). The size of the microgel particles was measured with an ALV/LSE-5004 DLS goniometer bearing a Multiple Tau Digital Correlator and Electronics. The instrument is equipped with a laser light wavelength of 633 nm and the scattered light was detected at a scattering angle set of 90°. The samples were measured at 20 °C and the temperature fluctuations were below 0.1 °C. Microgel samples were highly diluted (c < 0.01 wt %) with water for chromatography from Merck Millipore and subsequently filtered through a 1.2 μm filter before measurements were performed to eliminate dust, aggregation and impurities. The hydrodynamic radius R_h was calculated from second order cumulant fits via the

Stokes-Einstein equation. For temperature-dependent measurements, samples were measured between 10 and 60°C, in steps of 3°C and keeping the temperature fluctuations below 0.1°C. Three runs of 120 s each where performed at each temperature in order to calculate the standard deviation. The volume phase transition temperature (VPTT) of each microgel was determined as the inflection point of the temperature-dependent light scattering curve.

***In situ* irradiation within the DLS instrument**. The photo-induced size changes at different temperatures were detected by DLS. Samples were allowed to equilibrate thermally at the respective temperatures for 10 mins. The optical fibre coupled to LED (λ = 365 nm, 100 mW cm^{-2}) was placed 0.5 cm above the meniscus of the microgel solution in the cuvette. At each temperature, six runs of 10 s each were performed and repeated for over fifteen minutes to monitor the photo-responsive effect over time. The *in situ* photo-irradiation set-up is similar to the one shown in Fig. A2(1) of Appendix 2.

Atomic force microscopy (AFM). Images were recorded using a tapping mode on a Veeco Nanoscope Atomic Force Microscope. Cantilevers (NanoWorld, Neuchâtel, Switzerland) with resonance frequency of 250 – 300 kHz and spring constant of 42 N m^{-1} were used. The deposition of microgels on a silicon wafer was carried out on a spin-coater (Convac 1001S, Germany) at a speed of 3000 rpm for 30 s. The silicon wafer used for deposition was previously cleaned by sonication in isopropanol for 10 minutes, dried with an air stream, and treated with UV/O_2 for 15 min. The concentration of microgel solution used for spin coating was 1.0 mg/mL. At this microgel concentration, sufficient amount of particles could be adsorbed and be distributed evenly on the silicon wafer without clustering.

Cryogenic transmission electron microscopy (Cryo-TEM). Visualization was performed on a Carl Zeiss LibraTM 120 microscope (Oberkochen, Germany) with a bottom-mounted CCD camera. Freshly synthesized microgel dispersions were first diluted with 25 parts of deionized water, and 2 μl of the diluted suspension of each sample was withdrawn and deposited on one side of a plasma-treated lacey grid within a vitrobot system. Excess liquid was blotted away from the under side of the grid by a piece of filter paper so that no thick liquid film, i.e. above 200 nm thick, remained. Once prepared, the sample assemblage was immediately plunged into liquid ethane (−182.8°C). The frozen, or vitrified, sample was then mounted on a Gatan 626 cryo-holder and transferred into a JOEL 1210 TEM with an acceleration voltage of 120 KeV. The specimen temperature was maintained at −170°C throughout the observation.

Confocal laser scanning microscopy. Imaging was performed on a Leica TCS SP8 to visualize bright field and fluorescence images of P(VCL-bis$_{1.5}$-ABSA$_{10}$) microgel and self-assembled nanospheres from P(VCL-ABSA$_{10}$) chains and to analyze their dynamics. The sample chamber is made from a glass substrate and three stacked cover slides to form a closed channel. The channel is sealed using commercial fast curing adhesive. The particles were imaged by setting fixed laser intensity for the UV laser line (λ = 405 nm to induce *trans*-to-*cis* isomerization of ABSA) and fluorescence detection was set according to the emission profile as determined in the fluorometer (emission spectrum of P(VCL-bis$_{1.5}$-ABSA$_{10}$) is shown in Fig. A3(2) of Appendix 3)

3.3. Results and discussion

3.3.1. Morphology and topography of P(VCL-bis$_{1.5}$-ABSA$_{6.0}$) and P(VCL-bis$_{1.5}$-ABSA$_{10}$) microgels

We first observed particles showing hydrodynamic radii at 20°C ($R_{h,20°C}$) of ~ 260 nm and 230 nm (polydispersity index (Pd.I) < 0.1) in several reproducible DLS measurements of P(VCL-bis$_{1.5}$-ABSA$_{6.0}$) and P(VCL-bis$_{1.5}$-ABSA$_{10}$) respectively (see Fig. 3(1a)). Unbeknownst to us at that point was that these DLS measurements represent size information of dimeric assemblies of the microgel particles. DLS is a commonly employed and often very reliable technique to obtain information about size of spherical particles. However, it remains an indirect method since it relies on computing particle size based on diffusion coefficients obtained from the intensity of scattered light, via the Stokes-Einstein equation.[3(13)] Cryo-TEM imaging was then employed to capture the particles since it is regarded as one of the best technique to capture soft colloidal particles like microgels and to observe their structures in their native solution state.[3(14)]

During cryo-TEM imaging, the microgels are trapped within a thin vitrified ice layer that is typically less than 100 nm thick.[3(15)] Since the microgels have hydrodynamic diameters that are more than 100 nm, they are made to conform into a confined space within the vitrified ice layer. The trapped microgels should therefore adopt a more planar two dimensional structure as a result of being stretched laterally.[3(16)] This being the case, the particle size observed in cryo-TEM could be larger than that observed by DLS. However this, was not the case for single particles of P(VCL-bis$_{1.5}$-ABSA$_{6.0}$) and P(VCL-bis$_{1.5}$-ABSA$_{10}$) as seen in Fig. 3(2a) and 3(2c) respectively. The dangling chains on the particle periphery are clearly visible without the use of any contrast agents. The particle diameter was measured by considering the end of the dangling chains as the boundary between the particle and surrounding water. The average radius are found to be about ~ 183 ± 15 nm for P(VCL-bis$_{1.5}$-ABSA$_{6.0}$) and ~147 ± 12 nm for P(VCL-bis$_{1.5}$-ABSA$_{10}$). These values are significantly smaller than the R_h, obtained form DLS, as shown in Fig. 3(1a). This led us to believe that we were observing dimeric assemblies of particles in DLS. In Fig. 3(2b) and 3(2d), the clustering of the particles is evident and some particles are fused together to form dimeric or higher order assemblies. The confined environment of the vitreous ice layer enhanced the clustering effect of the microgels as compared to the case in solution, where they prefer to exist as dimeric assemblies.

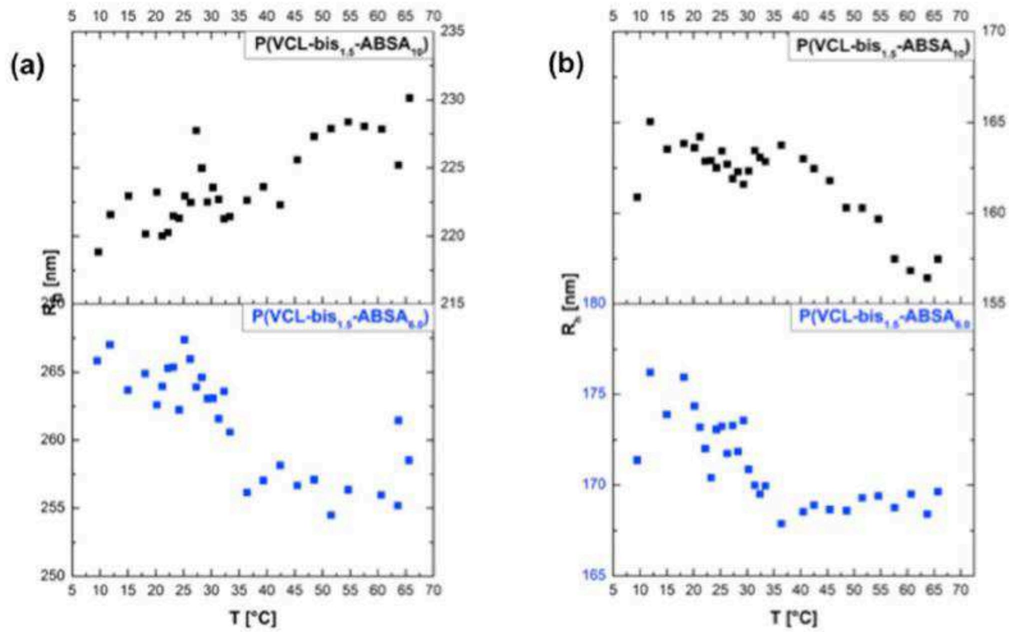

Figure 3(1). Size-temperature data obtained from DLS of (a) Dimeric assemblies, and (b) Single particles of P(VCL-bis$_{1.5}$-ABSA$_{6.0}$) and P(VCL-bis$_{1.5}$-ABSA$_{10}$).

In the AFM image of P(VCL-bis$_{1.5}$-ABSA$_{6.0}$) in Fig. 3(2e), islands of clustered particles are visible. The lateral diameters of the single particles adsorbed on the hydrophilized Si substrate are much larger than the size obtained by DLS. This can be attributed to the spreading of the particles on the surface, especially of the dangling chains on the particle periphery. The spreading is also most possibly aided by the attractive interactions between the surface and the high amount of sulfonic acid terminal groups of the ABSA that can form H-bonding interactions with the hydrophilized surface.

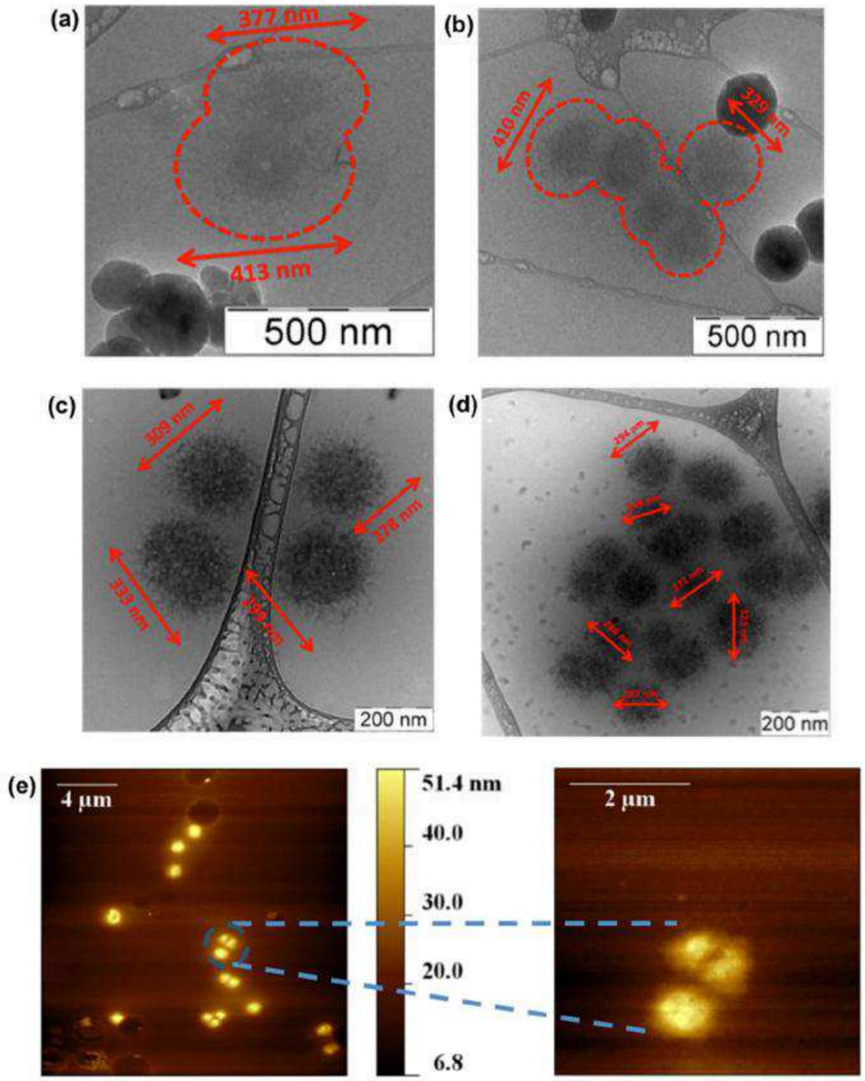

Figure 3(2). Cryo-TEM micrographs of (a & b) P(VCL-bis$_{1.5}$-ABSA$_{6.0}$), (c,d) P(VCL-bis$_{1.5}$-ABSA$_{10}$), and AFM topography images of (e) P(VCL-bis$_{1.5}$-ABSA$_{6.0}$). Original images of (a), (b), (c), and (d) without annotations can be found in Fig. A3(3a-d) respectively of Appendix 3.

3.3.2. The origin of clustering

With the benefit of having the direct visualization of the microgel structure via cryo-TEM, we then understood that the microgels in their native state preferred to exist as self-assembled particle pairs that are fused into each other. We consider this 'fusion' between particles to be the result of a combination of non-covalent, supramolecular attractive interactions that occur more easily due to the fuzzy surface morphology of the microgel particles contributed by the interlocking of the dangling chains. Two main attractive interactions most probably prevail, the first being the interactions due to complexations between the sulfonic end groups of ABSA and the polar C=O groups of the VCL units, leading to the formation of relatively strong H-bonds. The nature of H-bonding in our VCL-ABSA system can be classified as charge-assisted hydrogen bonding (CAHB) since the ABSA pendant group is essentially a molecular anion and the nitrogen atom of the vinylamide is likely to bear a partial positive charge in aqueous environments.[3(17)] Complexation between comonomers can be found in polymeric systems where the comonomers bear opposite charges or when one monomer is charged while the other has an easily polarizable functional group.[3(18)] For instance in copolymeric chains of P(*N*-vinylcaprolactam-co-methacrylic acid) [P(VCL-co-MAA)] as well as in mixtures containing homopolymeric chains of P(VCL) and P(MAA), macromolecular complexes have been observed to form in water by cooperative H-bonding between VCL and MAA units.[3(18c)] Since the sulfonic acid group is a stronger acid than the carboxylic group and is known to interact with macromolecular proton acceptors, the H-bonding interactions between the sulfonic acid terminal groups of ABSA and the C=O of VCL is very plausibly stronger in our microgel system.[3(19)]

A second prevailing supramolecular force that could contribute to the clustering phenomenon is the π-π stacking interactions of the aromatic rings of the ABSA pendant groups. The ABSA pendant groups are expected to exist predominantly in their *trans* form under normal conditions without UV irradiation.[3(20)] Given the relatively high concentration of ABSA pendant groups, and the proclivity of *trans* azobenzene to form stacking interactions, we investigated the existence of aggregates associated with azobenzene groups via UV/vis spectroscopy.[3(21)] We compared the absorption spectra of P(VCL-bis$_{1.5}$-ABSA$_{4.5}$) and ABSA comonomer that we reported in Chapter 2 to that of P(VCL-bis$_{1.5}$-ABSA$_{10}$) and observed a small hypsochromic shift of about 14 nm (from 337 nm to 323 nm) in the absorption wavelength of the π-π^* transition of trans-ABSA in P(VCL-bis$_{1.5}$-ABSA$_{10}$) (see Fig. A3(4) of Appendix 3). This indicates the presence of *H*-aggregation which is known to cause a hypsochromic shift.[3(22)] Given that the hypsochromic shift is small, the formation of micro-domains from the clustering of ABSA pendant groups can be excluded[3(22b)] Instead the observed *H*-aggregates can be assumed to arise from ABSA pendant groups that are roughly evenly distributed in the network.

The ABSA pendant groups are connected to the polymer backbone via a relatively flexible ester linkage that allows decoupling of the movement of the pendant groups from the segmental motion of the backbone. Hence, the ABSA moieties have a relatively high degree of independence to orient and organize themselves.[3(23)] The sulfonic acid terminal groups of ABSA could then extend their reach to be in the vicinity of the polar C=O groups of the VCL units on adjacent dangling chains since the VCL units themselves have restricted rotational freedom around the N-C bond connecting them to the polymer backbone.

Other non-covalent interactions that could further contribute to the clustering are the hydrophobic interactions between the aromatic rings of ABSA and the methine and methylene groups of VCL, and dipole-induced dipole forces that occur between the highly dipolar amide group of VCL and the highly polarisable aromatic groups of ABSA molecules.[3(17)] All of these non-covalent attractive interactions have an additive effect on the overall binding energies, reinforcing the strength of the supramolecular interactions and thereby contributing to the stability of the dimeric assemblies.[3(7),3(9a)]

3.3.3. Investigation of the thermo- and photo-responsive properties of dimeric assemblies of P(VCL-bis$_{1.5}$-ABSA$_x$) microgels via DLS measurements

The R_h versus temperature plots of the dimeric assemblies associated with the microgels of P(VCL-bis$_{1.5}$-ABSA$_{6.0}$) and P(VCL-bis$_{1.5}$-ABSA$_{10}$), as measured by dynamic light scattering, was shown in Fig. 3(1a). There is no clear volume phase transition in both microgels within the measured temperature range of 10-65°C and the R_h values fluctuate over a range of ~10 nm, about a mean of 260 nm and 230 nm for P(VCL-bis$_{1.5}$-ABSA$_{6.0}$) and P(VCL-bis$_{1.5}$-ABSA$_{10}$) respectively. P(VCL-bis$_{1.5}$-ABSA$_{10}$) shows a slight upward trend in the size of the dimeric assemblies with increase in temperature while P(VCL-bis$_{1.5}$-ABSA$_{6.0}$) shows the opposite trend. While the size fluctuations could be an artifact of measuring non-spherical particles via DLS, we hypothesize that the increase in size could be an indication of the loosening of the supramolecular inter-particle interactions, particularly of the π-π stacking interactions of ABSA. We base this on the findings of Dunitz *et al*. who reported that the strength of π-π stacking interactions is significantly lower than that of CABH and they are also more susceptible to thermal fluctuations, based on the measurements of their binding energies and force constants respectively.[3(10)] Moreover, the increase motions of the chains in the network affect the orientation of the azobenzene units.[3(22b)] Therefore, the *H*-aggregation of the ABSA groups is the likelier of the two strong supramolecular interactions to be weakened upon increasing the temperature above a certain threshold. Since the *H*-aggregation is expected to be more extensive in P(VCL-bis$_{1.5}$-ABSA$_{10}$), the weakening of π-π stacking interactions of the ABSA groups has an appreciable effect on increasing the size of the dimeric assembly. It is most probably unfavorable for the dimeric assemblies of P(VCL-bis$_{1.5}$-ABSA$_{10}$) to shrink since this would cause an increase in short-range repulsive forces especially when the chains at the fused interface are already in close proximity.

The small decrease in size with temperature observed in P(VCL-bis$_{1.5}$-ABSA$_{6.0}$) could be attributed to the disruption of some H-bonding interactions of water molecules with the carbonyl of VCL units. In P(VCL-bis$_{1.5}$-ABSA$_{6.0}$), the backbone positions are less crowded and therefore the VCL units are more hydrated than in P(VCL-bis$_{1.5}$-ABSA$_{10}$). As such, the increase in temperature would favor the disruption of hydrogen bonding to water molecules and the concomitant formation of hydrophobic interactions between chains. Assuming the CABH interactions between the sulfonic acid of ABSA and C=O of VCL remain stable at higher temperatures, and only the π-π stacking interactions can be disrupted, the size increase of the dimeric assemblies associated with their disruption in P(VCL-bis$_{1.5}$-ABSA$_{6.0}$) is less significant than the size decrease due to the disruption of H-bonding with water molecules.

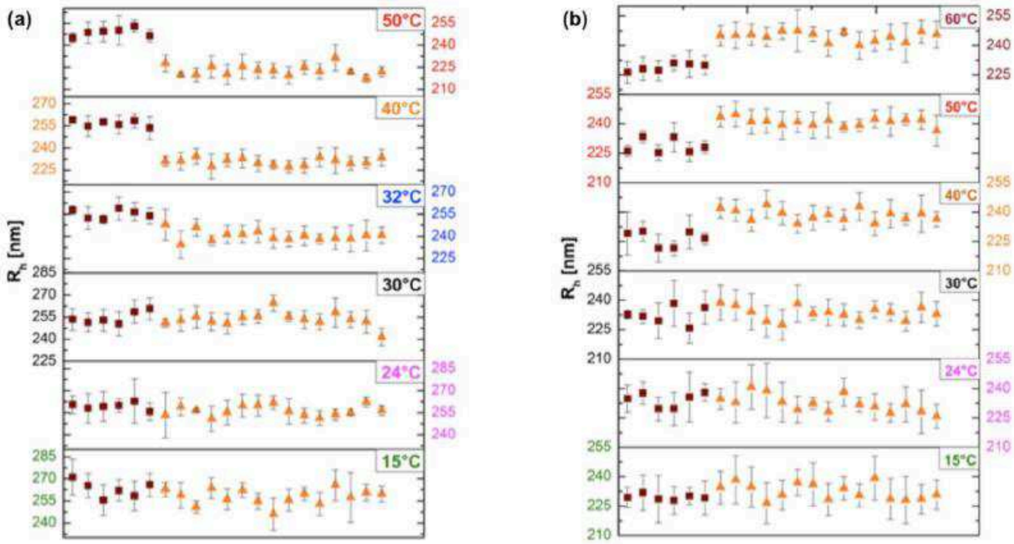

(c)

T [°C]	$R_{h,native}$ [nm]	$R_{h,irrad.}$ [nm]	% decrease in R_h
15	263.1	257.8	2.0
24	259.4	256.3	1.2
30	254.6	253.4	0.5
32	255.5	240.3	5.8
40	256.6	230.7	10.1
50	248.8	222.9	10.4

(d)

T [°C]	$R_{h,native}$ [nm]	$R_{h,irrad.}$ [nm]	% decrease in R_h
15	229.5	232.4	-1.3
24	234.2	232.3	0.8
30	232.4	233.5	-0.5
40	226.5	238.4	-5.3
50	228.6	240.9	-5.4
60	228.9	244.7	-6.9

Figure 3(3). Investigation of the photo-responsive behavior of dimeric assemblies of (a) P(VCL-bis$_{1.5}$-ABSA$_{6.0}$), and (b) P(VCL-bis$_{1.5}$-ABSA$_{10}$) irradiated (λ = 365 nm, 100 mW) at different temperatures. ■ points represent the R_h of the microgels in their native states while ▲ points represent the R_h reached with UV irradiation. Each measurement point represents the average of 6 x 10 seconds measurement runs in DLS. Percentage deswelling* of (c) P(VCL-bis$_{1.5}$-ABSA$_{6.0}$), and (d) P(VCL-bis$_{1.5}$-ABSA$_{10}$) at the different temperatures.* Values were calculated based on the mean R_h values before and after irradiation.

The dimeric assemblies of P(VCL-bis$_{1.5}$-ABSA$_{6.0}$) and P(VCL-bis$_{1.5}$-ABSA$_{10}$) show photo-responses that mirror their thermo-responses, as shown in Fig. 3(3a) and 3(3b) respectively. With UV irradiation, the respective responses are amplified. The photo-responses at temperatures below 30°C are marginal for both microgels. With increase in temperature, the photo-responses become more significant. Dimeric assemblies of P(VCL-bis$_{1.5}$-ABSA$_{6.0}$) decrease in size by about 10% at 50°C while those of P(VCL-bis$_{1.5}$-ABSA$_{10}$) increase in size by almost 7 % at 60°C, as summarized in Fig. 3(3c) and 3(3d) respectively. Although Han *et al*. reported several papers on the possibility of UV-induced aggregation of *cis* azobenzene-amphiphiles,[24] we do not think that the increase in the size of P(VCL-bis$_{1.5}$-ABSA$_{10}$)

particles at higher temperatures with UV irradiation is caused by higher order aggregates since the size increase is not of the order of the size of a particle. We postulate that the size of the P(VCL-bis$_{1.5}$-ABSA$_{10}$) dimeric assemblies increases further as a result of the concerted application of temperature and UV irradiation because the *trans*-to-*cis* isomerization of the ABSA pendant groups is able to disrupt the CABH interaction by virtue of the change in molecular geometry of the group. In the *cis* state, some of the ABSA groups on the dangling chains are removed from the vicinities of the C=O groups of VCL on adjacent dangling chains of the partnering particle. The *cis*-ABSA groups are instead brought closer to the backbone of the chain from which it is hanging, as per the deswelling mechanism proposed in our earlier paper, or to a chain of the same particle. In other words, some of the inter-particle CAHB interactions are replaced by intra-particle ones.

As with the application of only a temperature stimulus, the combined application of temperature and UV does not appear to lead to a disruption of the stable dimeric assemblies into discrete single particles.

3.3.4. Investigation of the thermo- and photo-responsive properties of single particles of P(VCL-bis$_{1.5}$-ABSA$_x$) microgels via DLS measurements

As discussed in the previous sections, the heating of the microgel solutions up to 65°C does not lead to the disruption of the dimeric assemblies and we deduced this from the very marginal size changes. We were however able to disrupt the dimeric assemblies by the addition of 0.1 ml of 50 mM KCl (aq) into 0.5 ml of the respective microgel solution (0.2 mg/ml), followed by mechanical agitation for 15 minutes via ultrasonic treatment, in an ice-water bath. KCl acts as a chaotropic agent and increases the ionic strength of the surrounding solution, thereby disfavoring the hydrophobic inter-particle interactions. Ultrasound treatment has been reported to disrupt intra-particle H-bonds in copolymeric microgels of *N*-isopropylacrylamide and acrylic acid.[25] We arrived at $R_{h,20°C}$ values of about 170 nm and 160 nm (Pd.I < 0.1) for microgels P(VCL-bis$_{1.5}$-ABSA$_{6.0}$) and P(VCL-bis$_{1.5}$-ABSA$_{10}$) respectively (see Fig. 3(1b)). These values of hydrodynamic size observed in DLS are similar to the sizes observed in cryo-TEM measurements shown in Fig. 3(2a-d). The size observed in DLS could sometimes be slightly larger given the presence of dangling chains on the microgel surface, which results in DLS measurements indicating a larger apparent size. This is because the chains cause an increase in the viscosity of the micro-environment in their direct vicinity, in this case, the surface of the particles. This then results in an overestimation of the actual viscosity in the Stokes-Einstein equation.[13] Consequently, this error is carried forth to an underestimation of the particle diffusion coefficient, leading to the DLS perceiving the particles to be larger than they actually are. The micrographic evidence of single particles seen in Fig 3(1a) and 3(1c), and the ability to disrupt the stable dimeric assemblies are proof that the particles are produced as single particles during the polymerization.

The thermo-responsive behavior of the single microgel particles was investigated via the same heating cycle that was performed on their dimeric assemblies. As seen in Fig. 3(1b), the R_h values remain relatively constant below 30°C. Beyond 30°C, there is a small and gradual downward trend in the R_h values. This can be attributed to the disruption of some H-bonding interactions of water molecules to the carbonyl groups of VCL. The decrease in R_h with increase in temperature is however very shallow and this is consistent with a suppression of the thermo-responsive behavior of the microgels. This is due to the formation of extensive physical cross-links within the network, which act to restrict the collapse of the particles.[18d,26] These physical cross-links are expected to arise from intra-particle supramolecular interactions similar to the inter-particle ones discussed earlier. These forces are the extensive charge-assisted hydrogen bonding (CAHB) interactions, and π-π stacking interactions. The expected high proportion of ABSA relative to VCL in the corona leads to the crowding of the polymer backbone in the corona with the ABSA pendant groups and also higher physical cross-link density. Since the corona is expected to be more responsive to stimuli compared to the core, it is reasonable to expect the overall thermo-responsive property of the microgels to be suppressed.[1]

The disruption of these extensive physical cross-links appears to be thermodynamically unfavorable. The entropic gain in the transition to the collapsed microgel state would not offset the increased enthalpy associated with the disruption of attractive interactions. Furthermore, a high content of ABSA comonomer contributes to a high concentration of α-methyl groups from the methacrylate functional group. The α-methyl groups have rotational freedom and can relax the increase in thermal energy in the network.[27] This increase in conformational entropy and flexibility in the backbone contributes further to the unfavorability of a coil to globule transition.[28] Moreover the collapse of our microgels could lead to increased steric crowding and electrostatic repulsion. We did not investigate the thermo-responsive behavior beyond 65°C but further increase in thermal motion as the temperature increases could facilitate the movement of the polymer chains to yield more favorable orientations that maximizes electrostatic complementarity.[29] Even if the attractive interactions are disrupted at higher temperatures, the transition is expected to be broader and more continuous since the network heterogeneity is expected to increase with increased cross-linking density.[30-31]

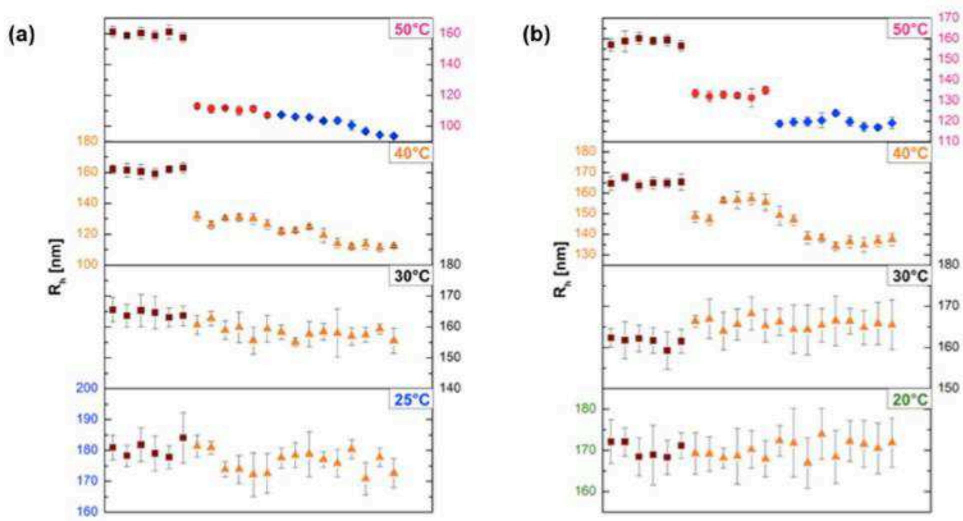

(c)

T [°C]	$R_{h,native}$ [nm]	$R_{h,irrad.}$ [nm]	% decrease in R_h
25	180.3	176.3	2.2
30	164.3	158.3	3.7
40	161.4	121.7	24.6
50	159.6	101.3*	36.5

(d)

T [°C]	$R_{h,native}$ [nm]	$R_{h,irrad.}$ [nm]	% decrease in R_h
20	170.2	170.2	0
30	161.5	165.7	-2.6
40	161.4	121.7	12.3
50	158.5	119.4*	24.7

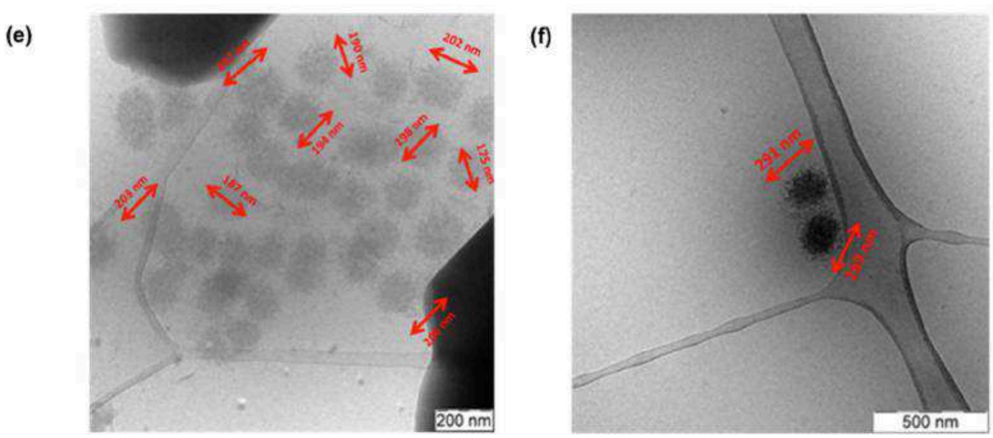

Figure 3(4). Investigation of the photo-responsive behavior of single particles of (a) P(VCL-bis$_{1.5}$-ABSA$_{6.0}$), and (b) P(VCL-bis$_{1.5}$-ABSA$_{10}$) irradiated (λ = 365 nm, 100 mW cm^{-2}) at different temperatures. ■ points represent the R_h of the microgels in their native states while ▲ points represent the R_h reached with UV irradiation. Points represented by the ● symbol show the R_h after equilibration for 1 hour at 50°C followed by 15 minutes of UV irradiation (λ = 365 nm, 100 mW cm^{-2}). Points represented by the ◆ symbol show the R_h after the UV source was left on for an additional 45 minutes. Each measurement point represents the average of 6 x 10 seconds measurement runs in DLS. Percentage deswelling* of (c) P(VCL-bis$_{1.5}$-ABSA$_{6.0}$), and (d) P(VCL-bis$_{1.5}$-ABSA$_{10}$) at the different temperatures. Values were calculated based on the mean R_h values before and after irradiation. *Only the ◆ points were considered in the calculation of the mean. Cryo-TEM micrographs of (e, f) P(VCL-bis$_{1.5}$-ABSA$_{6.0}$) after equilibration for 1 hour at 50°C followed by 15 minutes of UV (λ = 365 nm, 100 mW cm^{-2}) irradiation. Original images of (e) and (f) without annotations are found in Fig. A3(3e, f) respectively of Appendix 3.

The simultaneous application of UV irradiation and elevated temperatures on the single particles of P(VCL-bis$_{1.5}$-ABSA$_{6.0}$) and P(VCL-bis$_{1.5}$-ABSA$_{10}$) leads to enhanced deswelling compared to when temperature was applied as the sole stimulus. The mechanism of water loss under UV irradiation is presumed to be similar to the one proposed in Chapter 2. The size changes for the particles remain marginal at 30°C and below. For measurements above 30°C, the microgel solutions were kept at the respective temperatures for 30-60 minutes before UV irradiation was introduced. Subsequently, we see a two-step deswelling process. Significant deswelling is seen after 15 minutes of continuous UV irradiation, this is indicated by the measurement points represented by circular symbols in Fig. 3(4a,b). Additional 45 minutes of continuous UV irradiation led to further deswelling, indicated by the diamond-shaped measurement points in Fig. 3(4a,b). This suggests that certain conditions have to be fulfilled in order to achieve significant deswelling. First a relatively high temperature is required and secondly, the microgel solution has to be left to stand at this temperature for a prolonged period of time. Finally, UV irradiation (λ = 365 nm, 100 mW cm^{-2}) has to be supplied continuously for an extended period of time.

The heat treatment is required to supply sufficient energy to disrupt some of the non-covalent interactions (especially the stronger CAHB interactions) within the microgel network and to coax the polymer chains and especially the ABSA pendant groups into suitable conformations where they possess greater degrees of freedom. Extended UV irradiation is required to favor the isomerization to the *cis*-ABSA form, within the relatively tight confines of the matrix, in order to attain a photostationary state with a higher proportion of *cis*-ABSA. Presumably the isomerization can occur to a significant extent only when some of the physical cross-links have already been disrupted by the prolonged heat treatment.

The final extent of deswelling is slightly higher in P(VCL-bis$_{1.5}$-ABSA$_{6.0}$) than in P(VCL-bis$_{1.5}$-ABSA$_{10}$). Particles of P(VCL-bis$_{1.5}$-ABSA$_{10}$) and P(VCL-bis$_{1.5}$-ABSA$_{6.0}$) have similar sizes at 20°C, with particles of the latter being even slightly larger. It is therefore reasonable to consider that the chain segments in P(VCL-bis$_{1.5}$-ABSA$_{10}$) are expected to be more crowded than in P(VCL-bis$_{1.5}$-ABSA$_{6.0}$) due to the higher content of relatively large ABSA pendant groups. Since conformations in which different chain segments occupy the same space are not physically possible due to excluded volume demands, the network in P(VCL-bis$_{1.5}$-ABSA$_{10}$) has restricted free volume to accommodate *cis*-ABSA which has a higher free volume requirement than the *trans* isomer.[32] Furthermore, by comparing Fig. 3(1a) and 3(1c), one can discern an area of larger corona for particles of P(VCL-bis$_{1.5}$-ABSA$_{6.0}$), which show lower contrast in the cryo-TEM micrographs compared to the particle core. Since the corona is expected to be more responsive to stimuli compared to the core, the greater extent of deswelling in P(VCL-bis$_{1.5}$-ABSA$_{6.0}$) is expected.

The pH-responsive nature of the single microgel particles was investigated but will not be discussed at length here. The changes in R_h of the particles across the pH range from 2-12 are shown in Fig. A3(5) of Appendix 3. The particles of P(VCL-bis$_{1.5}$-ABSA$_{6.0}$) are largest in the pH range of about 6-8. Within this pH range, the sulfonic acid moieties of the ABSA pendant groups are assumed to be deprotonated. The excess of negative charges leads to repulsive forces which act to expand the microgel network. Above pH 8, R_h of the particles decreases slightly and progressively until the measured pH of 12. While the sulfonic acid groups should remain deprotonated, the addition of 0.1 M NaOH solution to the microgel solutions lead to an electrostatic screening of the negative charges by Na^+ counterions. In the acidic pH region, as the pH decreases below pH 6, the fraction of sulfonic acid groups that are protonated, increases. This favors the formation of intra-particle H-bond interactions between the sulfonic acid group and the C=O group of VCL. As a result of the increased physical cross-links, the particles decrease in size to its minimum value at pH 2.

3.3.5. Self-assembly of P(VCL-ABSA$_{10}$) chains in THF/water mixture.

Most self-assembled polymeric structures are made up of amphiphilic block copolymers,[33] but also include reports of hyperbranched polymers with a three-dimensional dendritic architecture that are capable of supramolecular self-assembly.[34] Meanwhile, random copolymers prepared via non-controlled radical polymerization methods, which can self-assemble, are less known.

We investigated the possibility of this by synthesizing linear chains of P(VCL-ABSA$_{10}$) via the same microgel polymerization procedure described above, while omitting the addition of BIS cross-linker. Under similar reaction conditions, chemical self-cross-linking of PVCL homopolymer is not known to occur.[31] ABSA is also not expected to undergo cross-linking with another azobenzene moiety under the reaction conditions employed.[3(35)]

DLS measurements of the linear chains in their native aqueous state (2 g/L) showed very low count rates and do not show a correlation function that indicates the presence of discrete globular particles. Without the addition of a chemical cross-linker, the self-cross-linking of P(VCL) during free radical polymerization in water via chain transfer reactions is not known to occur.[3(31)] The mechanism for nanosphere formation in 75% w/w water/THF is not completely clear, but it should be driven by similar non-covalent interactions between chains, as seen in the case of the microgel particles in the previous section. From the viewpoint of energy, it is known that vesicles are equilibrium structures formed under thermodynamic control.[3(36)] We could consider our system here to be a form of static self-assembly, since energy in the form of stirring was required for the formation of the nanospheres.[3(5)] As discussed earlier, the hypsochromic shift associated with the *H*-aggregation of ABSA in the microgel network is small and we deduced that the formation of nano-domains from the clustering of ABSA pendant groups could be excluded. It would then be reasonable to make the assumption that with feed amounts of ABSA as high as 10 mol%, leading to an incorporation of ~ 20 mol% ABSA in the microgel network, the copolymeric chains are non-blocky in nature. As a corollary, the linear P(VCL-$ABSA_{10}$) chains synthesized should also consist of a random distribution of ABSA units.

In aqueous solutions, the P(VCL) main chain is hydrophilic and exists in a loose coil conformation.[3(37)] Upon addition into THF, some hydrogen bonding interactions between water molecules and VCL is expected to be broken because THF is a better solvent than water for VCL. THF is also a better solvent for the aromatic ABSA pendant groups and in THF-rich regions, their sulfonic acid terminal ends are expected to remain in the uncharged form. As a result, their complexation to the C=O moieties of the VCL units through CAHB interactions should be enhanced. These electrostatic interactions produce tight ion pairs in the THF-rich regions due to the low dielectric constant of THF as compared to that of water.[3(38)] This would favor the collapse of the loose coils into globules and concomitantly brings the ABSA pendant groups into closer approach with one another. This in turn facilitates ordering of the azobenzene groups relative to each other via stacking interactions which are expected to be stronger in the more hydrophobic THF. The formation and strengthening of these non-covalent interactions in THF act to 'lock' the linear chains into conformations ideal for self-assembly. The large sizes of the nanospheres indicate that they are formed from the self-assembly of multiple chains involved in both intra and inter-chain non-covalent interactions. There most probably exists a dynamic interplay of inter-chain and intra-chain non-covalent interactions. An inhomogeneous mixture of large and small nanoparticles should be expected when the balance is not optimized. Seo *et al*. report that in the case of supramolecular assembly involving a substantial fraction of inter-chain association, ill-defined nanostructures and aggregates are formed.[3(34a)]

Self-assembled structures based on poly(*N*-vinylcaprolactam) P(VCL) are uncommon but have nonetheless been reported by Bronstein *et al*. They produced core−shell, P(VCL) single-molecule nanostructures (diameter less than 70 nm) due to interaction of PVCL with metal ions.[3(37)] Self-assembly of polymeric systems bearing azobenzene groups, on the other hand, are fairly common. For instance, Wang et *al*. report on the formation of nanospheres with diameters up to the micrometer range via self-assembly of an azobenzene-containing polymer. These nanospheres are held together by supramolecular forces and are reported to undergo photo-induced deformation properties.[26b] Seo and coworkers proposed that well-defined nanoparticles are formed only when there are sufficiently high amounts of groups along the polymer chains that can interact supramolecularly. These groups drive intra-chain collapse whereas a lower ratio of supramolecular units promotes inter-chain interactions instead, leading to aggregation.[3(34a)]

Cryo-TEM images in Fig. 3(5a-c) reveal the coexistence of dense nanospheres and vesicle-like nanospheres. During the capture of these images, exposure of the nanospheres to the electron beam for more than 10 seconds leads to sublimation of THF, in the vitrified THF/water layer. The effect of this is visible as bright empty holes in the matrix of the nanospheres, which are visible in Fig. 3(5a,b). This phenomenon compromises the quality of the captured images but it nonetheless reveals that the THF-rich regions are compartmentalized within the interior of the nanospheres, most likely associating favorably with the more hydrophobic ABSA groups.[3(39)]

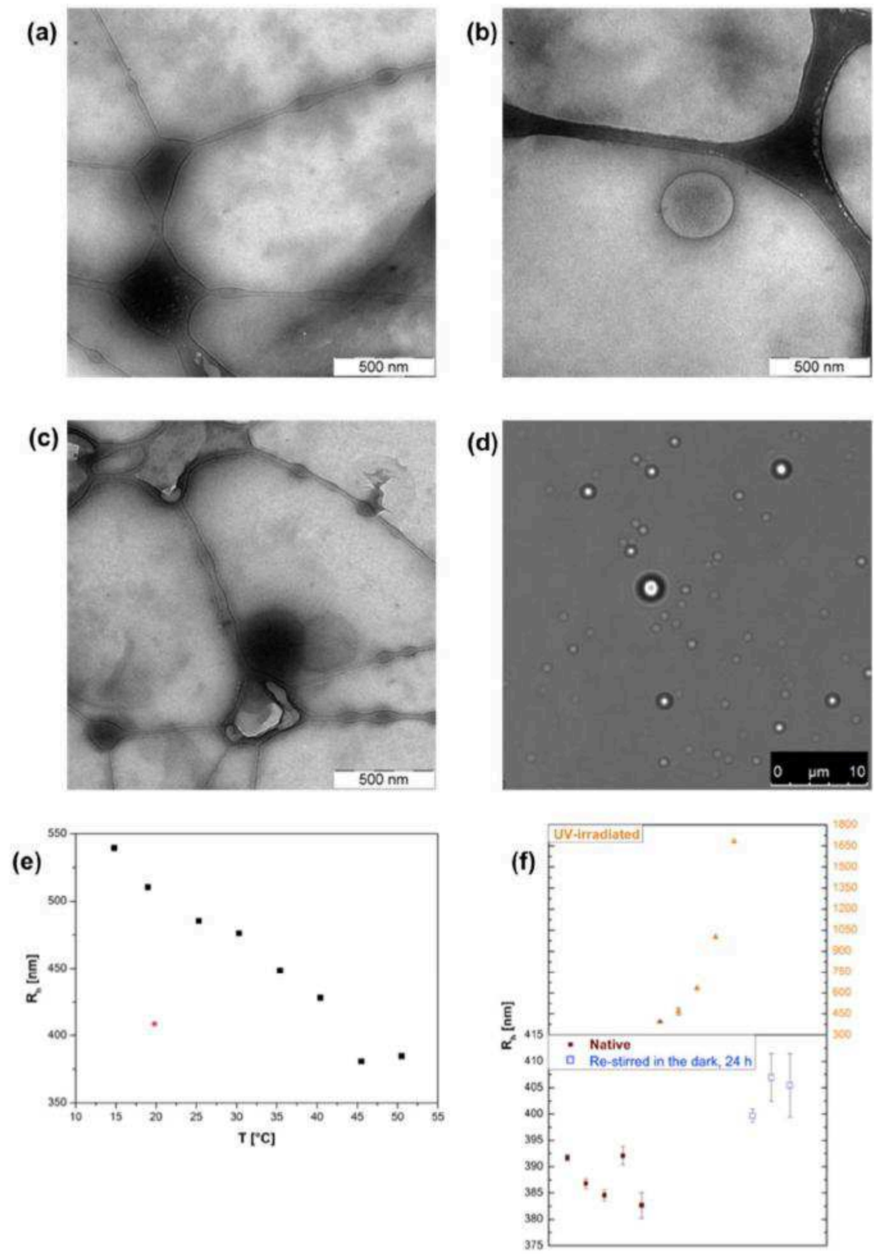

Figure 3(5). Cryo-TEM micrographs of linear P(VCL-ABSA$_{10}$) chains in 75 wt. % H_2O/THF, self-assembled into (a) to (c) Nanospheres and vesicles. (d) Confocal micrograph of particles self-assembled from linear P(VCL-ABSA$_{10}$) chains in 75 wt. % H_2O/THF. (e) Size-temperature data of self-assembled particles of P(VCL-ABSA$_{10}$). ■ represents points during the heating cycle while ★ represents the R_h upon cooling from 50°C to 20°C. (f) Monitoring the change in size of the cooled particles from (e) at 20°C (represented by ■ symbol), after 15 mins of UV irradiation (λ = 365 nm, 100 mW cm^{-2}, represented by ▲ symbol), and after re-stirring the dispersion in the dark for 20 hours (represented by □ symbol).

3.3.6. Investigation of the thermo- and photo-responsive properties of nanospheres assembled from linear P(VCL-ABSA$_{10}$) chains

Fig. 3(5e) shows the size-temperature data of the self-assembled nanospheres obtained via a heating cycle to 50°C. The square-shaped measurement points show the continuous change in R_h (obtained via a cumulant fit) during a heating cycle of the nanospheres assembled from the linear P(VCL-ABSA$_{10}$) chains. The nanospheres exhibit a deswelling with increase in temperature and this is to be expected for a VCL-containing polymer. Upon cooling to 20°C, the particle relaxes and its R_h (star-shaped measurement point in Fig. 3(5e)) is slightly larger than the R_h at 50°C. The initial size of the freshly prepared particles at 20°C is however not recovered. The smaller size upon cooling compared to the initial size suggests that water was removed from the self-assembled network during heating and was not fully regained when the attractive hydrophobic interactions that hold the network together were strengthened on heating.

After this heating cycle, the cooled solution of nanospheres was irradiated with UV (λ = 365 nm, 100 mW cm^{-2}) for 15 minutes *in situ* of the toluene bath of the DLS instrument maintained at 20°C. The triangular measurement points in Fig. 3(5f) represent the sizes captured after 15 minutes of UV irradiation. The time lapsed between measurement points was about 5 minutes. The margins of error associated with the disrupted particles are of the order of hundreds of nanometer and are not represented in Fig. 3(5f). These measurements were also associated with low count rates, further indicating that the nanospheres were disrupted. Re-stirring (600 rpm) in the dark at room temperature for more than 20 hours led to the re-assembling of the nanospheres. The unfilled, square-shaped measurement points in Fig. 3(5f) indicate the size of the re-assembled particles.

Evidently, photoisomerization with UV (λ = 365 nm, 100 mW cm^{-2}) is destructive to the nanosphere structure. This indicates a disruption of the non-covalent supramolecular forces holding the chains together. Presumably the isomerization of the ABSA pendant group from the *trans* to *cis* form results in the distancing of the sulfonic acid terminal end of ABSA away from the C=O group of VCL on an adjacent chain. The stacking interactions between the *trans*-ABSA can also be disrupted due to the large steric repulsion of the *cis* isomers, which have relatively weaker association constants than the *trans* isomer.[3(40)] The re-assembly of the nanospheres observed upon re-stirring could be attributed to the chain re-ordering and reestablishment of the non-covalent interactions.

A more rigorous analysis is required to account for the assembly, disruption and re-assembly of the P(VCL-ABSA$_{10}$) linear chains into stable nanospheres. The use of theoretical models and computer simulation approaches could be explored to derive a clear description.

3.3.7. Investigation of the fluorescence behavior of P(VCL-bis$_{1.5}$-ABSA$_x$) microgels and nanospheres assembled from linear P(VCL-ABSA$_{10}$) chains

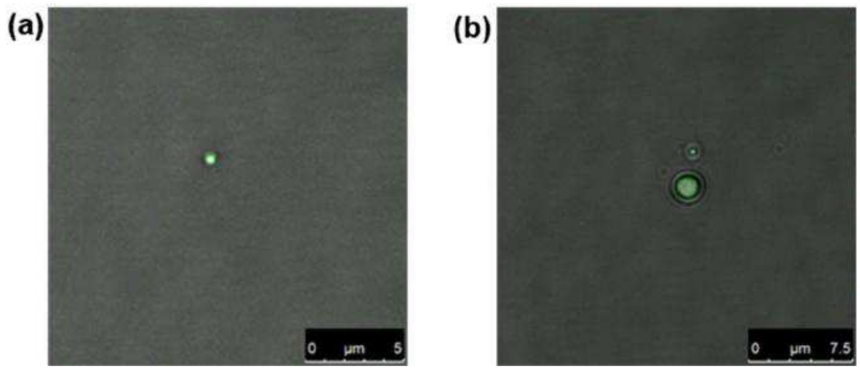

Figure 3(6). Confocal microscopy images of (a) P(VCL-bis$_{1.5}$-ABSA$_{10}$) microgel and (b) Self-assembled nanosphere of P(VCL-ABSA$_{10}$).

Interest in the use of azobenzene-based fluorescent material is fairly recent.[3(41)] This is because azobenzene molecules are mostly non-fluorescent in dilute solutions, having low quantum yields in the range of about 10^{-7}-10^{-5}.[3(24),3(42)] Compounds with enhanced fluorescence behavior that can be modulated have been molecularly designed by the clever coupling of a fluorescent dye with an isomerizable, π-conjugated azobenzene molecule.[3(41a)] However, to achieve fluorescence emission on its own, the azobenzene molecule or groups within polymeric systems have to fulfill a key criterion. The *trans*-to-*cis* isomerization of the azobenzene moiety should be suppressed to some extent so that the non-radiative relaxation process of the azobenzene groups in those compounds is prevented.[3(43a)] Suppression of the photo-isomerization of azobenzene can be achieved by confining the azobenzene molecules within restricted volumes via aggregation and self-organization phenomena.[3(43)] To attain self-organization, the azobenzene-containing system should be amphiphilic in nature, allowing it to self-assemble in suitable media into hierarchical structures.[3(24),3(43)] The use of specific, intramolecular forces that constricts the N=N bond freedom of the azobenzene molecule has also been reported by Yoshino et al.[3(41b)] In this case, they utilized N-B dative bonds to restrict both rotation and therefore the isomerization of the azobenzene molecule which resulted in the molecules exhibiting high fluorescence quantum yields.

From the discussions of the thermo- and photo-responsive behaviors of our microgel system, both as dimeric assemblies and as single particles, it is clear that our particles fulfills the criteria necessary to allow fluorescence emission of the ABSA moieties. Confocal microscopic investigations (see Fig. 3(6)) reveal that P(VCL-bis-$ABSA_{10}$) microgels and the self-assembled particles of P(VCL-$ABSA_{10}$) exhibit fluorescence emission detected at ~510 nm when excited by light of λ = 405 nm. P(VCL-bis-$ABSA_{6.0}$) microgels exhibited comparatively weaker fluorescence. [See Fig. A3(2) of Appendix 3 for the fluorescence emission spectrum of P(VCL-bis-$ABSA_{10}$)].

3.3.8. Possibility for higher order aggregation of microgel particles

We have discussed the proclivity of the particles of P(VCL-bis-$ABSA_{6.0}$) and P(VCL-bis-$ABSA_{10}$) to exist as dimeric assemblies in their native solutions. We did not however detect higher order aggregation of the particles in solution via DLS. Neither have we shown their assembly into more complex macrostructures. In Figs. 3(2b,d), however, we observe clusters of particles in very close proximity, indicating the potential for forming ordered assemblies of particles such as monolayers. The particles in Figs. 3(2b,d) are confined within a thin vitrified ice layer, and this suggests that aggregation could be induced by exerting homogeneous pressure around a certain concentration of microgel solution, within a confined volume. As pressure increases, the polymer-water interaction becomes increasingly unfavorable.[3(44)] As a result, the inter-particle interactions via supramolecular forces of CABH and π-π stacking could increase and drive the formation of ordered three dimensional suprastructures. Fig. A3(6) of Appendix 3 further demonstrates the possibility for confinement-induced aggregation. The particles of P(VCL-$bis_{1.5}$-$ABSA_{6.0}$), confined within glass plates for confocal microscopic measurements, are seen in Fig. A3(6) as a string of inter-linked particles. Since these microgel particles are also polyelectrolytic in nature, the ionic strength or pH of the solution are parameters that could be varied to induce particle aggregation.[3(45)]

3.4. Conclusion

In summary, P(VCL) copolymeric microgels were synthesized via a convenient surfactant-free precipitation polymerization procedure in water to contain relatively high incorporation levels (between 20 and 30 wt. %) of 4-[(4-methacryloyloxy)phenylazo] benzenesulfonic acid (ABSA). High ABSA incorporation results in the presence of extensive intra- and inter-particle charged-assisted H-bonding and π-π stacking interactions. These attractive interactions strongly influence the thermo- and photo-responsive behaviors of the dimeric and single particles.

In their native solutions, the microgels were found to display a curious anisotropic morphology. They prefer to exist as dimeric assemblies of particles whose peripheral dangling chains are interlocked with the inner network structure of their dimeric partner. In dimeric assemblies of P(VCL-bis$_{1.5}$-ABSA$_{6.0}$) we see a superficial decrease in size at temperatures above the VPTT of pure P(VCL-bis) microgels. This can be attributed to the disruption of some hydrogen bonding interactions with water molecules within the dimeric assemblies. P(VCL-bis$_{1.5}$-ABSA$_{10}$) on the other hand showed a marginal increase in size above the same temperature. This most probably arises from the loosening of the inter-particle interactions. UV irradiation magnifies the effect of the temperature stimulus in both microgels, to increasing extents at higher temperatures.

The individual particles in the dimeric assemblies were not separable by temperature or UV stimulus. We were nevertheless able to disrupt the dimers by slightly increasing the ionic strength of the microgel solution before subjecting them to short periods of mechanical agitation by ultrasonic treatment. In both P(VCL-bis$_{1.5}$-ABSA$_{6.0}$) and P(VCL-bis$_{1.5}$-ABSA$_{10}$) single particles, we observe a suppression of the thermo-responsive property normally associated with P(VCL)-based microgels. They exhibit a shallow deswelling from 30°C and the particle size continues to decrease gradually to a minimum at around 50°C. The extent of deswelling was significantly enhanced by UV irradiation, especially at higher temperatures, with sufficient equilibration times and with longer durations of UV irradiation. We also synthesized random copolymer chains of P(VCL-ABSA$_{10}$) using the same microgel polymerization procedure but eliminated the use of the chemical cross-linker BIS. Via similar non-covalent interactions as those present in the microgels, the linear chains were able to self-assemble into nanospheres of around 500 nm in diameter in a 75 wt. % water/THF mixture. These nanospheres could be disrupted via prolonged UV irradiation of 15 minutes and then re-assembled by stirring the irradiated solution overnight, in the dark. In addition, the P(VCL-bis$_{1.5}$-ABSA$_{10}$) particles and the self-assembled nanospheres of P(VCL-ABSA$_{10}$) were found to display fluorescence emission at 510 nm when excited by light of λ = 405 nm. The origin of this phenomenon is believed to be due to the restricted *trans-cis* isomerization of the ABSA pendant groups within the crowded and extensively physically cross-linked networks.

3.5. Outlook

The ability of the dangling chains of the microgel particles to dynamically complex with neighboring particles and surfaces via multiple, dynamic, non-covalent supramolecular forces should be further explored as a convenient and versatile strategy to bind to targets via specific interactions and to organize the particles into more complex ensembles. Such microgels could be used in the removal of organic pollutants, dyes, and metals in the water remediation field, for example.[3(46)] Furthermore, these microgels could be used to form interactions with quantum dots to produce semiconductor devices[3(47)] and be used as scaffolds for cell growth with control over the cell detachment.[3(48)]

The use of external forces or agents, for example, multivalent ions to direct the assembly of multiple microgel particles could be explored to obtain microgel ensembles of various architectures. This would be relevant since controlling interparticle interactions and aggregation are important in various areas such as the investigation of cluster formation in various disease processes, protein crystallography and the production of photonic crystals.[3(49)]

The reversible formation and disruption of supramolecular bonds like H-bond can bring additional functionality such as switchable electrical conductivity, proton conductivity or photonic band gap to materials derived from such particles.[3(50)] Furthermore, stimuli-dependent particles with potential for multiple, non-covalent interactions can be used as an easy and low-cost method to coat various interfaces for biomedical and environmental applications.[3(51)]

The self-assembling linear chains that are responsive to external stimuli presents a facile strategy to achieve chain collapse, and can be further formulated for use in the uptake, encapsulation, and triggered release of active agents. Improving the ability to effectively and efficiently control particle and chain self-assembly and disassembly, through the application of external stimuli, is a continuing research goal in the field of smart molecular systems development.

3.6. REFERENCES

3(1) Pich, A.; Richtering, W. *Chemical Design of Responsive Microgels*; Springer-Verlag: Berlin, Heidelberg, 2011.

3(2) Fernandez-Nieves, A.; Wyss, H. M.; Mattsson, J.; Weitz, D. A. eds. *Microgel Suspensions: Fundamentals and Applications*; Wiley-VCH Verlag; Weinheim, 2011.

3(3) Roy, D.; Cambre, J. N.; Sumerlin, B. S. Future Perspectives and Recent Advances in Stimuli-responsive Materials. *Prog. Polym. Sci.* **2010**, *35*, 278–301.

3(4) Gong, Y.; Zhu, A. I.; Zhang, Q. G.; Liu, Q. L. Colloidosomes from Poly(*N*-vinyl-2-pyrrolidone)-coated Poly(*N*-Isopropylacrylamide-co-acrylic acid) Microgels via UV Crosslinking. *RSC Adv.* **2014**, *4*, 9445-9450.

3(5) Whitesides, G. M.; Grzybowski, B. Self-assembly at All Scales. *Science* **2002**, *295*, 2418-2421.

3(6) Demirörs, A. F.; Pillai, P. P.; Kowalczyk, B.; Grzybowski, B. A. Colloidal Assembly Directed by Virtual Magnetic Moulds. *Nature* **2013**, *503*, 99–103 and references therein.

3(7) Shishkin, O. V.; Zubatyuk, R. I.; Shishkina, S. V.; Dyakonenko, V. V.; Medviediev, V. V. Role of Supramolecular Synthons in the Formation of the Supramolecular Architecture of Molecular Crystals Revisited from an Energetic Viewpoint. *Phys. Chem. Chem. Phys.* **2014**, *16*, 6773-6786.

3(8) (a) Desiraju, G. R. Supramolecular Synthons in Crystal Engineering—A New Organic Synthesis. *Angew. Chem. Int. Ed.* **1995**, *34*, 2311-2327.; (b) Desiraju, G. R. Designer Crystals: Intermolecular Interactions, Network Structures and Supramolecular Synthons. *Chem. Commun.* **1997**, 1475-1482.

3(9) (a) Son, S. U.; Reingold, J. A.; Carpenter, G. B.; Czech, P. T.; Sweigart, D. A. Charge-Assisted Hydrogen Bonding and Other Noncovalent Interactions in the Self-Assembly of the Organometallic Building Block [(η^6-hydroquinone)Rh(P(OPh)$_3$)$_2$]$^+$ with a Range of Counteranions. *Organometallics* **2006**, *25*, 5276-5285 and references therein; (b) Fang, Y.; Nguyen, P.; Ivasenko, O.; Aviles, M. P.; Kebede, E.; Askari, M. A.; Ottenwaelder, X.; Ziener, U.; Sirid, O.; Cuccia, L. A. Charge-assisted Hydrogen Bond-directed Self-assembly of an Amphiphilic Zwitterionic Quinonemonoimine at the Liquid–solid Interface. *Chem. Commun.* **2011**, *47*, 11255–11257.

3(10) Dunitz, J. D.; Gavezzotti, A. Supramolecular Synthons: Validation and Ranking of Intermolecular Interaction Energies. *Cryst. Growth. Des.* **2012**, *12*, 5873-5877.

3(11) Huheey, J. E.; Keiter, E. A.; Keiter, R. L. *Inorganic Chemistry: Principles of Structure and Reactivity 4th Ed*.; Harper Collins; New York, 1993.

3(12) Gong, C. B.; Wong, K. L.; Lam, M. H. W. Photoresponsive Molecularly Imprinted Hydrogels for the Photoregulated Release and Uptake of Pharmaceuticals in the Aqueous Media. *Chem. Mater.* **2008**, *20*, 1353-1358.

3(13) Rubinstein, M.; Colby, R. H. *Polymer Physics*; Oxford University Press: New York, 2003.

3(14) (a) Karg, M.; Hellweg, T. Smart Inorganic/Organic Hybrid Microgels: Synthesis and Characterisation. *J. Mater. Chem.* **2009**, *19*, 8714–8727.; (b) Herves, P.; Perez-Lorenzo, M.; Liz-Marzan, L. M.; Dzubiella, J.; Lu, Y.; Ballauff, M. Catalysis by Metallic Nanoparticles in Aqueous Solution: Model Reactions. *Chem. Soc. Rev.* **2012**, *41*, 5577–5587.; (c) Milne, J. L.; Borgnia, M. J.; Bartesaghi, A.; Tran, E. E.; Earl, L. A.; Schauder, D. M.; Lengyel, J.; Pierson, J.; Patwardhan, A.; Subramaniam, S. Cryo-Electron Microscopy - A Primer for the Non-Microscopist. *FEBS J*. **2013**, *280*, 28-45.

3(15) Cho, H.-J.; Hyun, J.-K.; Kim, J.-G.; Jeong, H. S.; Park, H. N.; You, D.-J.; Jung, H. S. Measurement of Ice Thickness on Vitreous Ice Embedded Cryo-EM Grids: Investigation of Optimizing Condition for Visualizing Macromolecules. *J. Anal. Sci. Technol.* **2013**, *4*, 7.

3(16) Tiwari, R.; Heuser, T.; Weyandt, E.; Wang, B.; Walther, A. Polyacid Microgels with Adaptive Hydrophobic Pockets and Ampholytic Character: Synthesis, Solution Properties and Insights into Internal Nanostructure by Cryogenic-TEM. *Soft Matter* **2015**, *11*, 8342-8353.

3(17) Saraydin, D.; Karadag, E. Binding of Some Dyes onto Crosslinked Poly(*N*-Vinylpyrrolidone). *Polym. Bull.* **2000**, *44*, 501–508.

3(18) (a) Kirsh, E.Y. Water-soluble Poly(*N*-Vinylamides): Microstructure, Solvation, Conformational State and Complex Formation in Aqueous Solutions. *Prog. Polym. Sci.* **1993**, *18*, 519-542.; (b) Makhaeva, E. E.; Tenhu, H.; Khokhlov, A. R. Behavior of Poly(*N*-vinylcaprolactam-co-methacrylic acid) Macromolecules in Aqueous Solution: Interplay between Coulombic and Hydrophobic Interaction. *Macromolecules* **2002**, *35*, 1870-1876.; (c) Okhapkin, I. M.; Nasimova, I. R.; Makhaeva, E. E.; Khohlov, A. R. Effect of Complexation of Monomer Units on pH- and Temperature-Sensitive Properties of Poly(*N*-vinylcaprolactam-co-methacrylic acid). *Macromolecules* **2003**, *36*, 8130-8138.; (d) Costa, E.; Coelho, M.; Illharco, L. M.; Aguiar-Ricardo, A.; Hammond, P. T. Tannic Acid Mediated Suppression of PNIPAAm Microgels Thermoresponsive Behavior. *Macromolecules* **2011**, *44*, 612-621.

3(19) Patai, S.; Rappoport, Z. eds. *The Chemistry of Sulphonic Acids, Esters and their Derivatives*; John Wiley; Chichester, 1991.

3(20) Natansohn, A.; Rochon, P. Photoinduced Motions in Azo-Containing Polymers. *Chem. Rev.* **2002**, *102*, 4139-4176 and references therein.

3(21) Tong, X.; Wang, G.; Soldera, A.; Zhao, Y. How Can Azobenzene Block Copolymer Vesicles Be Dissociated and Reformed by Light? *J. Phys. Chem. B.* **2005**, *109*, 20281-20287.

3(22) (a) Kasha, M.; Rawls. H. R.; El-Bayoumi, M. A. The Exciton Model in Molecular Spectroscopy. *Pure Appl. Chem.* **1965**, *11*, 371-392.; (b) Kuiper, J. M.; Engberts, J. B. F. N. H-Aggregation of Azobenzene-Substituted Amphiphiles in Vesicular Membranes. *Langmuir* **2004**, *20*, 1152-1160 and references therein.

3(23) (a) Geng, J.; Zhao, X.; Zhou, E.; Li, G.; Lam, J. W. Y.; Tang, B. Z. Shear Induced Molecular Alignments of a Side-Chain Liquid Crystalline Polyacetylene Containing Biphenyl Mesogens. *Polymer* **2003**, *44*, 8095–8102.; (b) Ganicz, T.; Stańczyk, W. Side-chain Liquid Crystal Polymers (SCLCP): Methods and Materials. An Overview. *Materials* **2009**, *2*, 95-128.; (c) Zheng, J.-F.; Yu, Z.-Q.; Liu, X.; Chen, X.-F.; Yang, S.; Chen, E.-Q. Side-chain Liquid-Crystalline Polymers based on Flexible Rod-like Mesogen Directly Attached to Backbone. *J. Polym. Sci. Part A: Polym. Chem.* **2012**, *50*, 5023-5031.

3(24) Han, M.; Hara, M. Intense Fluorescence from Light-Driven Self-Assembled Aggregates of Nonionic Azobenzene Derivative. *J. Am. Chem. Soc.* **2005**, *127*, 10951-10955 and references therein.

3(25) Venegas-Sanchez, J.; Kusunoki, T.;Yamamoto, M.; Kobayashi, T. Sono-respond on Thermosensitive Polymer Microgels Based on Cross-linked Poly(*N*-Isopropylacrylamide-co-acrylic acid). *Ultrason. Sonochem.* **2013**, *20*, 1271-1275.

3(26) (a) Cabrera, I.; Krongauz, V. Dynamic Ordering of Aggregated Mesomorphic Macromolecules. *Nature* **1987**, *326*, 582-585.; (b) Wang, S.; Zhang, N.; Ge, X.; Wan, Y.; Li, X.; Yan, L.; Xia, Y.; Song, B. Self-Assembly of an Azobenzene-containing Polymer Prepared by a Multi-Component Reaction: Supramolecular Nanospheres with Photo-Induced Deformation Properties. *Soft Matter* **2014**, *10*, 4833-4839.

3(27) Tirumala, V. R.; Ilavsky, J.; Ilavsky, M. Effect of Chemical Structure on the Volume-Phase Transition in Neutral and Weakly Charged Poly(*N*-alkyl(meth)acrylamide) Hydrogels Studied by Ultrasmall-Angle X-ray Scattering. *J. Chem. Phys.* **2006**, *124*, 234911.

3(28) Keerl, M.; Smirnovas, V.; Winter, R.; Richtering, W. Copolymer Microgels from Mono- and Disubstituted Acrylamides: Phase Behavior and Hydrogen Bonds. *Macromolecules* **2008***, 41,* 6830-6836.

3(29) Sun, H.; Ye, K.; Wang, C.; Qi, H.; Li, F.; Wang, Y. The π−π Stacked Geometries and Association Thermodynamics of Quinacridone Derivatives Studied by ^{1}H NMR. *J. Phys. Chem.* A **2006**, *110*, 10750-10756.

3(30) Crassous, J. J.; Wittemann, A.; Siebenbürger, M.; Schrinner, M.; Drechsler, M.; Ballauf, M. Direct Imaging of Temperature-Sensitive Core-Shell Latexes by

Cryogenic Transmission Electron Microscopy. *Colloid Polym. Sci.* **2008**, *286*, 805–812.
3(31) Schneider, F.; Balaceanu, A.; Feoktystov, A.; Pipich, V.; Wu, Y.; Allgaier, J.; Pyckhout-Hintzen, W.; Pich, A.; Schneider, G. J. Monitoring the Internal Structure of Poly(*N*-vinylcaprolactam) Microgels with Variable Cross-Link Concentration. *Langmuir* **2014**, *30*, 15317−15326.
3(32) El Halabieh, R. H.; Mermut, O.; Barrett, C. Using Light to Control Physical Properties of Polymers and Surfaces with Azobenzene Chromophores. *J. Pure Appl. Chem.* **2004**, *76*, 1445–1465.
3(33) (a) Li, Z.; Ding, J.; Day, M.; Tao, Y. Molecularly Imprinted Polymeric Nanospheres by Diblock Copolymer Self-Assembly. *Macromolecules* **2006**, *39*, 2629-2636.; (b) Hu, Z.; Verheijen, W.; Hofkens, J.; Jonas, A. M.; Gohy, J.-F. Formation of Vesicles in Block Copolymer-Fluorinated Surfactant Complexes. *Langmuir* **2007**, *23*, 116-122.; (c) Park, J.-S.; Akiyama, Y.; Yamasaki, Y.; Kataoka, K. Preparation and Characterization of Polyion Complex Micelles with a Novel Thermosensitive Poly(2-isopropyl-2-oxazoline) Shell via the Complexation of Oppositely Charged Block Ionomers. *Langmuir* **2007**, *23*, 138-146.; (d) Skrabania, K.; Kristen, J.; Laschewsky, A.; Akdemir, O.; Hoth, A.; Lutz, J.-F. Design, Synthesis, and Aqueous Aggregation Behavior of Nonionic Single and Multiple Thermoresponsive Polymers. *Langmuir* **2007**, *23*, 84-93.
3(34) (a) Seo, M.; Beck, B. J.; Paulusse, J. M. J.; Hawker, C. J.; Kim, S. Y. Polymeric Nanoparticles via Noncovalent Cross-Linking of Linear Chains. *Macromolecules* **2008**, *41*, 6413-6418.; (b) Wu, J.; Tang, H.; Wu, P. Self-Assembled Aggregates of Dendritic-Linear Copolymers: Vesicles and Microspheres. *Soft Matter* **2011**, *7*, 4166-4169.; (c) Chen, C.; Liu, G.; Liu, X.; Pang, S.; Zhu, C.; Lv, L.; Ji, J. Photo-responsive, Biocompatible Polymeric Micelles Self-Assembled from Hyperbranched Polyphosphate-based Polymers. *Polym. Chem.* **2011**, *2*, 1389-1397.; (d) Chen, C.-J.; Jin, Q.; Liu, G.-Y.; Li, D. D.; Wang, J.-L.; Ji, J. Reversibly Light-Responsive Micelles Constructed via a Simple Modification of Hyperbranched Polymers with Chromophores. *Polymer* **2012**, *53*, 3695-3703.; (e) Kurniasih, I. N.; Keilitz, J.; Haag, R.
Dendritic Nanocarriers Based on Hyperbranched Polymers. *Chem. Soc. Rev.* **2015**, *44*, 4145-4164 and references therein.
3(35) Jing, X.-K.; Wang, X.-S.; Guo, D.-M.; Zhang, Y.; Zhai, F.-Y.; Wang, X.-L.; Chen, L.; Wang, Y.-Z. The High-Temperature Self-Crosslinking Contribution of Azobenzene Groups to the Flame Retardance and Anti-Dripping of Copolyesters. *J. Mater. Chem. A* **2013**, *1*, 9264-9272

3(36) Luo, L.; Eisenberg, A. Thermodynamic Stabilization Mechanism of Block Copolymer Vesicles. *J. Am. Chem. Soc.* **2001**, *123*, 1012–1013.

3(37) Bronstein, L. M.; Kostylev, M.; Tsvetkova, I.; Tomaszewski, J.; B.; E. E.; Okhapkin, I.; Khokhlov, A. R. Core−Shell Nanostructures from Single Poly(*N*-Vinylcaprolactam) Macromolecules: Stabilization and Visualization. *Langmuir* **2005**, *21*, 2652–2655.

3(38) Cui, H.; Chen, Z.; Zheng, S.; Wooley, K. L.; Pochan, D. J. Block Copolymer Assembly via Kinetic Control. *Science* **2007**, *317*, 647-650.

3(39) Hu, J.; Yu, H.; Gan, L. H.; Hu, X. Photo-driven Pulsating Vesicles from Self-Assembled Lipid-like Azopolymers. *Soft Matter* **2011**, *7*, 11345-11350.

3(40) (a) Khoukh, S.; Oda, R.; Labrot, Th.; Perrin, P.; Tribet, C. Light-Responsive Hydrophobic Association of Azobenzene-Modified Poly(acrylic acid) with Neutral Surfactants. *Langmuir* **2007**, *23*, 94-104.; (b) Babu, S. S.; Praveen, V. K.; Ajayaghosh, A. Functional π-Gelators and Their Applications. *Chem. Rev.* **2014**, *114*, 1973−2129.

3(41) (a) Anwar, N.; Willms, T.; Grimme, B.; Kuehne, A. J. C. Light-Switchable and Monodisperse Conjugated Polymer Particles. *ACS Macro Lett*. **2013**, *2*, 766-769.; (b) Yoshino, J.; Kano, N.; Kawashima, T. Fluorescent Azobenzenes and Aromatic Aldimines Featuring an N–B Interaction. *Dalton Trans.* **2013**, *42*, 15826-15834.

3(42) (a) Rau, H. Spectroscopic Properties of Organic Azo Compounds. *Angew. Chem. Int. Ed.* **1972**, *12*, 224-235.; (b) Morgante, C. G.; Struve, W. S. $S_2 \rightarrow S_0$ Fluorescence in *trans*-Azobenzene. *Chem. Phys. Lett.* **1979**, *68*, 267-271.

3(43) (a) Ren, H.; Chen, D.; Shi, Y.; Yu, H.; Fu, Z. A Carboxylic Azo Monomer and its Homopolymer: Synthesis, Self-Organization and Fluorescence Behaviour in Solution. *Polym. Chem.* **2015**, *6*, 270-277 and references therein; (b) Han, M.; Takeoka, Y.; Seki, T. Facile Morphological Control of Fluorescent Nano/Microstructures via Self-Assembly and Phase Separation of Trigonal Azobenzenes Showing Aggregation-Induced Emission Enhancement in Polymer Matrices. *J. Mater. Chem. C* **2015**, *3*, 4093-4098.; (c) Bo, Q.; Zhao, Y. Fluorescence from an Azobenzene-Containing Diblock Copolymer Micelle in Solution. *Langmuir* **2007**, *23*, 5746-5751.

3(44) Liétor-Santos, J. J.; Sierra-Martín, B.; Gasser, U.; Fernández-Nieves, A. The Effect of Hydrostatic Pressure Over the Swelling of Microgel Particles. *Soft Matter* **2011**, *7*, 6370-6374.

3(45) Lebovka, N. I. Aggregation of Charged Colloidal Particles. *Adv. Polym. Sci.* **2014**, *255*, 57–96.

3(46) (a) Qu, X.; Alvarez, P. J.; Li, Q. Applications of Nanotechnology in Water and Wastewater Treatment. *Water Res.* **2013**, *47*, 3931-3146.; (b) Qu, X.; Brame, J.; Li, Q.; Alvarez, P. J. Nanotechnology for a Safe and Sustainable Water Supply: Enabling Integrated Water Treatment and Reuse. *Acc. Chem. Res.* **2013**, *46*, 834-843.; (c) Wan, D.; Chen, F.; Geng, Q.; Lu, H.; Willcock, H.; Liu, Q.; Wang, F.; Zou, K.; Jin, M.; Hongting Pu, H.; Du, J. A Multifunctional Azobenzene-Based Polymeric Adsorbent for Effective Water Remediation. *Scientific Reports* **2014**, *4*, 7296.; (d) Kuppusamy, S.; Thavamani, P.; Megharaj, M.; Naidu, R. Bioremediation Potential of Natural Polyphenol Rich Green Wastes: A Review of Current Research and Recommendations for Future Directions. *Environ. Technol. Innov.* **2015**, *4*, 17-28.; (e) Gehrke, I.; Geiser, A.; Somborn-Schulz, A. Innovations in Nanotechnology for Water Treatment. *Nanotechnol. Sci. Appl.* **2015**, *8*, 1–17.

3(47) Cai. Y.; Wu, X.; Liu, Q.; Liu, H. Alternative Procedure for the Incorporation of Quantum Dots into Poly(*N*-Isopropyl acrylamide-co-acrylic acid) Microgels based on Multiple Interactions. *J. Appl. Polym. Sci.* **2016**, *133*, 43277.

3(48) Xia, Y.; He, X.; Cao, M.; Wang, X.; Sun, Y.; He, H.; Xu, H.; Lu, J. R. Self-Assembled Two-Dimensional Thermoresponsive Microgel Arrays for Cell Growth/Detachment Control. *Biomacromolecules* **2014**, *15*, 4021-4031.

3(49) Min, Y.; Akbulut, M.; Kristiansen, K.; Golan, Y.; Israelachvili, J. The Role of Interparticle and External Forces in Nanoparticle Assembly. *Nature Materials* **2008**, *7*, 527 – 538.

3(50) (a) Soininen, A. J.; Rahikkala, A.; Korhonen, J. T.; Kauppinen, E. I.; Mezzenga, R.; Raula, J.; Ruokolainen, J. Hierarchical Structures of Hydrogen-Bonded Liquid-Crystalline Side-Chain Diblock Copolymers in Nanoparticles. *Macromolecules* **2012**, *45*, 8743−8751.; (b) Wang, R.; Wu, X.; Yan, X.; He, G.; Hu, Z. Proton Conductivity Enhancement of SPEEK Membrane Through n-BuOH Assisted Self-Organization. *J. Membr. Sci.* **2015**, *479*, 46-54.

3(51) Ejima, H.; Richardson, J. J.; Liang, K.; Best, J. P.; van Koeverden, M. P.; Such, G. K.; Cui, J.; Caruso, F. One-Step Assembly of Coordination Complexes for Versatile Film and Particle Engineering. *Science* **2013**, *341*, 154-157.

APPENDIX 3

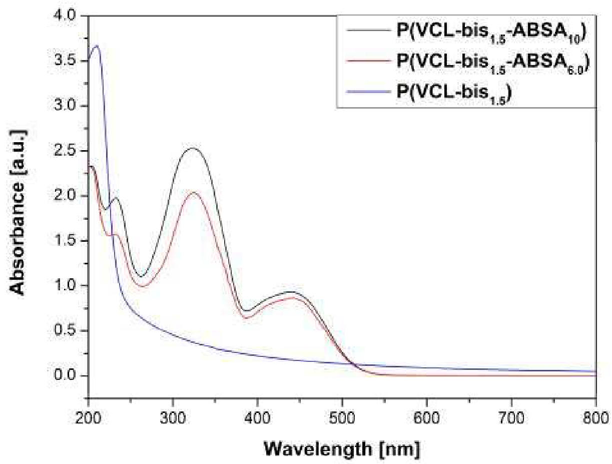

Figure A3(1). Absorption spectra of aqueous solutions of P(VCL-bis$_{1.5}$), P(VCL-bis$_{1.5}$-ABSA$_{6.0}$) and P(VCL-bis$_{1.5}$-ABSA$_{10}$).

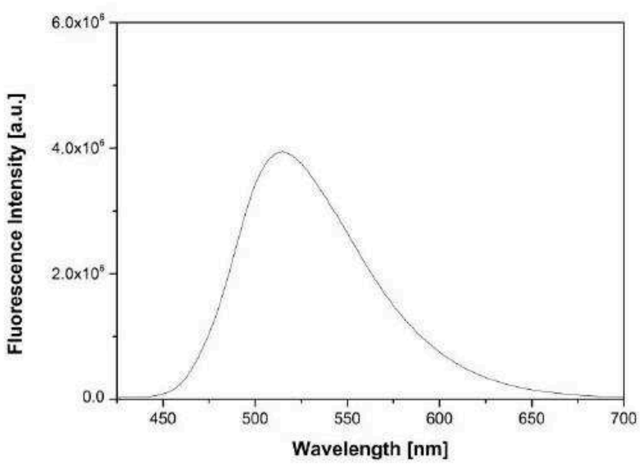

Figure A3(2). Fluorescence emission spectrum of P(VCL-bis-ABSA$_{10}$) microgel.

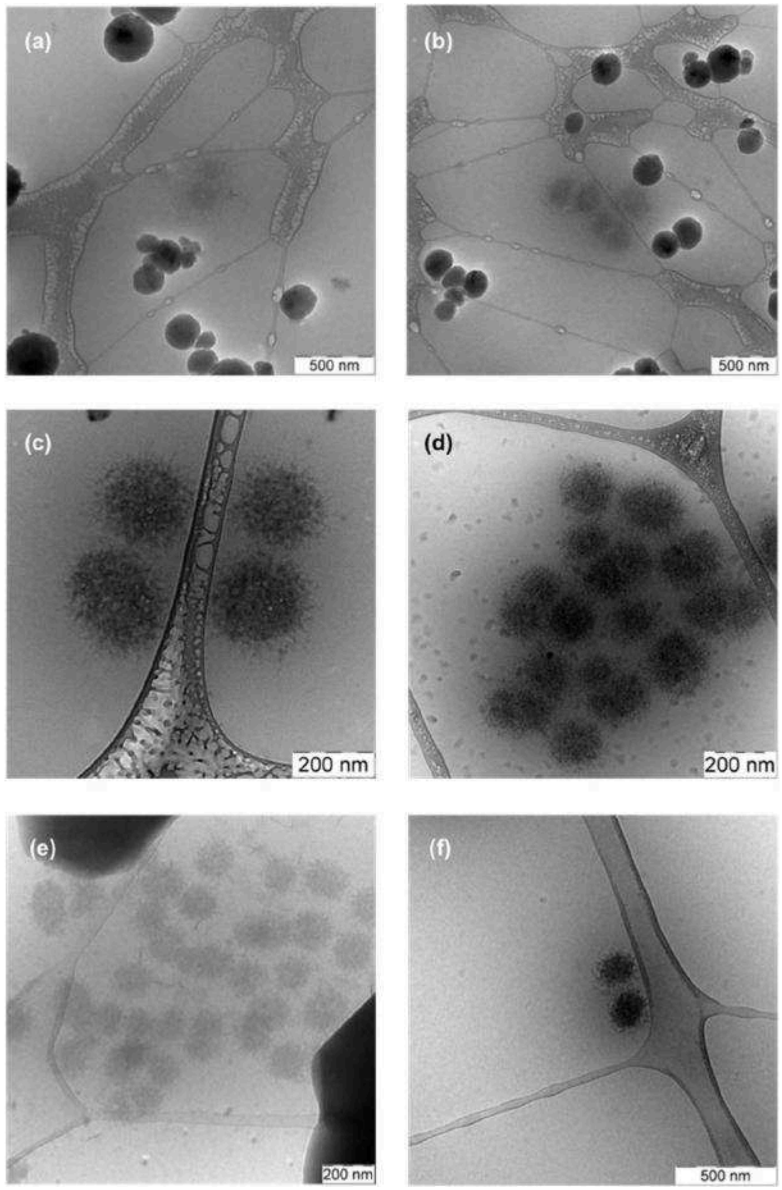

Figure A3(3). Cryo-TEM micrographs of (a, b) Native P(VCL-bis$_{1.5}$-ABSA$_{6.0}$) microgels, (c, d) P(VCL-bis$_{1.5}$-ABSA$_{10}$) microgels, and (e, f) P(VCL-bis$_{1.5}$-ABSA$_{6.0}$) microgels after equilibration for 1 hour at 50°C followed by 15 minutes of UV (λ = 365 nm, 100 mW cm^{-2}) irradiation.

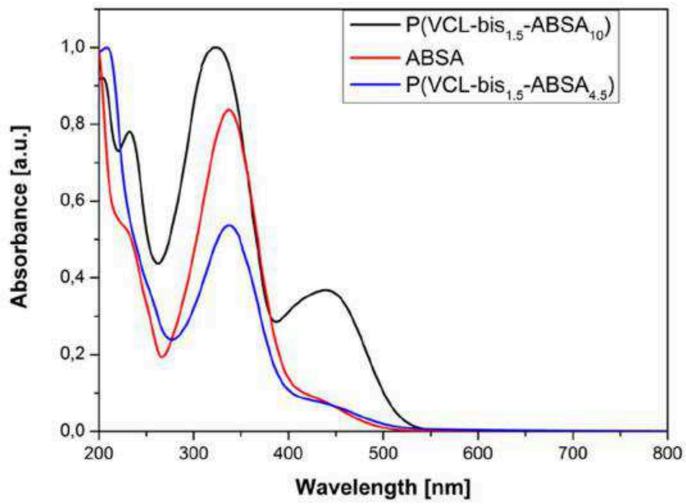

Figure A3(4). Normalized absorption spectra of aqueous solutions of free ABSA, P(VCL-bis$_{1.5}$-ABSA$_{4.5}$), and P(VCL-bis$_{1.5}$-ABSA$_{10}$).

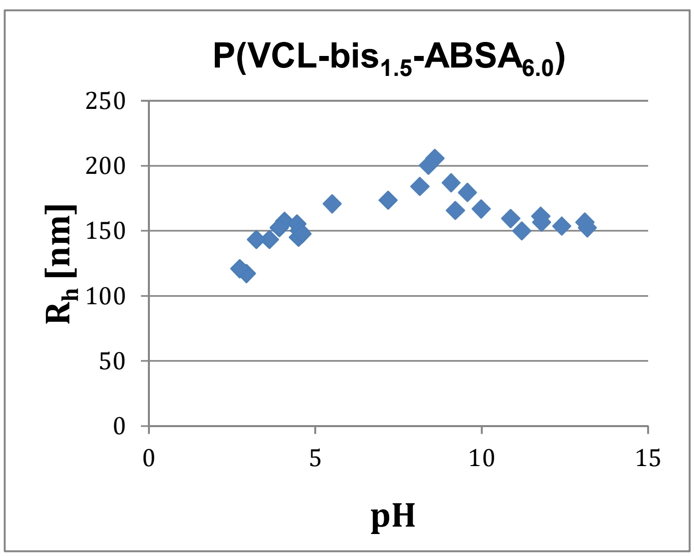

Figure A3(5). Change in R_h of P(VCL-bis$_{1.5}$-ABSA$_{6.0}$) as a function of pH.

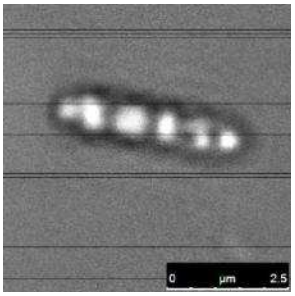

Figure A3(6). Inter-linked 'string' of P(VCL-bis$_{1.5}$-ABSA$_{6.0}$) particles, as seen under confocal microscopy.

CHAPTER 4. Thermo- and Photo-Responsive Properties of *N*-Vinylcaprolactam Microgels containing Azobenzene-based Cross-linkers

4.1. Introduction

Azobenzene cross-linkers have been used as photo-switches to directly trigger modifications in peptide and protein structures and thereby, their functions. This strategy relies on coupling the change in the end-to-end distance that occurs upon azobenzene isomerization to a peptide or protein structural/functional change.[4(1)] To the best of our knowledge, there are very few reports of azobenzene cross-linkers incorporated within a microgel matrix. The group of Serpe used an azobenzene crosslinker, 4,4′-di(acrylamido)-azobenzene, to synthesize P(NIPAM) microgels. They could control the volume of these microgels via temperature or light. The microgels shrink reversibly with temperature and they they reported the increased swelling of the microgels upon UV-induced *trans*-to-*cis* isomerization. This swelling was reversible with alternate application of UV and visible lights.[4(2)] Presumably this increased swelling can be attributed to the increase in hydrophilicity of the microgel matrix upon isomerization of the cross-linkers to the more polar *cis* form. Meanwhile, the group of Richtering reported on the physical photochemistry of azobenzene moieties within a poly(butyl methacrylate) (PBMA) nanoparticle matrix. The *cis*-azobenzene isomer, especially when the azobenzene is incorporated as a cross-linker show longer excited state lifetimes as compared to those of the free azobenzene in solution. They concluded that the lifetimes could be controlled by varying the tightness of the surrounding matrix.[4(3)]

Considering the results presented in Chapter 2, the isomerization to the more polar *cis* azobenzene attached as pendant groups within a P(VCL) microgel matrix led to a deswelling. The effect of *trans*-*cis* isomerization of the azobenzene cross-linkers on the swelling behavior of the microgels could be different from that of the microgels described in Chapter 2 where the azobenzene moieties are present as pendant groups. The azobenzene cross-linkers have lesser degrees of freedoms since they are more restricted due to the carbon atoms on each aromatic ring, *para* to the azo bond, being covalently linked to adjacent polymer chains in the network. Hence, the interaction of the azobenzenes with carbonyl groups of VCL should be more restricted. The decrease in the end-to-end distance of the azobenzene cross-linker could be the main driver to cause a deswelling of the microgel network upon its *trans*-to-*cis* isomerization. The group of Woolley *et al.* exploited the shorter end-to-end distance of *cis*-azobenzene cross-linkers to manipulate the helical content in peptides.[4(4)] Similarly, they demonstrated the photo-switching of protein conformation with azobenzene cross-linkers, thereby stabilizing one form over the other.[4(5)] By incorporating azobenzene cross-linkers into P(VCL) microgel, the effect of cooperative and simultaneous contraction of the *trans*-azobenzene to *cis*-azobenzene cross-linkers could lead to a significant deswelling of the microgel matrix.

The *trans-cis* isomerization of the azobenzene cross-linkers is expected to be sterically demanding.[4(6)] Lengthening of the spacers should enhance the flexibility of the resultant microgel matrix, thereby facilitating and increasing the rate of the *trans-cis* isomerization.[4(6b)] The flexibility of the spacers should also tend to increase the cross-linker's mobility even under ambient conditions,[4(7)] which could facilitate the propensity for *cis* azobenzene moieties to associate with each other.[4(8)] Furthermore, the length of spacer and presence of substituent groups on the aromatic rings could possibly influence the size of microgels and interactions of azobenzenes with each other and with the VCL units. Therefore, there should be changes in the balance of polymer-polymer and polymer-water interactions that govern the size of the microgels, especially when irradiated with UV. All things considered, increasing the spacer lengths could result in increased hydrophobic interactions, thereby enhancing the deswelling of the microgels.

The findings of the groups mentioned above inform our work here into incorporating azobenzene cross-linkers into P(VCL) microgel matrix. Therein lies our motivation for wanting to incorporate azobenzene cross-linkers with different spacer lengths into our microgels. In this study, we synthesized and characterized dual thermo- and photo-responsive microgels with VCL as monomer and azobenzene functionalized with different alkyl spacer lengths or functional groups as cross-linker. The different cross-linkers that were used are shown in Chart 4(1) and differ in length of alkyl spacers on the *para* carbon atoms while 4,4'-dimethacryloylazobenzen-3-carboxylic acid (**DACA**) has an additional hydrophilic carboxyl group as a substituent on one of the benzene rings. No additional chemical cross-linker, such as *N*,*N*'-methylenebisacrylamide (BIS) was used to obtain stable microgel particles. The effect of UV stimulus on microgel size is measured by *in situ* irradiation within the DLS instrument, while AFM is used to determine the topography of these novel microgels on hydrophilized silicon substrates.

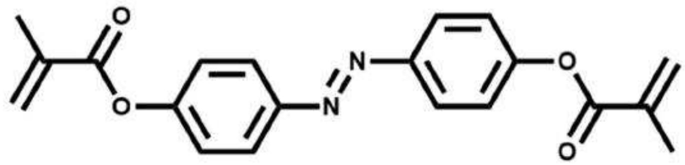

(1)

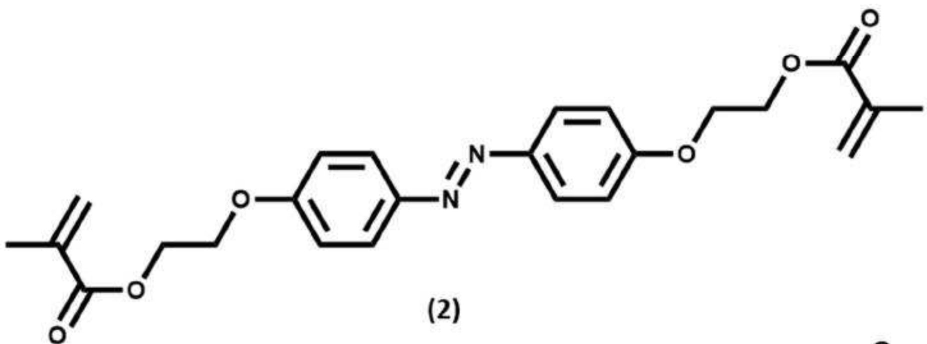

(2)

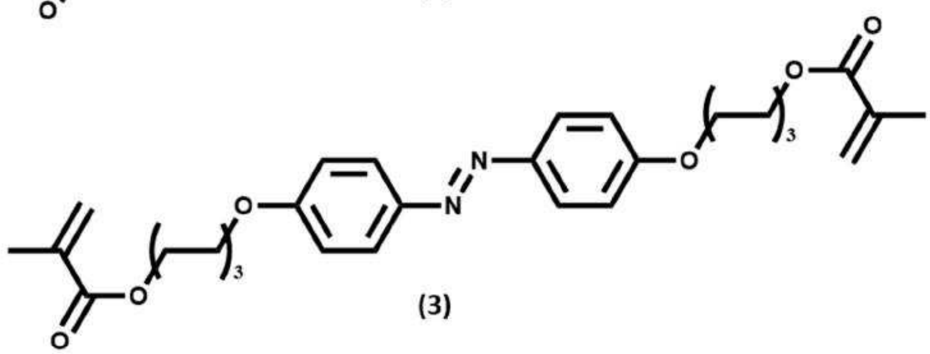

(3)

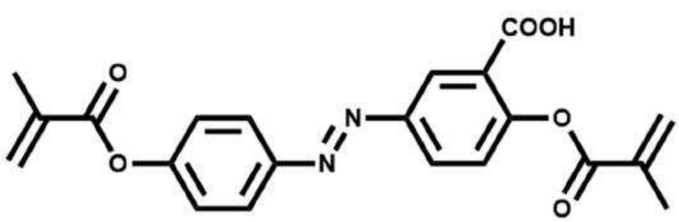

(4)

Chart 4(1). Azobenzene-based cross-linkers used in this study: (**1**) 4,4'-dimethacryloylazobenzene **DMAB**, (**2**) 4,4'-dimethacryloylethoxyazobenzene **DEAB**, (**3**) 4,4'-dimethacryloylhexoxyazobenzene **DHAB,** and (**4**) Synthesis of 4,4'-dimethacryloylazobenzen-3-carboxylic acid **DACA**.

4.2. Experimental section

4.2.1. Materials

N-Vinylcaprolactam (VCL) (Sigma-Aldrich, of 98% purity) was purified by a high-vacuum distillation at 80°C. *p*-aminophenol, 5-amino-2-hydroxybenzoic acid, phenol, sodium nitrite, methacryloyl chloride, sodium hydrogencarbonate, magnesium sulfate, 2-chloroethanol, 6-chlorohexanol, potassium carbonate, ethanol and potassium iodide were all purchased from Sigma-Aldrich and used as received. Triethylamine (puriss p.a., ≥99.5%), hydrochloric acid (ACS reagent, 37%), *N,N*-dimethylformamide (anhydrous, 99.8%) and tetrahydrofuran (anhydrous, ≥99.9%, inhibitor-free) were also obtained from Sigma-Aldrich and used as received. The initiator 2,2'-azobis[*N*-(2-carboxyethyl)-2 methylpropionamidine]hydrate (ACMA), was purchased from (Wako Pure Chemical Industries, Ltd., Specialty Chemicals) and used as received. Deuterated NMR solvents DMSO-d_6 (99 %) and $CDCl_3$ (99.8 %) were obtained from Deutero GmbH and used as received.

4.2.2. Cross-linker syntheses

The azobenzene-based cross-linkers were synthesized according to the respective procedures reported below. The ^{1}H NMR spectra of the synthesized compounds can be found in the Appendix 4.

Scheme 4(1). Synthesis of 4,4’dihydroxyazobenzene.

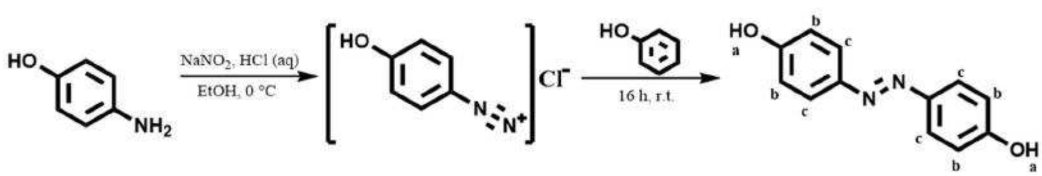

1 eq. *p*-aminophenol (1.6 g, 14.7 mmol) was dissolved in a mixture of concentrated hydrochloric acid (37 %) and 22 mL distilled water and cooled to <3°C in an ice-water bath. Subsequently, sodium nitrite ($NaNO_2$) (3.2 eq.) was dissolved in 14 mL distilled water, cooled to <3°C and added dropwise to the first solution to form the diazonium salt. 40 mL of pre-cooled ethanol was then added and the mixture was stirred for 30 min. In another flask, phenol (1 eq.) was dissolved in mixture of 22 mL 10 wt% sodium hydroxide solution and 20 mL ethanol, cooled to <3°C and added slowly to the diazonium salt under continuous stirring. The reaction was continued for 2 h under cooling and was stirred over night at room temparature. The mixture was neutralized with dilute HCl, concentrated in vacuo, filtered and washed with water. Dark, reddish brown solid was recrystallized from mixture of ethanol and water (1:1)

and dried under vacuum to give 70% yield. Synthesis procedure is adapted from that described by Alam *et al*.[4(9)]

^{1}H NMR (400MHz, DMSO-d6): δ = 10.17 ppm (s, O-H (2H), a), 7.72-7.70 ppm (m, Ar-H (4H), c), 6.92-6.90 ppm (m, Ar-H (4H), b). ^{1}H NMR spectrum is shown in Fig. A4(1) of Appendix 4.

Scheme 4(2). Synthesis of 4,4'-dimethacryloylazobenzene **DMAB (1).**

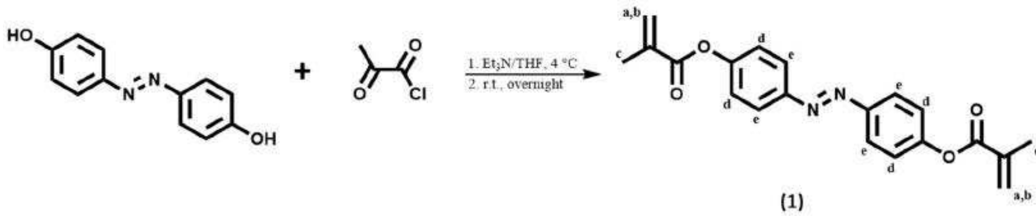

1 eq. 4,4'-dihydroxyazobenzene and 2.5 eq. of triethylamine (Et_3N) were dissolved in anhydrous THF, cooled to <3°C in an ice/water bath and purged with nitrogen for 30 min. Then 2.5 eq. methacryloyl chloride dissolved in a small amount of anhydrous THF was added dropwise to the cooled solution. The reaction was continued at r.t. for 24 h. The resulting product mixture was filtered, evaporated and dissolved in chloroform. The organic layer was washed with aqueous sodium hydrogencarbonate solution and brine until the methacrylic acid was removed. The resulting organic phase was dried over anhydrous magnesium sulfate, evaporated in vacuo and purified by recrystallization from 1:1 ethanol/water mixture to give brown solids in 65% yield.

^{1}H NMR (400 MHz, DMSO-d_6): 8.00-7.96 ppm (m, 4H, C*H*-arom, d); 7.46-7.42 ppm (m, 4H, C*H*-arom, e); 6.3 ppm (d, 2H, CH*H*-*cis*, b); 5.95 ppm (m, 2H, CH*H*-*trans*, a); 2.03 ppm (s, 6H, CH_3, c). Synthesis procedure was adapted from that of Gong *et al.*[4(6b)] ^{1}H NMR spectrum is shown in Fig. A4(2) of Appendix 4.

Scheme 4(3). Synthesis of 4,4'-dihydroxy-ethoxy/hexoxy-azobenzene.

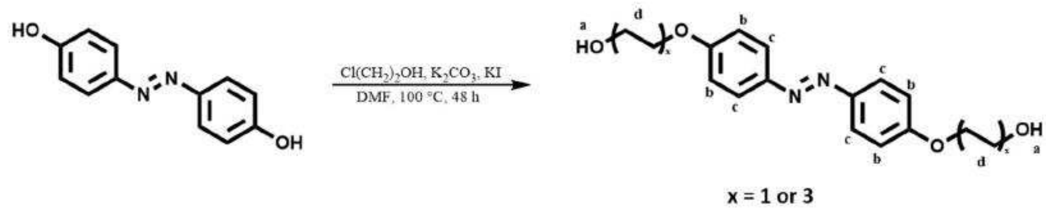

4,4'-dihydroxyazobenzene (1 eq.), potassium carbonate (2 eq.) and a pinch of potassium iodide were dissolved in anhydrous DMF and purged with nitrogen for 30 minutes. 4 eq. of spacer molecules (2-chloroethanol or 6-chlorohexanol) were then added. The reaction mixture was stirred for 48 h under reflux at 100°C. Subsequently, the product mixture was cooled and then diluted with excess of water. The formed precipitate was filtered off, washed with water, recrystallized from ethyl acetate and dried under vacuum. Synthesis procedure was adapted from that of Meng *et al.*[4(10)]

X=1: ^1H NMR (400MHz, $CDCl_3$): δ = 7.90-7.79 ppm (m, Ar-H (4H), c), 7.04-6.94 ppm (m, Ar-H (4H), b), 4.58-4.56 ppm (m, CH_2 (4H), d2), 4.01 ppm (s, OH (2H), a), 4.32-4.16 ppm (m, CH_2 (4H), d1). ^1H NMR spectrum is shown in Fig. A4(3) of Appendix 4.

X=3: ^1H NMR (400MHz, $CDCl_3$): δ = 7.87-7.85 ppm (m, Ar-H (4H), c), 7.00-6.98 ppm (m, Ar-H (4H), b), 4.04-4.03 ppm (m, CH_2 (4H), d6), 3.55-3.53 ppm (m, CH_2 (4H), d1), 1.84-1.40 ppm (m, CH_2 (16H), d2- d5). ^1H NMR spectrum is shown in Fig. A4(4) of Appendix 4.

Scheme 4(4). Synthesis of 4,4'-dimethacryloylethoxyazobenzene **DEAB (2),** and 4,4'-dimethacryloylhexoxyazobenzene **DHAB (3).**

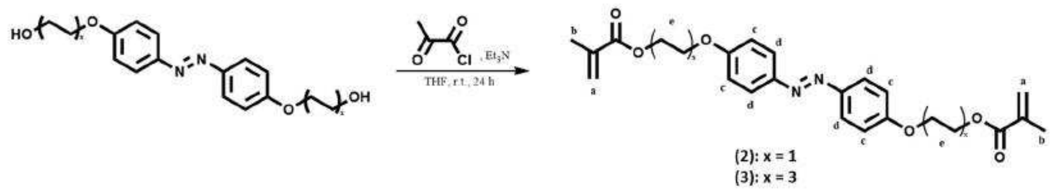

1 eq. 4,4'-dihydroxy-ethoxy/hexoxy-azobenzene and 2.5 eq. of triethylamine (Et_3N) were dissolved in anhydrous THF, cooled to <3°C in an ice/water bath and purged with nitrogen for 30 min. Subsequently, 2.5 eq. methacryloyl chloride dissolved in a small amount of anhydrous THF was added dropwise to the cooled solution. The reaction was continued at r.t. for 24 h. The resulting product mixture was filtered, evaporated and dissolved in chloroform. The organic layer was washed with aqueous sodium hydrogencarbonate solution and brine until the methacrylic acid was removed. The resulting organic phase was dried over anhydrous magnesium sulfate, evaporated in vacuo and purified by recrystallization from ethanol.

X=1: ^{1}H NMR (400MHz, $CDCl_3$): δ = 7.90-7.88 ppm (m, Ar-H (4H), d), 7.05-7.02 ppm (m, Ar-H (4H), c), 6.17 ppm (s, CH_2, (2H), a), 5.61 ppm (t, CH_2 (2H), a), 4.55 ppm (t, CH_2 (4H), e1), 4.32 ppm (t, CH_2 (4H), e2), 1.97 ppm (s, CH_3 (6H), b). ^{1}H NMR spectrum is shown in Fig. A4(5) of Appendix 4.

X = 3: ^{1}H NMR (400MHz, $CDCl_3$): δ = 7.89-7.86 ppm (m, Ar-H (4H), d), 7.00-6.98 ppm (m, Ar-H (4H), c), 6.11 ppm (s, CH (2H), a), 5.56 ppm (t, CH (2H), a), 4.18 ppm (t, CH_2 (4H), e1), 4.05 ppm (t, CH_2 (4H), e6), 1.95 ppm (s, CH_3 (6H), b), 1.88-1.46 ppm (m, CH_2 (16H), e2-e5). ^{1}H NMR spectrum is shown in Fig. A4(6) of Appendix 4.

Scheme 4(5). Synthesis of 4,4'-dihydroxyazobenzen-3-carboxylic acid.

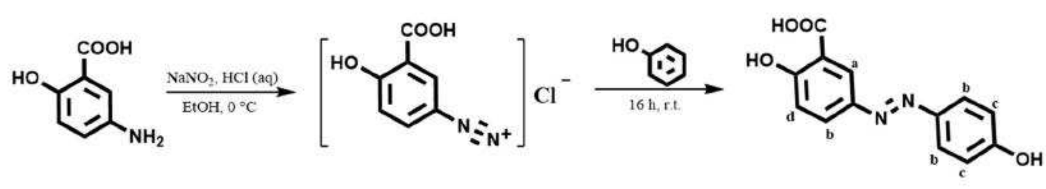

5-amino-2-hydroxybenzoic acid (1.6 g, 10.4 mmol) was dissolved in dilute hydrochloric acid (5.0 ml 37% aq. HCl + 16 ml of water) and cooled to 0–3 ºC. To this mixture an aqueous solution of sodium nitrite (2.30 g, 33.4 mmol in 18 ml of water) was slowly added dropwise under continuous stirring. Next the obtained diazonium salt was diluted with 40 cm^3 of pre-cooled ethanol. Separately phenol (0.98 g, 10.4

mmol) was dissolved in 10 ml 10% NaOH and 15 ml of ethanol, and this mixture was also cooled to 0–3ºC. The phenolate solution was added dropwise under stirring to the diazonium salt and the dark-red solution was obtained. Azo coupling was continued for 4 h at 5ºC, and then the solution was neutralized with dilute hydrochloric acid. The yielded red solid was filtered, washed with water and dried. The crude material was recrystallized from ethanol/water (1:1) mixture to give (50%) light brown solids. Synthesis procedure adapted from Mahkam *et al*.[4(11)]

^{1}H NMR (400 MHz, DMSO-d_6): δ = 8.18 ppm (d, 1H, C*H*-arom, a); 7.71-7.66 ppm (m, 3H, C*H*-arom, b); 6.87 ppm (dd, 2H, C*H*-arom, c); 6.72 ppm (d, 1H, C*H*-arom, d). ^{1}H NMR spectrum is shown in Fig. A4(7) of Appendix 4.

Scheme 4(6). Synthesis of 4,4'-dimethacryloylazobenzen-3-carboxylic acid **DACA (4).**

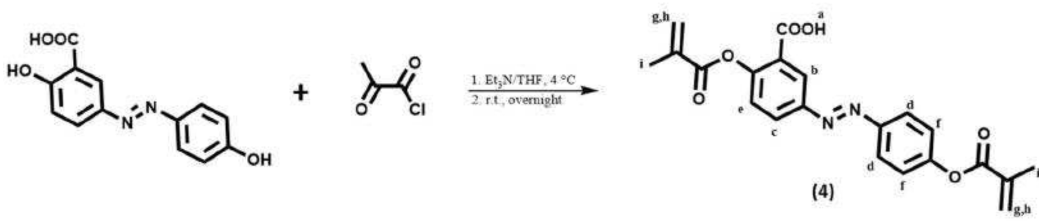

1 eq. 4,4'-dihydroxyazobenzen-3-carboxylic acid and 2.5 eq. of triethylamine (Et_3N) were dissolved in anhydrous THF, cooled to <3°C in an ice/water bath and purged with nitrogen for 30 min. Then 2.5 eq. methacryloyl chloride dissolved in a small amount of anhydrous THF was added dropwise to the cooled solution. The reaction was continued at r.t. for 24 h. The resulting product mixture was filtered, evaporated and dissolved in chloroform. The organic layer was washed with aqueous sodium hydrogencarbonate solution and brine until the methacrylic acid was removed. The resulting organic phase was dried over anhydrous magnesium sulfate, evaporated in vacuo and purified by recrystallization from 1:1 ethanol/water mixture to give light brown solids in 55% yield.

^{1}H NMR (400 MHz, DMSO-d_6): δ = 13.46 ppm (br-s, 1H, COO*H*, a); 8.40-8.33 ppm (m, 1H, C*H*-arom, b); 8.18 ppm (dd, 1H, C*H*-arom, c); 8.07-7.92 ppm (m, 2H, C*H*-arom, d); 7.52 ppm (d, 1H, C*H*-arom, e); 7.48-7.39 ppm (m, 2H, C*H*-arom, f); 6.32 ppm (d, 2H, CH*H*-*cis*, g); 5.96-5.92 ppm (m, 2H, CH*H*-*trans*, h); 2.03 ppm (s, 6H, CH_3, i). ^{1}H NMR spectrum is shown in Fig. A4(8) of Appendix 4.

4.2.3. Microgel synthesis

1.390 g VCL (monomer) and 5 mg SDS (surfactant) were dissolved in 90 mL distilled water, filled into a double-wall glass reactor equipped with stirrer and reflux condenser and purged with nitrogen at 70°C under stirring (250 rpm) for 30 min. 34.2 mg ACMA initiator was dissolved in 5 mL water and added to the reaction mixture. 30 seconds after the clear solution turned turbid, the cross-linker dissolved in 2.5 mL ethanol and 2.5 mL acetone was added gradually over ~1 min to the reaction mixture. The mixture turned instantly yellow and was purged with nitrogen for 30 min. The reaction was continued for 6 h at 70°C and 250 rpm. A few minutes after addition of the cross-linker, small amount of precipitated cross-linker could be observed on the reactor wall. After the reaction, the microgel solution was filtered and then dialyzed against distilled water for ~5 days. Afterwards the microgel solution was centrifuged 3 times at 10 000 rpm for 10 min. The small amount of sedimented solid after the first centrifugation was disposed off. For all microgel syntheses, a double-wall glass reactor (250 mL, Rettberg GmbH) equipped with reflux condenser and mechanic stirrer (IKA Eurostar 20 digital) was used. The VCL used in these reactions was purified by vacuum distillation. Dialysis was performed using Dialysis Membrane Spectra/Por® 2 (flat width: 25 mm, thickness: 20 μm, MWCO: Nominal 12 000-14 000). The steps in the synthesis of the microgels are presented in Scheme 4(7).

Table 4(1). Amount of reagents used in the synthesis of microgels.

Microgel	VCL [mmol]	AzoXlinker [mmol]	SDS [mg]	Acetone [ml]	Ethanol [ml]
P(VCL-$DMAB_{0.5}$)	10	0.05	10	2.5	2.5
P(VCL-$DMAB_{1.0}$)	10	0.1	10	2.5	2.5
P(VCL-$DEMA_{0.5}$)	10	0.05	10	2.5	2.5
P(VCL-$DHMA_{0.5}$)	10	0.05	10	2.5	2.5
P(VCL-$DACA_{0.25}$)	10	0.025	10	2.5	2.5
P(VCL-$DACA_{0.5}$)	10	0.05	10	2.5	2.5

*The nomenclature used in this paper for the microgels are based on the feed amounts of azobenzene cross-linker (indicated in subscripts in mol %).

Scheme 4(7). Schematic representation of the microgel synthesis via precipitation polymerization

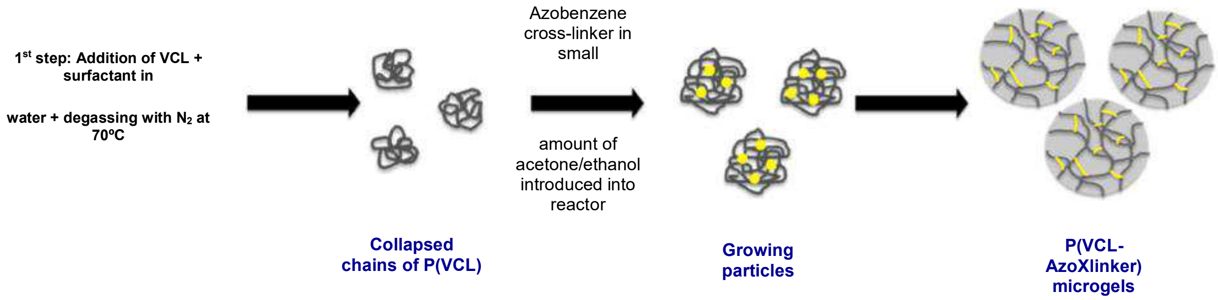

4.2.4. Microgel characterization

UV/vis-spectroscopy. The spectra were measured from 800-200 nm with a scan rate of 600 nm/min on a Cary 100Bio UV-Visible Spectrophotometer from Varian. A quartz cuvette was used for the measurement and a quartz cuvette filled with deionized water was used as a reference.

Dynamic light scattering. The size of the microgel particles was measured with an ALV/LSE-5004 DLS goniometer with a Multiple Tau Digital Correlator and Electronics. The instrument is equipped with a laser light wavelength of 633 nm and the scattered light was detected at a scattering angle set to 90°. The samples were measured at 20 °C and the temperature fluctuations were below 0.1 °C. Microgel samples were highly diluted ($c < 0.01$ wt %) with water for chromatography from Merck Millipore and subsequently filtered through a 1.2 μm filter before measurements were performed to eliminate dust, aggregation and impurities. The hydrodynamic radius R_h was calculated from second order cumulant fits via the Stokes-Einstein equation. For temperature-dependent measurements, samples were measured between 10 and 60°C, in steps of 3°C and the temperature fluctuations were kept below 0.1°C. Three runs of 120 s each were performed at each temperature in order to calculate the standard deviation. The volume phase transition temperature (VPTT) of each microgel was determined as the inflection point of the temperature-dependent light scattering curve.

***In situ* irradiation within the DLS instrument**. The photo-induced size changes at different temperatures were measured by DLS. Samples were allowed to equilibrate thermally at the respective temperatures for 10 minutes. The LED (λ = 365 nm or 450 nm) was placed 0.5 cm above the meniscus of the microgel solution in the DLS cuvette. At each temperature, six runs of 10 s each were performed and repeated for over fifteen minutes to monitor the photo-responsive effect over time.

Atomic force microscopy (AFM). Images were recorded using tapping mode on a Veeco Nanoscope Atomic Force Microscope. Cantilevers (NanoWorld, Neuchâtel, Switzerland) with resonance frequency of 250 – 300 kHz and spring constant of 42 N m^{-1} were used. The deposition of microgels on a silicon wafer was carried out on a spin-coater (Convac 1001S, Germany) at a speed of 3000 rpm for 30 s. The silicon wafer used for deposition was previously cleaned by sonication in isopropanol for 10 minutes, dried with an air stream, and treated with UV/O_2 for 15 minutes. The concentration of microgel solution used for spin coating was 1.0 mg/mL. At this microgel concentration, sufficient amount of particles could be adsorbed and be evenly distributed on the silicon wafer without clustering.

4.3. Results and discussion

4.3.1. Morphology of microgel on Si substrate

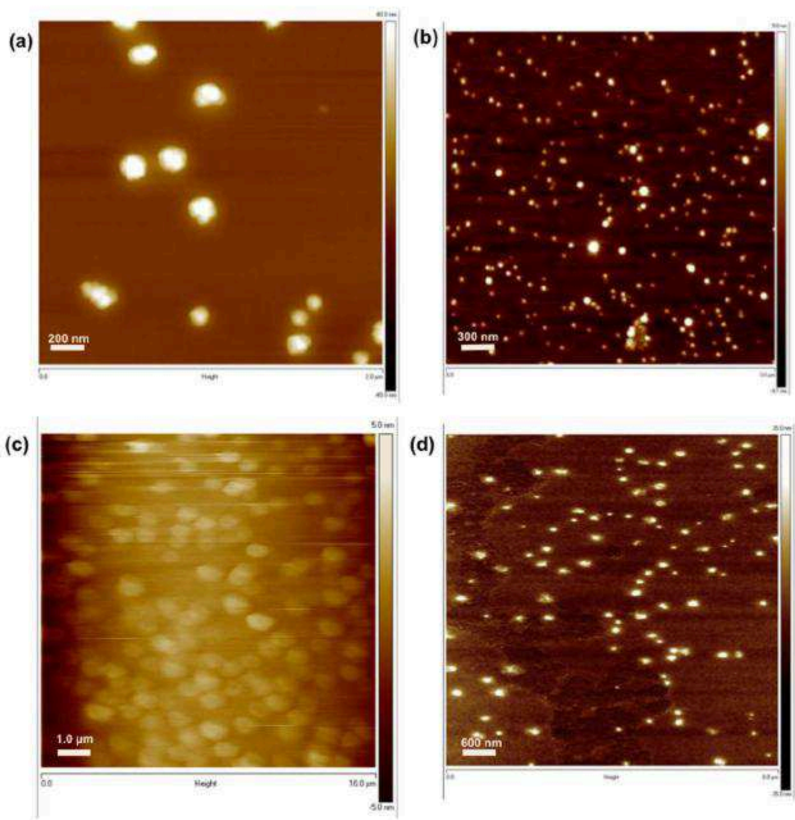

Figure 4(1). AFM images of (a) P(VCL-DMAB$_{1.0}$), (b) P(VCL-DEAB$_{0.5}$) (c) P(VCL-DACA$_{0.25}$), (d) P(VCL-DACA$_{0.5}$) microgels. Note the different scales in the images.

Fig. 4(1) shows the microgels as observed with AFM. The microgels containing DACA cross-linkers appear to be more deformed and more ellipsoidal in shape than the other microgels. This could be attributed to the presence of carboxylic acid groups of DACA which could form hydrogen bonds with the hydrophilized Si substrate. The particles of P(VCL-$DACA_{0.25}$) are especially soft and highly deformed on the Si substrate and this is to be expected given that the smallest amount of cross-linker was used in its synthesis.[4(12)]

4.3.2. Thermo-responsive behavior of microgel

The size-temperature data in Fig. 4(2) reveal that the microgels synthesized with small feed amounts of azobenzene cross-linkers have their VPTT at around 32ºC, close to that of P(VCL-bis) microgels, as described earlier in Chapter 2. The hydrophilic-hydrophobic balance of the microgel matrix appears unchanged by the incorporation of a small amount of hydrophobic azobenzene cross-linkers (less than or equal to 1.0 mol% feed amounts). Similarly, a co-worker in the group reported that the VPTT of PVCL/NIPAm microgels remained constant at ~ 35ºC with varying BIS cross-linker content (between 0.05 and 3.0 mol%).[4(12)]

When the same cross-linkers were used, a higher feed amount led to a slightly broader volume phase transition. This can be observed by comparing Fig. 4(1a) with 4(1b) and 4(1d) with 4(1e). A broader transition is indicative of a more heterogeneous cross-linking density within the microgel network.[4(13)]

Table 4(2) shows that the extent of deswelling by temperature stimulus of the microgels, represented by the normalized hydrodynamic radius ($R_{h,20ºC}/R_{h,50ºC}$). By comparing microgels of similar sizes, P(VCL-$DMAB_{0.5}$), P(VCL-$DEAB_{0.5}$) and P(VCL-$DACA_{0.5}$), show increasing extents of heat-induced dewelling, in that order. Deswelling in P(VCL) microgels is the result of the disruption of hydrogen bond interactions between the C=O of the VCL units and water molecules and the concomitant increase in hydrophobic interactions between the polymer chain segments.[4(14)] The presence of alkyl spacers and the polar carboxylic groups most possibly contributes to more extensive hydrophobic interactions during the temperature-induced volume phase transition, and therefore, a greater extent of deswelling in P(VCL-$DEAB_{0.5}$) and P(VCL-$DACA_{0.5}$) than in P(VCL-$DMAB_{0.5}$).

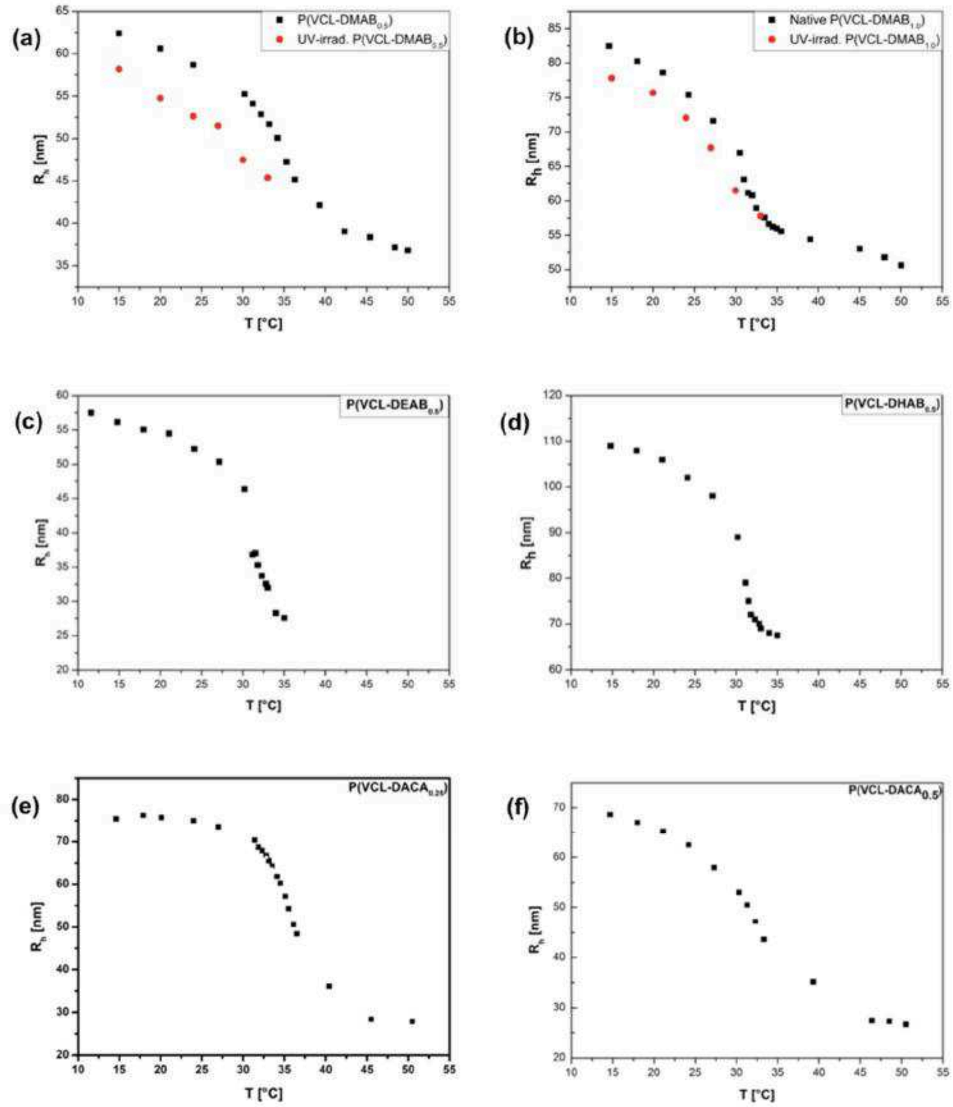

Figure 4(2). Size-temperature data of (a) P(VCL-DMAB$_{0.5}$) (b) P(VCL-DMAB$_{1.0}$), (c) P(VCL-DEAB$_{0.5}$), (d) P(VCL-DACA$_{0.25}$), (e) P(VCL-DACA$_{0.5}$) microgels. The circular points in red in (a) and (b) denote the R_h of the particles under UV irradiation (λ = 365 nm, 100 mW cm^{-2}). *The particles of P(VCL-DEAB$_{0.5}$) and P(VCL-DHAB$_{0.5}$) started to aggregate at 35°C, making it difficult to determine their R_h above this temperature.

As the temperature increases from 20ºC to 35ºC, the R_h of P(VCL-DEAB$_{0.5}$) decreases from 57.44 to 27.60 nm, which may not be the final collapsed R_h at 50ºC. P(VCL-DEAB$_{0.5}$) microgels started to aggregate above 35ºC and therefore it was difficult to determine the collapsed volume of the microgel at 50ºC.

Table 4(2). Swelling degrees of the microgels, represented by the normalized hydrodynamic radius ($R_{h,20ºC}/R_{h,50ºC}$).*The collapsed sizes of microgels P(VCL-DEAB$_{0.5}$) and P(VCL-DHAB$_{0.5}$) were those at 35ºC.

Microgel	$R_{h,20°C}$	$R_{h,50°C}$	Swelling degree ($R_{h,20°C}/R_{h,50°C}$)
P(VCL-DMAB$_{0.5}$)	60.6	36.4	1.7
P(VCL-DMAB$_{1.0}$)	78.6	51.9	1.5
P(VCL-DEAB$_{0.5}$)	57.7	26.5*	2.2
P(VCL-DHAB$_{0.5}$)	106.7	67.9*	1.6
P(VCL-DACA$_{0.25}$)	77.9	28.7	2.7
P(VCL-DACA$_{0.50}$)	72.7	26.5	2.7

4.3.3. Photo-responsive behavior of microgels

Similar to the case in Chapter 2, of the microgels containing ABSA as pendant groups, the microgels with azobenzene cross-linkers deswell upon UV irradiation (λ = 365 nm, 100 mW cm^{-2}) at temperatures below their respective VPTTs. By comparing Figs. 4(3a) and 4(3b), under isothermal conditions, a lower DMAB cross-linker content results in a greater UV-induced deswelling of the microgel. A higher cross-linker content results in more rigid particles that are less responsive to the UV stimulus. This was the reason we kept the cross-linker feed amounts to less than 1.0 mol%. According to Schneider *et al*., a higher cross-linker content results in shorter subchains which increase the stiffness of the microgel chains.[4(13)] Since azobenzenes are rather bulky and rigid molecules, even at low concentrations of cross-linkers, the chains would become stiff and have reduced mobility. As a result, the strength of hydrogen bonds between water molecules and C=O of VCL is increased, which could increase the energetic cost for UV-induced deswelling. By comparing microgels P(VCL-DMAB$_{0.5}$) with P(VCL-DMAB$_{1.0}$) and P(VCL-DACA$_{0.25}$) with P(VCL-DACA$_{0.5}$), it is clear from the data presented in Figs. 4(3), 4(4) and Table 4(3) that a lower cross-linker amount is desirable to achieve greater UV-induced deswelling.

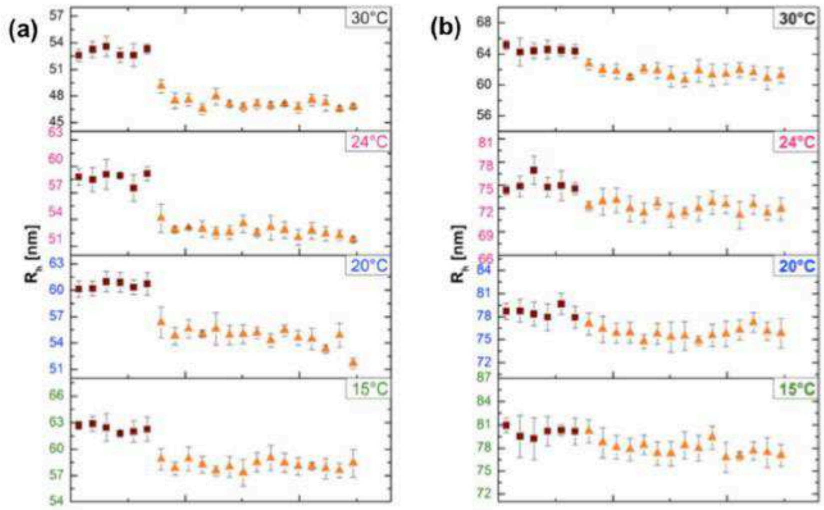

(c)

Temperature [°C]	% decrease in R_h
15	6.7
20	9.7
24	10.2
30	10.9

(d)

Temperature [°C]	% decrease in R_h
15	2.9
20	3.4
24	4.1
30	4.8

Figure 4(3). Investigation of the photo-responsive behavior of (a) P(VCL-DMAB$_{0.5}$), and (b) P(VCL-DMAB$_{1.0}$) at different temperatures. Percentage deswelling* of (c) P(VCL-DMAB$_{0.5}$), and (d) P(VCL-DMAB$_{1.0}$) at the different temperatures. *Values were calculated based on the mean R_h values before and after irradiation.

P(VCL-DMAB$_{0.5}$) showed comparable deswelling extents as P(VCL-bis$_{1.5}$-ABSA$_{1.5}$) in Chapter 2. However, in all the other microgels with azobenzene cross-linkers, the extents of deswelling are lower than those achieved in microgels of P(VCL-bis-ABSA), described in Chapter 2, where the azobenzene moieties were incorporated as pendant groups. Fig. 4(3c,d) summarizes the deswelling at different temperatures of P(VCL-DMAB$_{0.5}$) and P(VCL-DMAB$_{1.0}$) respectively. We observe a similar trend as the microgels in Chapter 2, where the extent of UV-induced deswelling increases with temperature, at temperatures below the VPTT of the microgel. The increase in temperature allows closer approach of the polymer segments, allowing for stronger hydrophobic interactions.

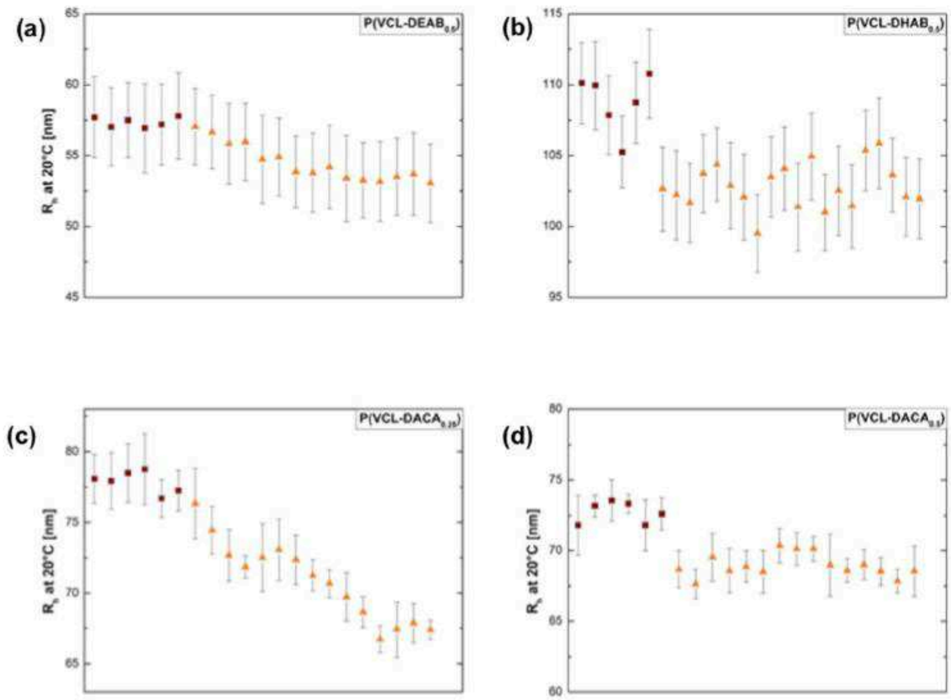

Figure 4(4). Investigation of the photo-responsive behavior of (a) P(VCL-DEAB$_{0.5}$), (b) P(VCL-DHAB$_{0.5}$), (c) P(VCL-DACA$_{0.25}$), (d) P(VCL-MACA$_{0.5}$) microgels irradiated by UV (λ = 365 nm, 100 mW cm^{-2}) at 20ºC.

Table 4(3). Summary of the R_h and Pd.I values of the native and irradiated microgels at 20ºC. *Values were calculated based on the mean R_h values before and after irradiation.⁺The $R_{h,irrad.}$ value of P(VCL-DACA$_{0.25}$) was taken at the median, not of the mean $R_{h,irrad.}$ value.

Microgel	$R_{h,native}$	Pd.I$_{native}$	$R_{h,irrad.}$	Pd.I$_{irrad.}$	ΔR_h [%]
P(VCL-DMAB$_{0.5}$)	60.6	0.104	54.9	0.12	9.7
P(VCL-DMAB$_{1.0}$)	78.6	0.101	75.9	0.135	3.4
P(VCL-DEAB$_{0.5}$)	57.7	0.34	53.4	0.36	7.5
P(VCL-DHAB$_{0.5}$)	106.7	0.37	102.9	0.38	3.6
P(VCL-DACA$_{0.25}$)	77.9	0.19	70.9⁺	0.26	9.0⁺
P(VCL-DACA$_{0.50}$)	72.7	0.19	68.9	0.21	5.2

Table 4(4). UV-induced deswelling of P(VCL-DEAB0.5) microgel at different temperatures.

Temperature [ºC]	$R_{h,native}$ [nm]	$Pd.I_{native}$	$R_{h,irrad.}$ [nm]	$Pd.I_{irrad.}$	ΔR_h [%]
20	57.7	0.37	53.4	0.38	7.5
30	47.0	0.33	43.4	0.32	7.7
32	34.2	0.41	31.5	0.40	7.9

The photo-responsive behavior of P(VCL-DEAB$_{0.5}$) was also measured at 30ºC and 32ºC. Table 4(4) shows that the percentage UV-induced deswelling did not vary much from the value recorded at 20ºC. This could be explained by the presence of pre-existing interactions between the alkyl chains of the azobenzene cross-linkers and the surrounding polymer segments, which are already critical before UV irradiation and contributes to more extensive hydrophobic interactions in the native microgel matrix.

While the distribution of cross-linkers in the microgel networks is not known, we initially hypothesized that lengthening the spacers connecting the cross-linkers to the polymer backbone should tend to increase the cross-linker's mobility even under ambient conditions and facilitate the *trans*-*cis* isomerization of azobenzene. By increasing the spacer lengths, the *cis* moieties could possibly approach each other in space within the microgel matrix to result in increased hydrophobic interactions, thereby enhancing the deswelling of the microgels. Presented with the data in Figs. 4(3), 4(4) and Table 4(3), however, in order of increasing deswelling extents, P(VCL-DEAB$_{0.5}$), P(VCL-DACA$_{0.25}$), and P(VCL-DMAB$_{0.5}$) showed the highest photo-responses. It should be noted that the Pd.I values are rather high for P(VCL-DEAB$_{0.5}$) and PVCL-DHAB$_{0.5}$), which could mean that the size analysis by the cumulant fit method in DLS could be inaccurate. Nonetheless, a case for having longer spacers to induce greater volume change in the particles upon a photo-response cannot be made.

Interestingly, as depicted in Fig. 4(4c), the UV-induced deswelling occurs in a gradual manner for P(VCL-DACA$_{0.25}$) compared to the other microgels. That the exclusion of water upon UV irradiation does not happen as rapidly as in the other microgels, suggests that the hydrophobic state is not as energetically favorable. Accounting for this would require a deeper investigation of the internal morphology of the particles via more direct approaches like NMR and SANS.[4(13)] In the temperature-induced deswelling of P(VCL-bis) microgels, the width or broadness of the transition is attributed to the degree of cooperativity of the hydrophobic associations in the microgel particle.[4(13)] If we were to draw parallels from this to explain the UV-induced deswelling of P(VCL-$DACA_{0.25}$), the gradual deswelling could be related to the low amount of DACA cross-linkers, thereby causing the cooperative effect of azobenzene isomerization to be mitigated. In addition, the low azobenzene cross-linker content could have resulted in more heterogeneous regions within the microgel matrix. As a result, different regions of the particle collapse at different rates.

4.4. Conclusion

N-Vinylcaprolactam (VCL) was cross-linked in a precipitation polymerization procedure in water with various azobenzene cross-linkers bearing different alkyl spacer lengths and substituent on the phenyl rings of the azobenzene. The hydrophobic azobenzene cross-linkers, dissolved in a small amount of acetone/ethanol co-solvent system, were added during an extra step after initiation of the VCL monomer. Novel thermo- and photo-responsive microgels were then produced.

Low azobenzene cross-linker feed amounts (< 1 mol %) was necessary to achieve reasonable UV-induced deswelling of the microgels. The lower the amount of azobenzene cross-linker, the softer and more deformable the particles and the more responsive they are to UV stimulus. With azobenzenes as cross-linkers, we achieved a smaller UV-induced deswelling of the microgels as compared to having azobenzenes as pendant groups in the microgels reported in Chapter 2.

The greatest extent of UV-induced deswelling was observed in the microgel containing the azobenzene cross-linker without any alkyl spacers or substituent groups. The initial hypothesis that increasing the flexibility of the spacers should tend to increase the cross-linker's mobility to facilitate the approach of the polar *cis*-azobenzene moieties to each other and to the VCL chains within the network to result in increased hydrophobic interactions, thereby enhancing deswelling, does not stand. Since the microgel with the azobenzene cross-linker with the shortest linking groups to the VCL chains exhibit the greatest UV-induced deswelling, this could be taken as preliminary evidence that rigid and taut connections to the VCL chains are optimal to observe the effect of the decrease in end-to-end distance of the azobenzene linkers.

It is known that hydrophobic interactions between the polymer segments play an important role in the deswelling of microgels. Based on the data presented in this chapter, it appears that the underlying, pre-existing interactions between the azobenzene cross-linkers and the surrounding VCL chain segments become critical in the native, non-irradiated state, especially when the azobenzene cross-linkers possess alkyl spacers and substituent group like COOH which are capable of forming more extensive interactions. The measure of heat-induced deswelling extents verifies that hydrophobic interactions are more robust in the systems with alkyl spacers and COOH substituent.

Further studies to probe the internal morphology and cross-linking distribution by more direct methods such as small angle neutron scattering (SANS), for instance would be required in order to better understand the mechanism of UV-induced deswelling and to be able to optimize and tune the extent of deswelling in P(VCL) microgel systems with azobenzene-based cross-linkers. Furthermore, improvements in their syntheses to produce more monodisperse microgels are required, if such systems should prove themselves worthy for a proper application.

4.5. REFERENCES

4(1) (a) Zhang, F.; Zarrine-Afsar, A.; Al-Abdul-Wahid, M. S.; Prosser, R. S.; Davidson, A. R.; Woolley, G. A. *J. Am. Chem. Soc.* **2009**, *131*, 2283-2289.; (b) Beharry, A. A. Characterization of Azobenzene-based Photo-switches and their Evaluation for *In Vivo* Applications. Ph.D Dissertation, University of Toronto, Toronto, Canada, 2012, and references therein.

4(2) Zhang, Q. M.; Li, X.; Islam, M. R.; Wie, M.; Serpe, M. J. Light Switchable Optical Materials from Azobenzene Crosslinked Poly(*N*-Isopropylacrylamide)-based Microgels. *J. Mater. Chem. C* **2014**, *2*, 6961-6965.

4(3) Bahrenburg, J.; Renth, F.; Temps, F.; Plamper, F.; Richtering, W. Femtosecond Spectroscopy Reveals Huge Differences in the Photoisomerisation Dynamics between Azobenzenes Linked to Polymers and Azobenzenes in Solution. *Phys. Chem. Chem. Phys.* **2014**, *16*, 11549-11554.

4(4) (a) Kumita, J. R.; Smart, O. S.; Woolley, G. A. Photo-Control of Helix Content in a Short Peptide. *Proc. Natl. Acad. Sci.* **2000**, *97*, 3803-3808.; (b) Cochran, A. G.; Skelton, N. J.; Starovasnik, M. A. Tryptophan Zippers: Stable, Monomeric β-Hairpins. *Proc. Natl. Acad. Sci.* **2001**, *98*, 5578-5583.; (c) Flint, D. G.; Kumita, J. R.; Smart, O. S.; Woolley, G. A. Using an Azobenzene Cross-linker to either Increase or Decrease Peptide Helix Content upon trans-to-cis Photoisomerization. *Chem. Biol.* **2002**, *9*, 391-397.; (d) Kumita, J. R.; Flint, D. G.; Smart, O. S.; Woolley, G. A. Photo-control of Peptide Helix Content by an Azobenzene Cross-linker: Steric Interactions with Underlying Residues are not Critical. *Protein Eng.* **2002**, *15*, 561-569.; (e) Zhang, Z.; Burns, D. C.; Kumita, J. R.; Smart, O. S.;

Woolley, G. A. A Water-Soluble Azobenzene Cross-linker for Photo-Control of Peptide Conformation. *Bioconjug. Chem.* **2003**, *14*, 824-829.; (f) Guerrero, L.; Smart, O. S.; Woolley, G. A.; Allemann, R. K. Photocontrol of DNA Binding Specificity of a Miniature Engrailed Homeodomain. *J. Am. Chem. Soc.* **2005**, *127*, 15624-15629.; (g) Woolley, G. A. Photocontrolling Peptide α-Helices. *Acc. Chem. Res.* **2005**, *38*, 486-493.; (h) Dong, S. L.; Loweneck, M.; Schrader, T. E.; Schreier, W. J.; Zinth, W.; Moroder, L.; Renner, C. A Photocontrolled β-Hairpin Peptide. *Chem. Eur. J.* **2006**, *12*, 1114-1120.

4(5) (a) Zhang, F.; Zarrine-Afsar, A.; Al-Abdul-Wahid, M. S.; Prosser, R. S.; Davidson, A. R.; Woolley, G. A. Structure-based Approach to the Photocontrol of Protein Folding. *J. Am. Chem. Soc.* **2009**, *131*, 2283-2289.

4(6) (a) El Halabieh, R. H.; Mermut, O.; Barrett, C. Using Light to Control Physical Properties of Polymers and Surfaces with Azobenzene Chromophores. *J. Pure Appl. Chem.* **2004**, *76*, 1445–1465.; (b) Gong, C. B.; Wong, K. L.; Lam, M. H. W. Photoresponsive Molecularly Imprinted Hydrogels for the Photoregulated Release and Uptake of Pharmaceuticals in the Aqueous Media. *Chem. Mater.* **2008**, *20*, 1353-1358.

4(7) (a) Yagai, S.; Okamura, S.; Nakano, Y.; Yamauchi, M.; Kishikawa, K.; Karatus, T.; Kitamura, A.; Ueno, A.; Kuzuhara, D.; Yamada, H.; Seki, T.; Ito, H. Design Amphiphilic Dipolar π-Systems for Stimuli-Responsive Luminescent Materials Using Metastable States. *Nat. Commun.* **2014**, *5*, 4013. (b) Kim, D.-Y.; Lee, S.-A.; Kim, H.; Kim, S. M.; Kim, N.; Jeong, K.-U. An Azobenzene-based Photochromic Liquid Crystalline Amphiphile for a Remote-Controllable Light Shutter. *Chem. Commun.* **2015**, *51*, 11080-11083.

4(8) (a) Han, M.; Hara, M. Intense Fluorescence from Light-Driven Self-Assembled Aggregates of Nonionic Azobenzene Derivative**.** *J. Am. Chem. Soc.* **2005**, *127*, 10951-10955.; (b) Liu, Y.-J.; Pallier, A.; Sun, J.; Rudiuk, S.; Baigl, D.; Piel, M.; Marie, E.; Tribet, C. Non-Monotonous Variation of the LCST of Light-Responsive, Amphiphilic Poly(NIPAM) Derivatives. *Soft Matter* **2012**, *8*, 8446-8455 and references therein.

4(9) Alam, M. Z.; Shibahara, A.; Ogata, T.; Kurihara, S. Synthesis of azobenzene-functionalized star polymers via RAFT and their photoresponsive properties. *Polymer* **2011**, *52*, 3696-3703.

4(10) Meng, X.; Natansohn, A.; Barett, C.; Rochon, P. Azo Polymers for Reversible Optical Storage. 10. Cooperative Motion of Polar Side Groups in Amorphous Polymers. *Macromolecules* **1996**, *29*, 946-952.

4(11) Mahkam, M.; Assadi, M. G.; Zahedifar, R.; Allahverdipoor, M.; Doostie, L.; Djozan, J. Synthesis and Evaluation of New Linear Azo-Polymers for Colonic Targeting**.** *Des. Monomer Polym.* **2004**, *4*, 351–359.
4(12) Wu, Y. Behavior of Temperature-Responsive Microgels at Interfaces: Deformability and Interfacial Activity. Ph.D Dissertation, RWTH Aachen University, Germany, 2014.
4(13) Schneider, F.; Balaceanu, A.; Feoktystov, A.; Pipich,V.; Wu, Y.; Allgaier, J.; Pyckhout-Hintzen, W.; Pich, A.; Schneider, G. J. Monitoring the Internal Structure of Poly(*N*-vinylcaprolactam) Microgels with Variable Cross-Link Concentration. *Langmuir* **2014**, *30*, 15317−15326 and references therein.
4(14) Ramos, J.; Imaz, A.; Forcada, J. Temperature-Sensitive Nanogels: Poly(*N*-Vinylcaprolactam) versus P(*N*-Isopropylacrylamide). *Polym. Chem.* **2012**, *3*, 852-856 and references therein.

APPENDIX 4

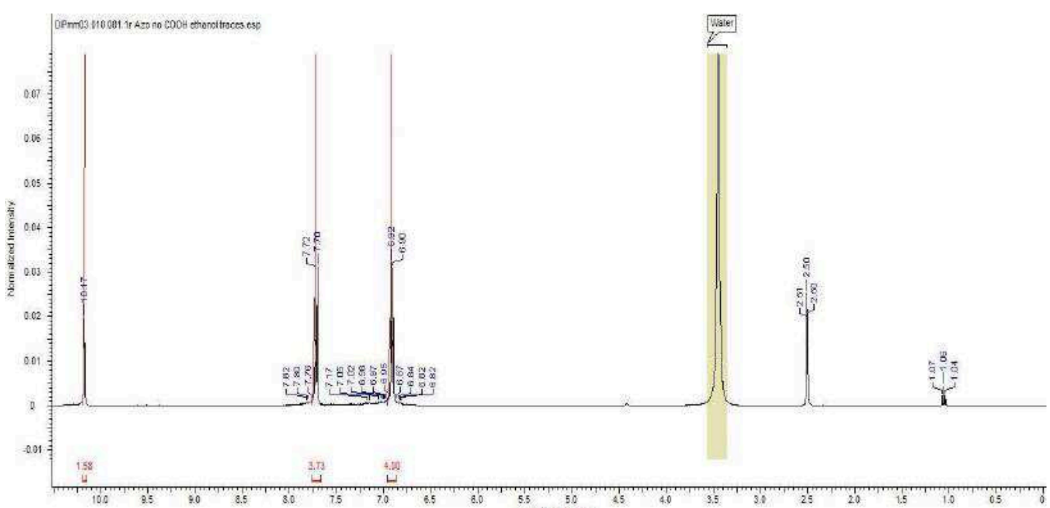

Figure A4(1). ^{1}H NMR spectrum of 4,4'dihydroxyazobenzene in DMSO-d_6.

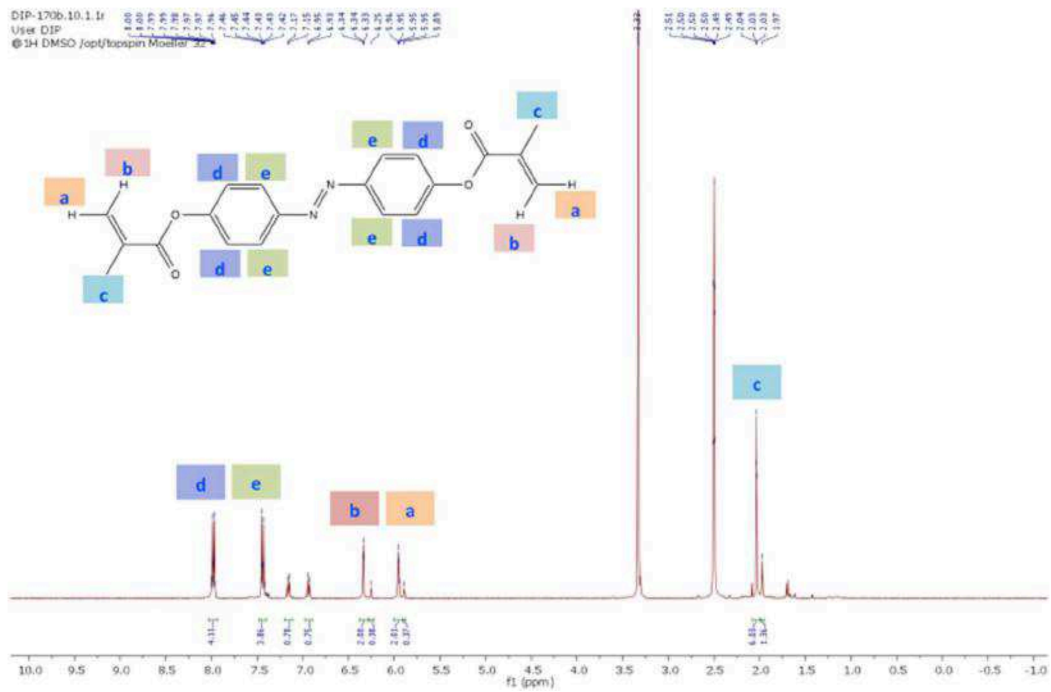

Figure A4(2). ^{1}H NMR spectrum of 4,4'-dimethacryoylazobenzene in DMSO-d_6.

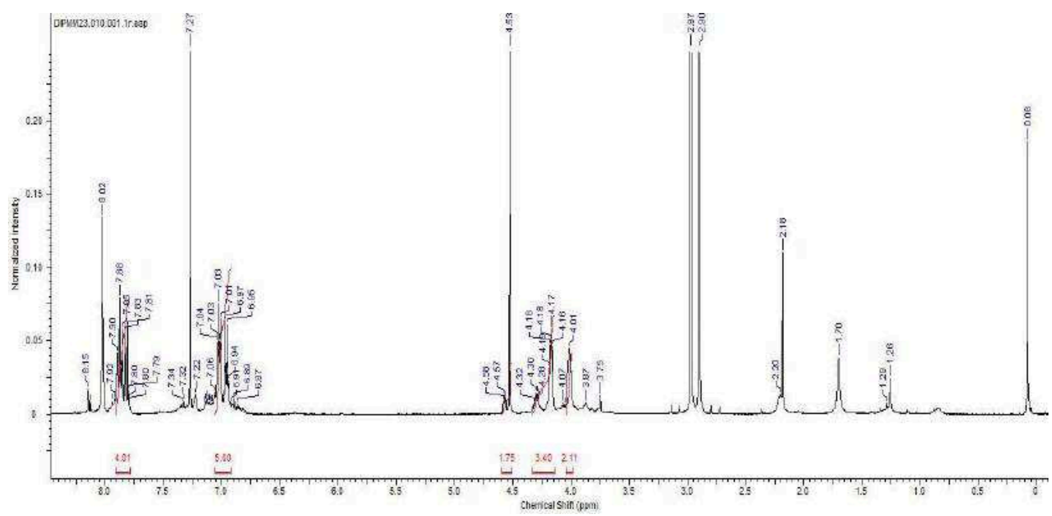

Figure A4(3). ^{1}H NMR spectrum of 4,4'-dihydroxyethoxyazobenzene in $CDCl_3$.

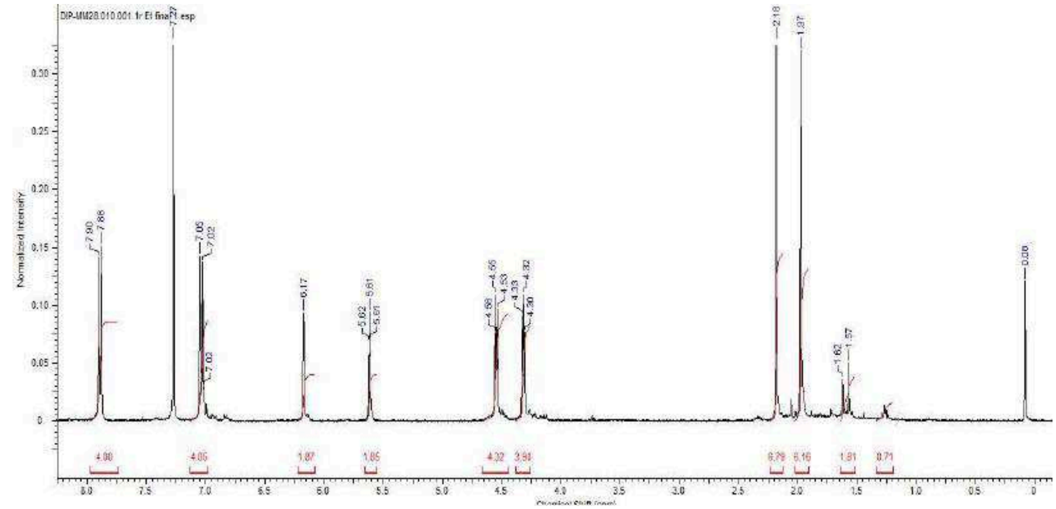

Figure A4(4). ^{1}H-NMR spectrum of 4,4'-dimethacryloylethoxyazobenzene in $CDCl_3$.

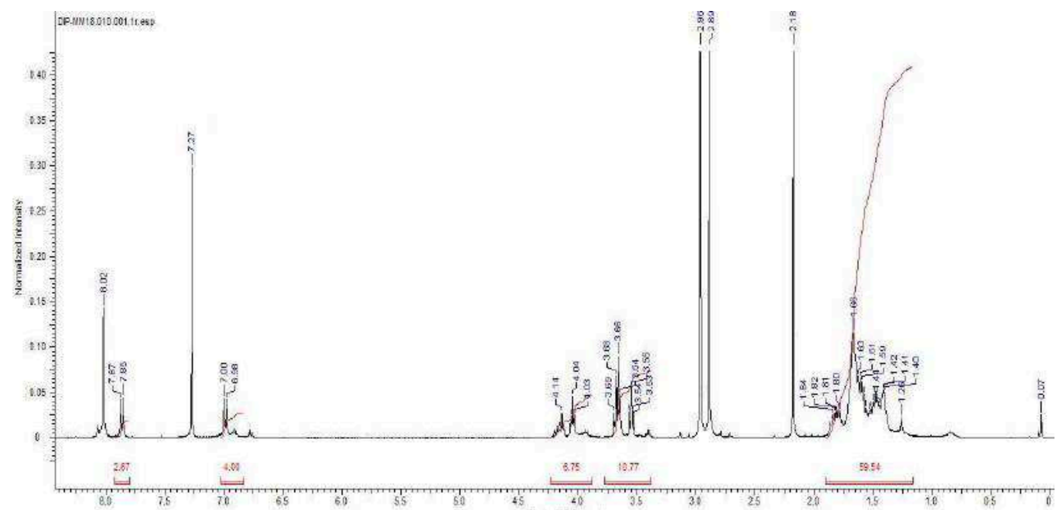

Figure A4(5). ^{1}H NMR spectrum of 4,4'-dihydroxyhexoxyazobenzene in $CDCl_3$.

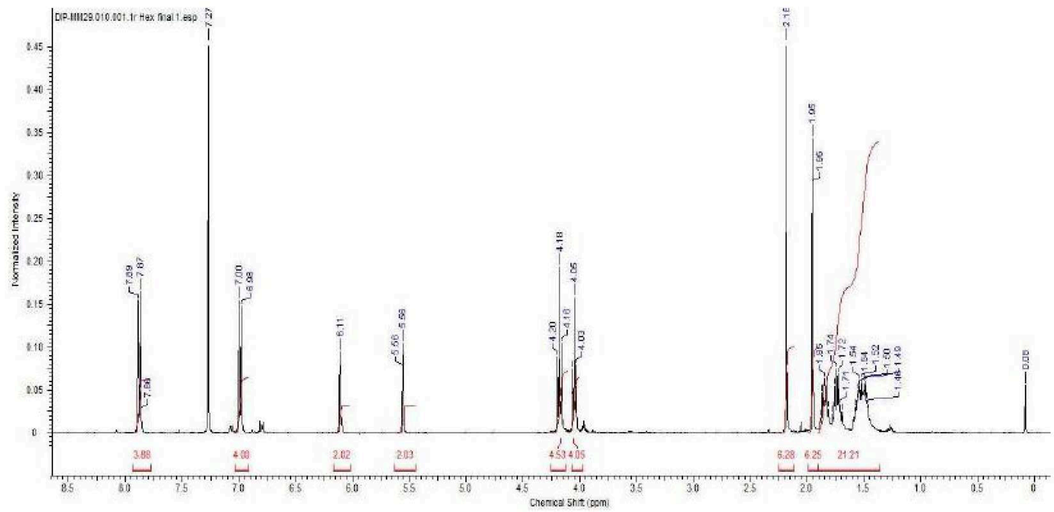

Figure A4(6). ¹H-NMR spectrum of 4,4'-dimethacryloylhexoxyazobenzene in $CDCl_3$.

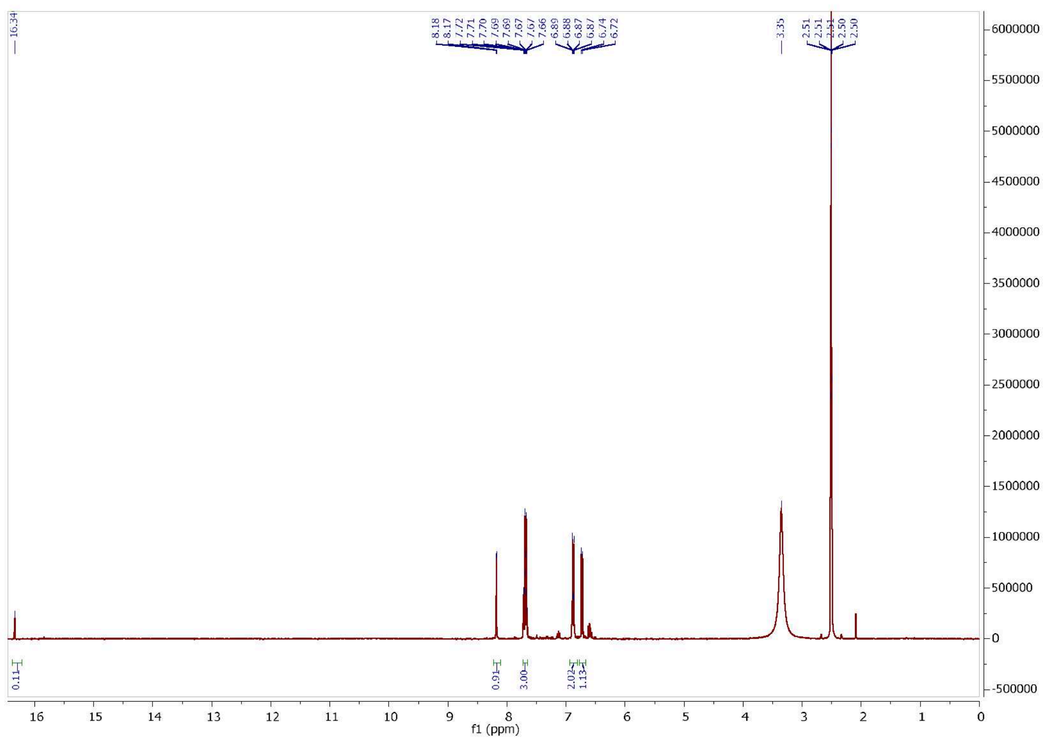

Figure A4(7). ¹H-NMR spectrum of 4,4'-dihydroxyazobenzen-3-carboxylic acid in DMSO-d_6.

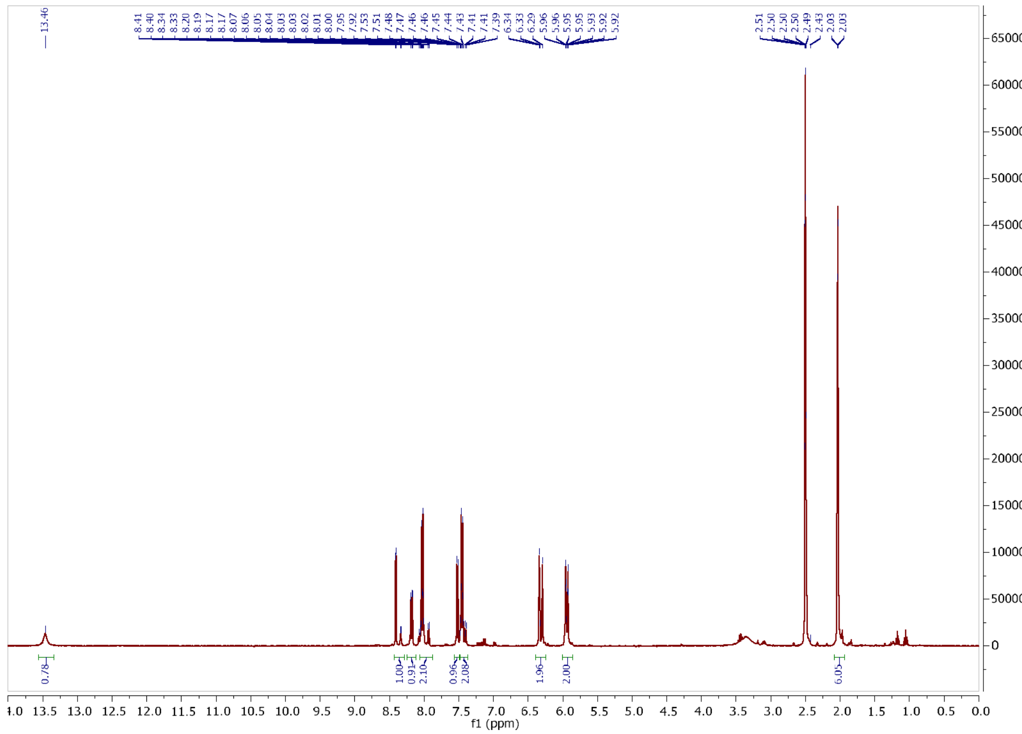

Figure A4(8). ^{1}H-NMR spectrum of 4,4'-dimethacryloylazobenzen-3-carboxylic acid in DMSO-d_6.

CHAPTER 5. UV-induced Swelling of Microgel Particles containing *β*-Dicarbonyl Groups

5.1. Introduction

β-dicarbonyl compounds (*β*-DCC) exist as enol and diketo structures that interconvert via a tautomeric equilibrium as shown in Scheme 5(1). This tautomerism is observable in the gas and liquid phases, as well as in films and even in isolated cryogenic matrices.[5(1)] The equilibrium between the diketo and enol forms can be shifted under illumination with UV light, in favor of the diketo form[5(2),5(3a)] and this property has been exploited in commercial sunscreen products for instance.[5(1),5(4)]

β-DCCs such as 2-acetoacetoxyethyl methacrylate (AAEM) that contain a polymerizable functionality have been widely used as a reactive co-monomer in various polymeric systems. The *β*-dicarbonyl moiety can undergo facile, chemical modifications such as ambient condition cross-linking reactions with functional groups such as diamines, aldehydes, and isocyanates.[5(8)] As such, they have been used in the production of coatings, latexes, resins, and dental adhesive formulations.[5(4-8a)] They are also important in architectural coating binders where improved hardness, scrub, stain, and dirt pick-up resistances are desired.[5(9)] However, the ability to influence the fraction of enol and diketo groups relative to each other via UV irradiation and in turn control the hydration behavior of *β*-DCC has scarcely been explored. This ability to respond to an external stimulus opens up the possibility for such molecules to be incorporated into polymeric networks to create a class of photoresponsive smart materials. An elegant example has been demonstrated by Watanabe and coworkers, who synthesized a hydrogel cantilever composed of a cross-linked network of acrylamide and acryloylacetone, a comonomer bearing the *β*-dicarbonyl functionality.[5(2)] They managed to achieve a maximum of 30% increase in swelling of the hydrogel which caused a 45° deflection upon 20 minutes of UV irradiation. Meanwhile, copolymeric gels containing AAEM have not been reported to exhibit photo-responsive behavior.[5(10-11)] They have nonetheless been employed as vessels for the synthesis and incorporation of metal nanoparticles.[5(10c-d)]

In this chapter, we provide a first investigation into the synthesis of monodispersed, discrete P(AAEM)-based microgel particles via precipitation polymerization in water and to consider their photo-responsive behavior. We report on the photo-induced swelling and size increase of the microgels and investigated how the extent and rate of swelling can be influence by differences in their internal morphology, which was varied via incorporation of different hydrophilic comonomers and cross-linkers. These microgels are attractive candidates, worthy of further investigation as a new class of smart, photo-responsive colloidal particles that are amenable to further chemical modifications and coordination to metal targets.

Scheme 5(1). Keto-enol tautomerization of AAEM and proposed interactions of the tautomers with water molecules.

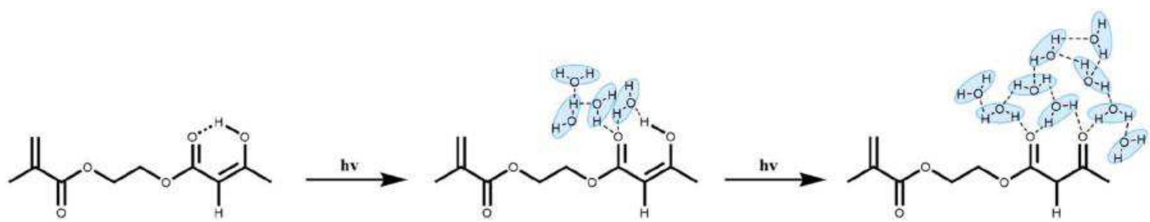

5.2. Experimental section

5.2.1. Materials

2-Acetoacetoxyethyl methacrylate (AAEM) was obtained from Aldrich and purified by running through an aluminum oxide column followed by vacuum distilled under nitrogen. 2,2'-azobis(2-methylpropyonamidine) dihydrochloride (AMPA), poly(ethylene glycol) methyl ether methacrylate, M_n = 500 g mol^{-1} (PEGMEMA 500), poly(ethylene glycol) methyl ether methacrylate, M_n = 950 g mol^{-1} (PEGMEMA 950), poly(ethylene glycol) diacrylate M_n = 700 g mol^{-1} (PEGDA), and *N,N´*-methylenebisacrylamide (BIS) were all obtained from Aldrich and used as received. These reagents are shown in Chart 5(1). Ethanol-d_6 (99.0%), Benzene-d_6 (99.5%) and $CDCl_3$ (99.8%)were all purchased from Deutero GmbH and used as received.

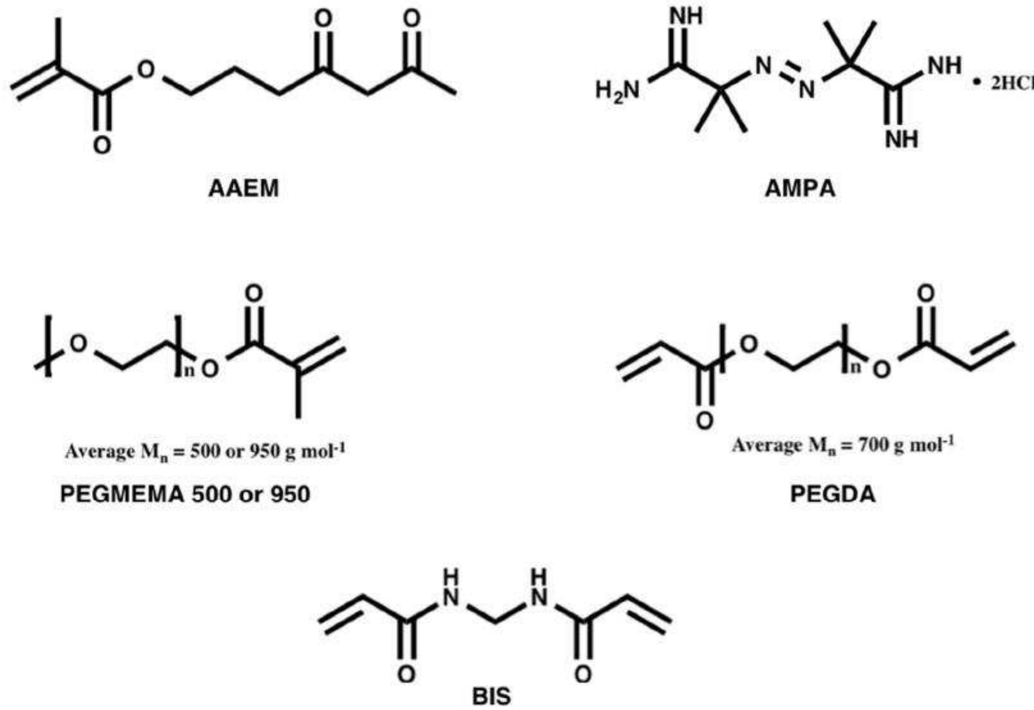

Chart 5(1). Chemical structures of the reagents used in the synthesis of the microgels.

5.2.2. Polymerization

Appropriate amounts of AAEM and respective co-reactants, listed in Table 5(1), were added to 145 ml of distilled water in a double-walled glass reactor, equipped with a stirrer. The polymerization mixture was purged with nitrogen flow under continuous stirring at 300 rpm for 30 minutes at a temperature of 70°C before initiation with the appropriate amount of AMPA (dissolved in 5 ml distilled water). The polymerization was carried out over 4 hours. In all cases stable milky dispersions were obtained. The microgel dispersions were subsequently purified by dialysis against distilled water using *Carl Roth ZelluTrans* regenerated cellulose membrane (MWCO: 12 000 - 14 000 Da).

Table 5(1). Reagents used for the synthesis of P(AAEM) microgels

Microgel	AAEM [mmol]	PEG 500 [mol %]	PEG diacrylate [mol %]	BIS [mol %]
MG1	10	-	-	-
MG2a	10	0.5	-	-
MG2b	10	1.0	-	-
MG3	10	-	0.5	-
MG4a	10	-	-	0.5
MG4b	10	-	-	1.0

5.2.3. Characterization

Dynamic light scattering (DLS). Particle size analysis of the microgels was carried out via dynamic light scattering (DLS) measurements and performed with an ALV/CGS-3 Goniometer with a JDS Uniphase Laser (λ = 632.8 nm) coupled to an ALV/LSE Tau Digital Correlator at a detection angle of 90°. Samples for DLS measurements were prepared by dilution of the stock microgel dispersions with water for chromatography (LiChrosolv®, Merck). The diluted dispersions were filtered through 1.2 µm syringe filters (Chromafil® Xtra PET-120/25, Macherey-Nagel) to eliminate dust particles. Filtered dispersions were placed into glass cuvettes (VWR, test tubes borosilicate 3.3, rimless, round bottom) and left to thermally equilibriate for 10 minutes before measurements in two runs of 60 seconds each were recorded at 20°C.

Measurement of particle size upon photo-response. The photo-response to UV light (λ = 254 nm, 4 W, compact lamp, UVP LLP) was also monitored by means of DLS. The diluted and filtered dispersions were placed in a Quartz cuvette (Quartz SUPRASIL®, Hellma Analytics) and irradiated *ex situ* with a handheld UV lamp (UVGL-25 Compact UV Lamp, 4 W, UVP) from a distance of 2 cm. Irradiation time was varied from 10 to 220 seconds. The irradiated dispersion was then transferred back to a glass cuvette and left to equilibriate at 20°C in the toluene bath of the DLS instrument for 10 minutes before size measurements were recorded. Most of the mean particle sizes reported in this paper was derived using the cumulant analysis method where the mean diffusion coefficient from the intensity autocorrelation function was fitted into the Stokes-Einstein equation for spherical particles.[5(12)] Where necessary to show the non-isotropic swelling and the consequent increase in particle size distribution, we presented the particle size distribution curves obtained from a CONTIN fit method.[5(13)]

UV/vis spectroscopy. UV/vis-spectroscopic studies were carried out with the Cary 100Bio UV-Visible Spectrophotometer from Varian. The spectra were measured from 800-200 nm with a scan rate of 600 nm/min. A quartz cuvette (Quartz SUPRASIL®, Hellma Analytics) was used for the measurement and a second cuvette filled with deionized water was used as a reference. UV irradiation (λ = 245 nm) of the solutions within the quartz cuvette was performed *ex situ* of the spectrophotometer with a handheld UV lamp (UVGL-25 Compact UV Lamp, 4 W, UVP) from a distance of 2 cm.

Microscopic attenuated total reflectance Fourier transform infrared (ATR FT-IR). Spectra were collected on a Thermo Nicolet Nexus 470 FTIR spectrometer instrument supplemented with a Ge crystal (2 mm, 45° face angle) overhead ATR cell from Specac. An amount of 1 μL of microgel dispersion in water (0.5 mg/ml) was placed directly on the Ge crystal and each spectrum was collected on the liquid-substrate interface.

^{1}H NMR spectra of AAEM monomer in various deuterated solvents were measured using an AV400 Bruker NMR spectrometer. In a typical sample preparation, 50 μl of destabilized AAEM monomer was dissolved in 0.5 ml of deuterated solvent.

Cryogenic transmission electron microscopy (cryo-TEM) visualization was performed on a Carl Zeiss LibraTM 120 microscope (Oberkochen, Germany) with a bottom-mounted CCD camera. The electron beam accelerating voltage was set to 100 kV. Freshly synthesized microgel dispersions were first diluted with 25 parts of deionized water, and 2 μl of the diluted suspension of each sample was withdrawn and deposited on one side of a plasma-treated lacey grid within a vitrobot system. Excess liquid was blotted away from the under side of the grid by a piece of filter paper so that no thick liquid film, i.e. above 200 nm thick, remained. Once prepared, the sample assemblage was immediately plunged into liquid ethane (−182.8°C). The frozen, or vitrified, sample was then mounted on a Gatan 626 cryo-holder and transferred into a JOEL 1210 TEM with an acceleration voltage of 120 KeV. The specimen temperature was maintained at −180°C throughout the observation.

The Cryo-FESEM images of the microgel were captured on a Hitachi S-4800 electron microscope. This device is equipped with a vacuum sample chamber with temperature control. The chamber is connected to the microscope, so that the sample can be observed in the same environment as in the chamber. A drop of the emulsion (~ 10 μL) was added into a cylindrical copper cuvette. The volume of the drop is slightly larger than that of the cuvette, and therefore, an excess of liquid is held at the top of the cuvette by surface tension. Liquid nitrogen was degassed in vacuum for 30 seconds before the cuvette containing the sample was frozen by being dipped into the liquid nitrogen and transferred into the sample chamber (T = -140°C, $p = 10^{-6}$ Pa), where a part of the frozen drop on top of the cuvette was cut away with a razor blade. The temperature in the chamber was raised to -90°C to create a clean surface. After 5-10 min, the sample was cooled again to -140°C and maintained at this temperature during the observation.

5.3. Results and discussion

5.3.1. Synthesis and particulate nature of non-chemically cross-linked microgels

AAEM has limited solubility in water, existing as oily droplets at room temperature but in the concentration employed in our polymerization, become sufficiently soluble at 70°C. We assume that the initiation starts in water and the growing P(AAEM) oligoradicals become increasingly hydrophobic. After a certain critical chain length, they precipitate to form stable nuclei, which subsequently grow by monomer diffusion. The linear, aliphatic nature of the AAEM monomer is not expected to confer much steric restriction on the entanglement of the chains, thereby enabling a dense packing of the polymer chains within the particles.

MG1 was prepared without the addition of any chemical cross-linkers. Nonetheless, discrete and monodispersed particles were detected by DLS, and cryo-electron microscopic imaging. This suggests that the P(AAEM) chains could form spherical three-dimensional networks without the use of a chemical cross-linker. Fig. A5(1) of Appendix 5 shows the fitting to a spherical model of an angle-dependent DLS measurement of MG1 performed at 20°C. The excellent fit affirms the discrete, spherical and particulate nature of an aqueous dispersion of MG1. The cryo-SEM and cryo-TEM micrographs of the different microgel particles are shown in Fig. 5(1). The particles are spherical with R_h that corresponds to that measured in DLS.

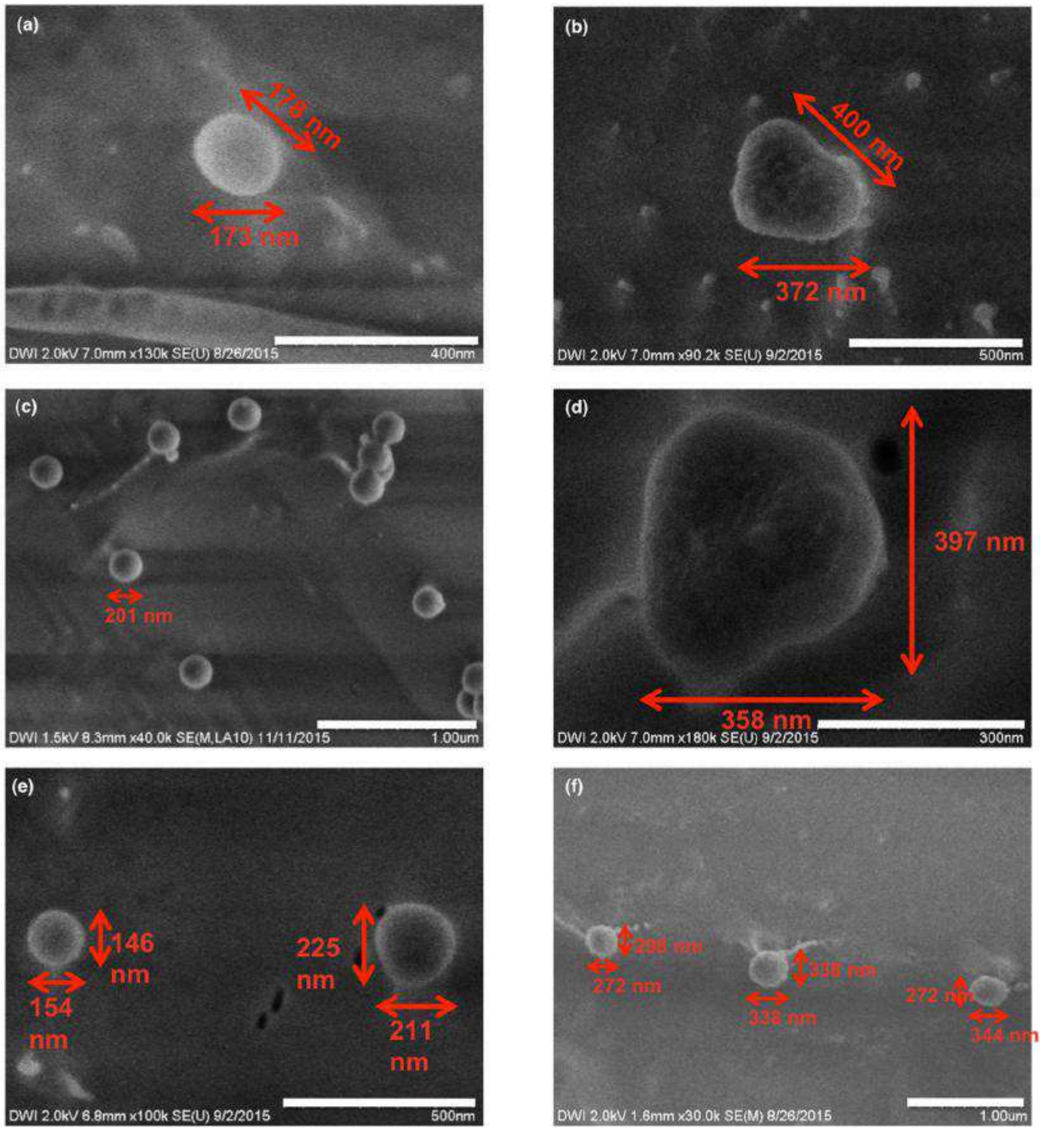

Figure 5(1). Cryo-FESEM micrographs of (a) MG1, (b) MG1 irradiated for 90 s, (c) MG2a, (d) MG2a irradiated for 30 s, (e) MG4a, and (f) MG4a irradiated for 30 s.

We dissolved a drop (~ 50 µl) of freshly prepared and dialyzed aqueous MG1 dispersion in 1 ml of THF in order to investigate if the MG1 particles are somehow chemically cross-linked or if they are formed merely from entangled, topologically constrained polymer chains in a poor solvent (water). THF is a good solvent for the AAEM monomer and if the MG1 particles were not chemically cross-linked, the entangled chains should unravel, uncoil to an extended conformation and dissolve in THF. Fig. A5(2) of Appendix 5 shows the size distribution curves of DLS measurements, obtained via a CONTIN fit, of MG1 dissolved in THF over time. The particles appear to swell progressively in THF until they start to unravel at around the twentieth minute mark. At the 30th minute mark, small particles of sizes less than 100 nm in hydrodynamic radius are detected. This could be attributed to aggregation of linear chains.

This indicates that the MG1 particles are probably not chemically cross-linked but are instead microphase-separated and entangled polymer chains with physical cross-links, as we initially assumed. Nonetheless, we cannot entirely exclude the existence of some degree of chemical cross-linking. Boyko contends that chemical cross-links could arise from chain transfer reactions during AAEM polymerization.[5(11)] Physical cross-links can arise from intra-particle, H-bonding interactions between groups adjacent to each other. These interactions most probably occur between the acidic hydrogen atoms on the acetylene carbon atom between the diketo groups and the carbonyl oxygen atoms on adjacent chains.[5(14)] Physical cross-links formed via hydrogen bonding between two enol moieties, between two diketo moieties or between an enol moiety and a diketo moiety, on adjacent chains could also be possible. The reality is probably a combination of all of these hydrogen bonding interactions.

5.3.2. Tautomeric nature of AAEM monomer and AAEM unit within microgel particle

The tautomeric nature of the AAEM monomer was investigated in the following deuterated solvents, listed in ascending polarity: benzene-d_6, $CDCl_3$, and ethanol-d_6. NMR measurement was not performed in D_2O since AAEM exists as phase-separated oily globules in aqueous media at room temperature. The respective ^1H NMR spectra can be found in Fig. A5(3) of Appendix 5. It is clear that in the monomeric form, AAEM exists predominantly as the diketo tautomer. This agrees well with the evidence that the keto form is usually the more thermodynamically stable form for most aldehydes and ketones due to bond energies, being about 48 kJ mol^{-1} more stable than the enol form.[5(15)] By examining the integral ratio of the methyl protons of the diketo form to the same protons of the enolic form, we see that the proportion of the diketo form increases with increasing solvent polarity. In the protic ethanol-d_6 solvent, the signal of the enolic proton is barely visible. This is an indication that the diketo form is strongly stabilized via hydrogen bonding with ethanol molecules. We did not perform ^1H NMR measurements on the microgel particles because the freeze-dried particles were not easily re-dispersable in the deuterated solvents. Instead, we carried out attenuated total reflectance measurement on MG1 in order to detect the predominant tautomeric species in its native aqueous environment. An analysis of the absorption bands reveals a relatively high degree of enolization before UV irradiation in MG 1, with the *cis*-chelated enol form being dominant. This can be seen by the relatively prominent absorption band at ~ 1657 cm^{-1} seen in Fig. 5(2). This band is associated with the stretching vibrations of the conjugated double bond (C=C) of the enolic form.[5(3a),5(16)] After irradiation, the band at ~ 1657 cm^{-1} is diminished while a new band at ~ 1739 cm^{-1} becomes prominent. This new band is associated with the stretching vibration of the ester carbonyl of the keto form.[5(16)] The sharp bands at ~ 2924 cm^{-1} and ~2854 cm^{-1} can be attributed to the CH_2 stretching modes while the broad band centered at ~ 3450 cm^{-1} is related to OH stretching.[5(3a)]

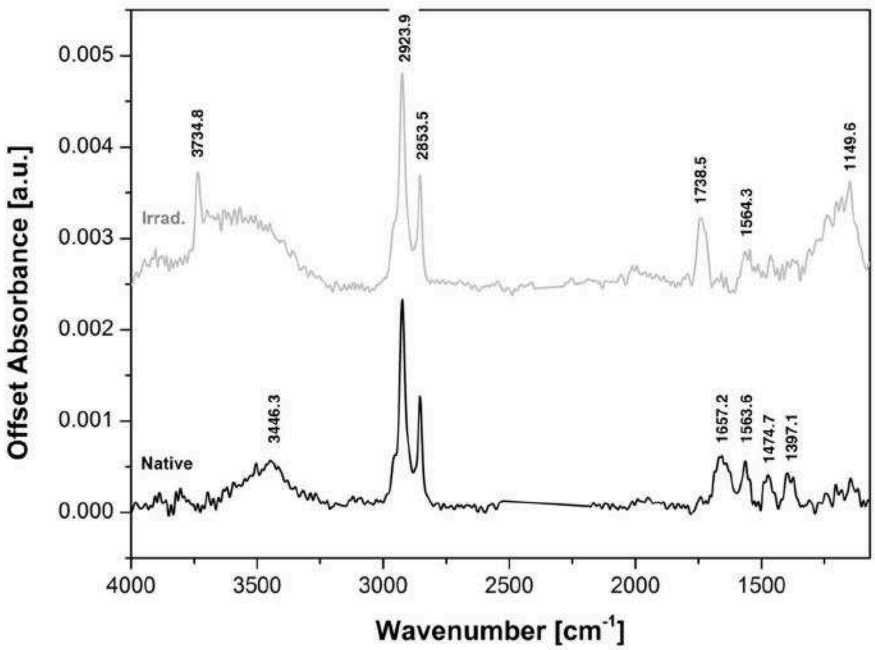

Figure 5(2). ATR spectra of native MG1 (5 wt. % in H_2O) and UV-irradiated (λ = 254nm) MG1 (5 wt. % in H_2O).

Table 5(2). Assignment of ATR absorption bands

Assignment	Wavenumber [cm^{-1}]
C=C vibrations of enolic form	1657
Ester C=O vibrations of the keto form	1739
CH_2 stretching modes	2854 and 2924 (sharp)
Rotational fine structures of water	3450 (broad)

This reversal in tautomeric equilibrium has been similarly observed during the transformation from monomeric acryloylacetone to poly(acryloylacetone).[5(17)] It was proposed that the enol form probably dominates within the polymer due to the hydrophobic microenvironment within the polymer coils. The enol form is stabilized by H-bonding to the Lewis basic neighbouring carbonyl group, forming what is known as a chelated enol species. The formation of a conjugated six-membered ring results in a resonance stabilization of the chelated enol.[5(18)] In the case of P(AAEM), Schlaad *et al*. found that the diketo form predominates both in the homopolymer and block copolymer, dissolved in $CDCl_3$.[5(14)] This appears to contradict our findings but we believe that the microenvironment within a dense globular P(AAEM) particle is inherently different from that of a homopolymer or copolymer coil, and it is this difference in the hydrophilicities of the two microenvironments that is key in determining the tautomeric equilibrium.

5.3.3. Detection of photo-ketonization

UV irradiation of 248 nm < λ < 280 nm is essential to trigger the ketonization process.[5(3a)] The photo-ketonization of the microgel particles was followed spectro-photometrically by irradiation of the diluted microgel dispersions with λ = 254 nm. The absorption peak at λ = 260 nm seen in the spectra in Fig. 5(3) is associated with the π-π* transition of the chelated enol tautomer.[5(19-20)] Upon irradiation, this peak decreases in intensity and is an indication of the photo-ketonization process. The absorption (n-π* transition) of the diketo species, known to appear at around 310 nm, is typically weak and usually not detected due to the very small extinction coefficient of the keto form.[5(19-21)] Hence, only changes in the absorption of the enol form can be followed spectro-photometrically.

As shown in the putative tautomerization pathway in Scheme 5(1), the photo-ketonization is expected to proceed from the *cis* chelated enol form to a transient non-chelated rotamer of the *cis* enol before the diketo form is produced.[5(1),5(19-22)] The equilibrium inter-conversion between the *cis* and *trans* enol form (with maximum absorption at around 230 nm)[5(20)] most possibly occurs on a timescale too fast to be captured by UV/vis measurements or unlikely to occur altogether within the polymeric particles due to reasons expounded by Masuda *et al*.[5(22)] They explain that within the polymeric chains, the formation of the *trans* enol form is bypassed most probably due to serious restrictions to rotation, which is necessary to form the *trans* enol. Fixing of the *cis* enolic H by formation of H-bond to C=O groups would further restrict rotation around the double bond, thereby excluding the formation of the *trans* enol. The increase in absorbance of the spectrum of MG1 over the entire wavelength [shown in Fig. 5(3a)] after 220 s of UV irradiation is an indication of particle aggregation.

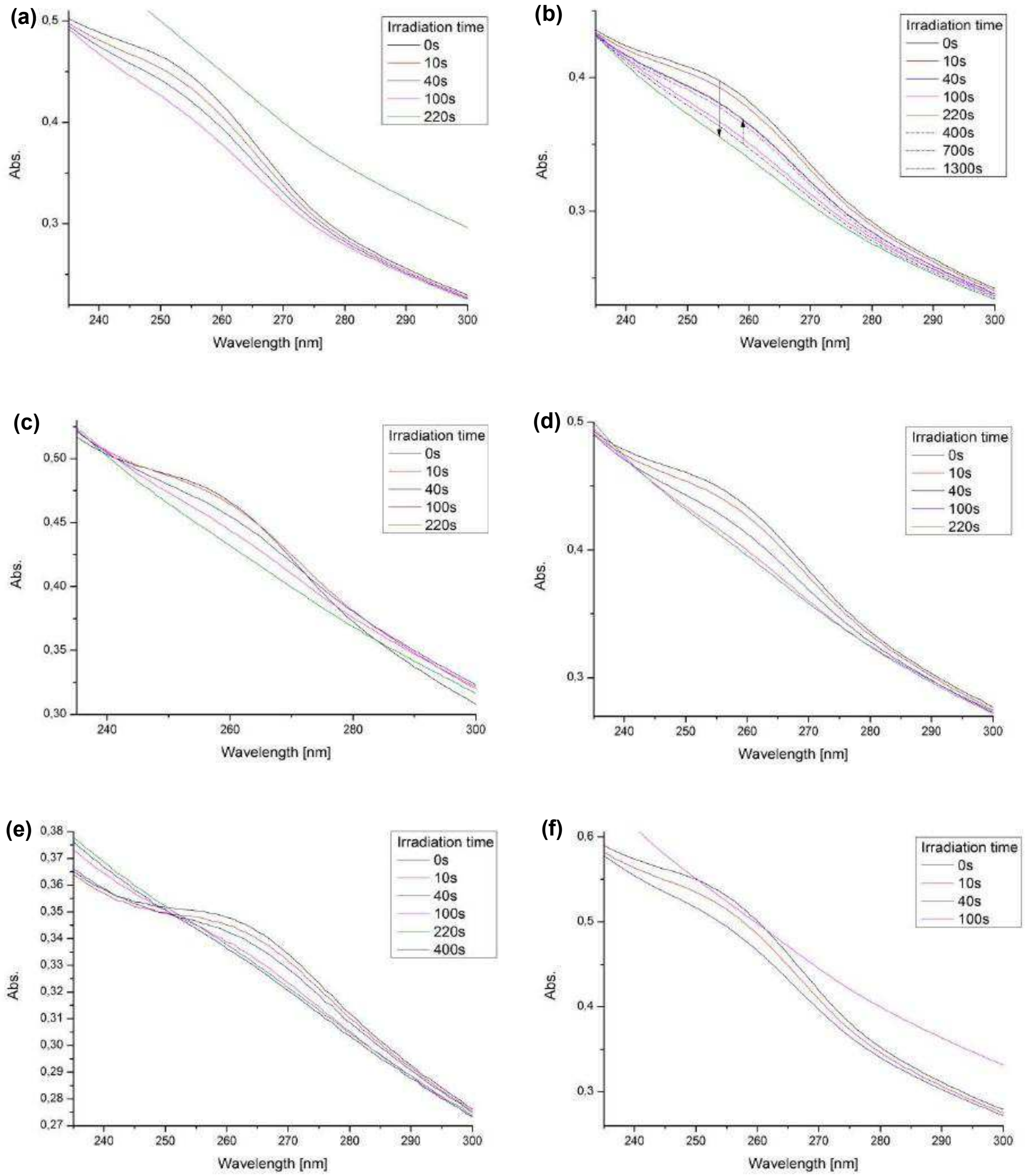

Figure 5(3). Change in the absorbances of the microgels upon UV (λ = 254 nm) irradiation. (a) MG1, (b) MG2a, (c) MG2b, (d) MG3, (e) MG4a, and (f) MG4b.

In Fig. 5(3b), the peak at 260 nm reappears after 400 s of irradiation. It would appear that the tautomeric equilibrium is shifted back to the enolic species in MG2a but not in the other microgel samples. The cause of the re-appearance of this peak in MG2a is not clear but we offer an explanation in the last section of this chapter.

5.3.4. Photo-ketonization-induced swelling of microgel

Photo-ketonization is fundamental to induce swelling of hydrogels containing *β*-dicarbonyl moieties.[2] Similarly, via DLS investigation, we determined that photo-ketonization leads to a swelling of our microgels. Fig. 5(4) shows the R_h of the respective microgels when subjected to ex situ UV irradiation progressively for increasing periods of time, as indicated.

Photo-ketonization leads to swelling because of the increased osmotic pressure to absorb water by the carbonyl moieties of the diketo group. Diffusion of water molecules is however limited by the dense topology of the chains, which restricts water permeability. We are of the opinion that in each particle, there is a radial gradient of decreasing topological restrictions from the core to the surface. The entanglement of the long linear P(AAEM) chains with each other and hence the topological restrictions are more severe in the interior of the microgels. Therefore, the chains existing closer to the surface are expected to have higher mobility, since their mobility or reptation is less hindered. This is analogous to the system investigated by Rubio Retama *et al*., who detected different diffusion coefficients of polymer chains in the core and the surface due to differing cross-linking densities within a single microgel particle.[5(23)]

Looser or more mobile chains facilitate the diffusion of water molecules into the particle. Hence, this radial gradient of decreasing topological restrictions should be well correlated with the progressive increase in hydrophilicity of the particle microenvironment on moving from the core to the surface. We discuss the data presented in Fig. 5(4) on the basis of the differences in topological restrictions and hydrophilicities of the microenvironments in each network. The hydrophilicity of the microenvironment in turn affects the tautomeric equilibrium of the acetoacetyl moieties along the polymer chains. In a hydrophilic microenvironment, the diketo form is most likely to predominate, as discussed in the obtained NMR spectra of the AAEM monomer. This is because of the tendency for the C=O groups to form hydrogen bonding with water molecules and in accordance with the Erlenmeyer rule of a shift in the tautomeric equilibrium towards the keto form with increasing solvent polarity.[5(24)]

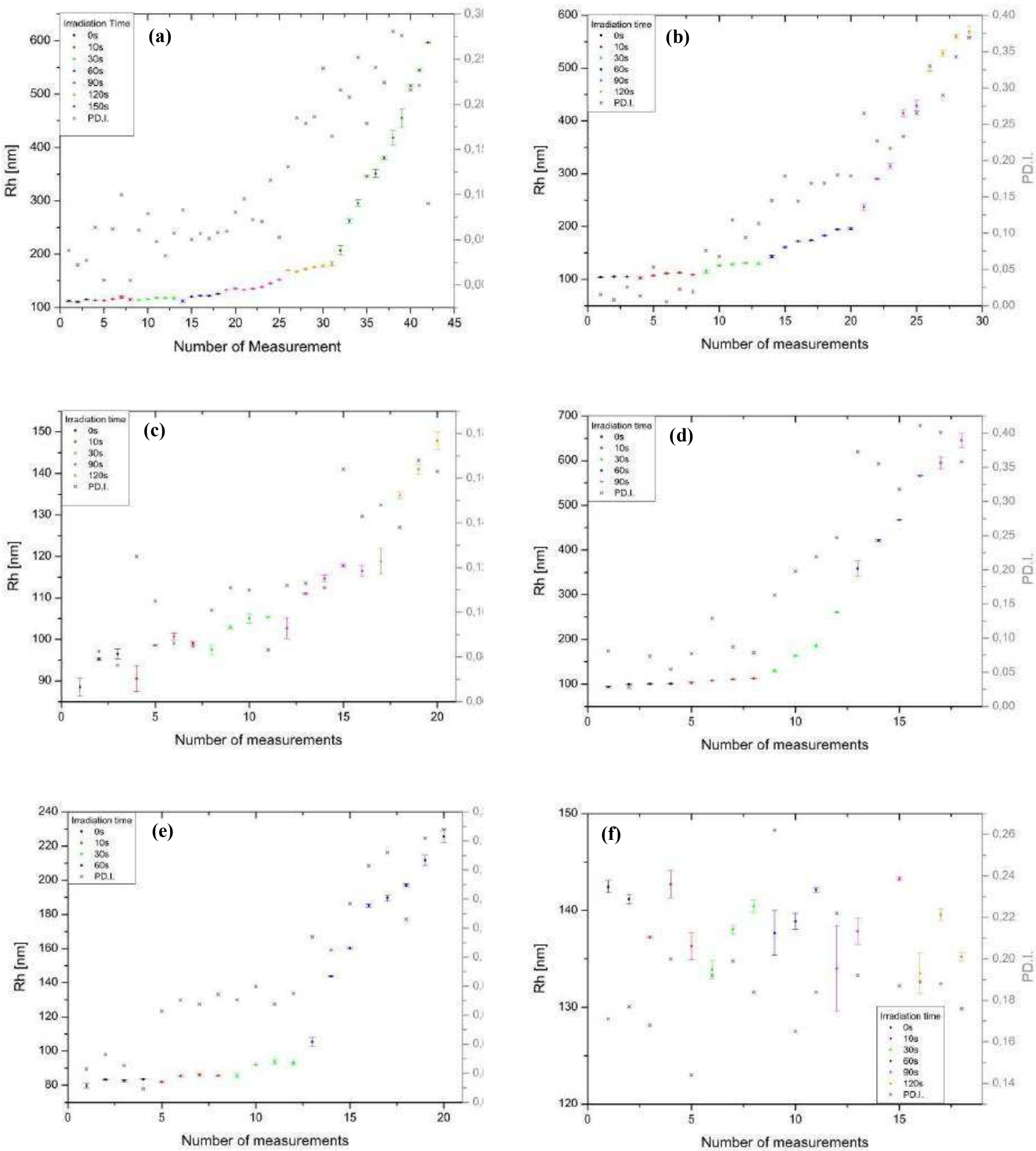

Figure 5(4). Change in the R_h of the microgels upon UV (λ = 254 nm) irradiation. (a) MG1, (b) MG2a, (c) MG2b, (d) MG3, (e) MG4a, and (f) MG4b.

In a more hydrophobic microenvironment, such as in the dense interior of the microgels, the chelated enol form is stabilized and predominates. Hence, we expect the gradient of hydrophilicity of the microenvironment to be well correlated with a gradient of increasing chelated enol tautomer on moving from the surface into the interior of the microgels.

PEG macromolecules are expected to increase the hydrophilicity of the network.[5(25)] At the same time the flexible PEG chains would disrupt the close packing of the P(AAEM) chains, easing some of the topological constraints in the net-work. BIS as a cross-linker is hydrophilic because of its amide functionality containing both H-bond accepting and donating moieties. The small and rigid nature of the BIS molecule is further expected to alleviate the topological constraints in the network by decreasing the extent of chain entanglement. This then leads to improved water permeability through a more porous network. A more hydrophilic internal micro-environment of the microgels, however, leads to two effects that tend to be antagonistic to one another. The first is that the existence of a higher proportion of diketo moieties in the interior of the microgels prior to UV irradiation would be favored in a more hydrophilic internal microenvironment. This would promote physical cross-linking within the particle as discussed earlier, and limits the photo-ketonization process upon UV irradiation, consequently limiting the extent of photo-induced swelling. The second effect is that a more hydrophilic network would be more amenable to wicking and permeation of water into its interior because of the minimization of topological constraints. The network should then be more elastic and porous when the reptation of the entangled P(AAEM) chains is less restricted. This facilitates swelling of the microgels due to the opening of channels for the diffusion of water molecules.

As seen in Fig. 5(4), the more flexible and/or porous networks in MG2a, MG2b, MG3b, and MG4a enable faster onset of swelling upon UV irradiation compared to MG1. Within a topologically constrained network, it is also to be expected that competition between two possible H-bonding interactions could arise as a result of photo-ketonization. The carbonyl moieties of the diketo groups could form hydrogen bond interactions with water molecules, resulting in swelling of the microgels or they could form hydrogen bond interactions with the acidic hydrogen atoms on acetylene carbon atoms of adjacent chains, leading to increased formation of physical cross-links within the particle network. We suspect the latter process to prevail in MG1, at least initially, before H-bonding to water becomes more favorable.

We observed that after each period of irradiation, the microgel solutions requires an equilibration time of ~10 minutes before the swelling stabilizes and the R_h reaches a constant value. This can be attributed to the fact that the long, heavy and densely-packed polymer chains have poor mobility. Time is required for the polymer chains to stretch and relax to accommodate water molecules. After a certain point when sufficient water has entered the dense interior of the network, the water acts as a good lubricant for segmental motion, relaxing topological constraints and allowing more rapid swelling. The rate of irradiation employed is an important factor to consider in minimizing particle aggregation. Irradiation in stages, using short bursts of 10-30 seconds irradiation times in stages is preferred over longer, single-dose irradiation times of 60 s and above. Gradual irradiation helps to control the rate of photo-ketonization which in turn ensures a more isotropic swelling of the microgels, prevents their rapid destabilization, and delays the onset of particle aggregation.

Even with short doses of irradiation, the diffusion of water molecules is expected to occur non-isotropically in all microgel particles since topological constraints in the network hinder uniform diffusion and permeation of water. This non-isotropic swelling is evident in the cryo-FESEM micrographs seen in Fig. 5(1b, d). This results in the broadening of the particle size distribution after irradiation, and leads to a destabilization of the microgels, thereby facilitating their aggregation. By looking at Fig. 5(4d), for instance, the onset of aggregation is apparent by the rapid increase in the polydispersity index (Pd.I), after 30 seconds of UV irradiation for MG3. The photo-ketonization process appears to promote aggregation of the microgel particles and this can be attributed to the decrease in stability of the particles as they swell non-isotropically. The increase in the concentration of diketo groups also drives inter-particle hydrogen bonding interaction, thereby accelerating the aggregation process.[5(12)]

Table 5(3). UV-Induced swelling degree before onset of particle aggregation.

Microgel	$R_{h,native}$*	$R_{h,max}$*	Degree of Swelling ($R_{h,max}/R_{h,native}$)
MG1	112.9	331.1 (150 s)#	2.7
MG2a	105.4	241.2 (90 s)	2.3
MG2b	95.9	115.0 (90 s)	1.2
MG3	100.3	203.5 (30 s)	2.0
MG4a	82.2	211.5 (60 s)	2.6

*Taken as the mean of three consecutive measurements.
Time in brackets indicates the period of UV irradiation required to attain maximum swelling before aggregation sets in.

The extents of swelling before the onset of aggregation of the respective microgels are listed in Table 5(3). $R_{h,max}$ is used to denote the largest hydrodynamic radius attained by UV irradiation before the extent of aggregation. The onset of aggregation for each microgel was arbitrarily set to begin when the Pd.I reached a value of between 0.12-0.15. This is usually the point after the first rapid swelling upon a certain period of irradiation before a second burst of size increase most probably associated with aggregation occurs.

MG4a appears to possess a balance of fast and high swelling extent upon UV irradiation, before aggregation sets in. This could be attributed to a relatively homogeneous distribution of cross-linking points in the network, which contributes to a more uniform mesh size throughout the particle. Well-defined network porosity enables a more homogeneous swelling process. In some microgel particles, aggregation could set in earlier before the full extent of swelling of each individual particle can be attained. This most probably happens when the rate of swelling is slower than the rate of aggregation. We believe this to be the case especially for MG2b and MG3. In Fig. 5(4c), the R_h values of MG2b particles after 60s of irradiation were omitted because the size of the particles remained similar to that after 30 s of irradiation. In addition, the R_h values beyond 120 s of irradiation were not included in Fig. 5(4c) due to space constraints but they indicate the start of particle aggregation.

We observe that MG3 appears more susceptible to aggregation on standing, even prior to irradiation. The long hydrophilic chains of PEGDA could be protruding from the dense globular network, enriching the surface.[5(25)] We believe this makes the particles open to inter-particle hydrogen bonding interactions, thereby hastening the aggregation phenomenon. Nonetheless a dilute solution of MG3 was prepared for DLS measurement. The R_h value of the non-irradiated sample was unvarying at ~101 nm for multiple size measurements over ten minutes. A cryo-FESEM micrograph, shown in Fig. A5(4a) of Appendix 5, captures a particle of MG3 in its native state. Upon 10 s of λ = 254 nm irradiation, the R_h of the solution was immediately measured by DLS. A size of R_h = 129.81 ± 6.13 nm (Pd.I 0.103) was recorded. A narrow particle size distribution is shown in Fig. A5(4b) of Appendix 5. The dispersion was left to stand in the DLS instrument before a second measurement was recorded ten minutes after the first. Here we see that the R_h obtained by the cumulant fit has more than doubled to 328.01 ± 8.10 nm (Pd.I 0.244). The particle size distribution curve obtained via a CONTIN fit reveals a bimodal distribution of particles, as shown in Fig. A5(4b) of Appendix 5. A non-isotropic swelling of the microgels leading to some particle aggregation is apparent from this measurement. A third measurement was performed fifteen minutes after the first and the result indicates further aggregation. R_h = 405.15 ± 11.08 nm (Pd.I = 0.222) was recorded. The aggregation process continues upon standing for longer periods (30 minutes) and the dispersion becomes increasingly unstable, causing the microgels to precipitate and sediment out of solution.

For the microgel with BIS as cross-linker (MG4), the particles are less likely to aggregate than the particles of the microgel with PEGDA as cross-linker (MG3). In contrast to PEGDA, BIS is a much smaller molecule that is expected to remain within the interior of the particles. Inter-particle hydrogen bonding interactions and aggregation are therefore minimized. It is known that for gels and elastomers, the modulus of the network is inversely related to the average molar mass between cross-links.[5(26)] This could explain the difference in swelling behavior associated with MG3 and MG4a where PEGDA and BIS are used as cross-linkers, in the same molar ratio, respectively. We could assume that the average molecular weight of the P(AAEM) subchains between cross-linking points are very similar in both MG3 and MG4a. By viewing the P(AAEM) chains as the cross-linkers in the network instead, we could say that in MG3, the average molar mass between cross-links is a lot higher than in MG4a since PEGDA has a much higher molecular weight than BIS. This accounts for the higher rigidity of MG4 particles compared to those of MG3.

MG4a particles have the smallest R_h of ~ 82 nm in the native state most probably due to the chemical cross-links and the absence of bulky high molecular weight constituents. A rapid onset of swelling is only observed after 60 seconds of irradiation. The particle size and Pd.I then continue to rise even without any further irradiation, if swelling is left unhalted. This is consistent with swelling followed by aggregation and hence no further irradiation was performed on MG4a beyond 60 seconds. It should be noted that in the microgel samples, the aggregation process could be arrested at any time by preventing or disrupting inter-particle hydrogen bonding interactions. This can be achieved by the addition of a small volume of dilute CTAB solution. The diketo groups bind preferentially to the cetyltrimethylammonium ions of CTAB, thereby minimizing the formation of inter-particle hydrogen bonding.[5(4)]

The microgel particles with BIS content of 1.0 mol%, MG4b, show the largest starting R_h and they do not swell upon UV irradiation. The R_h value fluctuates about a mean of ~ 137 nm. The high amount of BIS changes the microenvironment within the particles to be highly hydrophilic and this result in the larger initial size compared to the other microgel particles. This most probably alters the tautomeric balance of enol and diketo groups along the chains dramatically, in favor of the diketo form, even before UV irradiation. Abundance of the diketo moieties in turn facilitates the formation of additional physical cross-links via hydrogen bonding interactions. UV irradiation appears to trigger enol to keto tautomerization on the microscopic level along the polymer chain, as detected by UV/vis spectroscopy (Fig. 5(3f)). However, macroscopic volume increase of the particles is not observed in DLS. This could be attributed to the limited photo-ketonization that occurs which nonetheless could be detected in UV/vis spectroscopy. Similarly, microgels containing AAEM copolymerized with *N*-vinylcaprolactam P(VCL-AAEM) are not known to exhibit swelling with UV irradiation. These particles have been recognized to consist of a PAAEM-rich core and a PVCL-rich shell structure due to the rapid consumption of highly reactive AAEM in the first stage of reaction. Since BIS (2.5 mol%) is also used as cross-linker, a radial distribution of cross-linking density is expected from a more cross-linked core to a less cross-linked shell.[5(27)] The absence of UV-induced swelling in these particles can then be attributed to the highly hydrophilic environment within the microgel network which diminishes the proportion of chelated enol species, necessary for photo-ketonization.

Several groups have reported the photo-switchability of the diketo species of polymeric *β*-DCC back to the enol form in the dark, albeit partially and slowly. This can occur on the timescale of several hours after irradiation[5(17,21)] or even days after.[5(2,22)] If photo-ketonization is associated with increased swelling of the particles, a re-enolization should lead to a deswelling of the particles. As discussed earlier, in Fig. 5(3c) we see the reappearance of the peak in absorbance at λ = 260 nm in the absorption spectra of MG2a. Dynamic light scattering experiments do not however show a correlation of this re-enolization after 400 s of irradiation with a deswelling of the particles. As a matter of fact, DLS measurements started detecting rapid aggregation after 90 s of irradiation time. The higher concentration of dispersion used in DLS measurements most probably contributes to the fast onset of aggregation in MG2a which was not observed in the lower concentration used for UV/vis measurements. The re-enolization process is probably limited, but can nonetheless be detected by the very sensitive technique of UV/vis spectroscopy. Deswelling, as with swelling, is diffusion limited. The nature of the re-formed enol species is unknown but we deduce that it should not be the original *cis* chelated enol. The long PEG chains in MG2a with their multiple hydrogen bond accepting oxygen atoms probably drives the re-enolization by stabilizing the enolic structure via formation of hydrogen bonding interactions between the enolic protons and the oxygen atoms of the PEG chains.[5(28)] This is a reasonable speculation because, besides the polarity of the solvent, certain structural factors favor the shift of equilibrium towards the enolic species.[5(15,24)] The flexible PEG chains, with their relatively less restricted inter-segmental movements, can very closely approach the P(AAEM) chains to cause the re-enolization. Similarly, Lee *et al.* proposed H-bond formation between the acidic H atoms on the C_2 position of an imidazolium ring and the O atoms of PEG chains in their investigation of the lower critical solution temperature-type behavior of PEG dissolved in imidazolium-based tetrafluoroborate ionic liquids.[5(28)]

5.4. Conclusion

UV-responsive P(AAEM)-based microgels were conveniently synthesized via surfactant-free precipitation polymerization in water. UV irradiation induces a photo-ketonization reaction, which induces swelling in the microgel particles, causing particle size to at least double in four of the microgels synthesized. The extent of swelling is dependent upon the extent of UV-induced photo-ketonization which in turn can be controlled by manipulating the elasticity and hydrophilicity of the network. This was achieved by varying the type and amount of comonomer or cross-linker. The swelling process tends to occur non-isotropically and destabilizes the irradiated particles, leading to their agglomeration.

5.5. Outlook

P(AAEM) microgel systems could serve as prototypical candidates for further studies on the photo-induced processes occurring in colloidal particles containing *β*-DCC groups. This functional group is well-known to be strong bidentate ligands that are able to form complexes with a wide variety of metal ions.[5(29)] The resultant hybrid materials can be utilized as catalytic nanoreactors, colloidal semiconductors, and exploited for their novel optical and magnetic properties.[5(30)] The metal selectivity of such chelating systems can be tuned by changing the tautomeric equilibrium, since the enol form is known to possess higher chelator strength.[5(4)] Such particles can therefore adhere to metallic substrates, or be used to separate and concentrate metal ions.[5(31)] Since the *β*-DCC structure is also a familiar and consistent motif within biologically-relevant molecules, these particles could act as prototypical vessels for analogous biochemical reactions.[5(32)] A better understanding of the back reaction to the enolic form is required since for many applications, such as a photo-switchable scaffold, reversibility is a desirable feature. A portion of the colloidal particle could be bound covalently by controlled chemical reaction of the acetoacetoxy group under mild reaction conditions while still having free photo-triggerable groups remaining. For instance, the *β*-DCC moieties can undergo acetal reaction with OH groups of polysaccharide biopolymers in the building of biocompatible scaffolds. Since their responsiveness can be spatially controlled under ambient conditions, they are desirable as potential sensing materials. They are also potential candidates in biomineralization applications. The photo-induceable aggregation of the microgel particles could be potentially useful in wastewater treatment where flocculation is an important purification process. Moreover, precipitating non-ionic polymers can be exploited for their potential use in biotechnology and separation aids.[5(33)]

Modulation of the swelling behavior of the microgel particles can be further investigated by tuning their internal morphology through more precise control of the number and spatial distribution of cross-links. To achieve this, optimization of synthesis parameters is required and various other multifunctional monomers such as ethylene glycol dimethacrylate, butanediol diacrylate, triethylene glycol dimethacrylate, tetraethylene glycol dimethacrylate , 1,3-butanediol dimethacrylate, 1,4-butanediol dimethacrylate, glycerol dimethacrylate, pentaerythritol triacrylate and pentaerythritol propoxylate triacrylate could be used as cross-linkers.[5(34)]

5.6. REFERENCES

5(1) Verma, P. K.; Koch, F.; Steinbacher, A.; Nuernberger, P.; Brixner, T. Ultrafast UV-Induced Photoisomerization of Intramolecularly H-Bonded Symmetric ß-Diketones. *J. Am. Chem. Soc.* **2014**, *136*, 14981-14989 and references therein.

5(2) Watanabe, T.; Akiyama, M.; Totani, K.; Kueble, S. M.; Stellaci, F.; Wenseleers, W.; Braun, K.; Marder, S. R.; Perry. J. W. Photoresponsive Hydrogel Microstructure Fabricated by Two-Photon Initiated Polymerization. *Adv. Funct. Mater.* ***2002***, *12*, 611-614.

5(3) (a) Lozada-Garcia, R. R.; Ceponkus, J.; Chin, W.; Chevalier, M.; Crépin, C. Acetylacetone in hydrogen solids: IR signatures of the enol and keto tautomers and UV induced tautomerization. *Chem. Phys. Lett.* **2011**, *504*, 142–147; (b) Nagashima, N.; Kudoh, S.; Takayanagi, M.; Nakata, M. UV-Induced Photoisomerization of Acetylacetone and Identification of Less-Stable Isomers by Low-Temperature Matrix-Isolation Infrared Spectroscopy and Density Functional Theory Calculation. *J. Phys. Chem. A* **2001**, *105*, 10832-10838.

5(4) Krasia, T. *Synthesis and Colloidal Properties of a Novel Type of Block Copolymers bearing β-Dicarbonyl Residues*. Ph.D. Dissertation, Max-Planck-Institut für Kolloid- und Grenzflächenforschung, Universität Potsdam, Potsdam, Germany, 2003 and references therein.

5(5) (a) Jun, J. W.; Shek, P. N. Synthesis and characterization of a novel *in situ* forming gel based on hydrogel dispersions. *J. Biomed. Mater. Res. B* **2009**, *90*, 738; (b) Mastrorilli, P.; Nobile, C. F.; Suranna, G. P.; Taurino, M. R.; Latronico, M.

Synthesis and copolymerization of a ruthenium(II) complex with the deprotonated form of 2-(acetoacetoxy)ethylmetacrylate. *Inorg. Chim. Acta* **2002**, *335*, 107; (c) Qiang, X. H.; Xue, Q.; Zhang, H.; Yan, Z.; Li, M.; Xu, W.; Wang, Y. J. Preparation and characterization of acrylic resin/protein composite crosslinked films. *J. Coat. Technol. Res.* **2014**, *11*, 923-931.

5(6) Del Rector, F.; Blount, W. W.; Leonard, D. R. *Applications for the Acetoacetyl Functionality in Thermoset Coatings*. Water-Borne and Higher Solids Coatings Symposium, February 1988, New Orleans.

5(7) Park, Y.-J.; Monteiro, M. J; van Es, S.; Anton, L. Effect of ambient crosslinking on the mechanical properties and film morphology of PSTY-P(BA-co-AAEMA) reactive composite latexes. *Eur. Polym. J.* **2001**, *37*, 965–973.

5(8) (a) Ooka, M.; Ozawa, H. Recent developments in crosslinking technology for coating resins. *Prog. Org. Coat*. **1994**, *23*, 325–338.; (b) Geurink, P. J. A.; van Dalen, L.; van der Ven, L. G. J.; Lamping, R. R. Analytical aspects and film properties of two-pack acetoacetate functional latexes. *Prog. Org. Coat.* **1996**, *27*, 73-78.; (c) Carey, J. G.; Overbeek, G. C.; Heuts, M. P. J.; Smak, Y. W. (Imperial Chemical Industries Plc, UK). Aqueous Coating Compositions. US Patent 5,002,998, March 26, 1991.; (d) Lavoie, A. C.; Bors, D. A.; Brown, W. T. (Röhm and Haas) Functionalization of Polymers via Enamine of Acetoacetate. US Patent 5,494,975, February 27, 1996.; (e) Mao, C.-L.; Chen, N.; Tien, C.-F. (Air Products and Chemicals) Water-borne Cross-linkable Composition. US Patent 5,536,784, July 16, 1996.; (f) Taylor, J. W.; Salisbury, J. R. (Eastman Chemical Company) Waterborne Coating Compositions. US Patent 5,663,266, September 2, 1997.

5(9) Beshah, K.; Devonport, W. A study of acetoacetoxyethyl methacrylate hydrolysis in acrylic latex polymers as a function of pH. *J. Coat. Technol. Res.* **2013**, *10*, 821-828.

5(10) (a) Pich, A.; Lu, Y.; Boyko, V.; Arndt, K.-F.; Adler, H.-J. P. Thermo-sensitive poly(N-vinylcaprolactam-co-acetoacetoxyethyl methacrylate) microgels: 2. Incorporation of polypyrrole. *Polymer* **2003**, *44*, 7651-7659.; (b) Pich, A.; Tessier, A.; Boyko, V.; Lu, Y.; Adler, H.-J. P. Synthesis and Characterization of Poly(vinylcaprolactam)-Based Microgels Exhibiting Temperature and pH-Sensitive Properties. *Macromolecules* **2006**, *39*, 7701–7707.; (c) Agrawal, G.; Schürings, M. P.; van Rijn, P.; Pich, A. Formation of catalytically active gold-polymer microgel hybrids *via* a controlled *in situ* reductive process. *J. Mater. Chem. A* **2013**, *1*, 13244-13251.; (d) Agrawal, M.; Pich, A.; Gupta, S.; Zafeiropoulos, N. E:, Rubio-Retama, J.; Simon, F.; Stamm, M. Temperature sensitive hybrid microgels loaded with ZnO nanoparticles. *J. Mater. Chem.* **2008**, *18*, 2581–2586.; (e) Boyko, V.; Lu, Y.; Richter, A.; Pich, A. Preparation and Characterization of Acetoacetoxyethyl Methacrylate-Based Gels. *Macromol. Chem. Phys.* **2003**, *204*, 2031–2039.

5(11) Boyko, V. *N*-Vinylcaprolactam based Bulk and Microgels: Synthesis, Structural Formation and Characterization by Dynamic Light Scattering. Ph.D. Dissertation, Dresden University of Technology, Dresden, Germany, 2004.

5(12) Rubinstein, M.; Colby, R. H. Polymer Physics; Oxford University Press: New York, 2003.

5(13) (a) Provencher, S. W. A constrained regularization method for inverting data represented by linear algebraic or integral equations. *Comput. Phys. Commun.* **1982**, *27*, 213-217.; (b) Provencher, S. W. CONTIN: a general purpose constrained regularization program for inverting noisy linear algebraic and integral equations. *Comput. Phys. Commun.* **1982**, *27*, 229-242.

5(14) Schlaad, H.; Krasia, T.; Antonietti, M. Superhelices of Poly[2-(acetoacetoxy)ethyl methacrylate]. *J. Am. Chem. Soc.* **2004**, *126*, 11307-11312.

5(15) Keeler, J.; Wothers, P. Chemical Structure and Reactivity: An Integrated Approach, Second Edition; Oxford University Press: Oxford, 2014.

5(16) (a) Rudakov, O. B.; Gol'tsev, A. N.; Kaplin, Y. V.; Ternovskaya, I. A.; Lunev, A. S. IR spectroscopic investigation of the keto-enol tautomerism of ortho-octadecyloxybenzoylmethyl acetate. *J. Appl. Spectroscopy* **1991**, *54*, 13-16. (b) Ghorai, S.; Laskin, A.; Tivanski, A. V. Spectroscopic Evidence of Keto-Enol Tautomerism in Deliquesced Malonic Acid Particles. J*. Phys. Chem. A* **2011**, *115*, 4373–4380.

5(17) Petkov, I.; Masuda, S.; Sertova, N.; Grigorov, L. On the photosensitivity of poly(acryloylacetone) in solution. *J. Photochem. Photobiol. A: Chem*. **1996**, *95*, 189-193.

5(18) (a) Srinivasan, R.; Feenstra, J. S.; Park, S. T; Xu, S.; Zewail, A. H. Direct Determination of Hydrogen-Bonded Structures in Resonant and Tautomeric Reactions Using Ultrafast Electron Diffraction. *J. Am. Chem. Soc*. **2004**, *126*, 2266-2267. (b) Trivella, A.; Roubin, P.; Theule, P.; Rajzmann, M.; Coussan, S.; Manca, C. UV and IR Photoisomerization of Acetylacetone Trapped in a Nitrogen Matrix. *J. Phys. Chem. A* **2007**, *111*, 3074. and references therein.

5(19) Morton, R. A.; Hassan, A.; Calloway, T. C. Absorption spectra in relation to the constitution of keto-enols. *J. Chem. Soc*. **1934**, 883.

5(20) (a) Veierov, D.; Bercovici, T.; Fisher, E.; Mazur, Y.; Yogev, A. Photoisomerization of ß-diketones and ß-keto esters. *J. Am. Chem. Soc.* **1973**, *95*, 8173.; (b) Veierov, D.; Bercovici, T.; Fischer, E.; Mazur, Y.; Yogev, A.

Photoisomerization of the enol form of 1,3-dicarbonyl compounds. *J. Am. Chem. Soc.* **1977**, *99*, 2723.

5(21) Balashev, K.; Panchev, N.; Petkov, I.; Panaiotov, I. Photochemical behaviour of polyacryloylacetone; and polyethylacrylacetate monolayers at the air-water interface. *Colloid Polym. Sci.* **2000**, *278*, 301-311.

5(22) Masuda, S.; Sertova, N.; Petkov, I. Photochemical behavior of poly(ethylacryloylacetate) and poly(acryloylacetone) films. *J. Polym. Sci. Part A: Polym. Chem.* **1997**, *35*, 3683-3688.

5(23) Rubio Retama, J.; Frick, B.; Seydel, T.; Stamm, M.; Fernand Barbero, A.; Lopez Cabarcos, E. Polymer Chain Dynamics of Core-Shell Thermosensitive Microgels. *Macromolecules* **2008**, *41*, 4739.

5(24) (a) Drexler, E. J.; Field, K. W. An NMR study of keto-enol tautomerism in ß-dicarbonyl compounds. *J. Chem. Ed.* **1976**, *53*, 392-393 and references therein; (b) Mills, S. G.; Beak, P. Solvent effects on keto-enol equilibria: tests of quantitative models. *J. Org. Chem.* **1985**, *50*, 1216 and references therein; (c) Spencer, J. N.; Holmboe, E. S.; Kirshenbaum, M. R.; Firth, D. W.; Pinto, P.B. Solvent effects on the tautomeric equilibrium of 2,4-pentanedione. *Can. J. Chem*. **1982**, *60*, 1178; (d) Ishida, T.; Hirata, F.; Kato, S. Solvation dynamics of benzonitrile excited state in polar solvents: A time-dependent reference interaction site model self-consistent field approach. *J. Chem. Phys*. **1999**, *110*, 11423.; (e) Weedon, A. C. Photochemical Reactions Involving Enols. In The Chemistry of Enols; Rappoport, Z., Ed.; John Wiley & Sons, Chichester, UK, 1990, p 591-638.

5(25) (a) Das, I.; Gupta, S. K. Polyethylene glycol degradation by UV irradiation. *Indian J. Chem*. **2005**, *44A*, 1355-1358; (b) Nolan, C. M.; Reyes, C. D.; Debord, J. D.; Garcia, A. J.; Lyon, L. A. Phase Transition Behavior, Protein Adsorption, and Cell Adhesion Resistance of Poly(ethylene glycol) Cross-Linked Microgel Particles. *Biomacromolecules* **2005**, *6*, 2032-2039; (c) Dupin, D.; Fujii, S.; Armes, S. P. Efficient Synthesis of Sterically Stabilized pH-Responsive Microgels of Controllable Particle Diameter by Emulsion Polymerization. *Langmuir* **2006**, *22*, 3381-3387.

5(26) Treloar, L. R. G. Physics of Rubber Elasticity; Clarendon Press: Oxford, 1975.

5(27) Boyko, V.; Pich, A.; Lu, Y.; Richter, S.; Arndt, K.-F.; Adler, H.-J. P. Thermo-sensitive poly(N-vinylcaprolactam-co-acetoacetoxyethyl methacrylate) microgels: 1-synthesis and characterization. *Polymer* **2003**, *44*, 7821-7827.

5(28) Lee, H.-N.; Newell, N.; Bai, Z.; Lodge, T. P. Unusual Lower Critical Solution Temperature Phase Behavior of Poly(ethylene oxide) in Ionic Liquids. *Macromolecules* **2012**, *45*, 3627-3633.

5(29) (a) Maverick, A. W.; Klavetter, F. E. Cofacial binuclear copper complexes of a bis(ß-diketone) ligand. *Inorg. Chem.* **1984**, *23*, 4130-4131; (b) Powell, K. R.; McCleskey, T. M.; Tumas, W.; DeSimone, J. M. Polymers with Multiple Ligand Sites for Metal Extractions in Dense-Phase Carbon Dioxide. *Ind. Eng. Chem. Res.* **2001**, *40*, 1301-1305; (c) Southard, G. E.; Murray, G. M. Synthesis of Vinyl-Substituted ß-Diketones for Polymerizable Metal Complexes. *J. Org. Chem.* **2005**, *70*, 9036-9039.; (d) Papaphilippou, P.; Loizou, L.; Popa, N. C.; Han, A.; Vekas, L.; Odysseos, A.; Krasia-Christoforou, T. Superparamagnetic Hybrid Micelles, Based on Iron Oxide Nanoparticles and Well-Defined Diblock Copolymers Possessing ß-Ketoester Functionalities. *Biomacromolecules* **2009**, *10*, 2662–2671.

5(30) Papaphilippou, P.; Christodoulou, M.; Marinica, O.-M.; Taculescu, A.; Vekas, L.; Chrissafis, K.; Krasia-Christoforou, T. Multiresponsive Polymer Conetworks Capable of Responding to Changes in pH, Temperature, and Magnetic Field: Synthesis, Characterization, and Evaluation of Their Ability for Controlled Uptake and Release of Solutes. *ACS Appl. Mater. Interfaces* **2012**, *4*, 2139−2147.

5(31) Tomida, T.; Tomida, M.; Nishihara, Y.; Nakabayashi, I.; Okazaki, T.; Masuda, S. Properties of polyacryloylacetone for adsorption of divalent metal ions. *Polymer* **1990**, *11*, 102.

5(32) Kotha, S.; Deb, A. C.; Kumar, R. V. Spiro-annulation of barbituric acid derivatives and its analogs by ring- closing metathesis reaction. *Bioorg. Med. Chem. Lett.* **2005**, *15*, 1039-1043.

5(33) Galaev, I. Y.; Mattiasson, B. Thermoreactive water-soluble polymers, nonionic surfactants, and hydrogels as reagents in biotechnology. *Enzyme Microb. Technol.*, **1993**, *15*, 354-366.

5(34) Schneider, F.; Balaceanu, A.; Feoktystov, A.; Pipich,V.; Wu, Y.; Allgaier, J.; Pyckhout-Hintzen, W.; Pich, A.; Schneider, G. J. Monitoring the Internal Structure of Poly(*N*-vinylcaprolactam) Microgels with Variable Cross-Link Concentration. *Langmuir* **2014**, *30*, 15317−15326 and references therein.

APPENDIX 5

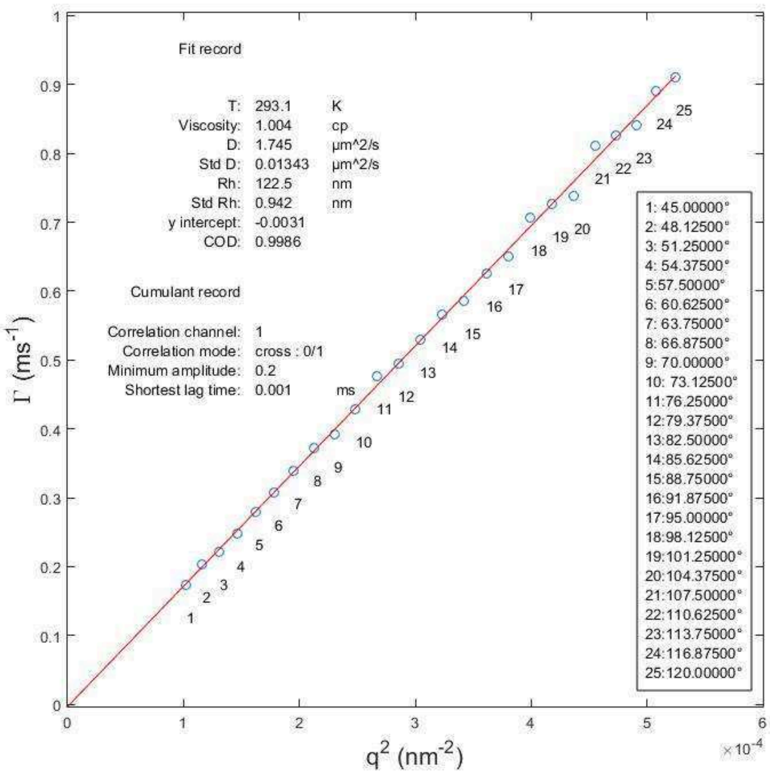

Figure A5(1). Angle-dependent dynamic light scattering measurement of MG1 performed at 20°C. A straight-line fit to a spherical model is shown.

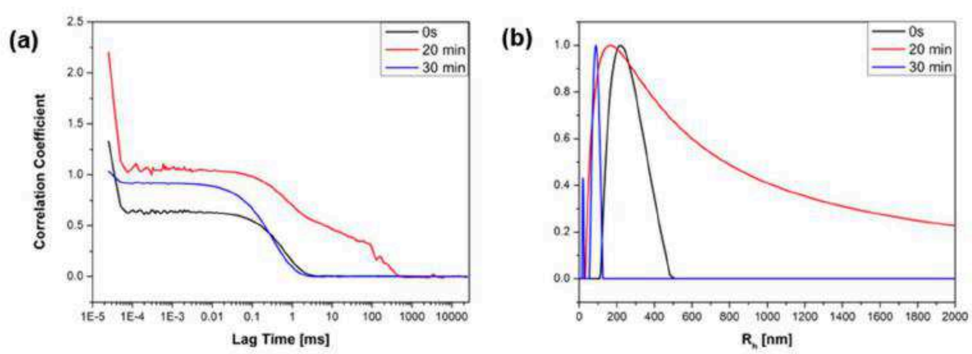

Figure A5(2). (a) Correlation function in DLS of MG1 dissolved in THF, after equilibration times of 0 seconds, 20 minutes, and 30 minutes, (b) Size distribution curves of MG1 dissolved in THF, obtained via CONTIN fits, after equilibration times of 0 seconds, 20 minutes and 30 minutes.

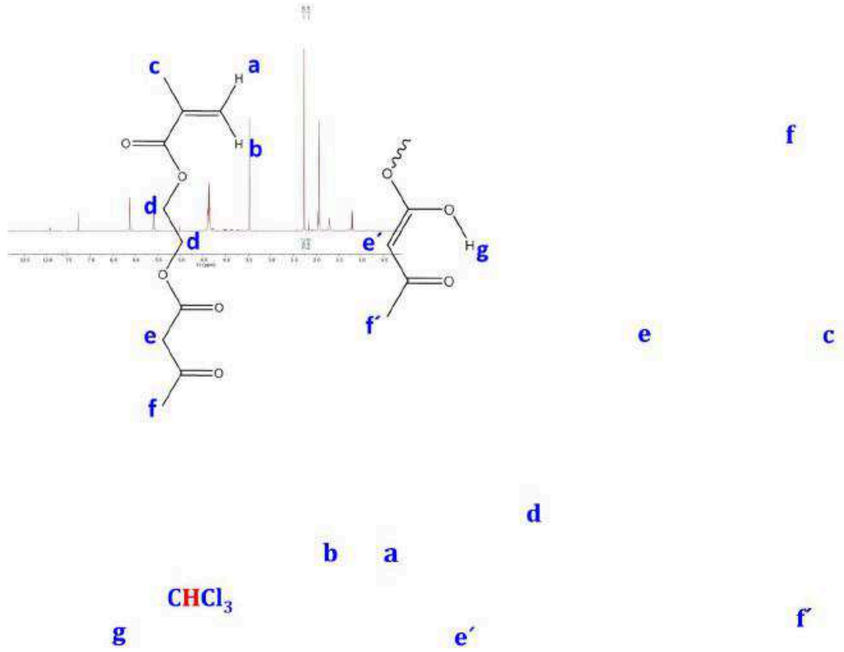

Figure A5(3a). ^{1}H NMR spectra of AAEM monomer in $CDCl_3$.

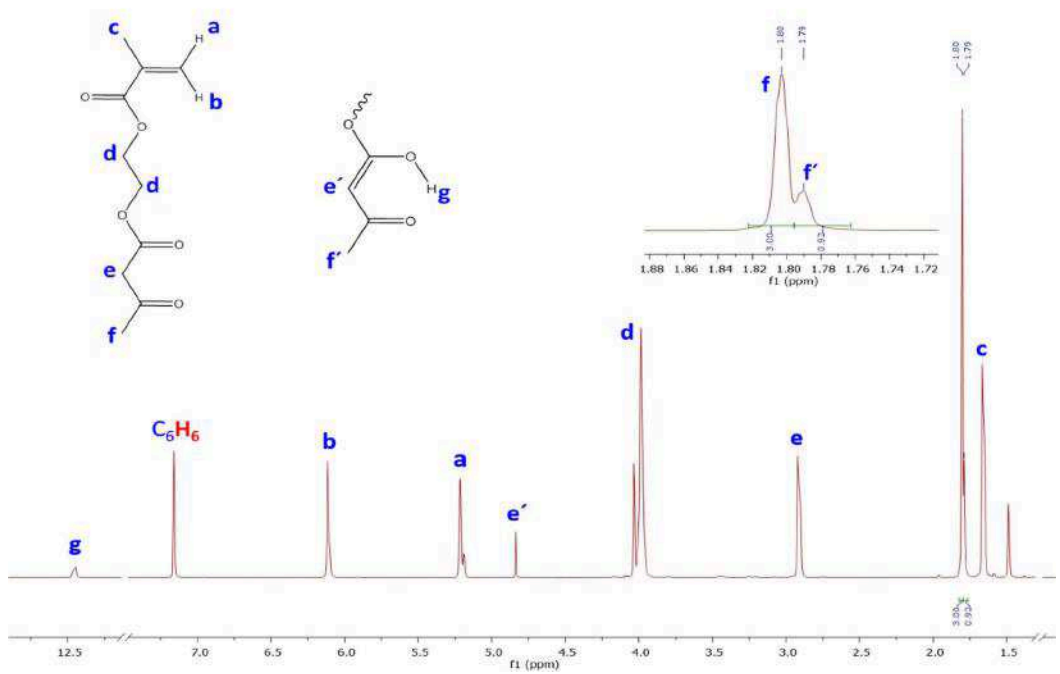

Figure A5(3b). ^{1}H NMR spectra of AAEM monomer in Benzene-d_6.

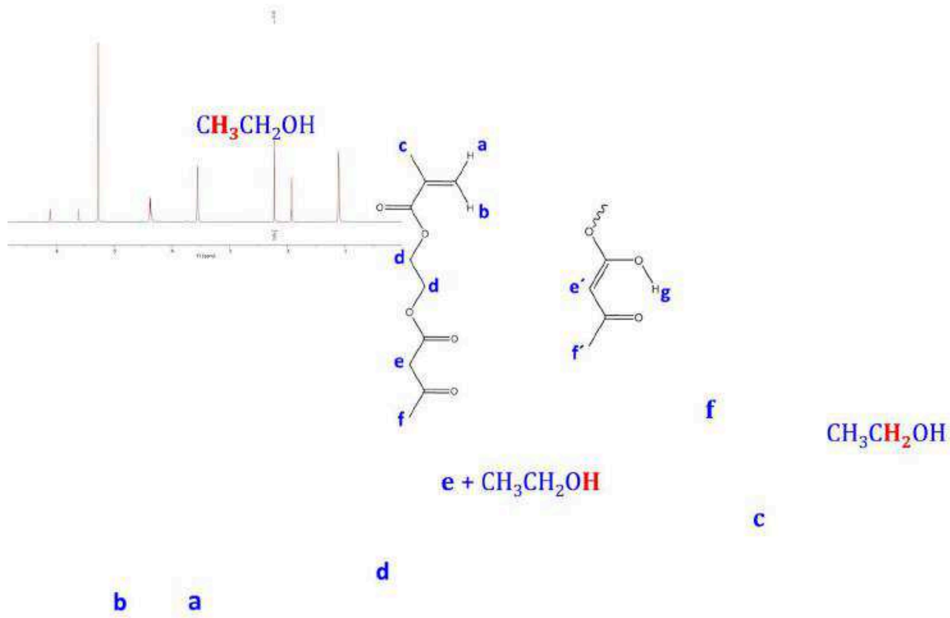

Figure A5(3c). ^{1}H NMR spectra of AAEM monomer in Ethanol-d_6.

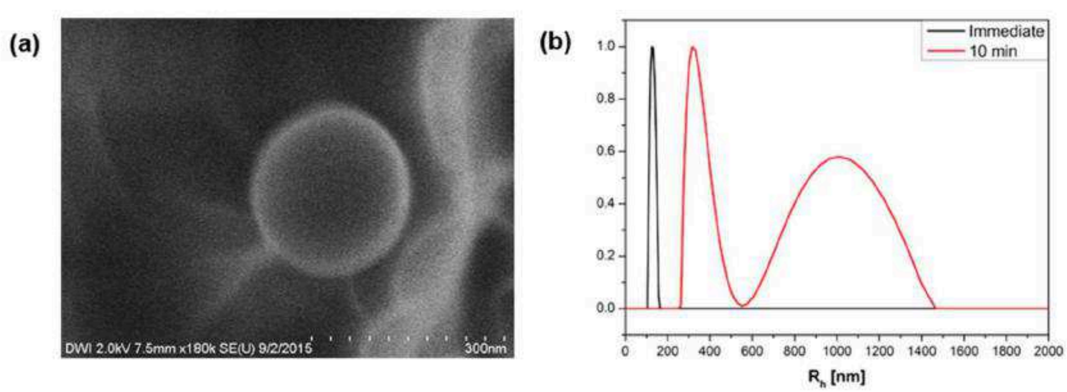

Figure A5(4). (a) Cryo-FESEM micrographs of MG3 in its native state, (b) Narrow particle size distribution of MG3, immediately after 10 sec of UV (254 nm) irradiation, obtained via a CONTIN fit from the DLS size measurement data (R_h derived from cumulant fit = 129.81 ± 6.13 nm, Pd.I 0.103), and particle size distribution of the size measurement recorded after 10 minutes of equilibration time for the same MG3 sample that had been UV-irradiated (254 nm) for 10 sec (R_h derived from cumulant fit = 328.01 ± 8.10 nm, Pd.I 0.244).

CHAPTER 6. Summary

Monodispersed thermo- and photo-responsive microgels were prepared via precipitation polymerization with *N*-vinylcaprolactam as the main monomer and the amount of photochromic azobenzene-based comonomer, 4-[(4-methacryloyloxy)phenylazo] benzenesulfonic acid (ABSA), incorporated was modulated. We offer a convenient and practical method to observe the photo-switchable size changes of such small particles, in real time, via *in situ* irradiation within the dynamic light scattering (DLS) instrument. Microgels with low and high loadings of ABSA were found to exhibit distinct thermo- and photo-responsive properties from one another.

Size-temperature data obtained from dynamic light scattering measurements show that the microgels with low loading of ABSA (≤ 10 wt. %) displayed volume phase transition temperatures that are shifted to lower temperatures relative to pure P(VCL-BIS) microgels. UV irradiation (λ = 365 nm) induces the isomerization of *trans* ABSA side groups in P(VCL-BIS-ABSA) microgels, producing up to 36% *cis*-ABSA in the photo-stationary state. As a result of this *trans*-*cis* isomerization, the microgels deswell at temperatures below their VPTT by up to 28% of their sizes in the native state. This deswelling was found to be rapidly reversible via irradiation of the microgel solution with blue light that initiated the back isomerization reaction. Above the VPTT of the microgels, no photo-response was detected by DLS. To the best of our knowledge, this is the first reported instance of rapid and significant deswelling of P(VCL)-based microgels upon UV-induced *trans*-to-*cis* isomerization of small amounts of incorporated ABSA pendant groups within the microgel matrix. The mechanism for the UV-induced deswelling is found to be analogous to that of a temperature induced deswelling of P(VCL-BIS) microgels. Within the microgels, the bent and bulky *cis*-ABSA side groups are most likely to be oriented toward the VCL units in the main chain. This results in increased hydrophobic interactions between the polar *cis* side groups with the main chain and causes a dehydrating effect on the VCL units.

With high loading of ABSA (between 20 and 30 wt. %), extensive intra- and inter-particle charged-assisted H-bonding and π-π stacking interactions arise. Inter-particle interactions result in the microgels existing preferentially as dimeric assemblies whose peripheral dangling chains are interlocked with the inner network structure of their dimeric partner. These attractive interactions strongly suppressed the thermo- and photo-responsive behaviors of the dimeric and single particles. The individual particles in the dimeric assemblies were not separable by temperature or

UV stimulus. We were nevertheless able to disrupt the dimers by increasing the ionic strength of the microgel solution before subjecting them to short periods of mechanical agitation by ultrasonic treatment. The single microgel particles exhibited shallow deswelling from 30°C and the particle size continued to decrease gradually to a minimum at around 50°C. The extent of deswelling was significantly enhanced by UV irradiation, especially at higher temperatures, with sufficient equilibration times and with longer durations of UV irradiation. Random copolymer chains with high loading of ABSA were also synthesized using the same microgel polymerization procedure but the addition of the chemical cross-linker BIS was eliminated. Via similar non-covalent interactions as those present in the microgels, the linear chains were able to self-assemble into nanospheres of around 500 nm in diameter in a 75 wt. % water/THF mixture. These nanospheres could be disrupted via prolonged UV irradiation of 15 minutes and then re-assembled by stirring the irradiated solution overnight, in the dark.

Photo-responsive microgels of P(VCL) bearing azobenzene-based cross-linkers were also synthesized. Low azobenzene cross-linker feed amounts (< 1 mol %) was necessary to achieve reasonable UV-induced deswelling of the microgels. The lower the amount of azobenzene cross-linker, the softer and more deformable the particles were and the more responsive they were to UV stimulus. With azobenzenes as cross-linkers, we achieved a smaller UV-induced deswelling of the microgels as compared to having ABSA as pendant groups in the microgels. Moreover, we observed that the underlying, pre-existing interactions between the azobenzene cross-linkers and the surrounding VCL chain segments become critical in the native, non-irradiated state, especially when the azobenzene cross-linkers possess alkyl spacers and substituent group like COOH which are capable of forming more extensive interactions. The measure of heat-induced deswelling extents verifies that hydrophobic interactions are more robust in the systems with alkyl spacers and COOH substituent.

UV-responsive P(AAEM)-based microgels were also conveniently synthesized via surfactant-free precipitation polymerization in water. This study presents the first investigation into the swelling of P(AAEM) microgels upon UV irradiation that induces a photo-ketonization reaction. The hydrodynamic radii of the microgels increased to at least twice their original values in four of the microgels synthesized. The extent of swelling is dependent upon the extent of UV-induced photo-ketonization which in turn can be controlled by manipulating the elasticity and hydrophilicity of the network. This was achieved by varying the type and amount of comonomer or cross-linker which affect the distribution of crosslinking points and the microstructure of the subchains.

In other words, the internal morphology of the microgel network affects its photo-responsiveness. The swelling process tended to occur non-isotropically and destabilized the irradiated particles, leading to their agglomeration, which is facilitated by inter-particle hydrogen bonding interactions.